

**TREATMENT OF NON-IDEALITY IN THE
MULTIPHASE MODEL SPACCIM AND
INVESTIGATION OF ITS INFLUENCE ON
TROPOSPHERIC AQUEOUS PHASE
CHEMISTRY**

Von der Fakultät für Umweltwissenschaften und Verfahrenstechnik der
Brandenburgischen Technischen Universität Cottbus zur Erlangung des
des akademischen Grades eines Doktor-Ingenieurs (Dr.-Ing.)

genehmigte Dissertation
vorgelegt von

M. Tech. Chemical Engineering
Ahahmad Jhony Rusumdar
geboren am 10. Juni 1983 in Guntur, India.

Gutachter: Prof. Dr. Detlev Möller
Prof. Dr. Hartmut Herrmann

Tag der mündlichen Prüfung: 21.02.2013

Contents

| | |
|---|-------------|
| List of Figures | V |
| List of Tables | IX |
| List of Symbols | XI |
| Acronyms and Abbreviations | XV |
| Acknowledgements | XVII |
| Abstract | XIX |
| 1 Introduction | 1 |
| 2 Scientific background | 6 |
| 2.1 Theoretical aspects of phase equilibria in multicomponent systems | 6 |
| 2.1.1 Gibbs energy | 6 |
| 2.1.2 The chemical potential | 7 |
| 2.1.3 Raoult's law | 9 |
| 2.1.4 Intermolecular forces in solutions | 10 |
| 2.1.5 Non-ideal solutions | 10 |
| 2.2 Equilibrium growth theory and microphysical processing | 12 |
| 2.2.1 Modeling of cloud droplet activation | 14 |
| 2.2.2 The effect of surface tension on droplet growth | 15 |
| 2.3 Multiphase models for atmospheric aerosols | 16 |
| 2.3.1 Equilibrium approach | 16 |
| 2.3.2 Dynamic approach | 17 |
| 2.3.3 Hybrid approach | 18 |
| 3 Activity coefficient models | 19 |
| 3.1 G^{Ex} models | 19 |
| 3.2 Group contribution methods | 20 |
| 3.3 Activity coefficient models for mixtures of organic and inorganic compounds | 21 |
| 3.4 Activity coefficient models for inorganic compounds: Pitzer model | 23 |
| 3.5 Activity coefficient models for organic compounds | 24 |
| 3.6 Description of activity coefficient module used in this study | 24 |
| 3.6.1 Long-range contribution | 25 |
| 3.6.2 Middle-range contribution-extended version | 26 |

| | | |
|----------|---|-----------|
| 3.6.3 | Short-range contribution | 31 |
| 3.6.4 | Total activity coefficients | 33 |
| 4 | The air parcel model SPACCIM | 35 |
| 4.1 | Microphysical processes | 35 |
| 4.1.1 | Equilibrating particle water content | 36 |
| 4.1.2 | Water condensation and evaporation | 37 |
| 4.2 | Multiphase chemistry model | 38 |
| 4.2.1 | Mass balance equations | 38 |
| 4.2.2 | Description of chemical reactions | 38 |
| 4.2.3 | Phase transfer processes | 40 |
| 4.2.4 | Microphysical fluxes | 42 |
| 4.3 | Coupling scheme and feedback processes | 42 |
| 5 | Model improvements and treatment of non-ideality | 44 |
| 5.1 | Multiphase chemistry approach considering non-ideal solutions | 45 |
| 5.1.1 | Numerical description of multiphase chemistry | 45 |
| 5.1.2 | Reaction kinetics and coefficients | 46 |
| 5.1.3 | Equilibrium and non-equilibrium across the gas and aerosol phases | 47 |
| 5.2 | Modified coupling scheme | 50 |
| 5.3 | Feedback of non-ideal multiphase chemistry on microphysics | 51 |
| 5.4 | Implementation and adjustment of numerical schemes | 52 |
| 5.4.1 | Major modifications performed in numerics | 53 |
| 5.4.2 | Time integration scheme | 53 |
| 5.4.3 | Linear system solver | 54 |
| 5.4.4 | Adjustment of Jacobian calculation and linear system solver | 55 |
| 6 | Model results and discussions | 58 |
| 6.1 | Activity coefficient model verification | 58 |
| 6.1.1 | Comparison with published activity coefficient models | 59 |
| 6.1.1.1 | Binary aqueous electrolyte solutions | 59 |
| 6.1.1.2 | Aqueous organic solutions | 61 |
| 6.1.2 | Intercomparison between activity coefficient models | 63 |
| 6.1.3 | Verification of activity models with water activity measurements | 68 |
| 6.1.4 | Verification of robustness: extended AIOMFAC | 70 |
| 6.1.5 | Importance of interactions | 73 |
| 6.1.6 | Conclusions | 75 |
| 6.2 | Multiphase processing in aqueous particles and clouds | 76 |
| 6.2.1 | Description of microphysical scenarios | 76 |

| | | |
|----------|--|------------|
| 6.2.2 | Applied multiphase chemistry mechanism: RACM-MIM2ext/CAPRAM 2.4+organicExt | 78 |
| 6.2.3 | Modeled microphysical conditions | 79 |
| 6.2.4 | Modeled activity coefficients | 80 |
| 6.2.4.1 | Inorganic compounds | 81 |
| 6.2.4.2 | Organic compounds | 83 |
| 6.2.5 | Particle acidity | 86 |
| 6.2.6 | Multiphase processing of inorganics | 88 |
| 6.2.6.1 | Sulphur processing | 88 |
| 6.2.6.2 | Iron chemistry | 90 |
| 6.2.7 | Multiphase processing of radicals | 95 |
| 6.2.7.1 | OH radical | 96 |
| 6.2.7.2 | NO ₃ radical | 102 |
| 6.2.7.3 | Multiphase HO ₂ /O ₂ ⁻ radical processing | 106 |
| 6.2.8 | Aqueous multiphase processing of organic compounds | 109 |
| 6.2.8.1 | C ₂ aqueous phase processing | 109 |
| 6.2.8.2 | C ₃ aqueous phase processing | 113 |
| 6.2.9 | Summary: Processing of multiphase chemistry under non-ideal conditions | 117 |
| 6.3 | Chemical sensitivity studies | 119 |
| 6.3.1 | Modeled activity coefficients | 119 |
| 6.3.2 | Inorganic compounds | 119 |
| 6.3.3 | Organic compounds | 122 |
| 6.3.4 | Particle acidity | 125 |
| 6.3.5 | Multiphase processing of inorganics | 127 |
| 6.3.6 | Multiphase OH radical processing | 128 |
| 6.3.7 | Aqueous multiphase processing of organic compounds | 131 |
| 6.3.8 | Summary: Influence of treatment of non-ideality on multiphase chemistry at different relative humidity levels | 134 |
| 7 | Summary and outlook | 135 |
| | Bibliography | 140 |
| | Appendix | 152 |
| A | Thermodynamics of phase equilibria in multicomponent systems | 152 |
| A.1 | Phase equilibria in heterogeneous system | 152 |
| A.2 | The Gibbs-Duhem relation | 153 |
| A.3 | Gibbs excess energy | 154 |
| A.4 | Multi-component reaction equilibria | 156 |
| B | Description of activity coefficient models | 158 |

| | | |
|----------|--|------------|
| B.1 | Concentration scales and reference states | 158 |
| B.2 | PITZER approach | 160 |
| B.3 | UNIFAC | 162 |
| B.4 | LIFAC | 163 |
| B.4.1 | Long-range contribution | 164 |
| B.4.2 | Middle-range contribution | 164 |
| B.4.3 | Short-range contribution | 165 |
| B.5 | AIOMFAC | 166 |
| B.5.1 | Long-range contribution | 166 |
| B.5.2 | Middle-range contribution | 167 |
| B.5.3 | Short-range contribution | 169 |
| B.6 | Ming and Russell model | 170 |
| C | Multiphase processing in aqueous particles and clouds | 173 |
| C.1 | Modeled activity coefficients | 173 |
| C.2 | Multiphase processing of inorganic compounds | 173 |
| C.3 | Multiphase processing of radical oxidants | 176 |
| C.4 | Aqueous multiphase processing of organic compounds | 181 |
| C.5 | Activity coefficient parameters | 184 |

List of Figures

| | | |
|-----|--|----|
| 2.1 | Ideal and real vapor pressure over a binary liquid mixture of species A and B. . . | 9 |
| 2.2 | Three major terms represent different types of molecular interactions in a solution and add up to the excess Gibbs energy. | 11 |
| 2.3 | Schematic representation of traditional Köhler curve. | 14 |
| 3.1 | Solution of groups contribution concept. | 21 |
| 3.2 | Description of computational methodology for the activity coefficients for mixtures. | 22 |
| 3.3 | Description of activity coefficient algorithm implemented in this study. | 30 |
| 3.4 | Scheme of the currently used interactions in the MR and SR part. | 33 |
| 4.1 | Schematic of transport and reactive processes for the uptake in gas-liquid interactions. | 41 |
| 4.2 | Schematic of the model coupling strategy implemented in SPACCIM. | 42 |
| 5.1 | Schematic of the microphysical processes included in SPACCIM microphysics model. | 44 |
| 5.2 | Schematic of the model coupling strategy and its implementation considering the treatment of non-ideality and surface tension effects in SPACCIM. | 50 |
| 5.3 | Schematic of activity coefficients used in the microphysics and multiphase chemistry models. | 52 |
| 5.4 | Sparse structure of Jacobian and two droplet classes. | 55 |
| 6.1 | Experimental and predicted mean activity coefficients for aqueous electrolyte solutions at 25 °C as a function of molality. | 60 |
| 6.2 | Experimental and predicted mean activity coefficients for aqueous electrolyte solutions at 25 °C as a function of molality. | 61 |
| 6.3 | Experimental and predicted mean activity coefficients for aqueous electrolyte solutions at 25 °C as a function of molality. | 62 |
| 6.4 | Experimental and predicted mean activity coefficients for aqueous electrolyte solutions at 25 °C as a function of molality. | 63 |
| 6.5 | Experimental and predicted water activities and mean activity coefficients of binary aqueous Cl ⁻ electrolyte's solutions. | 64 |
| 6.6 | Experimental and predicted water activities and mean activity coefficients of binary aqueous NO ₃ ⁻ electrolyte's solutions. | 65 |

| | | |
|------|--|-----|
| 6.7 | Experimental and calculated water activities (a_w) in aqueous glutaric acid solution as a function of water fraction (x_w) at 298.15K. | 66 |
| 6.8 | Experimental and calculated water activities (a_w) in aqueous citric acid solution as a function of water fraction (x_w) at 298.15K. | 67 |
| 6.9 | Intercomparison between models for NaCl + NH ₄ NO ₃ (1:1). | 68 |
| 6.10 | Intercomparison between selected models for Ca(NO ₃) ₂ salt. | 69 |
| 6.11 | Experimental and calculated water activities (a_w) in aqueous solutions composed of organic-electrolyte mixture. | 70 |
| 6.12 | Water activities of glycerol- water-ammonium sulphate mixture at 298 K. | 71 |
| 6.13 | Comparison of water activities of binary aqueous SO ₄ ²⁻ electrolyte's solutions. | 72 |
| 6.14 | Comparison of mean activity coefficients of binary aqueous SO ₄ ²⁻ electrolyte's solutions. | 73 |
| 6.15 | Importance of different interactions in the aqueous solution composed of organic-electrolyte mixture. | 74 |
| 6.16 | Schematic of used meteorological scenarios. | 77 |
| 6.17 | Schematic of multiphase mechanism employed in this study. | 79 |
| 6.18 | Evolution of supersaturation during the meteorological scenario | 80 |
| 6.19 | Evolution of LWC during the meteorological scenario. | 80 |
| 6.20 | Modeled pH value as a function of time for the urban environmental conditions. | 88 |
| 6.21 | Modeled S(VI) aqueous phase concentration in mol m ⁻³ vs. modeling time for the urban scenario. | 89 |
| 6.22 | Modeled Fe(II) aqueous phase concentration in mol m ⁻³ vs. modeling time for the urban scenario. | 90 |
| 6.23 | Modeled chemical sink and source mass fluxes of Fe(II) for the second day of modeling time for the urban scenario in aqueous phase in mol m ⁻³ s ⁻¹ | 91 |
| 6.24 | Modeled OH aqueous phase concentration in mol l ⁻¹ vs. modeling time for the urban scenario. | 97 |
| 6.25 | Modeled chemical sink and source mass fluxes of OH in aqueous phase in mol m ⁻³ s ⁻¹ for the second day of modeling time for the urban scenario. | 101 |
| 6.26 | Modeled NO ₃ aqueous phase concentration in mol l ⁻¹ vs. modeling time for the urban scenario. | 103 |
| 6.27 | Modeled chemical sinks and source mass fluxes of NO ₃ in aqueous phase in mol m ⁻³ s ⁻¹ for the second day of modeling time for the urban scenario. | 106 |
| 6.28 | Modeled HO ₂ /O ₂ ⁻ aqueous phase concentration in mol m ⁻³ s ⁻¹ vs. modeling time for the urban scenario. | 107 |

| | | |
|------|--|-----|
| 6.29 | Modeled chemical sink and source mass fluxes of HO_2/O_2^- in aqueous phase in $\text{mol m}^{-3} \text{ s}^{-1}$ for the second day of modeling time for the urban scenario. | 108 |
| 6.30 | Modeled aqueous phase concentrations in $\text{mol m}^{-3}_{(air)}$ and corresponding activity coefficients for the most important C_2 oxidation products. | 110 |
| 6.31 | Modeled chemical sink and source mass fluxes of oxalic acid/oxalate for the second day of modeling time for the urban scenario in aqueous phase in $\text{mol m}^{-3} \text{ s}^{-1}$ | 112 |
| 6.32 | Modeled aqueous phase concentrations in $\text{mol m}^{-3}_{(air)}$ for the most important C_3 oxidation products for the urban scenario. | 115 |
| 6.33 | Modeled chemical sink and source mass fluxes of keto malonic acid in aqueous phase in $\text{mol m}^{-3} \text{ s}^{-1}$ for the second day of modeling time for the urban scenario. | 116 |
| 6.34 | Schematic of used meteorological scenarios for sensitivity studies. | 120 |
| 6.35 | Modeled pH value as a function of time for the urban environmental conditions | 126 |
| 6.36 | Modeled Fe(II) aqueous phase concentration in mol m^{-3} vs. modeling time for the urban scenario at three different relative humidity levels. | 128 |
| 6.37 | Modeled OH aqueous phase concentration in mol l^{-1} vs. modeling time for the urban scenario at three different RH levels. | 129 |
| 6.38 | Modeled chemical sinks and source mass fluxes of OH radical in aqueous phase $\text{mol m}^{-3} \text{ s}^{-1}$ for the simulation 70%-NIDU. | 130 |
| 6.39 | Modeled aqueous phase concentrations in $\text{mol m}^{-3}_{(air)}$ and corresponding activity coefficients for the most important C_2 oxidation products at three difference relative humidity levels. | 132 |
| A.1 | Thermodynamic relationships between Gibbs energy and other measurable quantities. | 155 |
| B.1 | Schematic of the activity of the solute in ideal and real solutions. | 160 |
| C.1 | Modeled activity coefficients of inorganic ions vs. modeling time for urban scenario. | 173 |
| C.2 | Modeled Fe(II) aqueous phase concentration in mol l^{-1} vs. modeling time for the remote scenario. | 174 |
| C.3 | Modeled activity coefficients of Fe(II) vs. modeling time for urban scenario at different relative humidities. | 174 |
| C.4 | Modeled OH and NO_3 aqueous phase concentration in mol l^{-1} vs. modeling time for the remote scenario. | 176 |
| C.5 | Modeled pH value as a function of time for the remote environmental conditions. | 179 |
| C.6 | Modeled chemical sink and source mass fluxes of OH in aqueous phase in $\text{mol m}^{-3} \text{ s}^{-1}$ for the second day of modeling time for the remote scenario. | 179 |
| C.7 | Modeled aqueous phase concentrations in $\text{mol m}^{-3}_{(air)}$ and corresponding activity coefficients for the most important C_2 oxidation products for the remote scenario. | 181 |

| | |
|--|-----|
| C.8 Modeled aqueous phase concentrations in mol m ⁻³ _(air) and corresponding activity coefficients for the most important C ₃ oxidation products. | 182 |
|--|-----|

List of Tables

| | | |
|-----|---|-----|
| 2.1 | Approaches to simulate gas/particle mass transfer | 17 |
| 5.1 | Description of activities implemented in SPACCIM. | 47 |
| 6.1 | Description of the microphysical model scenario and its acronym used in this study. 78 | |
| 6.2 | Predicted activity coefficients of the selected ions and water activity in the deliquescent particles for the remote and urban scenario. | 82 |
| 6.3 | Predicted activity coefficients of organic compounds in the deliquescent particles for the remote and urban scenario. | 84 |
| 6.4 | Integrated percentage contributions of the most important Fe(II) source and sink reactions for the urban case classified regarding to the various microphysical conditions during the simulation time. | 93 |
| 6.5 | Integrated percentage contributions of the most important OH radical source and sink reactions for the urban case classified regarding to the various microphysical conditions during the simulation time | 99 |
| 6.6 | Integrated percentage contributions of the most important NO ₃ radical source and sink reactions for the urban case classified regarding to the various microphysical conditions during the simulation time | 105 |
| 6.7 | Predicted activity coefficients of ions and water activity in the particles for the remote and urban scenario at three different RH levels | 121 |
| 6.8 | Predicted activity coefficients of key organic compounds in the particles for the remote and urban scenario at three different RH levels. | 124 |
| B.1 | UNIFAC group interaction parameters | 163 |
| C.1 | Integrated percentage contributions of the most important Fe(II) sources and sink reactions for the remote case classified regarding to the various microphysical conditions during the simulation time. | 175 |
| C.2 | Integrated percentage contributions of the most important OH radical sources and sink reactions for the remote case classified regarding to the various microphysical conditions during the simulation time. | 177 |
| C.3 | Integrated percentage contributions of the most important NO ₃ radical sources and sink reactions for the remote case classified regarding to the various microphysical conditions during the simulation time. | 180 |

| | | |
|------|---|-----|
| C.4 | Integrated percentage contributions of the most important glycolic acid source and sink reactions for the urban case classified regarding to the various microphysical conditions during the simulation time. | 183 |
| C.5 | Integrated percentage contributions of the most important glyoxylic acid sources and sink reactions for the urban case classified regarding to the various microphysical conditions during the simulation time. | 183 |
| C.6 | AIOMFAC binary cation-anion MR interaction parameters. | 184 |
| C.7 | AIOMFAC additional aqueous electrolyte interaction parameters. | 184 |
| C.8 | AIOMFAC binary MR parameters of organic-inorganic interactions between the functional main groups and the ions. | 185 |
| C.9 | Modified LIFAC binary MR interaction parameters of organic ↔ inorganic interactions between the functional main groups and the ions. | 185 |
| C.10 | Relative van der Waals subgroup volume (R_t) and surface area (Q_t) parameters for solvent subgroups. | 186 |
| C.11 | Relative van der Waals subgroup volume (R_t^H) and surface area (Q_t^H) parameters for cations and anions considering dynamic hydration. | 187 |

List of symbols and Abbreviations

| Symbol | Description |
|---------------------------------|---|
| $a_i, a_w, a_{m,n}$ | activity of species i ; activity of water; subgroup interaction parameter |
| A | Helmholtz energy; Kelvin term; Debye-Hückel parameter |
| B | Raoult term; Debye-Hückel parameter |
| $B_{c,a}, B_{k,i}$ | Binary adjustable MR coefficients of cation-anion |
| $b, b_{c,a}^1, b_{c,a}$ | Binary adjustable MR parameters of cation-anion |
| $b_{k,i}^1, b_{k,i}$ | Binary adjustable MR parameters of solvent-ion |
| $c_i, c_w, c_{i,j}, c_{aq}$ | Mole concentration of species i ; liquid water; electrolyte (i, j); of aqueous solute |
| $C'_{s,i}, C_{s,i}, C_i$ | Equilibrium concentration of trace species i ; saturation concentration of water over a flat surface; particle-phase concentration; local ambient concentration |
| $c_{c,a}^1, c_{c,a}^2, C_{c,a}$ | Ternary adjustable MR parameters of cation-anion |
| D | Molecular diffusion coefficient |
| e_s, E_A | Equilibrium vapor pressure over the surface of a spherical droplet; activation energy |
| f_i, f | Fugacity of species i , function value |
| $g, G, G_{i,j}$ | Gibbs energy; group interaction value |
| H_l | Dimensionless Henry's law constant of l^{th} species |
| I | Ionic strength, condensation/evaporation rate; intensity of solar radiation |
| J | Photolysis reaction rate; Jacobian |
| k, k_t, K_{eq} | Thermal conductivity; solvent; reaction rate; mass transfer coefficient; equilibrium coefficient |
| L | Liquid water content |
| m, m_p, m_{sol} | Molality; mass of the particle p ; mass of the solvent material |
| M_i, M_s, M_c, M | Molecular weight of component i ; molar mass of solute; molar mass of carbon; droplet classes |
| M_{av} | Average molar mass |
| n_i, n_w, n_s, n_c | Number of moles of species i ; number of water moles in the drop; number of all solute moles; number of carbon atoms |
| N_A, N_G | Number of aqueous phase species; number of gas phase species |
| P, P_0, P_1, \dots | Group interaction property; polynomial coefficients |
| p, p_a, p_g, p_w | Pressure; pressure of total air; partial pressure exerted by gas g ; by water vapor |
| p^{sat} | Saturation pressure |
| q_j, Q_t | UNIFAC area parameter of species j ; pure component t |
| $Q_{c,c',a}, Q_w, Q_t$ | Adjustable ternary MR parameters of cation-anion; relative van der Waals subgroup surface area of water; of component |

| | |
|----------------------------|---|
| r^*, r_i, r_a, r_A | Critical radius for growth of cloud drops; radius of the particles in bin i ; radius of the aqueous particle a ; rate of the reaction |
| R, R_w, R_t | Universal gas constant; relative van der Waals subgroup volume of water; of component |
| $R_{c,c',a}, R_l^A, R_l^G$ | Adjustable binary MR parameters of cation-anion; reaction terms in aqueous phase; gas phase |
| s_i | Molar entropy of species i |
| S | Entropy |
| S' | Equilibrium saturation ratio of water vapor |
| t | Time |
| T | Temperature, MR terms; microphysical fluxes |
| U | Internal energy |
| V | Volume |
| x_i, x_s, X_w | Mole fraction of aqueous phase species i ; salt-free mole fraction; mole fraction of subgroup in the mixture; water residual |
| y_i | Mole fraction of gas phase species i |
| z_i | Charge number of ion i |

Greek letters

| | |
|--|---|
| α | Mass accommodation coefficient |
| $\nu_w, \nu, \nu_i^{(j)}, \nu$ | Partial molar volume of water; stoichiometric factor; number of functional groups in species i ; molecular speed |
| μ | Chemical potential, Pitzer model parameter; entrainment/detrainment rate |
| $\rho, \rho_w, \rho_v, \rho_{v,r}$ | Density; density of water; of water water vapor; water vapor at the droplet surface |
| $\sigma_p, \sigma_{s/a}, \sigma_w$ | surface tension of particle p , at solid-aqueous interface; of water |
| $\gamma_i, \gamma_+, \gamma_-, \gamma$ | Activity coefficient of species i ; of cation; of anion; uptake coefficient |
| $\gamma_{\pm}, \gamma_{i,j}, \gamma^C, \gamma^R$ | Mean; mean binary activity coefficient; combinatorial part; residual part |
| Γ, Γ_s | Surface excess; of surfactant |
| $\Gamma_{diff}, \Gamma_{sol}$ | Resistance to uptake as a result of the rate of gas-phase diffusion; resistance to uptake as a result of partitioning |
| λ | Pitzer model parameter |
| φ | Solar quantum yield |
| ε_w | Static permittivity of water |
| Θ_m | Relative surface area fraction of subgroup |
| ψ_w | Temperature dependent function of the subgroup interaction parameter |

Superscripts

| | |
|-------------|---------------------|
| C | Combinatorial |
| E, Ex | Excess property |
| $*, o$ | Equilibrium states |
| LR | Long-range |
| MR | Middle-range |
| x, ∞ | Mole fraction scale |

| | |
|-----------------|-----------------|
| α, β | Phase indices |
| R | Residual |
| $ref, 0$ | Reference state |
| SR | Short-range |

Subscripts

| | |
|--------|---|
| a | Anion |
| c | Cation |
| ion | Ion |
| k | Solvent group |
| i, j | Ions, species, additional counter indices |

Acronyms and Abbreviations

| | |
|---------|--|
| AIM | Aerosol Inorganic Model |
| AIOMFAC | Aerosol Inorganic Organic Mixtures Functional groups Activity Coefficients |
| AMF | Approximate Matrix Factorization |
| AR4 | Assessment Report Four |
| BDF | Backward Differentiation Formula |
| CAPRAM | Chemical Aqueous Phase RAdical Mechanism |
| CCN | Cloud Condensation Nuclei |
| DGM | Discontinuous Galerkin Method |
| EQSAM | Equilibrium Simplified Aerosol Model |
| GDE | General Dynamic Equation |
| IMEX | Implicit-Explicit scheme |
| IPCC | Intergovernmental Panel on Climate Change |
| MADM | Multicomponent Aerosol Dynamics Model |
| LSODE | Linear Solver of ODEs systems |
| LWC | Liquid Water Content |
| ODE | Ordinary Differential Equation |
| SCAPE | Size Composition Aerosol Equilibrium Model |
| SPACCIM | SPectral Aerosol Cloud Chemistry Interaction Model |
| UNIFAC | UNIversal quasi-chemical Functional group Activity Coefficients |
| UNIQUAC | UNIversal QUAsi-Chemical activity coefficient model |
| WSOC | Water Soluble Organic Content |

Acknowledgements

I would like to express my sincere gratitude to Dr. Ralf Wolke, without whose mentoring this research would not have been possible. I am indebted to him for his constant encouragement and support that made this research success. I extend gratitude to Dr. Andreas Tilgner, who has been instrumental in the research especially for making data available and continuous help during the modeling issues as well as interpretation of results to make this dissertation successful.

I owe Prof. Dr. Eberhard Renner and Prof. Dr. Hartmut Herrmann special thanks for guiding me through the technical aspects used in this research. I appreciate their patience in answering all of my questions regarding the concepts used in this research. I would like to thank the people I have been working with. I am especially thanks to Peter Bräuer, Martin Schlegel, Dr. Olaf Hellmuth, Wolfram Schröder for their support in modeling issues. The special environment at the modeling and chemistry department of the Institute for Tropospheric Research (IFT) do deserve credit in the progress of this thesis. I extend my sincere thanks to the colleagues from the modeling and chemistry department.

I am also grateful to Prof. Dr. Detlev Möller, Dr. Klaus Keuler and Prof. Dr. Eberhard Schaller for showing interest in my work and being on my committee.

Finally, thanks to my beloved parents, for their patience and understanding during the entire process of my doctoral program. Their moral and emotional support has helped me a long way throughout my life. I also extend sincere thanks to my brothers, my beloved sister and friends for their constant support and encouragement during this time. Of course, I owe since thanks to the Lord, Almighty Allah, without whose grace and blessings this effort would not have been possible.

Abstract

The troposphere is a complex multiphase and multicomponent environment with simultaneously occurring gas and aqueous phase as well as heterogeneous chemical transformations which can potentially alter the physico-chemical composition of aerosols. The current knowledge of heterogeneous or multiphase chemistry in which aerosol particles participate, is noticeably less understood than homogeneous gas-phase atmospheric chemistry. Moreover, decades of cloud microphysical research have not provided conclusive understanding of the complex physical processes responsible for droplet growth. Growth and chemical changes in multicomponent aerosols are under investigation for a longer period of time, but the results are rather heterogeneous. In such multicomponent systems mass transfer between the phases are quite intricate, to treat the non-ideality in kinetic models considering complex multiphase processes. Molecular interactions between different organic-electrolyte mixture in the particle phase affect the water uptake and release (hygroscopicity), lead to modification of chemical reaction rates, and define the gas/particle partitioning of semi-volatile compounds apart from the chemical transformations. While the interactions between inorganic compounds included in inorganic chemistry are relatively well known, however, the interactions between organic compounds as well as mixture of inorganic-organic compounds comprised in a multiphase chemistry have remained elusive, due to the large number of organic species available in the atmosphere with greatly variable properties.

In light of this, a modeling framework has been developed in the context of multiphase air parcel model to treat the kinetic description of phase transfer processes considering complex multiphase chemistry and an extended description of non-ideal solutions for the aqueous phase chemistry by means of activity coefficient models. The developed framework can flexibly use a different combinations of mixing rules and accurate utilization of activity coefficient models. The current available activity coefficient models developed for electrolyte-organic-water mixtures are evaluated in the first part of the thesis. The model investigations cover a scale, ranging from very simple to complex simulations. In order to validate the model performance and the capability of the applied activity models, predicted results were compared with water activity measurements. Furthermore, simulation results for a simple and complex inorganic-organic chemical systems were compared with the results of thermodynamic equilibrium model E-AIM. Based on the model deviations with experimental data and intercomparison between the chosen models, AIOMFAC was selected to further extend the model interaction parameters. The interaction parameters from mod. LIFAC were used to extend the database, in order to compute the activity coefficients consistent with AIOMFAC model equations.

In the second part of the thesis, the extended activity coefficient model was implemented in the parcel model framework SPACCIM, in order to investigate the influence of treatment of non-ideality on multiphase chemistry. The effect of considering non-ideal solutions were studied for two different aerosol types (remote, urban) regarding complex multiphase chemistry. It has been shown, by these more realistic model simulations, under which circumstances it is important to consider non-ideal solutions and how will be the simulated particle/droplet growth and chemical transformations affected. The modeled activity coefficients and their pattern which decides the multiphase chemical transformations were investigated for inorganic and organic systems. The

present results have shown that, the inclusion of the treatment of non-ideality can substantially extend our ability to model complex multiphase processing of aqueous phase chemistry especially in the particle phase. Various sensitivity studies were performed at various relative humidity levels in order to investigate the influence of treatment of non-ideality on multiphase chemical processing. The aqueous phase particles becomes more acidic when considering the aqueous phase chemistry as non-ideal solutions. The multiphase processing in the aqueous particles is predominantly observed as declined at lower relative humidities when non-ideal solutions are assumed for aqueous phase chemistry. The tropospheric radical budget was observed mostly as decreased. The phase partitioning is rather not affected by the treatment of non-ideality, due to the coupled microphysics. The consideration of non-ideal solutions, influences on multiphase processing of organic compounds in a compound-specific manner, however, the processing is observed as decreasing for most of the subsystems. Due to the available water soluble organic compounds, the considered functions and approaches to predict the water activity and activity coefficients, seems to be good approximation to find the new equilibrium between the droplet and surrounding water vapor. All in all, more comprehensive modeling framework was designed and implemented to study the realistic processes descriptions while treating the aqueous phase chemistry as non-ideal solutions.

Keywords: Multiphase modeling, aerosol-cloud interactions, phase transfer, non-ideal solutions, activity coefficients, surface tension

Chapter 1

Introduction

Earth's atmosphere started to form billions of years ago and it has gone through some major changes since then (Seinfeld and Pandis, 1998). From the original atmosphere that was dominated by hydrogen and helium it has changed into current chemical mixture in which nitrogen is dominant constituent, oxygen enables life, and carbon dioxide contributes to the greenhouse effect that helps to maintain a steady enough temperature, etc. One of the most pressing problems facing the nations of the world during the 1990's and into the 21st century is the effect of human activities on the atmospheric environment. One of such climatic threat, which is popularly known as "global warming", has received great attention and recently been the topic of debates on various news media, as well as the focus of large national and international research programs. Motivated by climate change and the adverse health effects of various sources of air pollution, aerosol research has increasingly intensified over the past couple of decades.

The occurrence of pure air or water is impossible in nature. Some foreign mass may be present either naturally or mixed with the air or water, moreover particles consisting of only one compound do not exist in the atmosphere. Cloud phase in the tropospheric multiphase system is the dominant place in the atmosphere where trace components can exist in a condensed phase. These components become partially or completely dissolved in the cloud water content absorbed by cloud ice, or remains nonvolatile which under goes into chemical transformations subsequently in the atmosphere. Another important part of the atmosphere is made up by non-gaseous substances; particles, which consist of liquid and solid material. The mixture of gases with suspended liquids and solids is called aerosol. Aerosol particles and clouds play a crucial role in the troposphere e.g due to their influence on the earth radiation budget, viz. its relevance for climate (IPCC, 2007), the hydrological cycle and air pollution.

Hence, aerosols play a vital role in many fields and on many scales of atmospheric and climate science. However, the influences are differed, ranging from the nanometer scale of molecular interactions and chemical reactions to the global scale of the climate system. The recently published Fourth Assessment Report (AR4) of the United Nations Intergovernmental Panel on Climate Change (IPCC) states that the comprehensive processes, which leads to modify the cloud properties by aerosols is not characterized in appropriate way and the magnitudes of associated indirect radiative effects are poorly determined (Solomon et al., 2007). The tropospheric aerosol consists of water, inorganic acids, salts and many different organic compounds originating from natural and anthropogenic processes. Thus, one can define concerning to both physical and chemical properties, tropospheric aerosol is a complex mixture composed of organics and inorganics. Moreover, tropospheric aerosols, especially the very fine particles emitting from anthropogenic activities, have an impact on air quality and human health (Pöschl, 2005). Additionally, scattering and absorption of solar and terrestrial radiation influence the visibility and the earth's radiative budget. Aerosol particles can contain various liquid and solid phases as well as the composition of the particles controls the partitioning of semi-volatile organic

compounds (e.g. emissions from fossil fuel burning) partition between the particle and the gas phase. In this complex multiphase system many chemical and physical processes take place. Apart from the photochemical reactions caused by solar radiation, aqueous chemical reactions occurring in particles or in fog and cloud droplets. Moreover, phase transfer processes and heterogeneous chemical reactions occur between the aerosol particles and cloud droplets for instance, the formation of sulphuric acid from dissolved sulphur dioxide or between the solid and liquid phase (Seinfeld and Pandis, 1998).

In summary, these processes influence the particle and droplet formation and growth, the transport, as well as wet and dry deposition. Hence, these processes are crucial for the modeling of particle/droplet formation and growth. The presence of water soluble species in the particles plays an important role for example in the ability to act as cloud condensation nuclei through the so called solute (Raoult) effect, which is an important factor in the growing of particles and droplets. These transformation processes include condensation and evaporation, homogeneous nucleation, coagulation, and chemical reactions. Indeed, chemical conversions can essentially be determined by the mass transfer between different phases. In many mass transport processes existing in the nature in which, the transfer phenomena is a consequence of buoyancy effects caused by diffusion of chemical species (Treybal, 1980). Mass transfer from a gas phase to a liquid or solid phase proceeds via interface, which can be defined in this context, as those related to the interaction of at least one bulk phase (solid or liquid) with another phase (solid, liquid or gas) in the narrow region, in which the transition from one phase to the other occurs (Treybal, 1980).

Mass transfer processes, like adsorption or condensation of gas onto a droplet may be limited either by the flux to the particle surface, the rate of some surface reaction (and thus the surface area), or the rate of some internal chemical reaction (and thus the particle volume) (Treybal, 1980). As is common in modeling, the current models assume that diffusion limits condensation and use the appropriate form of Fick's law of diffusion Pruppacher and Klett (1997); Suryanarayana (2002). In this formulation, gradients of condensable vapor density (ρ_v) between the ambient environment and the particle surface, drives condensation. In view of the fact, that for explicit treatment for aqueous chemistry and mixed organic-inorganic behavior, volume limitation in principle, be required to effectively incorporate into the model as well as surface limitations (Krishna and Wesselingh, 1997). Diffusion-limited transfer is driven by concentration gradients between the ambient gas phase and the particle surface. The mass transfer limitations of surface and volume, occur where diffusion is rapid compared to the rate of the surface or internal chemical reaction that leads to a net transfer between the gas and particle phases (Treybal, 1980; Seinfeld and Pandis, 1998).

In clouds, droplets form primarily through the condensational growth of aerosol particles, while a majority of the trace species found dissolved in the droplets entered via dissolution after the droplets are formed. During the preceding existence there has been a mounting intensity of research on hygroscopic growth of atmospheric aerosol particles and on their activation to cloud droplets. This interest was driven by the necessity to increase the knowledge about the interaction of atmospheric particles with water vapor in the atmosphere. Both hygroscopic growth and activation of atmospheric particles can be described by Köhler theory (Köhler, 1936). It has recently become evident that, in a manner unforeseen by Köhler, chemical processes, compositional influences on physical properties and mass transfer kinetics also influence the formation of cloud droplets via condensation of water vapor. Moreover, modifications of Köhler theory have been proposed to incorporate various chemical effects, including slightly-soluble compounds (Shulman et al., 1996), dissolution of soluble gases (Kulmala et al., 1997), reduction of surface tension (Facchini et al., 1999) and film-forming compounds (Feingold and Chuang, 2002).

Mathematical models are often used to develop such relationships which can better describe the phase transfer of multi-component particles. However, detailed modeling of the aerosol dynamics is demanding because of the wide aerosol size range (e.g. diameters) spanning from a few nanometers to tens of microns. Since, the mass transfer rate between gas and aerosol phases is strongly dependent on aerosol size, the mass transfer rates for the smallest and the largest particles can be different by several orders of magnitude. The timescale for the diffusion of a molecule from the bulk gas phase to the surface of a particle increases with the diameter of the particle. Therefore, fine particles will tend to reach equilibrium rapidly whereas coarse particles can remain in non equilibrium conditions [e.g., [Wexler and Seinfeld \(1990\)](#); [Dassios and Pandis \(1999\)](#)]. Processes like heterogeneous reactions at the aerosol surface, mass transfer between aerosol and cloud droplets, as well as aqueous-phase chemistry inside cloud droplets represent some of the most important mechanisms for altering the aerosol size/composition distribution. The mathematical description of such systems results in a set of extremely stiff differential equations, due to the highly non-linear nature of the chemistry, coupled with widely different reaction time scales of different species ([Schwartz and Freiberg, 1981](#); [Schwartz, 1986](#); [Seinfeld and Pandis, 1998](#)). The mass transfer fluxes between the gas, solid and liquid phases in the aerosol can be described by aerosol multiphase models. These models can be integrated for example into global aerosol models, chemistry transport models, or plume dispersion models. The request for an increasing accuracy of model results demands a more and more precise description of the physical and chemical processes that influence droplet formation and growth. One of the challenging tasks of the recent research on this field is the consideration of non-ideal solutions in the multiphase models of mixed inorganic/organic aerosols ([Pilinis, 1999](#)).

Non-ideal circumstances occur when a small amount of liquid water is available in the particles. Such conditions can be found in the initial phase of cloud droplet activation. Furthermore these non-ideal conditions can be expected in particles below 100% relative humidity and in case of small particles above 100% of relative humidity, more precisely in deliquescent state. In a highly concentrated solution, the ions and molecules are close to each other, therefore they influence each other through electrostatic forces or other physical interactions. These intermolecular forces modify the affinity of a substance to transfer from one phase into another phase or to enter into a chemical reaction ([Smith et al., 1996](#)). Hence, the assumption of ideal solution in aerosol models has to be abandoned and non-ideal behavior has to be considered. Thus, activities have to be used instead of concentrations and the appropriate calculation methods have to be applied in the models.

Growth and chemical changes in multicomponent aerosols are under investigation for a longer period of time, even though the results are heterogeneous. For simple inorganic chemical systems under non-ideal conditions several modeling approaches exist which are able to describe such processes with increasing accuracy: e.g. MARS ([Saxena et al., 1986](#)), SCAPE ([Kim et al., 1993](#)), EQUISOLV ([Jacobson et al., 1996](#); [Jacobson, 1999](#)), AIM ([Clegg et al., 1998a](#)), ISORROPIA ([Nenes et al., 1998, 1999](#)), EQSAM ([Metzger, 2000](#)). The above mentioned models assume that the particles are in thermodynamic equilibrium with the corresponding gases. This assumption means that the mass transfer between the phases is instantaneous. However, mainly in case of coarse particles this approach is not valid, indeed, the mass transfer must be described as dynamical: e.g. MADM ([Pilinis et al., 2000](#)), SPACCIM ([Wolke et al., 2005](#)). A dynamical aerosol model must include the size resolved description of the mass transfer, it is reasonable since aerosols of various sizes have different chemical compositions and growth characteristics. The above mentioned models include either complex thermodynamics for inorganic electrolyte solutions, or they consider also organic species, but do not consider non-ideal solutions in the particles.

Atmospheric particles are complex mixtures of electrolytes and non-electrolytes. For this reason the description of non-ideal behavior of chemically complex particles is only possible with the combination of different methods (Clegg et al., 2001). While utilizing the basic laws of thermodynamics, a reliable thermodynamic model enables the calculation of the phases that develop in an aerosol particle at equilibrium conditions. Thus, to predict the stable phases, which can potentially alter the physico-chemical processing in a particle, the equilibrium aerosol composition (and size), and gas/particle partitioning of organics (and water), a precise and robust thermodynamic model needs is prerequisite. The prediction of vapor-liquid equilibria in mixed solvent electrolyte systems (solutions containing electrolytes and more than one solvent) is not new in industrial chemical applications. Combined electrolyte/non-electrolyte models were presented in the last years for example by Kikic et al. (1991), Yan et al. (1999) and Aznar and Telles (2001). However, such applications in the atmospheric chemistry are not yet common. A thermodynamic equilibrium model for mixed inorganic/organic aerosols was developed by Ming and Russel (2002), which includes the Pitzer approach (Pitzer, 1973; Pitzer and Mayorga, 1973; Pitzer, 1991) for inorganics and UNIFAC (Fredenslund et al., 1975) activity coefficient models. Furthermore, recently Zuend et al. (2008) developed the activity coefficient model, called AIOMFAC which can treat the complex organic-inorganic liquid mixtures up to lower relative humidities (RH), but currently this model is limited to three organic functional groups only. This model can predict the hygroscopic growth of multicomponent particles including relatively, a very simple chemistry.

The non-ideal behavior and surface effects of multicomponent aerosol systems, is not yet described satisfyingly in one complex model. The gas/particle partitioning models with detailed thermodynamics include simple chemistry; considering a set of chemical equilibrium reactions of inorganic species. This so called thermodynamic equilibrium models can not handle the mass transfer processes dynamically. Some of the aerosol dynamic models consider complex multiphase chemistry, but they do not consider the thermodynamics of real solutions. There is a lack of an improved model, however the developed model, in this thesis, would include the detailed multiphase chemistry of organic and inorganic species, as well as detailed thermodynamic comprehension of non-ideal solutions and the size resolved description of dynamical particle growth. This work is mainly motivated by the lack of knowledge in several of the mentioned topics related to aerosol thermodynamics. Especially, the role of inorganic and organic species as well as their interactions within the solutions are not well understood. Only very few thermodynamic model approaches exist so far, that consider organic-inorganic interactions in mixtures combined with complex multiphase chemistry (e.g. Zaveri et al. (2008)).

The aim of this thesis is to provide an improved description of gas/aerosol mass transfer processes under non-ideal conditions with the treatment of complex multiphase chemistry, including inorganic and organic species, as well as time and size dependent description of the mass transfer. Thus this thesis contributes to a more realistic modeling of mixed inorganic/organic aerosols also at low relative humidities. For this reason a combined approach for activity coefficient calculation in mixed solvent electrolyte systems was implemented into the Spectral Aerosol Cloud Chemistry Interaction Model (SPACCIM, Wolke et al. (2005)) framework. SPACCIM originally has been developed for the dynamical description of cloud microphysical processes with the consideration of complex multiphase chemistry for a size-resolved particle/drop spectrum. Up till now, SPACCIM was able to describe the transformation and growth of particles and droplets from shortly before cloud forming, through the cloud life time and shortly after cloud evaporation. The new version of SPACCIM can able to simulate the physico-chemical processes within aerosols also at low relative humidities, and thus almost during their whole life-time.

The model investigations cover a scale, ranging from very simple to complex simulations. In order to validate the model performance and the capability of the applied activity model the results were compared, with water activity measurements. The simulation results for a simple inorganic chemical system were also compared with the results of a thermodynamic equilibrium model for gas/particle partitioning developed by [Clegg et al. \(2001\)](#) and [Clegg and Seinfeld \(2006a,b\)](#). The effect of considering non-ideal solutions has been studied in two different aerosol types (remote, urban) with regarding complex multiphase chemistry. Simulations are carried out for meteorological scenarios in which an air parcel moves along a predefined trajectory including aerosol stages and phases with high relative humidity. Such more realistic model simulations will throw light on the issues like, under which circumstances it is important to consider real solutions, and how will be the simulated particle/droplet growth and chemical transformations affect while considering the non-ideal solutions.

Chapter 2

Scientific background

2.1 Theoretical aspects of phase equilibria in multicomponent systems

The thermodynamics of mixtures introduced in this chapter is more closely related to what is called the chemical thermodynamics, with some discussion of the nature of the chemical potential, the need of standard states, and then introduces the auxiliary functions of fugacity, activity and activity coefficients. Thus, the focus here is, on the changes in a thermodynamic system, when the chemical composition changes at constant temperature and pressure. Initially, the fundamental concept of Gibbs energy is introduced. The Gibbs energy state function is an important property in thermodynamics. Chemical potential and its relation to phase equilibrium is also explained to establish the link between this property and phase equilibrium. Both fugacity and activity coefficient relates chemical potential to measurable properties (Smith et al., 1996). The fugacity coefficients, described here, are usually used to quantify the departure from ideality for real gases via residual properties. The activity coefficient is preferred when defining the departure of real liquids from ideality. The detailed description and supporting information for the thermodynamics of phase equilibria in multicomponent systems is explained in Appendix. A.

2.1.1 Gibbs energy

Classical thermodynamics provides a number of state functions, the most well known being internal energy (U), enthalpy (H), Helmholtz energy (A) and Gibbs free energy (G). Changes in these functions depend on the changes in two state variables, or in case of open systems with material exchange with the surrounding, three state variables. Commonly used state variables are temperature (T), entropy (S), pressure (p), volume (V), chemical potential (μ) and mole number (n). If these two or three state variables are kept constant, the state function is also a potential with a minimum value at equilibrium. The Gibbs energy is a convenient state function since it is a potential function at constant temperature, pressure and number of moles in the system. The Gibbs energy is an important generating property since it provides a tangible link between equilibrium, mathematics and classical thermodynamics.

For a closed system in equilibrium, the basic relation connecting the Gibbs energy to the temperature and pressure can be expressed as:

$$d(nG) = (nV) dp - (nS) dT. \quad (2.1)$$

One can apply Eq. 2.1 to a single phase fluid in a closed system wherein no reactions occur. For such system the composition is necessarily constant, and thus

$$\left[\frac{\partial (nG)}{\partial p} \right]_{T,n} = nV \quad \text{and} \quad \left[\frac{\partial (nG)}{\partial T} \right]_{p,n} = -nS. \quad (2.2)$$

The subscript n indicates that the number of moles of all chemical species are held as constant. If one can consider the more general case of single-phase, open system that can interchange matter with its surroundings, the total Gibbs energy nG is still a function of T and p . Thus, at constant T and p (the typical case of practical interest) the change of G in equilibrium must be zero. Hence, Eq. 2.1 is only applicable to a system without exchange of material with the surrounding. To evaluate the vapor-liquid equilibrium problem one has to consider the case of mutual exchange of material between the phases (Prausnitz et al., 1986).

Since, material may be taken from or added to the system, nG is also a function of number of moles of chemical species present i.e. the Gibbs energy function is also influenced by a change in the amount of material. Thus,

$$nG = f(p, T, n_1, n_2, \dots, n_i, \dots), \quad (2.3)$$

where n_i refers to the number of moles of species i . Hence, one can write the differential of nG as:

$$d(nG) = \left[\frac{\partial (nG)}{\partial p} \right]_{T,n} dp + \left[\frac{\partial (nG)}{\partial T} \right]_{p,n} dT + \sum_i \left[\frac{\partial (nG)}{\partial n_i} \right]_{p,T,n_{j \neq i}} dn_i. \quad (2.4)$$

The summation indicates the over all species present in the system, and subscript n_j indicates that all mole numbers except i^{th} component/species is held constant. The derivative in the final term is important enough to be represent by its own nomenclature. Thus, by definition, the chemical potential of species i in the mixture is:

$$\mu_i \equiv \left[\frac{\partial (nG)}{\partial n_i} \right]_{p,T,n_j}. \quad (2.5)$$

With this definition and using Eq. 2.2, one can rewrite the Eq. 2.4 as follows:

$$d(nG) = (nV) dp - (nS) dT + \sum_i \mu_i dn_i. \quad (2.6)$$

Moreover, the Gibbs energy function plays an integral role in the computation of other system properties.

2.1.2 The chemical potential

The distribution of every component among all phases present can be described quantitatively by phase-equilibrium thermodynamics. In order to describe the phase equilibrium thermodynamics and chemical reactions in precise and abstract way one should relate the chemical potential. Therefore it is required to describe the chemical potential in terms of physically measurable quantities. The chemical potential of any pure substance i , is related to the physically measurable quantities such as temperature and pressure in the form of differential equation according to Eq. 2.6:

$$d\mu_i = -\frac{S}{n_i} dT + \frac{V}{n_i} dp. \quad (2.7)$$

With the basic properties molar entropy $s_i = S/n_i$ and molar volume $v_i = V/n_i$ and integral of Eq. 2.7 to obtain the chemical potential at a certain temperature and pressure:

$$\mu_i(T, p) = \mu_i(T^*, p^*) - \int_{T^*}^T s_i dT + \int_{p^*}^p v_i dp, \quad (2.8)$$

here superscript $*$ refers to an arbitrary reference state, which is also known as standard state. This equation is can compute the chemical potential at a particular temperature and pressure. Moreover, this equation can only be expressed relative to the value at the chosen standard state, where v_i is a simply substitution, of the ideal-gas equation ($v_i = RT/p$). However, the relation for a pure, ideal gas at constant temperature can be written as:

$$\mu_i(T, p) = \mu_i(T, p^*) + RT \ln\left(\frac{p}{p^*}\right), \quad (2.9)$$

where R is the universal gas constant. This equation shows the change in the chemical potential at constant temperature of an ideal gas, Furthermore, it is a simple logarithmic function with the measurable quantity in terms of pressure. The standard state pressure is usually defined to be $10^5 \text{ Pa} (\approx 1 \text{ atm})$ at standard temperature and pressure (STP) conditions, hence mathematically, it can written always $\mu^o(T)$ as standard state chemical potential. If we consider the mixture of ideal gases, out of that, for the pure ideal gas the chemical potential of species i can be defined as:

$$\mu_i(T, p) = \mu_i^o(T) + RT \ln\left(\frac{p}{p^o}\right) + RT \ln y_i, \quad (2.10)$$

where y_i is the mole fraction in the gas phase mixture:

$$y_i = \frac{n_i}{\sum_j n_j}, \quad (2.11)$$

Thus, while expressing the Eq. 2.10 in terms of the partial pressures $p_i = py_i$:

$$\mu_i(T, p) = \mu_i^o(T) + RT \ln\left(\frac{p}{p^o}\right), \quad (2.12)$$

as result a generic form of Eq. 2.10 will be obtained. Although it is hypothetical, the assumption of an ideal gas mixture for gases phase at ambient pressure and temperature, e.g. air, is usually valid for practical purposes (Pruppacher and Klett, 1997). Moreover, the fluids (pure liquids and liquid mixtures) usually, have dissimilarities to gases, since they also pose the disordered molecular structure, but they are incompressible. Based on this, one can define the chemical potential of an ideal solution similar to the expression of an ideal gas mixture, as:

$$\mu_i(T, p) = \mu_i^*(T, p) + RT \ln x_i, \quad (2.13)$$

where x_i is the mole fraction of component i in the liquid mixture and $\mu_i(T, p)$ is the standard chemical potential of pure species ($x_i = 1$). However, gas phase mixtures don't show strong intermolecular forces as liquids exhibit. Thus, one can't describe the pure liquids as ideal liquid, nevertheless a mixture of liquids is called an ideal mixture, where the molecular interactions between the molecules of different species are equal to the interactions between those of the same species.

2.1.3 Raoult's law

Let us consider the equilibrium distribution of a component in a binary system between a liquid phase and a vapor phase. In such situations, a simple relation can describe the distribution of the components between the phases, i.e., an equation relating x , the mole fraction in the liquid phase, to y , the mole fraction in the vapor phase. Hence, let A be a chemical species in a heterogeneous, closed system consisting of a liquid phase (l) and gas phase (g) given by Prausnitz et al. (1986):



This phenomenon can be explained with the help of chemical potentials. For instance, an ideal solution containing substance A in thermodynamic equilibrium with an ideal gas mixture, then:

$$\mu_A^{(g)} = \mu_A^{(l)}, \quad (2.15)$$

while using Eq. 2.12 and Eq. 2.13 one can write as follows:

$$\mu_A^o(T) + RT \ln \left(\frac{p_A}{p^o} \right) = \mu_A^*(T, p) + RT \ln x_A. \quad (2.16)$$

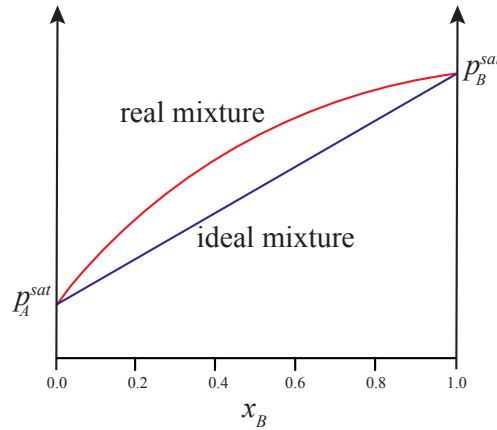


Figure 2.1: Ideal and real vapor pressure over a binary liquid mixture of species A and B . In this case the real vapor pressure shows a positive deviation from Raoult's law.

For pure liquid A ($x_A = 1$), the pressure over the liquid is the saturation pressure $p_A^{sat}(T)$ of A , gives us:

$$\mu_A^*(T, p_A^{sat}) = \mu_A^o(T) + RT \ln \left(\frac{p_A^{sat}}{p^o} \right). \quad (2.17)$$

Upon substitution of this relation into Eq. 2.16 gives in the form of:

$$\ln \left(\frac{p_A}{p^o} \right) = \frac{\mu_A^o(T) + RT \ln \left(\frac{p_A^{sat}}{p^o} \right) - \mu_A^o(T)}{RT} + \ln x_A \quad (2.18)$$

$$= \ln \left(\frac{p_A^{sat}}{p^o} x_A \right). \quad (2.19)$$

or

$$p_A = p_A^{sat} x_A, \quad (2.20)$$

where p_A^{sat} is usually written in the form of p_A^o to denote the reference state of pure A . At the same time, Eq. 2.20 is known as Raoult's law for ideal mixtures. Fig. 2.1 shows the vapor pressure over a mixture of two volatile liquids. The ideal curve (blue line) attempted to calculated from the Raoult's law mentioned above. Where as, non-ideal mixtures (red line) which shows either a positive or negative deviation, comes from the influence of interactions as well as the intermolecular forces between molecules of two substance A and B available in the system.

2.1.4 Intermolecular forces in solutions

As shown in Fig. 2.1, the fact that the vapor pressure is higher than ideal in these mixtures, means that molecules are breaking away more easily than they do in the pure liquids. This is because the intermolecular forces between molecules of A and B are less/greater than they are in the pure liquids. Furthermore, in general the properties of solutions depend on two characteristics: the manner in which the molecules arrange themselves (the geometric array in which the different size and shape molecules occupy space), and the nature as well as strength of the forces that affect between the molecules.

Intermolecular interactions in the solution play a crucial role for many reasons; they have an impact on the solubility, vapor pressure above the solution, boiling point of the solution or on the chemical reactivity (Adkins, 1983; McQuarrie and Simon, 1997). All molecules in the solution exert weak attractions on one another due to the mutual attraction of nuclei and electrons. These attractive forces are only significant at such short distances, where the intermolecular repulsion of the electrons on different atoms is also significant (Prausnitz et al., 1999). There are four main types of intermolecular forces, from strongest to weakest: ion-dipole, dipole-dipole, dipole-induced dipole, and induced dipole-induced dipole (also called dispersion or London forces). The aforementioned intermolecular forces occurring in a solution can be shown schematically as Fig. 2.2. Intermolecular attractions have some other effects on liquids. Surface tension is also a result of intermolecular forces (Prausnitz et al., 1999). Molecules at the surface of a liquid are attracted to the molecules beneath and beside them, leading to an inward force on the liquid and a kind of skin on the surface. This tension also causes drops of water to contract into spheres, minimizing surface area (Gibbs, 1928).

The balance between the above described forces controls the solubility properties of solvents and solutes. In an ideal solution of two or more components, the interacting forces between all kinds of molecules are exactly the same. This means that, it takes the same amount of energy for a solvent molecule to break away from the surface of the solution as it would take to leave the pure solvent. But, non-ideal solutions are those, where the forces between the components of the solute and solvent are diverse in compare to the pure materials (Smith et al., 1996; Prausnitz et al., 1999; Atkins and de Paula, 2002).

2.1.5 Non-ideal solutions

As described earlier, in reality, almost all solutions belong to the category of non-ideal mixtures, on contrary the concept of an ideal solution would be a just assumption to make the studies simple. However, to generalize the equations for ideal mixtures, Lewis who first defined a function

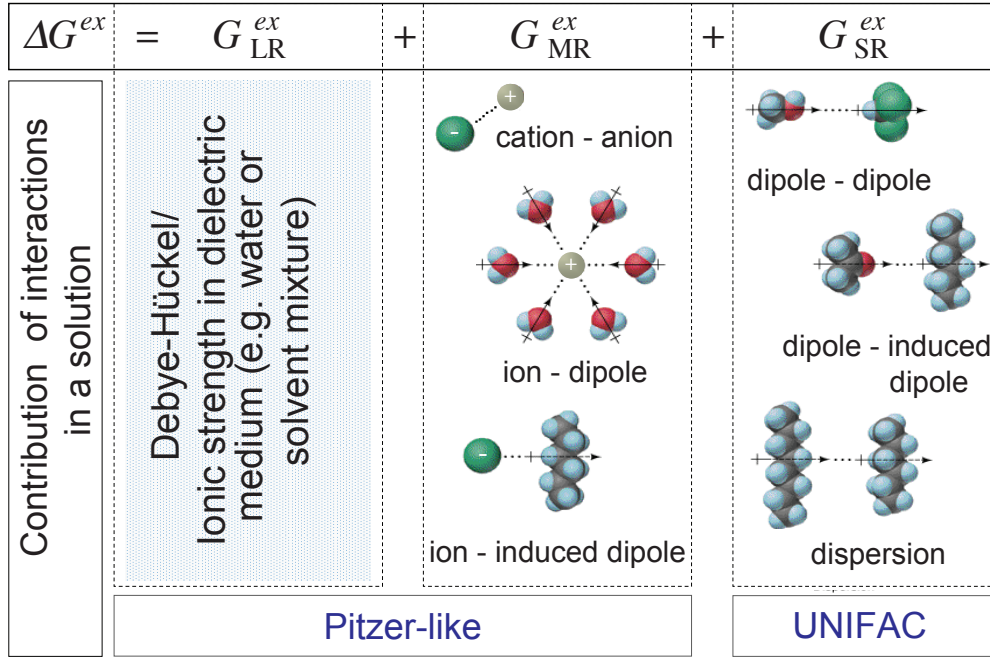


Figure 2.2: Three major terms represent different types of molecular interactions in a solution and add up to the excess Gibbs energy (G^{ex}) of a certain system along with the approaches to treat of these interactions (modified from Zuend et al. (2008)).

f , called fugacity (Lewis, 1907; Lewis and Randall, 1961). With change in the temperature (often called as isothermal expansion at constant pressure), of any component in the system irrespective of solid, liquid or gas, either pure or mixed, either ideal or not (Prausnitz et al., 1986):

$$\mu_i - \mu_i^o = RT \ln \frac{f_i}{f_i^o}. \quad (2.21)$$

In case of gaseous mixture, if it is assumed as ideal gas, the fugacity is almost equal to its pressure. Hence, for an ideal gas mixture, fugacity, f_i is equal to the partial pressure p_i . One should keep in mind that μ_i^o and f_i^o are not independent of each other. Lewis named the ratio f_i/f_i^o the "activity". The activity of a substance indicates how "active" the substance is relative to its standard state. More over in the technical point of view it is called It is a corrected/effective concentration (in whatever concentration scale). In addition, it has the concentration dependence due to non-ideal mixing (tendency to change the properties). If, one introduces the activity of substance i , a_i , into Eq. 2.13, the expression for the chemical potential of any mixture is:

$$\mu_i(T, p) = \mu_i^*(T, p) + RT \ln a_i. \quad (2.22)$$

Thus, the so called activity coefficient, γ_i , can be defined in compare with the equation for ideal solutions:

$$\gamma_i = \frac{a_i}{x_i}. \quad (2.23)$$

In general, the activity coefficient is a dimensionless "correction" factor relating the real behavior of a mixture to a hypothetical ideal behavior of that mixture.

While utilizing this conceptual idea, one can interrelate the chemical potential of a solution as:

$$\mu_i(T, p) = \mu_i^*(T, p) + RT \ln x_i + RT \ln \gamma_i, \quad (2.24)$$

where the first two terms on the right hand side describe the ideal contribution, μ_i^{id} , and the last term, describing the correction or excess contribution, μ_i^{ex} , to the chemical potential. As described in the Sec. 2.1.3, for any infinitely dilute solution of substance A in B , $\gamma_B \rightarrow 0$ if mole fraction of A , x_A approaches to zero i.e. $x_A \rightarrow 0$ (and $x_B \rightarrow 1$). In some sense, the ideal solutions can be described as the limiting solution for every mixture when becoming pure in one component. This consideration also shows that Raoult's law becomes valid in the limit of virtually pure substances.

$$p_i = p_i^0 x_i \gamma_i. \quad (2.25)$$

As a result, the activity coefficients of the components are widely used to represent the non-ideality of mixtures. Furthermore, the fundamental Gibbs free energy can be easily calculated, if the activity coefficients and standard potentials are known. Hence, the activity coefficient models aiming to estimate activity coefficients are thus obvious, since the experimental data is lacking.

2.2 Equilibrium growth theory and microphysical processing

Theoretically a droplet containing water and dissolved solutes are in equilibrium with ambient water vapor when droplet and gas phase partial vapor pressures are equal (Seinfeld and Pandis, 2006). To be able to fully understand the broader picture of this activation, it is necessary to study these variables in a simplified manner. One of the simple way to describe droplet growth is to use the equilibrium growth theory, also known as Köhler theory (Köhler, 1936).

Köhler theory gives the equilibrium saturation ratio of water vapor (S) for a certain droplet radius. In other words, it gives the water vapor pressure at which the droplet is in equilibrium with its surrounding ambient humid air, assuming spherical diluted particles can be written as follows (Jacobson, 1999):

$$S' = \frac{p_w}{p_w^0} = a_w \exp\left(\frac{2\sigma_{s/a} m_p}{r_a RT \rho}\right), \quad (2.26)$$

where p_w is the water vapor pressure at the droplet surface, p_w^0 is the saturation vapor pressure over a flat surface, a_w is the activity of water in solution, $\sigma_{s/a}$ is the surface tension, ν_w is the partial molar volume of water, R is the universal gas constant, T is the temperature, and ρ_w is the density of water.

In solution droplets, some solute molecules replace water at the gas-liquid interface and hydrate, thereby reducing the overall saturation vapor pressure over the drop and increasing the condensational mass flux onto its surface (Pruppacher and Klett, 1997). The adjusted vapor pressure over the flat surface of a solution is approximated by Raoult's law:

$$\left(\frac{C'_{s,i}}{C_{s,i}}\right)_{Solute} \equiv B \equiv a_w \approx \frac{n_w}{n_w + n_s} \equiv \left(\frac{3m_\nu i_\nu M_s}{4\pi \rho_w m_s}\right). \quad (2.27)$$

Here, $C'_{s,i}$ is the equilibrium concentration of trace species i , over a solution uncorrected for solute interference at the surface. $C_{s,i}$ is the saturation concentration of water over a flat surface corrected for solute properties, n_w is the number of water molecules in the drop, and n_s the number of all solute molecules (Pruppacher and Klett, 1997; Tester and Modell, 1997). Eq. 2.27 is a monotonically increasing function, which asymptotes to zero for the smallest (driest) particles and unity for the largest (Jacobson, 1999). This is the so-called solute effect.

Opposing the solute effect is the drive to reduce surface energy which leads molecules to desorb more readily from curved surfaces than from flat. This is the Kelvin effect, which can be approximated by:

$$\left(\frac{C'_s}{C_s}\right)_{Kelvin} \equiv A \equiv \exp\left(\frac{2\sigma_{s/a}m_p}{r_aRT\rho}\right). \quad (2.28)$$

Here, $\sigma_{s/a}$ is the surface tension of the droplet, R (J mol⁻¹ K⁻¹) is the universal gas constant, T (K) is the temperature, m_p is the mass and ρ is the density of the solution particle (Pruppacher and Klett, 1997). This function monotonically decreases with increasing particle size, and asymptotes to infinity for the smallest particles and unity for the largest. In the case of dilute droplets, while ignoring other effects i.e. radiative cooling effects, one can combine Eq. 2.27 and Eq. 2.28. The derived expressions for the solute and Kelvin effects, which is an appropriate estimate of S' for dilute droplets.

$$S' \approx \left(\frac{C'_{s,i}}{C_{s,i}}\right)_{Solute} \left(\frac{C'_s}{C_s}\right)_{Kelvin} = \frac{n_w}{n_w + n_s} \exp\left(\frac{2\sigma_{s/a}m_p}{r_aRT\rho}\right). \quad (2.29)$$

Note that Eq. 2.29 is the product of one function that monotonically decreases and one that monotonically increases with increasing r_a can be schematically shown as Fig. 2.3. The curvature of the product of the two curves is very important to understand the cloud activation. Now, the final equation, which describes the droplet growth, while taking the right sides of Eq. 2.27 and Eq. 2.28, gives the Köhler equation (Köhler, 1936),

$$S' = 1 + \frac{A}{r} - \frac{B}{r^3}, \quad (2.30)$$

where S' is the saturation ratio at equilibrium. This Köhler equation relates the saturation vapor pressure of water over a curved surface containing solute to that over a flat surface without solute. By minimizing the derivative of S' , the Eq. 2.30 gives the critical radius for growth and critical saturation ratio highlighted in Fig. 2.3 are given by Jacobson (1999):

$$r^* = \sqrt{\frac{3B}{A}} \quad S^* = 1 + \sqrt{\frac{4A^3}{27B}}, \quad (2.31)$$

Schematic illustration of the Köhler curve including its two opposite effects on the saturated vapor pressure p_w is shown in Fig. 2.3. As can be seen from the Eq. 2.26, the partial pressure of vapor over curved, diluted surface depends mainly on two opposite running processes with decreasing radius. As can be seen, S_{eq} reaches a maximum, critical value (S^*), when the particle reaches some associated critical radius (r_a^*) during condensational growth. Once the aerosol grows larger than (r_a^*), it is considered activated. (S^*) is greater than unity, meaning activation may only occur in an environment super saturated with respect to liquid water. The comparison of the solute and curvature effects shown in Fig. 2.3, the Raoult term which is proportional to $1/r^3$, dominates the equilibrium saturation ratio for relatively small cloud droplets and particles,

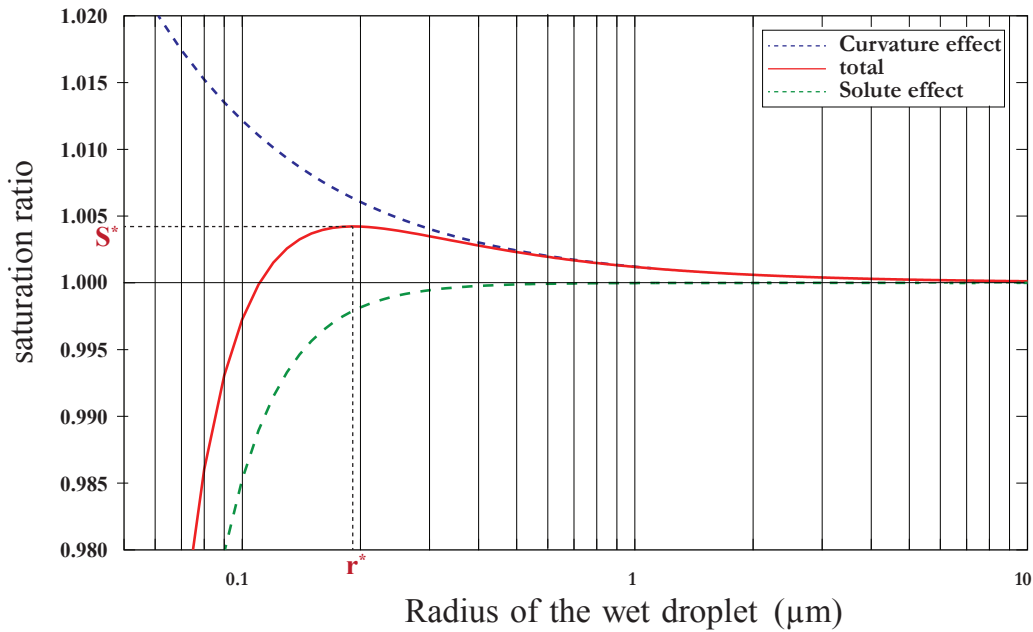


Figure 2.3: Schematic representation of traditional Köhler curve. Kelvin and Raoult effects are shown separately. The characteristic extremum of the curve represented by its critical saturation S^* and its corresponding critical radius r^* .

respectively. Apart from this, the $1/r$ proportional curvature effect contributes significantly for growing of particles. Finally, both effects converge to conditions over a flat and pure water surface and can be therefore neglected for those particles larger than $10 \mu m$.

2.2.1 Modeling of cloud droplet activation

Equilibrium growth theory describing the growth of a single particle is a simple way to study the effect of certain factors on cloud droplet activation. Another benefit of the Köhler theory (Köhler, 1936) is that with a fairly simple laboratory setup, it is possible to verify the theoretical results. Köhler theory (Köhler, 1936) can also be used to calculate the equilibrium growth of polydisperse droplet populations (Kokkola et al., 2003), but it may fail in describing the growth of droplets in a population as it neglects the kinetic nature of droplet growth (Chuang et al., 1997; Nenes et al., 2001).

In a polydisperse particle population, smaller particles require a higher supersaturation than larger ones in order to activate. When, some of the larger particles are activated, the rapid condensation growth of those droplets is causes water to deplete from the gas phase. The depletion of water together with the release of latent heat in condensation eventually causes the saturation ratio to start decreasing. Droplets with lower critical saturation ratio than the maximum reached by the parcel are activated and the rest are left inactivate. Thus condensation

alters the particle size distribution. The rate of change of mass (dm/dt) of a single drop can be estimated with the condensation equation:

$$\frac{dm}{dt} = 4\pi D_v (\rho_v - \rho_{v,r}), \quad (2.32)$$

where D_v is the molecular diffusion coefficient of water vapor in air, ρ_v is the density of water vapor, and $\rho_{v,r}$ is the density of water vapor at the droplet surface.

It may be that condensation of water vapor on larger droplets causes the saturation ratio in the parcel to decrease so rapidly. Then, the droplets start to evaporate those are already activated, as the ambient vapor pressure decreases below the vapor pressure at the droplet surface. The saturation ratio in the air parcel can also stay above the critical saturation ratio of droplet for such a short period that the droplet does not have time to exceed its critical size. In these cases, the droplet is left unactivated even though according to the equilibrium theory, the droplet would indeed continue to grow as a cloud droplet. There is a special case where the droplet is left unactivated but can still be considered as cloud droplet. Time plays a role in this case: it is when particle is so large that the cloud life time is shorter than the time requires for the particle to reach its critical size (Chuang et al., 1997; Nenes et al., 2001). The influences of slightly soluble and surface active compounds on the formation of cloud droplet populations have been studied with cloud parcel models (Abdul-Razzak and Ghan, 2004, 2005; Anttila and Kerminen, 2002; Ervens et al., 2005; Lohmann and Feichter, 2005; Nenes et al., 2001). Both of the effects have been found to alter droplet populations. It has also been suggested that, if the effects of low solubility and surface tension suppression together with increasing molecular weight considered simultaneously, the effects may counteract one another and lead to much similar changes in droplet population.

2.2.2 The effect of surface tension on droplet growth

Surface tension, σ (N/m or J/m²), can be defined as the energy needed to increase solution surface area. When a solution species is brought from interior to solution surface, energy is needed to break some intermolecular bonds as there are less interacting molecules in the surface (Prausnitz et al., 1999). As mentioned above, droplets experience increased pressure, which depends directly on surface tension and droplet diameter (curvature). As a result, volatile species have higher partial vapor pressures compared with those over flat solution surfaces. This increased vapor pressure is described by the Kelvin term (see Eq. 2.26). In order to model and describe surface concentrations, a simplified view of the gas-liquid interface is needed (Gibbs, 1928). When the surface is approximated, the Gibbs adsorption equation (Gibbs, 1928) relates the surface tension gradient ($\frac{\partial\sigma}{\partial\ln a_s}$, derivative of solution surface tension with respect to surfactant activity) to the surfactant surface excess Γ_s . The simple form of the Gibbs adsorption equation, where only one surfactant species has a non-zero surface excess is (Gibbs, 1928):

$$\Gamma_s = -\frac{1}{\psi RT} \frac{\partial\sigma}{\partial\ln a_s}. \quad (2.33)$$

Stoichiometric coefficient ψ is needed for dissociating surfactants and for mixtures with common ions. Surface activity, or tendency of a solute to accumulate on solution surface, depends on molecular or ion size, shape and interactions. Because of the strong interactions of the anions with the cations in the bulk solution, the drop has a slightly higher surface tension $\sigma_{(NH_4)_2SO_4} \sim 85$ (dynescm⁻¹) than pure water $\sigma_{H_2O} \sim 72$ (dynescm⁻¹) (Pruppacher and Klett, 1997). Organic

molecules in aqueous solution often cause lower surface tension since their hydrophobic parts are oriented toward the surface and lead to an expansion of the droplet. A specific relationship between concentrations of organic aerosol constituents and surface tension, has been given by [Facchini et al. \(1999\)](#):

$$\sigma_s = \sigma_w - 0.01877 \cdot T \cdot \ln(1 + 628.14 \cdot [C]), \quad (2.34)$$

where T is the temperature K and $[C]$ the concentration of WSOC ($molCL^{-1}$). On the basis of Eq. 2.34, a combined approach for accounting for a simultaneous change in σ_s and M_s derived by [Ervens et al. \(2004\)](#)

$$\sigma_s = \sigma_w - 0.01877 \cdot T \cdot \ln(1 + 628.14 \cdot n_C \cdot c_{aq}), \quad (2.35)$$

where c_{aq} is the solute concentration $molL^{-1}$, n_C is the number of carbon atoms ($M_C = 12 gmol^{-1}$):

$$n_C = \frac{M_s}{2.2M_C}. \quad (2.36)$$

2.3 Multiphase models for atmospheric aerosols

The mass transfer rate between gas and aerosol phases is strongly dependent on aerosol size, the mass transfer rates for the smallest and the largest particles can be different by several orders of magnitude. The mathematical description of such systems results in a set of extremely stiff differential equations. Gas/particle mass transfer is a process that transfers mass of condensable species from bulk gas phase to the particle surface. The timescale for the diffusion of a molecule from the bulk gas phase to the surface of a particle increases with the diameter of the particle. Therefore fine particles will tend to reach equilibrium rapidly whereas coarse particles can remain in non-equilibrium conditions (e.g., [Wexler and Seinfeld \(1990\)](#) and [Dassios and Pandis \(1999\)](#)). The conceptual description regarding these approaches was discussed in [Zhang et al. \(2004\)](#).

2.3.1 Equilibrium approach

Equilibrium approach always assumes an instantaneous chemical equilibrium between the bulk gas phase and the whole particulate phase (liquid/solid). One can categorize this approach into: bulk equilibrium approach and non-bulk equilibrium approach ([Bassett and Seinfeld, 1983, 1984](#)). The former one, assume the same chemical composition for all particles over all size sections (i.e. internal mixture). At the same time, in the later approach (also referred to as the size resolved equilibrium approach; see [Moya et al. \(2002\)](#)), particles in different size sections may have different chemical compositions. The bulk equilibrium approach of [Binkowski and Shankar \(1995\)](#) and the simple bulk equilibrium approach of [Hudischewskyj and Seigneur \(1989\)](#) and [Seigneur et al. \(1997\)](#) are examples of simple bulk equilibrium approaches, has been widely used in 3-D AQM applications([Zhang et al., 2004](#)). Due to its computational efficiency, in which the transferred material is allocated to the particle size distribution using weighting factors, that are derived based on either initial particle mass/surface area or a given distribution. These models, either assume mono-dispersed aerosols, or use bulk equilibrium with redistribution of the bulk material to different particle sizes following the equilibrium calculation ([Lurmann et al., 1997](#); [Capaldo et al., 2000](#); [Zhang et al., 2004](#)). While assuming an internal mixture with a potential

mixing of acidic particles with alkaline particles one may introduce errors, since both methods neglect the differences in chemical driving forces for different aerosol sections (or bins) (Ansari and Pandis, 1998; Moya et al., 2002; Myhre et al., 2004).

Size resolved equilibrium approach assuming an internal mixture over the entire size range, simulate equilibrium between gas phase and individual size sections. Examples of non-bulk equilibrium approach include those of Pilinis and Seinfeld (1987); Kleeman et al. (1997); Jacobson et al. (1996); Jacobson (1999) and Moya et al. (2002), in which a system of nonlinear algebraic equations are solved for each size range to determine the partitioning of semi-volatile species, while the mass transfer between the bulk gas-phase and bulk particulate phase is still considered to occur at an instantaneous thermodynamic equilibrium. In summary, the calculation of composition in each section is not based on the thermodynamic properties of that section, instead, it is based on the thermodynamic equilibrium of the bulk liquid/solid phases.

2.3.2 Dynamic approach

Dynamic/Kinetic approach does not rely on the instantaneous equilibrium. Furthermore this approach explicitly simulates gas/particle mass transfer for each size section by solving the equation for mass fluxes between the bulk gas-phase and individual particles or particles in a given size range (Zhang et al., 2004). Chemical concentrations in the bulk gas phase and in the particles in a given size section may or may not be in equilibrium. Since no equilibrium assumptions are made and the magnitude of the chemical driving force may vary with size sections, this approach provides the most accurate solution when an appropriate solver and sufficiently fine size-resolution are used (Zhang et al., 1999). Examples of the dynamic approaches for multicomponent aerosols include those of Meng and Seinfeld (1996); Meng et al. (1998); Jacobson (1997a,b); Sun and Wexler (1998a,b) and Pilinis et al. (2000). Existing kinetic approaches are applied primarily in box models (e.g. (Meng and Seinfeld, 1996; Pilinis et al., 2000)) although there exists few 3-D applications for episodes of few days (e.g. Meng et al. (1998)).

Table 2.1: Approaches to simulate gas/particle mass transfer

| Approaches | Methodology | Equilibrium Considered? | Equation solvers ^a |
|-----------------|---|--|-------------------------------|
| Equilibrium | Instantaneous chemical equilibrium between gas and particulate phases | Yes, between gas phase and bulk aerosol phase | No |
| Dynamic/Kinetic | Explicit simulation of gas/particle mass transfer for each size section | No | Yes, for all bins |
| Hybrid | Combination of both Equilibrium and kinetic approaches | No, for coarse bins (gas/particle mass transfer is solved kinetically), and yes for fine particles | Yes, for coarse bins only |

^a for condensation/evaporation

2.3.3 Hybrid approach

Hybrid approach is a combination of both dynamic and equilibrium approaches by providing a compromise between accuracy and efficiency. The CMU hybrid approach of [Capaldo et al. \(2000\)](#) is an example of such a hybrid approach, in which the mass transfer is treated explicitly for the coarse particles and the gas/particle equilibrium is assumed for the fine particles; but uncertainties exist in the selection of the cutoff size (i.e. threshold diameter) between the two approaches. Particles are usually assumed to be internally mixed (i.e., all particles within a given size range have the same chemical composition) and are distributed according to size sections. Therefore the mass transfer equation is solved between the bulk gas phase and the surface of the particles. On the other hand, the equilibrium approach is computationally efficient and has been used extensively in many 3-D models. [Zhang et al. \(1999\)](#) compared the CIT bulk equilibrium approach and the simple bulk equilibrium approach with the CIT dynamic approach in a box model. They found that the simple bulk equilibrium approach is inaccurate under many ambient conditions, whereas the CIT bulk equilibrium approach is appropriate when chloride and carbonate concentrations are insignificant. While the bulk equilibrium approach introduces errors in the partitioning calculation, particularly for cases with highly reactive coarse particles, the non-bulk equilibrium approach provides a more accurate representation of the interphase partitioning. However, the non-bulk equilibrium approach may lead to infinite solutions for solids and the equilibrium assumption is usually not valid for coarse particles.

Chapter 3

Activity coefficient models

The chemical conversions connected to the mass transfer between the phases in the aerosol can be described in models by the help of chemical equilibrium reactions; as condensation and evaporation between the gas and liquid phases, dissolution/dissociation of dissolved species, dissolution/precipitation of the solid species. Hence, development of appropriate tools are necessary, in order to understand the physico-chemical processing of aerosol particles impacts on the surrounding. It has been clear that particulate matter in the atmosphere may exist as a completely solid, completely liquid or a combined solid/liquid system. Hence, prediction of the phase state in relation to the associated chemical composition requires the use of thermodynamic models/approaches. The fundamental relationships for non-ideality present two ways of searching for the chemical equilibrium of aerosol. The first utilizes equilibrium constants defined for a set of reactions, which the user assumes to occur in the aerosol and the gaseous phase, based on varying levels of iteration. The second one focused on a search for the global minimum (see GFEMN (Ansari and Pandis, 1998), AIM online (Clegg et al., 1998a,b)).

For over decades, many frameworks were developed in order to estimate the activity coefficients of either electrolyte solutions or organic solutions (electrolyte-free systems) and mixture of organic-electrolyte systems. However, limited models available to combine organic-inorganic interactions in a single framework. On the whole, some of them were aimed to multicomponent atmospheric aerosol solutions. Among all, the available model approaches to treat the inorganic systems, organics and mixtures of organic-inorganic compounds will be outlined in the next following subsections followed by the description of activity coefficient module used in this thesis.

3.1 G^{Ex} models

As described in the previous chapter, the calculation of phase equilibria is based on fugacity or activity coefficients, depending on the Gibbs excess energy. In general G^{Ex}/RT is a function of T , P and composition, but for liquids at low to moderate pressures it is a weak function of P . Therefore the pressure dependence of activity coefficients is usually neglected. Thus, the G^{Ex}/RT at constant T for k number of species:

$$\frac{G^{Ex}}{RT} = f(x_i, x_j, \dots, x_k). \quad (\text{const } T) \quad (3.1)$$

Starting from the Gibbs-excess energy, an expression for the deviation from an ideal behavior can be written as:

$$RT \ln \gamma_i = \left(\frac{\partial G^{Ex}}{\partial n_i} \right)_{T,p,n_{j \neq i}} = g_i^E \Leftrightarrow \ln \gamma_i = \frac{g_i^E}{RT}. \quad (3.2)$$

A number of equations are in common use for correlation of activity coefficients. For binary systems (species i and j) the function most often represented as a power series

$$\frac{G^{Ex}}{RT} = A + Bx_i + Cx_i^2 + \dots \quad (\text{const } T). \quad (3.3)$$

Upon substituting the Eq. 3.3 in Eq. 3.2, the mean binary activity coefficients for species i and j can be parameterized with a polynomial fit of the form:

$$\ln \gamma_{i,j} = P_0 + P_1 x_{i,j}^{1/2} + P_2 x_{i,j} + P_3 x_{i,j}^{3/2} + \dots, \quad (3.4)$$

where P_0, P_1, \dots are experimental fitting coefficients. These polynomial coefficients are used to compute the activity coefficients of the particular species. One should note that, these coefficients will vary from species to species. The mean activity coefficient ($\gamma_{i,j}$) is related to single ion-activity coefficients by:

$$\gamma_{i,j} = (\gamma_+^{V_+} \cdot \gamma_-^{V_-})^{1/(V_+ + V_-)} \quad (3.5)$$

where γ_+ and γ_- are the activity coefficients of a cation and anion, respectively, V_+ and V_- are the corresponding stoichiometric coefficients. Empirical mixing rules are available, such as Bromley (1973) or Kusik and Meissner (1978)¹. These schemes have been used extensively in atmospheric models, and shown to accurately predict activity coefficients over a range of molalities. Mathematical relations to describe the activity coefficient (γ_i) in binary systems are given by the Margules equation (Margules, 1895), the van Laar equation (Van Laar, 1910) or the Redlich-Kister equation (Redlich and Kister, 1948). Furthermore, the limitation for the computation of activity coefficients to binary systems was eliminated with the use of concept of local composition (Wilson, 1964), in UNIQUAC (UNiversal QUAsiChemical) (Abrams and Prausnitz, 1975) method. In this approach the local concentration around one central molecule is assumed to be independent from the local composition around another type of molecule. However, the main disadvantage of these aforementioned models is the necessity of experimental data for the considered system to obtain model parameters. Due to the lack of experimental data, consequently, group contribution methods to predict activity coefficients have been developed and most widely used for the prediction of non-electrolyte activity estimation in non-ideal mixtures.

3.2 Group contribution methods

The models discussed previously utilize interaction parameters which must be obtained from the regression of experimental data. When experimental data is limited, the use of group contribution methods are preferred. As pointed out by Saxena and Hildemann (1996), treating each compound as a molecule would not only be cumbersome but also require binary aqueous data for each and every compound. Indeed, ultimately a technique is required where experimental data are bound to be lacking given the range of compounds often identified. As a result, a robust approach UNIFAC (Fredenslund et al., 1975) was developed. Here a molecule is fragmented into structural groups. It is assumed that the functional groups behave as if they were isolated from the molecule they are contained in. Thus, the intermolecular interactions are "weighted sums of group-group interactions" (Prausnitz et al., 1986). This allows to quantify the molecular interactions by reducing the experimental data for structural group interactions. For the prediction of mixture

¹These equations are not presented here, but can be found in the literature (see Pilinis (1999))

properties it is in most cases not sufficient to use a purely additive method. Instead, the property is determined from group interaction parameters (Gmehling, 2009) as follows:

$$P = f(G_{ij}), \quad (3.6)$$

where P stands for property and G_{ij} for group interaction value.

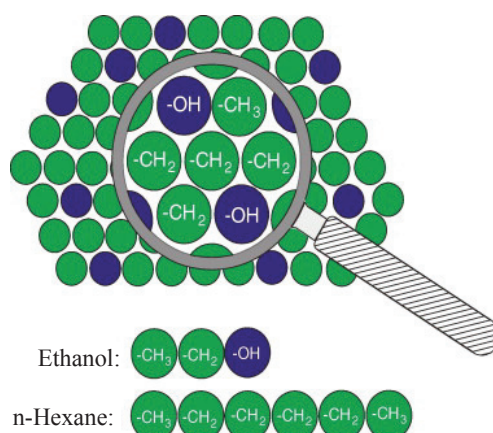


Figure 3.1: Solution of groups contribution concept [adapted from Gmehling (2009)].

The great advantage of group contribution methods is that the number of functional groups is much smaller than the number of possible molecules. For example, when the group interaction parameters between the alcohol and the alkane group are fitted using, e.g. the VLE data for the system shown in Fig. 3.1, the VLE behavior not only of this system but also of all other i.e. alkane + alkane, alcohol + alkane, and alcohol + alcohol systems can be predicted.

3.3 Activity coefficient models for mixtures of organic and inorganic compounds

For mixtures of organic and inorganic species, combinations of models are used as shown in Fig. 2.2. The main limitation regarding calculation of mixed organic/inorganic activity coefficients in aqueous systems stems from not being able to treat the complex interactions taking place in solution between the inorganic and organic fraction. Clegg et al. (2001) highlights the two main limitations. The first is a lack of experimental data from which important interaction parameters can be derived. The second is the lack of suitable theoretical models. The main reason is that atmospheric particles contain thousands of organic species. In fact, most of the published experimental data as well as activity coefficient models which are suitable to treat organic-electrolyte mixtures were designed for industrial purposes, and the compounds in these models are usually different from major species found in atmospheric aerosols (Raatikainen and Laaksonen, 2005).

The description of non-ideal behavior of chemically complex solutions is only possible with the combination of different methods (Clegg et al., 2001). Electrolytes might have a strong influence on the phase equilibrium behavior. Unfortunately, UNIFAC (Universal (Quasi chemical) Functional group Activity Coefficients) which are used to treat non-electrolytes cannot handle electrolyte systems. Therefore, parallel to the development of UNIFAC, the development of an electrolyte model for strong electrolytes were also developed. Hence, the models utilizing the combination of various approaches compute the activity coefficients by three contributions as shown in Fig. 2.2 (see Li et al. (1994) and Yan et al. (1999)). While these interactions for the Gibbs excess energy can be classified as (1) a Debye-Hückel term that represents the long-range (LR) interactions, (2) a virial term that accounts for the middle-range (MR) interactions caused by ion \leftrightarrow dipole effects and (3) the UNIFAC term that accounts for the short-range (SR) interactions (Raatikainen and Laaksonen, 2005). The required parameters for the MR term are fitted for the individual ions, which reduces the number of required parameters drastically. For the short range interactions, first the UNIQUAC equation, later the UNIFAC method (see Li et al. (1994)) was used. Moreover, there are some other activity models available in technical chemistry and chemical engineering, those are suitable to treat mixed solvent-electrolytes [e.g. Chiavone and Rasmussen (2000); Iliuta et al. (2000); Gros and Dussap (2003); Thomsen et al. (2004)].

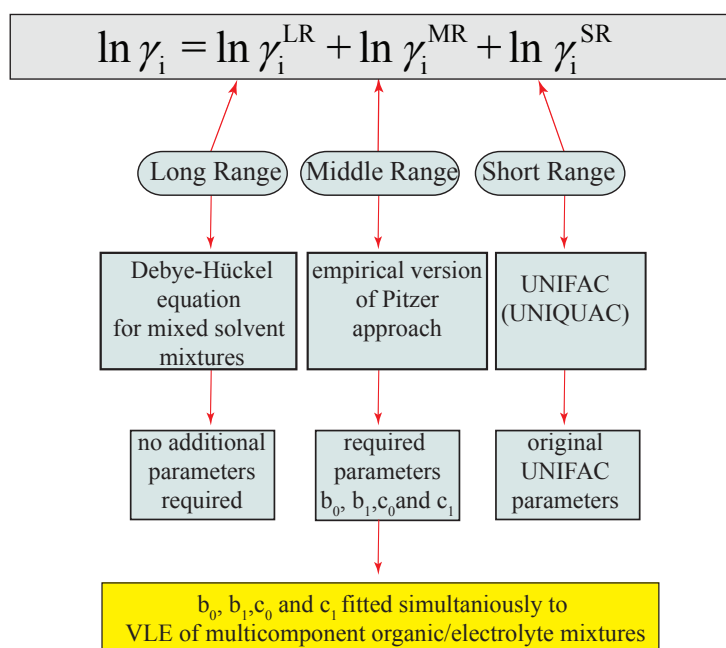


Figure 3.2: Description of computational methodology for the activity coefficients in multicomponent organic-electrolyte mixtures.

The different kinds of interactions between the molecules and ions of such systems are reasonable to describe with different terms for the Gibbs excess energy.

$$\ln \gamma_i = \ln \gamma_i^{LR} + \ln \gamma_i^{MR} + \ln \gamma_i^{SR} \quad (3.7)$$

Fig. 3.2, illustrate the computational methodology combining the different approaches into single model framework. As shown in this illustration, compare with Fig. 2.2, the methodology is described, how the mixtures of organic-inorganic mixtures are treated. As mentioned earlier

for the inorganic LR part no additional parameters are required and for the SR interactions, the UNIFAC method is commonly used. However, the interaction parameters for the MR part, caused from the ion↔ ion and ion↔ dipole are fitted against experimental data (parameters b_0 , b_1 , c_0 and c_1 shown in Fig. 3.2). Furthermore, for the description of activity coefficients for the inorganic compounds, the Pitzer approach (Pitzer, 1973; Pitzer and Mayorga, 1973; Pitzer, 1991) and their modified versions are extensively used in most of the model frameworks. The methods that are commonly used in these combined model frameworks will be outlined in the following subsections.

3.4 Activity coefficient models for inorganic compounds: Pitzer model

The LR nature of Columbic interactions between ions means, it is likely to be responsible for departures from ideality in ionic-solutions and to dominate contributions to non-ideality. This is the basis of the Debye-Hückel theory of ionic-solutions. However, it generally cannot be used to describe the properties of real solutions above 0.1 mol kg^{-1} . Indeed, the effect of complex ion-specific short-range forces that dominate in solutions at high concentrations must be described empirically. One can treat these non-Columbic interactions of ions in a series expansion of individual ion concentrations analogous to the virial expansion used for studying imperfect gases (Vaslow, 1972). While doing this, several attempts have been made to model the excess Gibbs free energy of the solution, which leads to the development of semi-empirical models. They are semi-empirical as SR interaction forces, dealt with through empirical theoretical in nature. In a solution of mixtures of strong electrolytes where association of ions are assumed not to occur, an ion-interaction rather than ion-pairing model is an appropriate choice (Smith et al., 1996). One of such powerful approach which is being used is Pitzer-like method as shown Fig. 2.2 using Pitzer equations (Pitzer, 1973; Pitzer and Mayorga, 1973; Pitzer, 1991) and the Pitzer-Simonson-Clegg model (Clegg and Pitzer, 1992; Clegg et al., 1992, 1998a). The theory behind the Pitzer's equations, along with required interaction parameters, is given in the literature (see Pitzer (1991) and references there in). The activity coefficient equations are based on a model for the excess Gibbs free energy that was represented by a virial expression of terms in concentration similar to Eq. 3.3. Hence, the activity coefficients are calculated by solving the equation for the Gibbs excess energy in the form of a series expansion given by Pitzer (1973) and Pitzer and Mayorga (1973):

$$\frac{G^{ex}}{m_{sol} \cdot RT} = f(I) + \sum_i \sum_j m_i m_j \lambda_{ij}(I) + \sum_i \sum_j \sum_k m_i m_j m_k \mu_{ijk}(I) + \dots, \quad (3.8)$$

where m_{sol} is the mass of the solvent material, m_i , m_j and m_k are the ion concentrations in the molality scale, λ and μ are model parameters and I is the ionic strength. The excess energy comprises a Debye-Hückel term $f(I)$ that represents the LR interactions, which dominate very dilute solutions. The SR interactions are accounted for by virial coefficients for binary and ternary interactions. One of the merits of Pitzer's technique was dependence of the binary interactions on the ionic strength of solution, which was not accounted for in earlier techniques as described in detail in Appendix. B.2.

3.5 Activity coefficient models for organic compounds

Unlike electrolytes, organic components have diverse chemical structures and possess quite different properties, both from each other and from electrolytes. This necessitates activity coefficient model frameworks that are different to inorganic models. Indeed, because electrolytes and organics have different interactions in aqueous solutions, a large fraction of all activity coefficient models are applicable either for non-electrolytes solutions or for aqueous electrolyte solutions. One of the most frequently used group contribution model approach to calculate the activity coefficients of mixtures of water and organic compounds is the UNIFAC model of [Fredenslund et al. \(1975\)](#). In the UNIFAC model, the activity coefficient of component i in the solution mixture is described by:

$$\ln \gamma_i = \ln \gamma_i^C + \ln \gamma_i^R, \quad (3.9)$$

where γ_i^C is the combinatorial part and γ_i^R is the residual part of the activity coefficient (γ_i). The combinatorial part provides the contribution due to molecular size and shape. On the other hand, the residual part describes molecular interactions between the functional groups. Furthermore, model equations requires large number of coefficients derived from experimental data. In literature (see [Hansen et al. \(1991\)](#); [Peng et al. \(2001\)](#)), several sets of fitted model coefficients are available for the UNIFAC model. The model interaction parameters used in this study are available in the Appendix of this work along with model description (see Appendix [B.3](#)).

3.6 Description of activity coefficient module used in this study

In this section, the used mixed organic-electrolyte model that is designed to yield comprehensive results to predict phase equilibria and activity coefficients is outlined. As explained in the previous subsection, the non-ideality of a thermodynamic system is usually described by an expression for the excess Gibbs energy $G^{ex}(J)$ as the characteristic state variables depending on the parameters pressure p and temperature T . A detailed description of typical expressions for interaction potentials and contributions, which play a role in inorganic mixtures or in organic-inorganic mixtures has been given in the literature (see [Pitzer \(1991\)](#); [Li et al. \(1994\)](#); [Yan et al. \(1999\)](#); [Clegg et al. \(2008\)](#) and references there in). Note that when no electrolytes are in the mixture, the total Gibbs energy shown in Eq. [3.7](#) reduces to short range interactions, i.e. $\Delta G^{ex} = G_{SR}^{ex}$. In the following section, the detailed description of LR, MR, and SR model parts that was specifically designed to perform speciation calculations will be outlined.

Based upon the extensive literature review, in the current study the aqueous phase liquid mixtures considered are composed of different inorganic salts, inorganic acids, organic compounds dissolved in water at STP conditions (i.e. $298K$ and $100kPa$). As described in [Li et al. \(1994\)](#) and [Zuend et al. \(2008\)](#) following the idea of UNIFAC and LIFAC, a group contribution concept is used to describe interaction effects of organic compounds in a solution, thereby covering a large number of organics by means of functional groups.

As discussed earlier, based on the model performance and comparison, four models have been selected and implemented in this study. However, all the models have their own advantages and disadvantages. After the critical evaluation of the models (see Sec. [6.1](#)), to compute the activity coefficients of the mixed organic-electrolyte-water system, at lower relative humidity and high ionic strength AIOMFAC ([Zuend et al., 2008](#)) model has been selected for further

model development, since, this model is originally designed only for the hydroxyl and alcohol groups. Apart from these organic functional groups, other organic groups, which have strong impact on multiphase chemical processing, were also identified in the atmosphere. In order to treat the non-ideality for the aqueous phase chemistry, within the known complexity, including the organic functional groups, which are commonly encounter in the atmosphere, the original AIOMFAC model interaction parameters are extended. Furthermore, one should keep in mind, that deriving or fitting the new parameters for all the organic and inorganic compounds identified in the atmosphere, is not the scope of this work. Hence, without altering the model equations of original AIOMFAC, the interaction parameters have been updated, while introducing a new algorithm, to compute the activity coefficients from the mod. LIFAC (Kiepe et al., 2006) as shown in Fig. 3.3. Thus, this new algorithm allows to predict the activity coefficients of the considered organic \leftrightarrow electrolyte mixture, flexibly, from these two approaches AIOMFAC (Zuend et al., 2008) and mod. LIFAC (Kiepe et al., 2006), within a single framework.

3.6.1 Long-range contribution

The long range interactions are same as original AIOMFAC, based on the Debye-Hückel theory (Debye and Hückel, 1923). As a consequence of the choice of the reference solvent water for inorganic ions, the Debye-Hückel expression is different from the one in original LIFAC (see Zuend et al. (2008)). Hence the similar assumption is considered in this model also. In contrast with Li et al. (1994); Yan et al. (1999) and Chang and Pankow (2006), in the AIOMFAC the water properties have been used for all solvent components for density and dielectric constant of the solvent mixture, instead of using mixing rules. Similar assumptions were made for the LR part of mixed solvent models in the field of technical chemistry and chemical engineering (see Iliuta et al. (2000) and references there in). With this assumption, the corresponding LR activity coefficient expressions for the solvents $\ln \gamma_s^{LR,(x)}$ and the ions $\ln \gamma_i^{LR,(x),\infty}$ according to Zuend et al. (2008)

$$\ln \gamma_s^{LR,(x)} = \frac{2AM_s}{b^3} \left(1 + b\sqrt{I} - \frac{1}{1 + b\sqrt{I}} - 2 \ln(1 + b\sqrt{I}) \right), \quad (3.10)$$

$$\ln \gamma_i^{LR,(x),\infty} = \frac{-z_i^2 A \sqrt{I}}{1 + b\sqrt{I}}. \quad (3.11)$$

Eq. 3.11 gives the activity coefficient of ion i in the mole fraction basis (x) with the reference state (see Appendix. B.1) of infinite dilution in water, indicated by super script ∞ . M_s is the molar mass of solvent s , z_i the number of elementary charges of ion i , and the ionic strength I (mol/kg) is:

$$I = \frac{1}{2} \sum_i m_i z_i^2. \quad (3.12)$$

The Debye-Hückel parameters $A(\sqrt{kg/mol})$ and $b(\sqrt{kg/mol})$ depend on temperature $T(K)$, density $\rho_w(kg/m^3)$ and static permittivity ε_w (dimension less) of water, calculated based on a distance of closest approach of $0.4nm$ between ions since, ions are hard spheres, with a unique closest approach parameter (Demaret and Gueron, 1993). Moreover, the computation of the free energy (for instance, surface potential and hard sphere distance) involves approximations. Agreement with the experiments for distance between the ions and the counter ion, in conjunction with an ion-pairing equilibrium, was obtained as $0.4nm$ (see (Demaret and Gueron, 1993; Antypov and Holm, 2007) and references there in).

$$A = 1.327757 \cdot 10^5 \frac{\sqrt{\rho_w}}{(\varepsilon_w T)^{3/2}}, \quad (3.13)$$

$$b = 6.359696 \sqrt{\frac{\rho_w}{\varepsilon_w T}}, \quad (3.14)$$

As pointed out by Raatikainen and Laaksonen (2005), the simplification to a water-property based expression for LR activity coefficients are beneficial. Due to the uncertainties to estimate unknown dielectric constants of certain organic compounds and maintaining the thermodynamic consistency regarding the selection of reference states, this assumption would be profitable. In a real mixture, solvents have densities and dielectric properties different from those of pure water, which was the reason for the models available in the chemical engineering or in technical chemistry, use to avoid applying this simplification. Compensation of these inaccuracies are controlled from this simplification, in the semi-empirical MR part as performed in original AIOMFAC (Zuend et al., 2008).

3.6.2 Middle-range contribution-extended version

The semi-empirical character of the MR part in AIOMFAC, containing most of the adjustable parameters, can be considered as the model part, which describes all the interaction effects involving ions not considered by the LR and SR contributions (see Zuend et al. (2008)). Hence, this includes corrections to assumptions made in the LR and SR parts with respect to approximations of physical parameters similar to Zuend et al. (2008). MR interactions of solvent compounds (organics and water) with ions are calculated using functional main groups. The MR contribution for the species included in the in the extended version follows the same computation as original AIOMFAC (see Zuend et al. (2008)) for further details.

The three interaction coefficients are parameterized as functions of ionic strength I . In contrast to LIFAC, in AIOMFAC the expressions, which were developed similar to the ones used for the Pitzer model of Knopf et al. (2003) are employed here as:

$$B_{k,i}(I) = b_{k,i}^{(1)} + b_{k,i}^{(2)} e^{-b_{k,i}^{(3)} \sqrt{I}}, \quad (3.15)$$

$$B_{c,a}(I) = b_{c,a}^{(1)} + b_{c,a}^{(2)} e^{-b_{c,a}^{(3)} \sqrt{I}}, \quad (3.16)$$

$$C_{c,a}(I) = c_{c,a}^{(1)} + e^{-c_{c,a}^{(2)} \sqrt{I}}, \quad (3.17)$$

where $b_{k,i}^{(1)}$, $b_{k,i}^{(2)}$, $b_{c,a}^{(1)}$, $b_{c,a}^{(2)}$, $c_{c,a}^{(1)}$, $c_{c,a}^{(2)}$ are adjustable parameters, which are determined by fitting AIOMFAC activity coefficients to experimental data sets. The parameter $b_{c,a}^{(3)}$ was found to describe most aqueous salt solutions when assuming a fixed value of $0.8 \text{ (kg}^{1/2}/\text{mol}^{1/2})$. The parameter $b_{k,i}^{(3)}$ was fixed for all mixed organic-inorganic solutions assuming a value of $1.2 \text{ (kg}^{1/2}/\text{mol}^{1/2})$. All interaction coefficients in the MR part are symmetric, i.e. $B_{c,a}(I) = B_{a,c}(I)$.

The MR activity coefficients are obtained for a specific solvent main group k^*

$$\begin{aligned}
\ln \gamma_{k^*}^{MR,(x)} &= \sum_i B_{k^*,i}(I) m_i - \frac{M_{k^*}}{M_{av}} \sum_k \sum_i [B_{k,i}(I) + IB'_{k,i}(I)] x'_k m_i \\
&\quad - M_{k^*} \sum_c \sum_a [B_{c,a}(I) + IB'_{c,a}(I)] m_c m_a \\
&\quad - M_{k^*} \sum_c \sum_a [2C_{c,a}(I) + IC'_{c,a}(I)] m_c m_a \sum_i m_i |Z_i| \\
&\quad - M_{k^*} \sum_c \sum_{c'} R_{c,c'} m_c m_{c'} \\
&\quad - M_{k^*} \sum_c \sum_{c' \geq c} \sum_a 2Q_{c,c',a} m_c m_{c'} m_a.
\end{aligned} \tag{3.18}$$

Where m_i , m_c , m_a are the molalities of ions, cations and anions, respectively, x'_k are the salt-free mole fractions of solvent main groups k , and $M_{av} = \sum_s x'_s M_s$ is the average molar mass of the solvent mixture. M_{k^*} is the molar mass of main group k^* , calculated from the molar masses of the corresponding subgroups and their partial contributions to k^* . $B_{k,i}(I)$ ($kg \text{ mol}^{-1}$) and $B_{c,a}(I)$ ($kg \text{ mol}^{-1}$) are binary interaction coefficients between solvent main groups and ions, and between cations and anions, respectively. $C_{c,a}(I)$ ($kg^2 \text{ mol}^{-2}$) are interaction coefficients between cation-anion pairs with respect to the total charge concentration. The coefficients $R_{c,c'}$ ($kg \text{ mol}^{-1}$) and $R_{c,c',a}$ ($kg^2 \text{ mol}^{-2}$) describe binary and ternary interactions involving two different cations $B'_{k,i}(I)$, $B'_{c,a}(I)$ ($kg^{1/2}/\text{mol}^{1/2}$). The parameter $b_{k,i}^{(3)}$, and $C'_{c,a}(I)$ (kg^3/mol^3) are the partial derivatives with respect to I , e.g. $B'_{c,a}(I) = \partial B_{c,a}(I)/\partial I$.

The activity coefficient of solvent compound s is then obtained from the main group contributions by:

$$\ln \gamma_s^{MR,(x)} = \sum_k \nu_k^{(s)} \ln \gamma_k^{MR,(x)}. \tag{3.19}$$

In analogy to Eq. 3.18 the expressions for a specific cation c^* are:

$$\begin{aligned}
\ln \gamma_{c^*}^{MR,(x),\infty} &= \frac{1}{M_{av}} \sum_k B_{k,c^*}(I) x'_k + \frac{z_{c^*}^2}{2M_{av}} \sum_k \sum_i B'_{k,i}(I) x'_k m_i \\
&\quad + \sum_a B_{c^*,a}(I) m_a + \frac{z_{c^*}^2}{2} \sum_c \sum_a B'_{c,a}(I) m_c m_a \\
&\quad + \sum_a C_{c^*,a}(I) m_a \sum_i m_i |z_i| \\
&\quad + \sum_c \sum_a \left[C_{c,a}(I) |z_{c^*}| + C'_{c,a}(I) \frac{z_{c^*}^2}{2} \sum_i m_i |z_i| \right] m_c m_a \\
&\quad + \sum_c R_{c^*,c} m_c + \sum_c \sum_a Q_{c^*,c,a} m_c m_a,
\end{aligned} \tag{3.20}$$

and for anion a^*

$$\begin{aligned}
\ln \gamma_{a^*}^{MR(x),\infty} &= \frac{1}{M_{av}} \sum_k B_{k,a^*}(I) x'_k + \frac{z_{a^*}^2}{2M_{av}} \sum_k \sum_i B'_{k,i}(I) x'_k m_i \\
&+ \sum_c B_{c,a^*}(I) m_c + \frac{z_{a^*}^2}{2} \sum_c \sum_a B'_{c,a}(I) m_c m_a \\
&+ \sum_c C_{c,a^*}(I) m_c \sum_i m_i |z_i| \\
&+ \sum_c \sum_a \left[C_{c,a}(I) |z_{a^*}| + C'_{c,a}(I) \frac{z_{a^*}^2}{2} \sum_i m_i |z_i| \right] m_c m_a \\
&+ \sum_c \sum_{c' \geq c} Q_{c,c',a^*} m_c m_{c'}.
\end{aligned} \tag{3.21}$$

Specific interaction coefficients (and the corresponding fit parameters) between the reference solvent, i.e. water, and the inorganic ions are set to zero ($B_{k=w,i}(I) = 0$). Moreover, the unsymmetrical reference state condition for infinite dilution of ions in water $\ln \gamma_i^{MR} \rightarrow 1$ is indeed also fulfilled for $\ln \gamma_{c^*}^{MR,(x),\infty}$ (normalized) instead of $\ln \gamma_{c^*}^{MR,(x)}$ according to original AIOMFAC (Zuend et al., 2008). The description of normalization realized in this implementation is explained in Appendix (see Appendix. B.1).

However, original AIOMFAC was not fitted for the whole range of inorganic and organic species, can found in atmosphere. In order to treat the important inorganic \leftrightarrow organic compounds, the modification is performed in the MR interactions, according to mod. LIFAC approach of Kiepe et al. (2006). For a better understanding, Eq. 3.21 can be divided into different terms:

$$\ln \gamma_i^{MR} = T_i^{solvent} + T_i^{ion-solvent} + T_i^{ion} + T_i^{ion-ion} + T_i^{ion-ion-ion} \tag{3.22}$$

with

$$T_i^{solvent} = \frac{1}{M_{av}} \sum_k B_{k,a^*}(I) x'_k, \tag{3.23}$$

$$T_i^{ion-solvent} = \frac{z_{a^*}^2}{2M_{av}} \sum_k \sum_i B'_{k,i}(I) x'_k m_i, \tag{3.24}$$

$$T_i^{ion} = \sum_c B_{c,a^*}(I) m_c, \tag{3.25}$$

$$T_i^{ion-ion} = \frac{z_{a^*}^2}{2} \sum_c \sum_a B'_{c,a}(I) m_c m_a, \tag{3.26}$$

$$\begin{aligned}
T_i^{ion-ion-ion} &= \frac{z_{a^*}^2}{2} \sum_c \sum_a B'_{c,a}(I) m_c m_a \\
&+ \sum_c C_{c,a^*}(I) m_c \sum_i m_i |z_i| \\
&+ \sum_c \sum_a \left[C_{c,a}(I) |z_{a^*}| + C'_{c,a}(I) \frac{z_{a^*}^2}{2} \sum_i m_i |z_i| \right] m_c m_a \\
&+ \sum_c \sum_{c' \geq c} Q_{c,c',a^*} m_c m_{c'}.
\end{aligned} \tag{3.27}$$

As mentioned earlier, the model has been extended by including the new interaction parameters for the species shown in Fig. 3.4, based on the mod. LIFAC (Kiepe et al., 2006). A sufficient evaluation was performed using the actual experimental database, which has been significantly enlarged within the last years (see Raatikainen and Laaksonen (2005) and Tong et al. (2008)).

However, the general concentration dependence of the interaction parameters can be written as analogous to Eq. 3.15:

$$B_{i,j} = b_{i,j} + c_{i,j} \exp^{a_1 \sqrt{I}}, \quad (3.28)$$

where, $b_{i,j}$, $c_{i,j}$ and a_1 are adjustable interaction parameters. However, according to mod. LIFAC (Kiepe et al., 2006), the second virial coefficient $B_{i,j}$ is the interaction coefficient between the species i and j . The relation of ion \leftrightarrow ion interaction parameter $B_{c,a}$ ion \leftrightarrow solvent group interaction parameter $B_{k,ion}$ to the ionic strength are described by Kiepe et al. (2006).

$$B_{c,a} = b_{c,a} + c_{c,a} \exp\left(-I^{1/2} + 0.125I\right), \quad (3.29)$$

$$B_{k,i} = b_{k,i} + c_{k,i} \exp\left(-1.2I^{1/2} + 0.25I\right). \quad (3.30)$$

The equation for interaction parameters shown in the two versions (Eq. 3.15 - 3.16 and Eq. 3.29 - 3.30) was compared and the final model equations are derived. As a result, Eq. 3.29 can be written as similar to Eq. 3.16:

$$B_{c,a}(I) = b_{c,a} + c_{c,a} \exp^{-(1.2+0.125\sqrt{I})\sqrt{I}} \quad (3.31)$$

Based on this, while using the similar model equations, the database was utilized with the ion-ion interaction parameters as:

$$b_{c,a}^{(1)} = b_{c,a}, \quad (3.32)$$

$$b_{c,a}^{(2)} = c_{c,a}, \quad (3.33)$$

$$b_{c,a}^{(3)} = -\left(1.2 + 0.125\sqrt{I}\right). \quad (3.34)$$

Since ion \leftrightarrow ion \leftrightarrow ion interaction parameters (ternary interactions) were not available with mod. LIFAC the interaction parameters for $c_{c,a}^{(1)}$ and $c_{c,a}^{(2)}$ were assigned to zero. Similar to ion-ion interaction parameters, the model equation to compute the solvent-ion interaction parameters were also modified. Compare with Eq. 3.15 and Eq. 3.30 the parameters are assigned as:

$$b_{k,i}^{(1)} = b_{k,i}, \quad (3.35)$$

$$b_{k,i}^{(2)} = c_{k,i}, \quad (3.36)$$

$$b_{c,a}^{(3)} = -\left(1.2 + 0.25\sqrt{I}\right). \quad (3.37)$$

Afterwards the same model equations were employed similar to Zuend et al. (2008) to compute the activity coefficients of each species. Even, the ternary and quaternary interactions were also assigned to zero during the computation of activity coefficients for solvent groups. Hence, the model equations reduced to original model equations as described in Kiepe et al. (2006) and Yan et al. (1999). Similarly the ternary interactions shown above for ions (see Eq. 3.26) also doesn't included in the computation of the activity coefficients those are not explicitly described in the original AIOMFAC. So this term leads to zero, and hence the Eq. 3.19 and Eq. 3.21 leads to the original model equations (see Eq. 12 in Kiepe et al. (2006)). The algorithm for computing the activity coefficient module is schematically shown in Fig. 3.3.

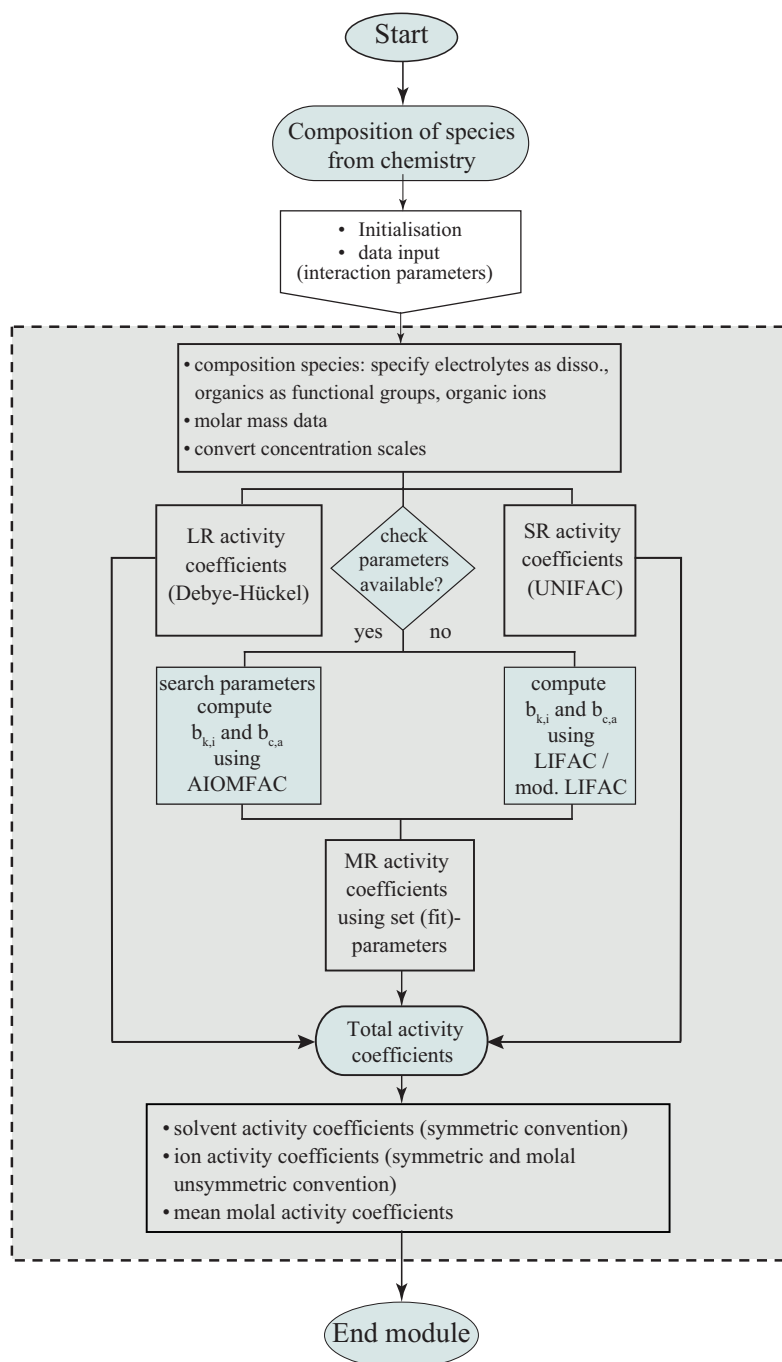


Figure 3.3: Description of activity coefficient algorithm implemented in this study.

3.6.3 Short-range contribution

This extended model of AIOMFAC follows the same as original version for short range contribution represented by the group-contribution method UNIFAC (Fredenslund et al., 1975). The UNIFAC expressions in AIOMFAC include some modifications to better meet the specific properties of atmospheric semi-volatile organics, which typically contain molecules carrying several strongly polar functional groups. In this way, the relative distances of a molecule's functional groups are taken into account explicitly (see Zuend et al. (2008)). However, original AIOMFAC comprises only alkane, alcohol and water groups. Hence the organic functional groups were extended as well. The interaction parameters for these organic functional groups are shown in Appendix B.5.3.

As a result, in the current version of UNIFAC (is similar to the original UNIFAC, except extending the database) the activity coefficient γ_j of mixture component j (j used for solute or solvent) is in general expressed as the contributions of a combinatorial part (C), accounting for the geometrical properties of the molecule, and a residual part (R), which reflects inter-molecular interactions:

$$\ln \gamma_j^{SR} = \ln \gamma_j^C + \ln \gamma_j^R. \quad (3.38)$$

The combinatorial contribution is calculated with the equation (Marcolli and Peter, 2005) as performed in original AIOMFAC (Zuend et al., 2008):

$$\ln \gamma_j^C = \ln \frac{\Phi_j}{x_j} + \frac{z}{2} q_j \ln \frac{\Theta_j}{\Phi_j} + l_j - \frac{\Phi_j}{x_j} \sum_{j'} x_{j'} l_{j'}, \quad (3.39)$$

where

$$\Phi_j = \frac{r_j x_j}{\sum_{j'} r_{j'} x_{j'}}; \Theta_j = \frac{q_j x_j}{\sum_{j'} q_{j'} x_{j'}}, \quad (3.40)$$

and

$$l_j = \frac{z}{2} (r_j - q_j) - (r_j - 1), \quad (3.41)$$

with $z = 10$. x_j is the mole fraction, $q_j = \sum_t \nu_t^{(j)} Q_t$ is the area parameter, $r_j = \sum_t \nu_t^{(j)} R_t$ is volume parameter and $\nu_t^{(j)}$ is the number of functional group k in species i . The only parameters in the combinatorial part are the pure component area (Q_k) and volume (R_k) parameters for sub groups. The residual contribution is calculated with the equation:

$$\ln \gamma_j^R = \sum_t \nu_t^{(j)} \left[\ln \Gamma_t - \ln \Gamma_t^{(j)} \right], \quad (3.42)$$

where Γ_t and $\Gamma_t^{(j)}$ are the group residual activity coefficients in the mixture and in a reference solution containing only compound j , a (hypothetical) pure liquid of j , respectively. The expression for the residual activity coefficient of subgroup t is:

$$\ln \Gamma_t = Q_t \left[1 - \ln \left(\sum_m \Theta_m \psi_{m,t} \right) - \sum_m \left(\frac{\Theta_m \psi_{t,m}}{\sum_n \Theta_n \psi_{n,m}} \right) \right], \quad (3.43)$$

with

$$\Theta_m = \frac{\Theta_m X_m}{\sum_n \Theta_n X_n}; \psi_{m,n} = e^{-a_{m,n}/T}, \quad (3.44)$$

where Θ_m is the relative surface area fraction of subgroup m , X_m is the mole fraction of m in the mixture, and $\psi_{m,n}$ is the temperature dependent function of the subgroup interaction parameter $a_{m,n}$. Note that the subgroup interaction parameters are unsymmetrical, i.e. $a_{m,t} \neq a_{t,m}$. The sums are over all different subgroups. Since, ions are treated like solvent components in the SR terms, resulting activity coefficients Eq. 3.38 are with respect to the symmetrical convention on mole fraction basis. For ions i , the unsymmetrical normalized activity coefficient is determined from:

$$\ln \gamma_i^{SR,(x),\infty} = \ln \gamma_i^{SR,(x)} - \ln \gamma_i^{SR,(x),ref}. \quad (3.45)$$

The symmetrically normalized value at the reference state is computed from Eq. 3.39 and Eq. 3.43 by introducing the reference state conditions of the ions (setting $x_w = 1$, $\sum_s x_s = 0$ for $s \neq w$ and $\sum_i x_i = 0$):

$$\begin{aligned} \ln \gamma_i^{SR,(x),ref} = & \ln \frac{r_i}{r_w} + 1 - \frac{r_i}{r_w} + \frac{z}{2} q_i \left[\ln \left(\frac{r_w q_i}{r_i q_w} \right) - 1 + \frac{r_i q_w}{r_w q_i} \right] \\ & + q_i (1 - \ln \psi_{w,i} - \psi_{i,w}), \end{aligned} \quad (3.46)$$

where subscript w stands for the reference solvent (water). The last term on the right-hand side of Eq. 3.46, reflecting the residual part reference contribution, becomes zero as we defined the SR ion-solvent interactions to be zero. Fig. 3.4 shows the binary species combinations, for which the specific parameters have used in this study. Mean interactions between ions and water are indirectly represented by the parameters of the cation \leftrightarrow anion interaction pairs according to Zuend et al. (2008), since the aqueous solution is defined as the reference system similar to the assumption as in conventional Pitzer models (Pitzer, 1991). The relative van der Waals subgroup volume and surface area parameters, R_t and Q_t , account for pure component properties, and these values for the ions can be estimated from the ionic radii. Hence, similar to the procedure according to Zuend et al. (2008), to be consistent with the parameters, the hydrated group volume and surface area parameters R_t^H and Q_t^H are calculated using an empirical parametrization given by Achard et al. (1994), for the ions, which are implemented from the mod. LIFAC. Since, fitting of new parameters is not the scope of this work, hence the final values R_t^H and Q_t^H instead of R_t and Q_t were used in the SR part. For those ions, the N_t^{ADH} are available in the literature, the R_t^H and Q_t^H values were computed and used in this PhD thesis to be consistent for the model equations (see Table. C.11 for the values).

$$R_t^H = R_t + N_t^{ADH} \cdot R_w, \quad (3.47)$$

$$Q_t^H = Q_t + N_t^{ADH} \cdot Q_w, \quad (3.48)$$

where R_w and Q_w refer to the values of the water molecule and N_t^{ADH} are measured apparent dynamic hydration numbers at 303.15 K (Kiriukhin and Collins, 2002). As shown in Fig. 3.4, the ions Mg^{2+} , Ca^{2+} , F^- , I^- , OH^- , NO_2^- , CO_3^- and CH_3COO^- are implemented from Kiepe et al. (2006). Due to the mounting interest of remaining ions, such as Fe^{2+} , succinate, malonate, included in the mechanism, the activity coefficients are computed according to LR and SR interactions. However, due to the lack of data for the interaction parameters are kept as 0 for these ions. Furthermore, while treating the non-ideality for the aqueous phase chemistry, all the ions were used to compute the activity coefficients, while simply deciding the ions are whether cations or anions. The LR contributions are computed for these ions, simply based on

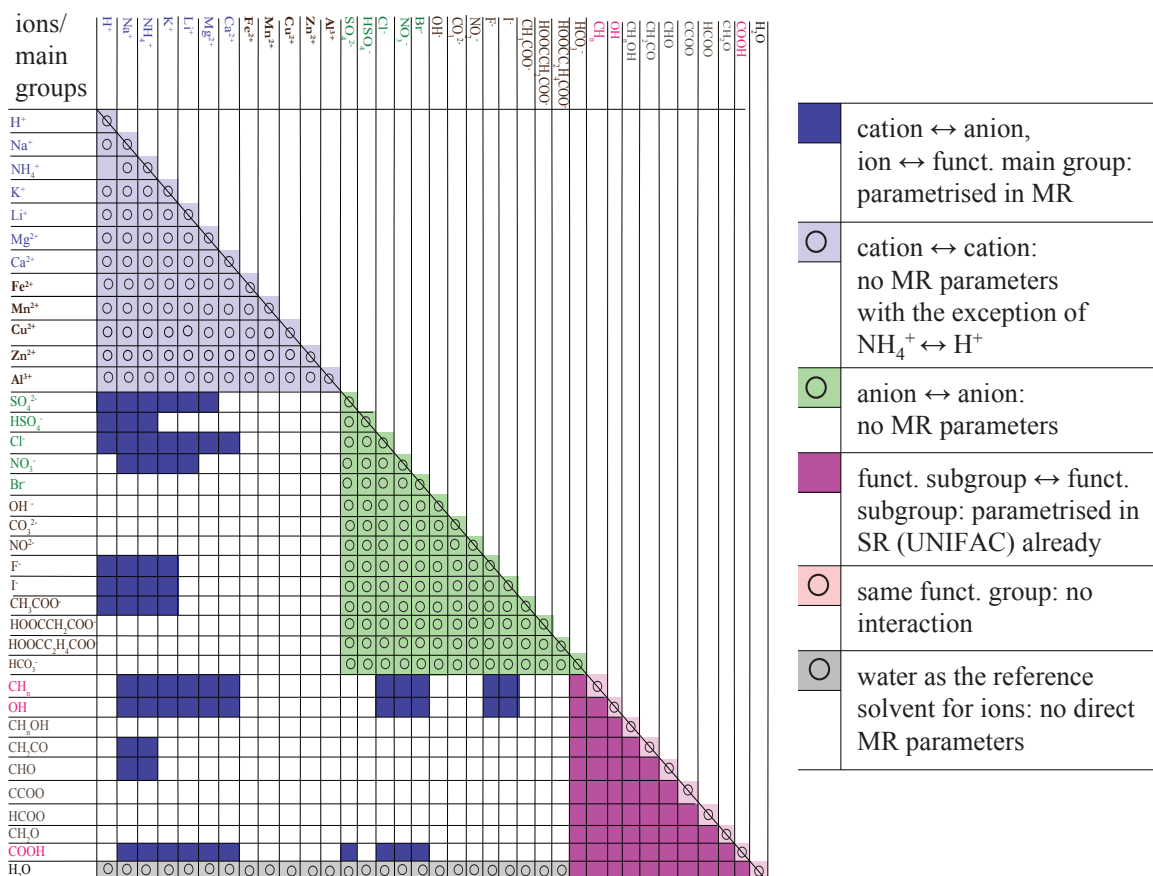


Figure 3.4: Scheme of the currently used interactions in the MR and SR part. Parameters for ion ↔ ion and ion ↔ organic main group interactions are all incorporated in the MR part and set to zero in the SR (UNIFAC) part.

the molalities, and charge equations, (see Eq. 3.11), where as the SR interactions are computed according to Eq. 3.45 and Eq. 3.46.

3.6.4 Total activity coefficients

Finally, the total activity coefficients for the each species can be computed according to the Gibbs energy and Eq. 3.7, the complete expression for the activity coefficient of solvent species s is (Li et al., 1994; Yan et al., 1999; Kiepe et al., 2006; Zuend et al., 2008):

$$\ln \gamma_s^{(x)} = \ln \gamma_s^{LR,(x)} + \ln \gamma_s^{MR,(x)} + \ln \gamma_s^{SR,(x)}, \quad (3.49)$$

where as these specific contributions of each interactions computed from Eq. 3.10, Eq. 3.19 and Eq. 3.38. Accordingly, the complete expression for the ions, with regard to the unsymmetrical convention on molality basis can be written as follows:

$$\ln \gamma_i^{(m)} = \left[\ln \gamma_i^{LR,(x),\infty} + \ln \gamma_i^{MR,(x),\infty} + \ln \gamma_i^{SR,(x),\infty} \right] - \ln \left[\frac{M_w}{\sum_s x'_s M_s} + M_w \sum_{i'} m_{i'} \right], \quad (3.50)$$

where M_s is the molar mass of solvent component s , x'_s its salt-free mole fraction, and $m_{i'}$ is the molality of ion i' . The total interaction contributions for ions are from Eq. 3.11 for LR, Eq. 3.19 or Eq. 3.21 for MR (depending on whether i is a cation or an anion) from extended AIOMFAC, additionally the SR part was computed from Eq. 3.46. The last term on the right-hand side of Eq. 3.50 converts the activity coefficient $\ln \gamma_s^{(x)}$ (infinitely diluted reference state on the mole fraction basis) to the activity coefficient on molality basis and infinitely diluted (in water) reference state. One can derive this term based on convention-independence of the chemical potentials $\left(\mu_i^{(m)}(p, T, n_j) = \mu_i^{(x)}(p, T, n_j) \right)$ and the definitions of the chosen reference states (Zuend et al., 2008).

However, concerning the conceptual model uncertainties as well as the limited experimental data sets, it should admit that the extended AIOMFAC cannot predict the activity coefficients of multicomponent organic \leftrightarrow electrolyte mixtures, with same high level of accuracy, as the Pitzer-like part of AIOMFAC (since most of the MR interaction parameters are assigned to zero) or other detailed thermodynamic models, such as the AIM model (Clegg et al., 1998a,b), as attained for aqueous electrolyte solutions (organic-free). Although, the model interaction parameters are fitted against experimental findings, these predictive models doesn't hold the same level of accuracy to compute the activity coefficients, when these models were compared with each other. However, due to the available possibilities and considering the advantages, where AIOMFAC can compute the activity coefficients at low concentrations this model is selected for further extension. Whenever, the more robust model come exists, the current model framework, can easily relax these limitations, due to the flexibility of the implemented code.

Chapter 4

The air parcel model SPACCIM

It has been well received in the atmospheric community that clouds play an decisive role in the processing and cycling of chemical constituents in the atmosphere. Moreover, in reality the multiphase processing of different constituents in the clouds as well as in the deliquescent particles, are closely associated with the microphysical processes. Since, the experimental effort can't provide the understanding about these processes along with the interactions in the molecular level, multiphase modeling frameworks including detailed microphysics are widely used. While reflecting the simplified description of reality, they merely provide a limited information. Hence, during the last two decades, several modeling frameworks were developed within the climate research community, ranging from detailed process models to statistical models, from 0-dimensional to 3-dimensional models and from local area to global models. Depending on the spatial and temporal scale and the nature of the studied atmospheric phenomenon, different models will be appropriate while receiving the great advances on developing model representations of these processes for instance, microphysics, heterogeneous chemistry and gas-particle partitioning.

One of such detailed modeling framework, SPACCIM was developed while integrating the detailed microphysical processes and the treatment of multiphase chemistry, for a size-resolved deliquescent particle as well as drop spectrum in a box model framework (see [Wolke et al. \(2005\)](#)). Atmospheric box models ([Gregoire et al., 1994](#)) are usually based on a set of ordinary differential equations (ODE) describing these aforementioned processes with appropriate formulations for modeling the gas-liquid mass transfer. The time evolution of the concentrations of chemical species in the gas and in the aqueous phases can be usually, described through a set of ODE in the box model frameworks. In this parcel model SPACCIM, the air parcel follows a predefined artificial trajectory, which depends on the meteorological forcing, including the cloud passages and intermediate aerosol states while varying the pressure and relative humidity. Their interaction including the information exchange was realized using a coupling scheme with a fixed coupling time step. Thus, the model allows a detailed description of the processing of gases and deliquescent particles before the cloud formation, under cloud conditions and after cloud evaporation. In subsequent sections, the description of the existing model, where the aqueous phase chemistry is considered as "ideal" solutions, will be outlined sequentially (i) microphysical model formulation, (ii) numerical description of multiphase chemistry, (iii) coupling between microphysical and multiphase chemistry model and their intercommunication.

4.1 Microphysical processes

The microphysical model in SPACCIM model framework built upon the work of [Simmel et al. \(2002\)](#), [Simmel et al. \(2005\)](#) as well as [Simmel and Wurzler \(2006\)](#). While using an artificial adiabatic air parcel, this model can able to describe the sectional cloud microphysical processes such as growing and shrinking of aerosol particles by water vapor diffusion, evaporation and

condensation...etc. The description of both equilibrium growth theory and modeling of cloud droplet activation explained in Sec. 2.2 were integrated in this model. The most relevant processes and their representation in the microphysical model will be described in preceding subsections.

4.1.1 Equilibrating particle water content

The equilibrium condition for gas-aerosol water vapor transfer for an aerosol particle is more complicated than that for a bulk liquid that shares across interface with the vapor phase. Unlike the bulk phase case, liquid-phase droplets are small and usually near-spherical and so the Eq. 2.26 must be considered for the curvature of the droplet (Pruppacher and Klett, 1997). For the mass transfer and the aqueous chemistry, well-diluted droplets are assumed. As a result, the water activity was considered as unity, since the solutions were considered as ideal, and the surface tension was same with pure water surface tension.

Hence, the solution for this equilibrium by holding the ambient relative humidity as fixed and changing the particle water content, and thus solute fraction, until Eq. 2.29 is satisfied within some specified error. This assumption during the equilibration process is fair since the particles are equilibrated one at a time and each particle contains very little water in absolute terms. The search can be explained for a single particle, by calculating a water residual, X_w , which can compare to an error tolerance. Hence the water residual can be computed as follows:

$$X_w = \frac{n_w}{n_w + n_s} \exp\left(\frac{2\sigma_{s/a}m_p}{r_aRT\rho}\right) - RH \quad (4.1)$$

If X_w is less than zero, the particle is too dry compared to the vapor phase and one can add more water to the aerosol; if X_w is greater than zero, the particle is too moist thus one can take water away. Using this directional guideline, the equilibration is a simple bisectional search:

1. Depending on whether X_w is positive or negative, the water content can be halve or double repeatedly. Recalculate X_w after each successive iteration and stop after X_w changes sign which illustrate us, that we overshoot the equilibrium point, while set aside the absolute size of the last halving or doubling step in terms of water molecules.
2. Then halve the last step size and retreat that much towards the equilibrium point, using the sign of X_w to determine, if that amount is to be added or subtracted.
3. Now recalculate the water residual (X_w). If obtained absolute value is smaller than some error tolerance, the Eq. 2.29 should be satisfied and the routine should end. Otherwise, proceed with step 2.

Note that this equilibration is performed especially during the initialization. While changing the water vapor content in the local system by the appropriate amount to offset the liquid water added or subtracted from the equilibrated particle. As alluded to above, this equilibration routine is useful primarily for initialization or studies in environments less moist than saturated. Among the assumptions implicit in this equilibrium model are that equilibration is effectively instantaneous with respect to the time scales on which the background environment changes, and that aerosols equilibrate dependent of one another.

4.1.2 Water condensation and evaporation

The both equilibrium and dynamic growth was implemented according to [Simmel and Wurzler \(2006\)](#). The dynamical description of condensation/evaporation rate $I(m)$ due to water vapor diffusion processes in General Dynamic Equation (GDE) ([Friedlander, 1977](#)), which governs the physical processes undergone by particles can be described by growth equation and the mass flux of the water vapor onto a deliquescent particle with the size k (see [Rogers and Yau \(1989\)](#); [Pruppacher and Klett \(1997\)](#) and references therein) is given by:

$$I(m) = \frac{dm_k}{dt} = \frac{4\pi r_k \left(S - 1 - \frac{A}{r_k} + \frac{B}{r_k^3} \right)}{[T_{therm} + T_{diff}]}, \quad (4.2)$$

where S can be taken into account as ambient saturation ratio and

$$T_{therm} = \left(\frac{L}{R_v T} - 1 \right) \frac{L \rho_w}{KT}; \quad T_{diff} = \frac{\rho_w R_v T}{De_s(T)}, \quad (4.3)$$

including the thermodynamic term associated with heat conduction and that considering the vapor diffusion respectively. D stands for the molecular diffusion coefficient, e_s is the equilibrium vapor pressure over the surface of a spherical droplet of radius r and density ρ_w at the temperature T , R_v is the universal gas constant for water vapor. Apart from these, the correction terms were also considered here for instance, the correction term for diffusivity $D_{\nu,k}^*$ as:

$$D_{\nu,k}^* = \frac{D_{\nu,k}}{\left(\frac{r_k}{r_k + \Delta_v} + \frac{D_{\nu,k}}{\alpha_c r_k} \sqrt{\frac{2\pi M_w}{RT_\infty}} \right)}, \quad (4.4)$$

with diffusivity $D_{\nu,k}$ of water vapor in $cm^{-2}s^{-1}$ (at $T_0 = 273.15K$ and $p_0 = 1013.25$ hPa)

$$D_{\nu,k} = 0.211 \left(\frac{T}{T_0} \right)^{1.94} \left(\frac{p_0}{p_\infty} \right) = 4.0122 \cdot 10^{-5} \left(\frac{T^{1.94}}{p_\infty} \right), \quad (4.5)$$

and the corrected thermal conductivity $\kappa_{a,k}^*$

$$\kappa_{a,k}^* = \frac{\kappa_{v,k}}{\left(\frac{r_k}{r_k + \Delta_T} + \frac{\kappa_{v,k}}{\alpha_T C_p \rho_{air} r_k} \sqrt{\frac{2\pi M_{air}}{RT_\infty}} \right)}, \quad (4.6)$$

with the thermal conductivity $\kappa_{v,k}$

$$\kappa_{v,k} = 418.5 * 10^{-5} [5.69 + 0.017 (T_\infty - 273.15)]. \quad (4.7)$$

The corrected thermal conductivity $\kappa_{a,k}^*$ of moist air and the diffusivity of water vapor $D_{\nu,k}^*$ are used in the growth equation due to the kinetic effects near the particle interface (see [Pruppacher and Klett \(1997\)](#)). In this regarding please note that, the rate of condensation/evaporation strongly depends on the size and chemical composition of the particles. The free energy barrier which has to be surmounted for coating the particles increases with decreasing size and salt content. The formulation of growth by diffusion is based on some assumptions which are not always satisfied ([Sehili et al., 2005](#)). When dealing with particles ranging in size from sub microns to several hundred of microns the so called kinetic effect has to be considered. For large particles, the continuum theory is the appropriated framework and for smaller ones the kinetic theory of

the gases governs the flow. Interpolation formulas exist, (for instance [Fukuta and Walter \(1970\)](#)) allowing a correction for the transition regime.

4.2 Multiphase chemistry model

As described earlier SPACCIM treats the multiphase chemistry and microphysical processes for a size-resolved droplet spectrum in a box model. The droplets are subdivided into several classes $k = 1, \dots, M$. This decomposition of the droplet spectrum into classes is based on their droplet size and the amount of scavenged material inside the drops, respectively. The assumption was, that the size distribution and all other microphysical parameters were given a priori by a microphysical cloud model. In each of the M droplet classes, N_A aqueous phase species are considered. Some of these aqueous phase species interact with one of the N_G gas phase species. One should have to note that the number of species in the gas phase must not be necessarily the same as the number of aqueous species which occur in all droplet classes.

4.2.1 Mass balance equations

The prognostic equations for the mass concentration of gas phase chemical species $c_{l^*}^G$ and an aqueous phase chemical species c_l^k in the k -th size bin inside of a box can be described by the following mass balance equation.

$$\frac{dc_{l^*}^G}{dt} = R_{l^*}^G(t, c_1^G, \dots, c_{N_G}^G) - \kappa_l \sum_k^K L_k \cdot k_t^{kl} \cdot \left[c_{l^*}^G - \frac{m_l^k}{H_l} \right] - \mu \cdot [c_{l^*}^G - c^{G_{ent}}], \quad (4.8)$$

$$\begin{aligned} \frac{d(c_l^k)}{dt} = & L_k \cdot R_l^A(t, m_1^k, \dots, m_{N_A}^k) + \kappa_l \cdot L_k \cdot k_t^{kl} \cdot \left[c_{l^*}^G - \frac{m_l^k}{H_l} \right] \\ & + T(c_l^1, \dots, c_l^M) + \mu \cdot [c_l^k - c_l^{k_{ent}}], \end{aligned} \quad (4.9)$$

with $l^* = 1, \dots, N_G$; $l = 1, \dots, N_A$; $k = 1, \dots, M$,

where L_k denotes the volume fraction $[V_k/V_{box}]$ of the k^{th} droplet class inside the box volume. The variables $m_l^k, k = 1, \dots, M$, are the liquid-phase concentrations of the l^{th} species in the k^{th} liquid water fraction and $c_{l^*}^G$ is the concentration of the "corresponding" gas phase species. The chemical reaction terms are denoted by $R_{l^*}^G$ and R_l^A . The second term on the right-hand side describes the interchange between the gas and aqueous phases. It will be referred to as the Henry term in the following. The pre factor κ_l of the Henry term is a solubility index and defined to be equal to 1 as well as 0 for soluble and insoluble species, respectively (see [Wolke et al. \(2005\)](#)). The term $T(c_l^1, \dots, c_l^M)$ in Eq. 4.9 stands for the mass transfer between different droplet classes by microphysical exchange processes of liquid water (e.g., by aggregation, break up, condensation). The time-dependent natural and anthropogenic emissions as well as dry and wet deposition are parameterized in the last terms of the right hand sides using the time dependent entrainment/detrainment rate μ .

4.2.2 Description of chemical reactions

In the aforementioned mass balance equations $R_{l^*}^G$ and R_l^A describes the chemical reaction terms. To get the information about the kinetics of phase transfer from gas-phase to condensed phase

of aerosols is necessary for accounting the corresponding atmospheric processes for instance multiphase or heterogeneous chemistry (Charlson et al., 1992; Seinfeld and Pandis, 1998). This is realized by incorporating the multiphase chemistry mechanism containing generally two chemical reaction types. (i) irreversible reactions such as photolysis reactions, temperature dependent and temperature independent reactions, (ii) equilibrium reactions such as dissociation and hydration reactions. However, the chemistry in the aqueous phase differs from the gas phase chemistry by the occurrence of fast dissociations. These reaction types in both gas and aqueous phase are presented here with examples.

Irreversible reaction types: Irreversible reactions or forward reactions, which proceed forward direction only, such as photolysis reactions, temperature dependent and temperature independent reactions, contains different formulations as well as a variety of other special reactions. In particular, the gas phase mechanism RACM (Stockwell et al., 1997) includes various reactions which depend on both the temperature and additionally the air pressure or the air density. For the description of these dependencies different reaction parameterizations are used in the mechanism.

Photolysis: The first order photo-dissociation reaction initiated by solar radiation in gas phase chemistry (see Karl et al. (2006)) is explained here with an example of photodissociation of nitrogen dioxide:



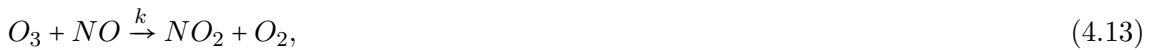
which contributes to the time rate of change of concentrations:

$$\frac{d[NO_2]}{dt} = -J \cdot [NO_2]. \quad (4.11)$$

The reaction rate constant J depends on the intensity of solar radiation I , the absorption cross section of the dissociating molecule (ρ), the quantum yield (i.e. the probability that the molecule dissociated when absorbing solar radiation) φ , and temperature (T) given by Jacobson (1999).

$$J = \int_{\lambda_1}^{\lambda_2} \sigma(\lambda, T) \varphi(\lambda, T) I(\lambda) d\lambda. \quad (4.12)$$

At the same time another most important reaction type is bimolecular or second order reaction, which can be explained with the following example (Karl et al., 2006):



Hence, the time rate of change of mass concentration, which contributes to the mass balance equations shown above:

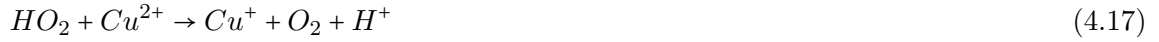
$$\frac{d[O_3]}{dt} = \dots - k \cdot [O_3] \cdot [NO] + \dots, \quad (4.14)$$

$$\frac{d[NO_2]}{dt} = \dots + k \cdot [O_3] \cdot [NO] + \dots \quad (4.15)$$

The term k is the reaction rate constant. In bimolecular reactions, k depends on the temperature and is usually given in Arrhenius form:

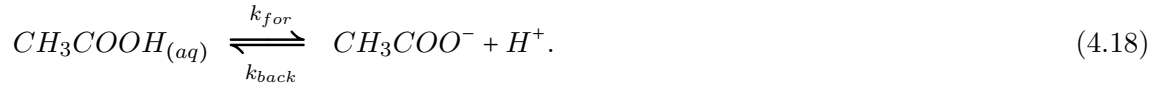
$$k = A_0 \exp(-E_A/RT) \quad (4.16)$$

Accordingly, the temperature dependent irreversible reactions in the aqueous phase can be given as example:



The reaction rates can be constant or take different temperature dependent. If it is constant, the reaction is then temperature independent.

Equilibrium reactions: Equilibrium reactions are those such as dissociation and hydration reactions. These kind of reversible reactions are treated in the model as forward and backward reactions based on the equilibrium constant as well as the backward reaction rate constant. For instance, the treatment of dissociation of acetic acid is implemented in the multiphase chemistry as:



where, the equilibrium constant is $K_{eq} = \frac{k_{for}}{k_{back}}$, which is known in many cases, contributes to the mass balance equations:

$$\begin{aligned} \frac{d[CH_3COOH]_{(aq)}}{dt} &= -k_{for}(T_\infty) \cdot [CH_3COOH]_{(aq)} + k_{back} \cdot [CH_3COO^-] \cdot [H^+] \\ &= -k_{back} \cdot K_{eq, CH_3COOH}(T_\infty) \cdot [CH_3COOH] \\ &\quad + k_{back} \cdot [CH_3COO^-] \cdot [H^+]. \end{aligned} \quad (4.19)$$

4.2.3 Phase transfer processes

By incorporating Schwartz approach (Schwartz, 1986) the interchange between the gas and liquid phases was specified. The eventual equilibrium concentration reached by a molecule A between the gas and the liquid phase can be described as Eq. 2.14. The value H_l denotes dimensionless Henry's law coefficient (the ratio between concentration in aqueous phase to gas phase) for the l^{th} species. The mass transfer coefficient

$$k_t^{kl} = \left(\frac{r_k^2}{3D_g} + \frac{4r_k}{3\nu\alpha_l} \right)^{-1}, \quad (4.20)$$

depends on the droplet size r_k , the gas diffusion coefficient D_g , the molecular speed ν and the mass accommodation coefficient α_l of the l^{th} species. Two key quantities are important to aerosol gas-liquid mass transfer are the mass accommodation coefficient, α , and the uptake coefficient, γ . These quantities play a decisive role in determining the rate of uptake of gaseous species by, and evaporation from aerosol particles, respectively, governing the timescale for a droplet to attain a equilibrium size (Schwartz, 1986). When a gas-phase species incorporating into a liquid aerosol droplet, that can involve the combination of a several processes as illustrated in Fig. 4.1. Moreover, these contributions taking into account of individual influences of each process

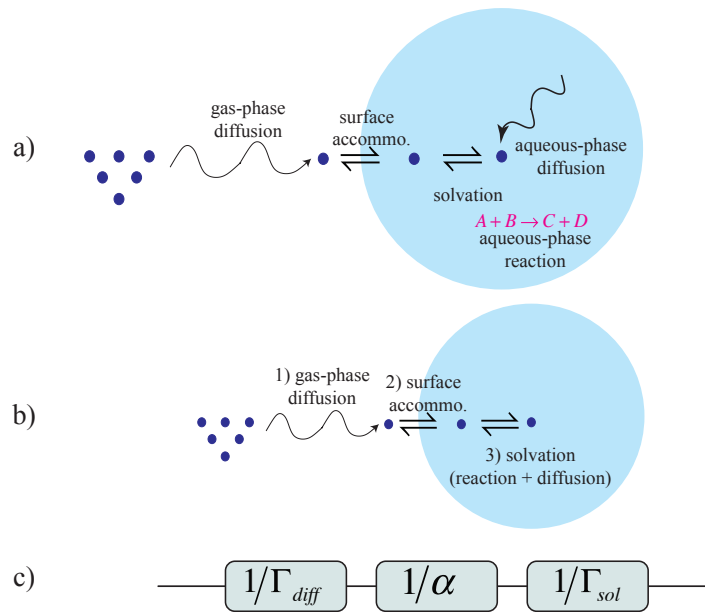


Figure 4.1: Schematic of transport and reactive processes for the uptake in gas-liquid interactions a) Processes involved in uptake of a gas-phase species by a liquid particle. b) Illustration of uptake of three-step process c) electrical resistance analogy for uptake [modified from Davidovits et al. (2006)].

considerably affecting the uptake coefficient γ , by representing the coupled differential equations which can't be solved analytically (Shi et al., 1999). These influences, however, effectively included in the resistance model of gas uptake, an approach first proposed by Schwartz (Schwartz and Freiberg, 1981; Schwartz, 1986). It was always assumed that these individual factors can be decoupled and so allows the individual effects to be interpreted individually. As a result, the following expression was given using the resistance model, which describing the effect of the each and every resistances included independent of reactive or non-reactive uptake processes (Hanson and Ravishankara, 1993; Shi et al., 1999; Davidovits et al., 2006).

$$\frac{1}{\gamma} = \frac{1}{\Gamma_{diff}} + \frac{1}{\alpha} + \frac{1}{\Gamma_{sol}}, \quad (4.21)$$

where $1/\Gamma_{diff}$ is used to describe the resistance to uptake as a result of the rate of gas-phase diffusion, α is the mass accommodation coefficient and $1/\Gamma_{sol}$ describes the resistance to uptake as a result of gas/liquid partitioning. The resistance model for gas uptake is analogous to that of electrical resistance in an electrical circuit. Fig. 4.1 shows an electrical circuit analogy for the uptake processes. As described, continuing the electrical analogy, Γ_{diff} , α and Γ_{sol} can be considered to be conductances for mass transfer. As shown in Fig. 4.1, diffusion stands for the process, as a gas-phase molecules of interest enter the surface their concentration is depleted near to the surface and more must travel to the region close to the surface of the particle. Later, surface accommodation, the proportion of colliding molecules which become incorporated into the particle. Finally, the solvation refers to the combined effect of aqueous phase diffusion and reactions taking place in the aqueous phase.

4.2.4 Microphysical fluxes

From the microphysical point of view, the exchange of liquid water between different droplet classes by aggregation and break up, for instance, takes place in a slower time scale than the aqueous phase chemistry and the phase interactions (Sehili et al., 2005). The liquid water fluxes transport of the corresponding fractions of all included aqueous phase species into other classes. For further presentation, the mass transfer term T was used in the linearized form (Wolke et al., 2005):

$$T(c_l^1, \dots, c_l^M) = \sum_{i=1}^M [T_{ik}c_l^i - T_{ki}c_l^k]. \quad (4.22)$$

In the ODE system Eq. 4.8 and Eq. 4.9, the species within one class are coupled through the chemical reaction system. Furthermore, two types of coupling between different droplet classes can be identified. Firstly, the aqueous phase species within different classes interact directly by the exchange term $T(c_l^1, \dots, c_l^M)$. Additionally, they are indirectly coupled over the gas phase by the phase interchange described by the Henry term.

4.3 Coupling scheme and feedback processes

Since the microphysical and multiphase processes in the troposphere proceed in coupled manner, the microphysical key values such as liquid water content and the droplet surface decide about phase transfer processes of water soluble trace gases and hence the occurring multiphase processes. Due to this reason, a detailed description of multiphase processes combining a complex multiphase chemistry mechanism and a detailed microphysical processes are coupled. Besides, the description of both separate processes were performed for a highly size resolved particle and droplet spectrum, allowing the processing of gases and deliquescent particles before cloud formation, cloud conditions and after cloud evaporation.

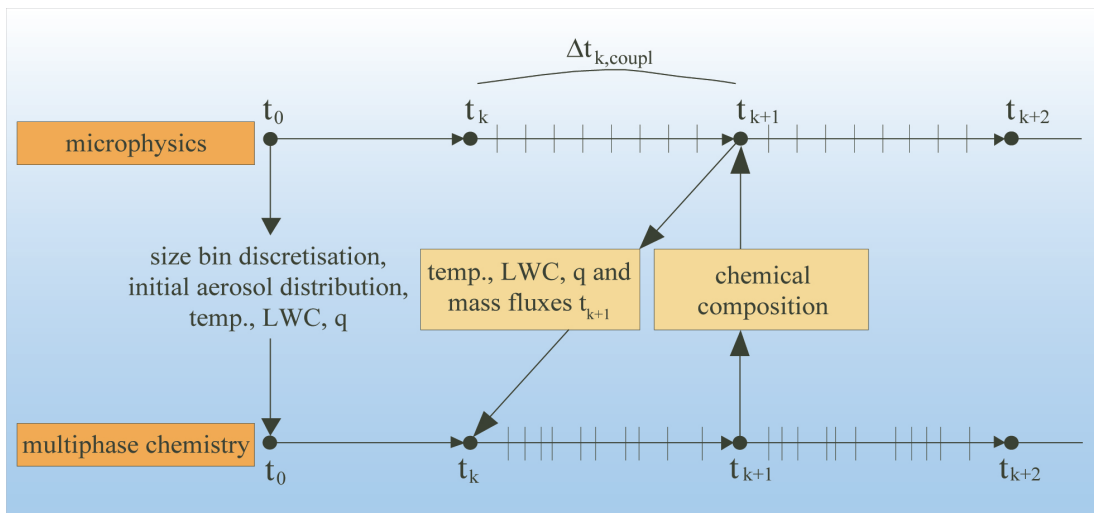


Figure 4.2: Schematic of the model coupling strategy implemented in SPACCIM [source Wolke et al. (2005)].

The coupling between microphysical and multiphase chemical processes realized in SPACCIM is shown schematically in Fig. 4.2. It is implemented in SPACCIM by using so called "operator splitting" techniques. The coupling strategy was explained in detail in Wolke et al. (2005). As shown in Fig. 4.2, the microphysical model is proceeds at first forward. Subsequently, all

microphysical and meteorological parameters as well as mass fluxes $T(L_1c_1^k)$ required for the calculation of the multiphase chemistry are taken over from the microphysical model after a coupling time step. The microphysical model provides both time-interpolated values of the required meteorological variables mainly scalar variables, (like temperature, liquid water content) and averaged mass fluxes $T(L_1c_1^k)$ for each particle/droplet class. After that, the multiphase chemistry is modeled based on the time-averaged mass fluxes. Finally, chemical information regarding changes in chemical composition due to phase transfer and multiphase chemical processes is delivered back to the microphysical model. This allows a continuous feedback of the multiphase chemistry in the microphysical processes such as water condensational growth fluxes as mentioned above. Moreover, both separate operating models uses its individual time-step control. This approach allows the coupling of the complex multiphase chemistry model with microphysical codes of different types. Furthermore, the exchange of information is organized over well-defined interfaces. This is necessary to allow a high regarding the usage of the models with different complexities and numerical costs.

Chapter 5

Model improvements and treatment of non-ideality

An aerosol multiphase chemistry model requires an accurate thermodynamic module to reliably predict particle deliquescence, water content and vapor-liquid phase equilibrium in multicomponent aerosols at a given relative humidity (RH) and temperature (T). It is also needed to compute the mass transfer driving forces for dynamic gas-particle partitioning of various semi-volatile species. An accurate prediction of the competitive growth of different aerosol particles via condensation/evaporation processes requires a dynamic treatment instead of equilibrium processes, driven and constrained by multiphase chemical equilibria. Prediction of these characteristics for a complex, multi-component aerosol is the purview of SPACCIM's thermodynamic and surface tension module, while incorporating efficient calculation of activity coefficients of electrolytes, non-electrolytes and other dissociating species, equilibria for dissociation reactions, equilibrium water content and surface tension. Solid phase species are only included insofar as they are absolutely insoluble species inside the aerosol particles. At the core of the thermodynamic module that estimates the activity coefficients of various organic-inorganic mixtures in multicomponent aqueous aerosols was implemented. Furthermore, the activity coefficients are repeatedly required and calculated for gas-particle partitioning calculations. The schematic of the complete microphysical processes including the aqueous phase thermodynamics and surface tension is shown in Fig. 5.1.

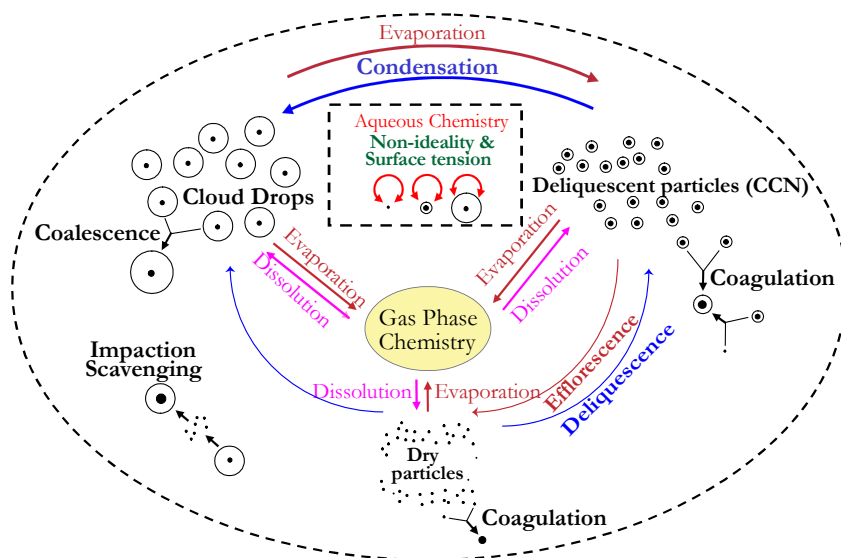


Figure 5.1: Schematic of the microphysical processes included in SPACCIM microphysics model.

Unlike most modules available in the literature, SPACCIM's activity coefficient module is written to be easily specialized or extended to include new species e.g. non-electrolytes. All of the specifics of the activity coefficient model and chemical reactions are read from input files. As a result, updates in interaction parameters can be easily incorporated. Besides, the flexibility of the computer code can facilitate changes easily for the future inclusions.

5.1 Multiphase chemistry approach considering non-ideal solutions

The implementation and consideration of chemical processes follows the same reaction types as explained in Sec. 4.2.1. The gas phase mixture is assumed to behave like ideal gas phase mixture. Hence, the modifications are performed for the aqueous phase reactions, along with gas-particle phase transfer. The description of the performed modifications for the aqueous phase chemistry will be explained in detail in next preceding subsections.

5.1.1 Numerical description of multiphase chemistry

In the original mass balance equations of SPACCIM (see Eq. 4.8 and Eq. 4.9), the molalities were replaced by activities. Activities are considered only in the aqueous phase, the gas phase was considered as ideal gas. The activities are calculated by $a_i = \gamma_i^m \cdot m_i$, where γ_i^m molality based activity coefficient computational methodology was explained in Sec. 3.6. Furthermore, computation of multiphase reactions along with phase transfer is rather difficult under non-ideal conditions. Thus, in a model that resolves aerosol, cloud, and droplets over multiple size bins, aqueous ODEs must be solved between the gas phase and all bins. Thus, the activity coefficients are continuously utilized resulting from aforementioned activity coefficient module. Subsequently, the prognostic equations were developed for the mass concentration of a gas phase chemical species $c_{l^*}^G$ and an aqueous phase chemical species c_l^k in the k -th size bin considering chemical production and degradation, phase transfer along with emission and deposition inside of a box under non-ideal conditions. The modified mass balance equations can be described as:

$$\frac{dc_{l^*}^G}{dt} = R_{l^*}^G(t, c_1^G, \dots, c_{N_G}^G) - \kappa_l \cdot \sum_k^K L_k \cdot k_t^{kl} \cdot \left[c_{l^*}^G - \frac{a_l^k}{H_l} \right] + \mu \cdot [c_{l^*}^G - c^{G_{ent}}], \quad (5.1)$$

$$\begin{aligned} \frac{d(c_l^k)}{dt} &= L_k \cdot R_l^A(t, a_1^k, \dots, a_{N_A}^k) + \kappa_l \cdot L_k \cdot k_t^{kl} \cdot \left[c_{l^*}^G - \frac{a_l^k}{H_l} \right] \\ &+ T(c_l^1, \dots, c_l^M) + \mu \cdot [c_l^k - c_l^{k_{ent}}], \end{aligned} \quad (5.2)$$

with L_k denotes the volume fraction $[V_k/V_{box}]$ of the k -th droplet class inside the box volume. The vectors $a^k, k = 1, \dots, K$, are the activities of the species in the k -th liquid water fraction and the vector c^G stands for the concentrations of the gas phase species. The modified mass balance equations that can treat the non-ideality along with phase transfer has been presented in, Eq. 5.1 and Eq. 5.2 in comparison with equations Eq. 4.8 and Eq. 4.9. The main differences in these two versions can be observed in (i) the mass transfer term and (ii) the chemistry term. The modifications are necessary in these terms, since the activities have to be used instead of concentrations under the non-ideal conditions.

5.1.2 Reaction kinetics and coefficients

The first term in the right hand side of the aforementioned mass balance equations, gives the information about the chemical transformations. However, the reaction term included in Eq. 5.1 is only a function of gas phase species. Therefore, the non-ideality is not considered in this term, since the gas phase chemistry is treated as ideal gas phase at STP conditions. The activity coefficients are considered only in the aqueous phase reaction kinetics.

Suppose, for an irreversible reaction $A + B \rightarrow C$, the rate of the reaction, r_A can be written for ideal solutions as:

$$r_A = -k_A \cdot [A] \cdot [B] \quad (5.3)$$

However, the reactivities of A, B, C, and D have to be used in place of the concentrations. The reactivity of A ($\{A\}$) is proportional to $[A]$, and the proportional constant is the activity coefficient γ . Hence, the rate constant for this reaction, considering non-ideal solutions can be written as:

$$r_A = -k_A \cdot [a_A] \cdot [a_B] = -k_A \cdot \gamma_A [A] \cdot \gamma_B [B] \quad (5.4)$$

However, apart from the irreversible reactions the equilibrium reaction types were also can explained for the change in the number of moles dn_i of each reactant $i = A, B, D, E$, etc. Such processes are described by

$$dn_D D + dn_E E + \dots \rightleftharpoons dn_A A + dn_B B + \dots, \quad (5.5)$$

where the each equilibrium reaction must conserve mass. Thus,

$$\sum_i k_i (dn_i) M_i = 0, \quad (5.6)$$

where M_i is the molecular weight of the species i , $k_i = +1$ for forward reactions, and $k_i = -1$ for backward reactions. Dividing each dn_i by smallest dn_i among all species in Eq. 5.5 gives a set of dimension less stoichiometric coefficients ν_i that can be substituted into Eq. 5.5 to yield the following equilibrium reaction.

$$\nu_D D + \nu_E E + \dots \rightleftharpoons \nu_A A + \nu_B B + \dots, \quad (5.7)$$

Thermodynamic activities in a reversible reaction, such as Eq. 5.7, are related to an equilibrium coefficient, which can be written for the ideal solutions as:

$$\frac{[A]^{\nu_A} \cdot [B]^{\nu_B} \cdot \dots}{[D]^{\nu_D} \cdot [E]^{\nu_E} \cdot \dots} = K_{eq}, \quad (5.8)$$

The similar relation for the equilibrium constant while treating the non-ideality, the expression can be written as:

$$\prod_i \{a_i\}^{k_i \nu_i} = \frac{\{A\}^{\nu_A} \cdot \{B\}^{\nu_B}}{\{D\}^{\nu_D} \cdot \{E\}^{\nu_E}} = \frac{(\gamma_A^{\nu_A} \cdot [A]^{\nu_A}) \cdot (\gamma_B^{\nu_B} \cdot [B]^{\nu_B})}{(\gamma_D^{\nu_D} \cdot [D]^{\nu_D}) \cdot (\gamma_E^{\nu_E} \cdot [E]^{\nu_E})} = K_{eq}, \quad (5.9)$$

where K_{eq} called as equilibrium coefficient, $\{a_i\}$ is the thermodynamic activity of species i , $\{A\}$, etc., are individual thermodynamic activities, $k_i = +1$ for products, and $k_i = -1$ for reactants.

Based on this criterion, for the multiphase chemical processes the reaction rates and reactivity terms were relaxed by the activities. The concept of activity introduced in Sec. 2.1.5 is a relative quantity of a substance and is determined differently for each phase. The activity of a gas over a particle surface is its saturation vapor pressure (atm) i.e. the activity coefficient of the gas phase species is considered as unity. Thus,

$$\{A(g)\} = p_{A,s}, \quad (5.10)$$

The activity of an ion in solution or of an undissociated electrolyte is its molality (moles of solute per kilogram of solvent) multiplied by its activity coefficient γ (unit less). Thus

$$\{A^+\} = m_{A^+}\gamma_{A^+}; \quad \{A(aq)\} = m_A\gamma_A, \quad (5.11)$$

respectively. The activity of a liquid water in a particle is the ambient relative humidity. Thus,

$$\{H_2O(aq)\} = a_w = \frac{p_v}{p_{v,s}} = RH, \quad (5.12)$$

where a_w denotes the activity of water, p_v is the partial pressure of water vapor, $p_{v,s}$ is the saturation vapor pressure of water over a bulk liquid surface, and RH is the relative humidity, expressed as a fraction. Solid phase species are only included insofar as they are absolutely insoluble species inside the aerosol and their concentrations do not affect the molalities or activity coefficients of soluble species. Hence, the activity of a pure solid is same as the molarity of the corresponding species i.e. activity coefficient is considered as unity. Hence,

$$\{A(s)\} = m_s, \quad (5.13)$$

which is the concentration of pure solid. Furthermore, the activity coefficients for neutral species that are non-polar (such as $O_{2(aq)}$, $H_{2(aq)}$ and $N_{2(aq)}$) and radicals are also defined as unity, since their reactivity is quite fast and their life time is rather small. The consideration of activities for different types of species are summarized in Table. 5.1

Table 5.1: Description of activities implemented in SPACCIM.

| Activites | Description |
|---|---|
| Activity of a gas over a particle surface | $\rightarrow \{A(g)\} = p_{A,s}$ |
| Activity of an un-dissociated compound | $\rightarrow \{A(aq)\} = m_A\gamma_A$ |
| Activity of an ion in solution | $\rightarrow \{A^+\} = m_{A^+}\gamma_{A^+}$ |
| Activity of liquid water in a particle | $\rightarrow \{H_2O(aq)\} = a_w$ |
| Activity of a solid | $\rightarrow \{A(s)\} = m_s$ |

5.1.3 Equilibrium and non-equilibrium across the gas and aerosol phases

This model framework allows, gas-to-particle transfer of volatile species, besides water vapor. The standard path of an ambient gas-phase molecule into an aerosol particle follows a two step process (see Fig. 4.1). Away from equilibrium, the Fickian diffusion-limited growth model Pruppacher and Klett (1997) has been included, driven by the gradient between the actual

and equilibrium surface concentrations of a given species. The primary difference between dissolution of volatile non- H_2O species and condensation of water vapor is in the way we define $C'_{a,i}$. For condensation, a simple scaling of the local saturation water vapor concentration has been used, while for dissolution the generalized form of Henry's law which depends on particle-specific as well as ambient environmental conditions has been used. As described about the condensation in Sec. 4.1.2, the focus is to develop an appropriate formulation for $\left(\frac{dc_i}{dt}\right)_{\text{gas/aerosol transfer}}$ in a diffusion limited framework, under non-ideal conditions. In this case, a gradient expressing the extent of disequilibrium drives the trace species towards the equilibrium condition. Moreover, the saturation vapor pressure of gas A can be determined from the equilibrium relationship $A_{(g)} \rightleftharpoons A_{(aq)}$. Thus, in terms of an arbitrary gas q the Henry's constant can be defined as

$$p_{q,s,i} = \frac{m_{q,i}}{H_q}. \quad (5.14)$$

The above equation can be expressed in terms of concentrations rather than molalities and partial pressures, under non-ideal conditions as:

$$C'_{a,i} \approx \frac{p_{a,i}}{RT} = \frac{m_i \gamma_i}{H_i RT} = \frac{c_i \gamma_i}{M_w c_w H_i RT}, \quad (5.15)$$

where H is known as Henry's law constant in $M \text{ atm}^{-1}$. Apart from the chemical transformations, using appropriate form of the equation of state ($p = c \cdot R \cdot T$) and defining the mass transfer coefficient (k_t) shown in Eq. 4.9, we may restate the mass transfer rate as a simple ordinary differential equation in which the rate of change of the particle-phase concentration (c_i) of species i is proportional to the gradient between the local ambient (C_i) and effective saturation concentration or activity just above the interface of the particle and gas phases:

$$\frac{dc_i}{dt} = k_t \left(C_i - \frac{a_i}{H_i} \right). \quad (5.16)$$

Here H_i is dimensionless Henry's law constant for i^{th} species, M_w is the molecular mass of water and H . Eq. 5.15 pertains to the case of a single gas phase species equilibrating between the gas and aqueous aerosol phases. H may also be defined for a dissolving species that dissociates after the phase transfer process has done as single or multi step process. This can be explained with the example of acetic acid which comes from gas phase and further dissociates in to aqueous phase:



Hence, the time rate of change of mass concentration, due to the phase transfer which contributes to the mass balance equations shown above:

$$\frac{d[CH_3COOH_{(aq)}]}{dt} = k_t \left(C_{CH_3COOH_{(g)}} - \frac{m_{CH_3COOH_{(aq)}}}{H} \right) \Big|_{ideal}. \quad (5.19)$$

For the treatment of non-ideality, in the above reaction the aqueous phase concentrations are replaced by activities:

$$\frac{d[CH_3COOH]_{(aq)}}{dt} = k_t \left(C_{CH_3COOH(g)} - \frac{a_{CH_3COOH(aq)}}{H} \right) \Big|_{non-ideal}. \quad (5.20)$$

The discussion for the formulation of Henry's law constant in detail, is not the main focus, however, as they follow directly from equation Eq. 5.8. However, one must note briefly that H_i involves two aqueous species when the dissolving gas species dissociates or incorporates an ion. This can be explained as follows:

$$\begin{aligned} \frac{d[CH_3COOH]_{aq}}{dt} \Big|_{ideal} &= -k_{for}(T_\infty) \cdot [CH_3COOH] + k_{back} \cdot [CH_3COO^-] \cdot [H^+] \\ &= -k_{back} \cdot K_{eq,CH_3COOH}(T_\infty) \cdot [CH_3COOH] \\ &\quad + k_{back} \cdot [CH_3COO^-] \cdot [H^+]. \end{aligned} \quad (5.21)$$

However, the above equation for the non-ideal solutions can be written as:

$$\begin{aligned} \frac{d[CH_3COOH]_{(aq)}}{dt} \Big|_{non-ideal} &= -k_{for}(T_\infty) \cdot [CH_3COOH] \cdot \gamma_{CH_3COOH} \\ &\quad + k_{back} \cdot [CH_3COO^-] \cdot \gamma_{CH_3COO^-} \cdot [H^+] \cdot \gamma_{H^+} \\ &= -k_{back} \cdot K_{eq,CH_3COOH}(T_\infty) \cdot [CH_3COOH] \cdot \gamma_{CH_3COOH} \\ &\quad + k_{back} \cdot [CH_3COO^-] \cdot \gamma_{CH_3COO^-} \cdot [H^+] \cdot \gamma_{H^+}. \end{aligned} \quad (5.22)$$

Comparing the Eq. 5.21 and Eq. 5.22, the equilibrium constant K_{eq} can be written as for ideal solutions:

$$K_{eq}|_{ideal} = \frac{[CH_3COO^-] \cdot [H^+]}{[CH_3COOH]_{(aq)}}. \quad (5.23)$$

Similarly, the equilibrium constant for non-ideal solutions, which includes the activities ($a = f(\gamma)$) instead of concentrations can be written as:

$$K_{eq}|_{non-ideal} = \frac{[CH_3COO^-] \cdot [H^+]}{[CH_3COOH]_{(aq)}} \times \frac{\gamma_{CH_3COO^-} \cdot \gamma_{H^+}}{\gamma_{CH_3COOH}}. \quad (5.24)$$

Hence, the correction factor including the ratio of activity coefficients gives the equilibrium (K_{eq}) in the non-ideal solutions, which are implemented in this study. Considering the population of N_A particles associated, we state the appropriate expression for gas-phase loss (following Jacobson (1997b)):

$$\frac{dC_i}{dt} = - \sum_{A=1}^{N_A} k_t \left(C_i - \frac{a_{s,A,i}}{H_i} \right). \quad (5.25)$$

Thus, a set of ordinary differential equations can be define, that includes Eq. 5.25 for each aerosol or group of aerosols. The numerical solution methods to solve these equations will be discussed in succeeding subsections.

5.2 Modified coupling scheme

The mass fluxes T and all meteorological parameters needed by the multiphase chemistry are taken from the microphysical model, since the microphysical and multiphase chemical processes proceed in coupled manner. Thus, the current coupling scheme has been modified between microphysical and multiphase chemical models where the activity coefficients and surface tension effects must be considered in both multiphase chemistry and microphysical models. As described in [Sehili et al. \(2005\)](#), the coupling scheme provides time-interpolated values of the meteorological variables (temperature, water vapor, liquid water content), can generate time averaged mass fluxes T over the coupling time interval. The changes in the chemical aerosol composition by gas scavenging and the chemical reactions, have a continuous feedback on the microphysical processes (e.g., water condensation growth rates via changes in surface tension and the Raoult term). Therefore,

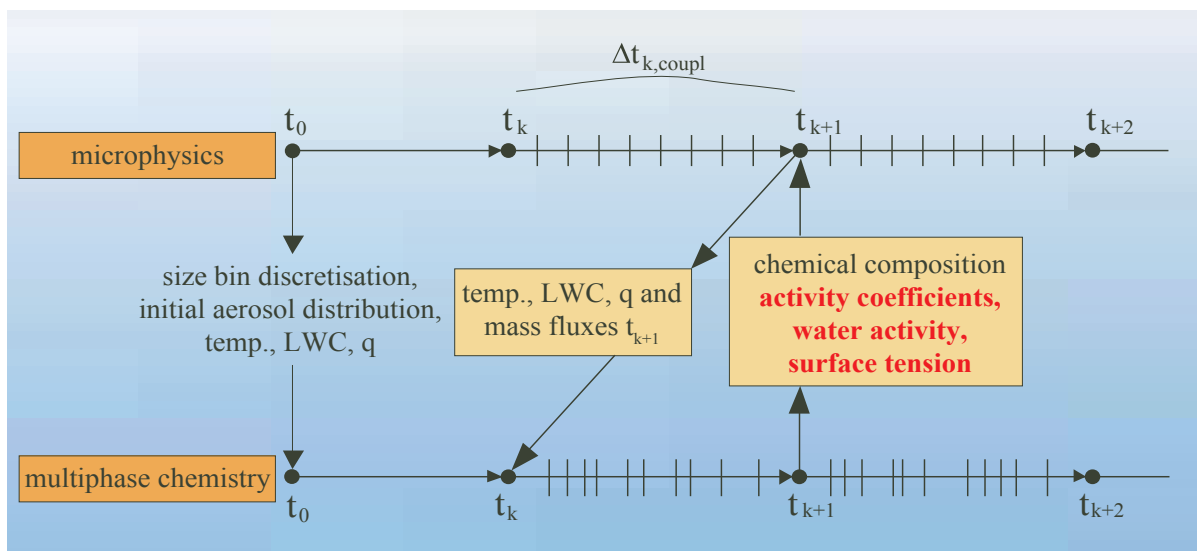


Figure 5.2: Schematic of the model coupling strategy and its implementation considering the treatment of non-ideality and surface tension effects in SPACCIM.

the modified chemical composition of the particle/drop spectrum, has to be taken into account by the microphysical model similar to [Wolke et al. \(2005\)](#). Apart from the chemical information regarding changes in chemical composition due to phase transfer, the activity coefficients as well as surface tension, computed in each time step are delivered back to the microphysical model. The schematic representation of the coupling scheme between microphysical and multiphase chemical models, their inter exchange and feedback while considering the non-ideal solutions and surface tension effects, implemented in the coupling scheme has been shown in Fig. 5.2. As highlighted in the Fig. 5.2, the description of microphysical and multiphase chemical processes are realized in SPACCIM, follows the same "operator splitting technique" as discussed in [Sehili et al. \(2005\)](#). This coupling strategy also allows a continuous feedback of the multiphase chemistry in the microphysical processes such as water condensational growth fluxes as mentioned above. Moreover, both separate operating models also use its individual time-step control as performed in [Wolke et al. \(2005\)](#), in order to allow a high regarding the usage of the models with different complexities and numerical costs. Coupling between the complex multiphase chemistry model and the detailed microphysical model under non-ideal conditions presented above implies the

definition of an interface for intercommunication of codes. For that, the different kind of variables are arranged and implemented, compatible with [Sehili et al. \(2005\)](#).

5.3 Feedback of non-ideal multiphase chemistry on microphysics

As presented in coupling scheme in Fig. 5.2, SPACCIM also, allows the feedback of chemical particle composition onto microphysics. The original Raoult term in the condensation rate was replaced by the sum of the molar ratios of all soluble species included in the multiphase system (see [Wolke et al. \(2005\)](#)):

$$Raoult_{chem}^k = \sum_i^{N_A} mol_{sol_i}^k / mol_w^k. \quad (5.26)$$

Here, the quantities $mol_{sol_i}^k$ of soluble material are obtained from the multiphase chemistry and kept constant in the microphysical calculations over the coupling time interval. The molar water fraction mol_w^k is taken directly from the microphysics. The sum $\sum_i^{N_A} mol_{sol_i}^k / mol_w^k$ goes through all soluble species.

While treating the aqueous phase chemistry as non-ideal solutions, the water activity given by the activity coefficient model is used directly for the Raoult term in microphysics. The condensation/evaporation of water vapor was described after [Pruppacher and Klett \(1997\)](#) by Eq. 4.2. The curvature effect (Kelvin term) represented by A and the solution effect (Raoult term) represented by B are computed according to the Eq. 2.28 and Eq. 2.27, respectively in the current version of SPACCIM. As can be seen, in Fig. 5.2, the chemical composition modified by their corresponding activities, activity coefficient, water activity and the surface tension, those are delivered back to microphysics model at every coupling time step. For this, the water activity of the solution is related to ambient conditions and chemical composition. However, the simple Köhler equation shows that for a curved surface the activity of water is equal to the RH divided by the Kelvin term. Hence, by iterating the Eq. 4.2, a new solution for this equation is calculated, and defined the new equilibrium, since, the water activity is at equilibrium depending on the chemical composition available in the solution at each water content. In order to obtain the solution of Eq. 2.29, a simple bisectional approach was employed to find the exact root. At the same time, the physical characteristics of the chemical composition define a new Kelvin term with the help of appropriate surface tension parameterizations. As soon as the equilibration of Eq. 2.29 is accomplished with certain convergence, the equilibrium saturation ratio is estimated. Subsequently the model proceed further to compute the microphysical variables like LWC, T as well as the mass fluxes at corresponding time step. The description of this algorithm is schematically shown in Fig. 5.3.

In the modified version of the feedback implementation, considering non-ideality and surface tension effects, Eq. 2.29 is iterated in each and every coupling step (Δt) as shown in Fig. 5.3. The Raoult term shown in in Eq. 5.26 is modified in the current version of SPACCIM. The ratios of concentrations in Eq. 2.27 is equal to the ratio of partial pressures shown in Eq. 2.26, therefore, Raoult's law is truly an approximation of the water activity (a_w), as indicated in Eq. 2.27. The resulting water activity from the activity coefficient model and the surface tension from the surface tension models, were updated continuously at every coupling time step as shown Fig. 5.3.

5.4 Implementation and adjustment of numerical schemes

The current version of SPACCIM also uses the same numerical techniques and the nomenclature used in Wolke et al. (2005), i.e., the essence of mathematical arrangements are unchanged. In order to treat the non-ideality for the aqueous phase chemistry the currently using numerical schemes are required to modify in order to solve the mass balance equations (Eq. 5.1 and Eq. 5.2).

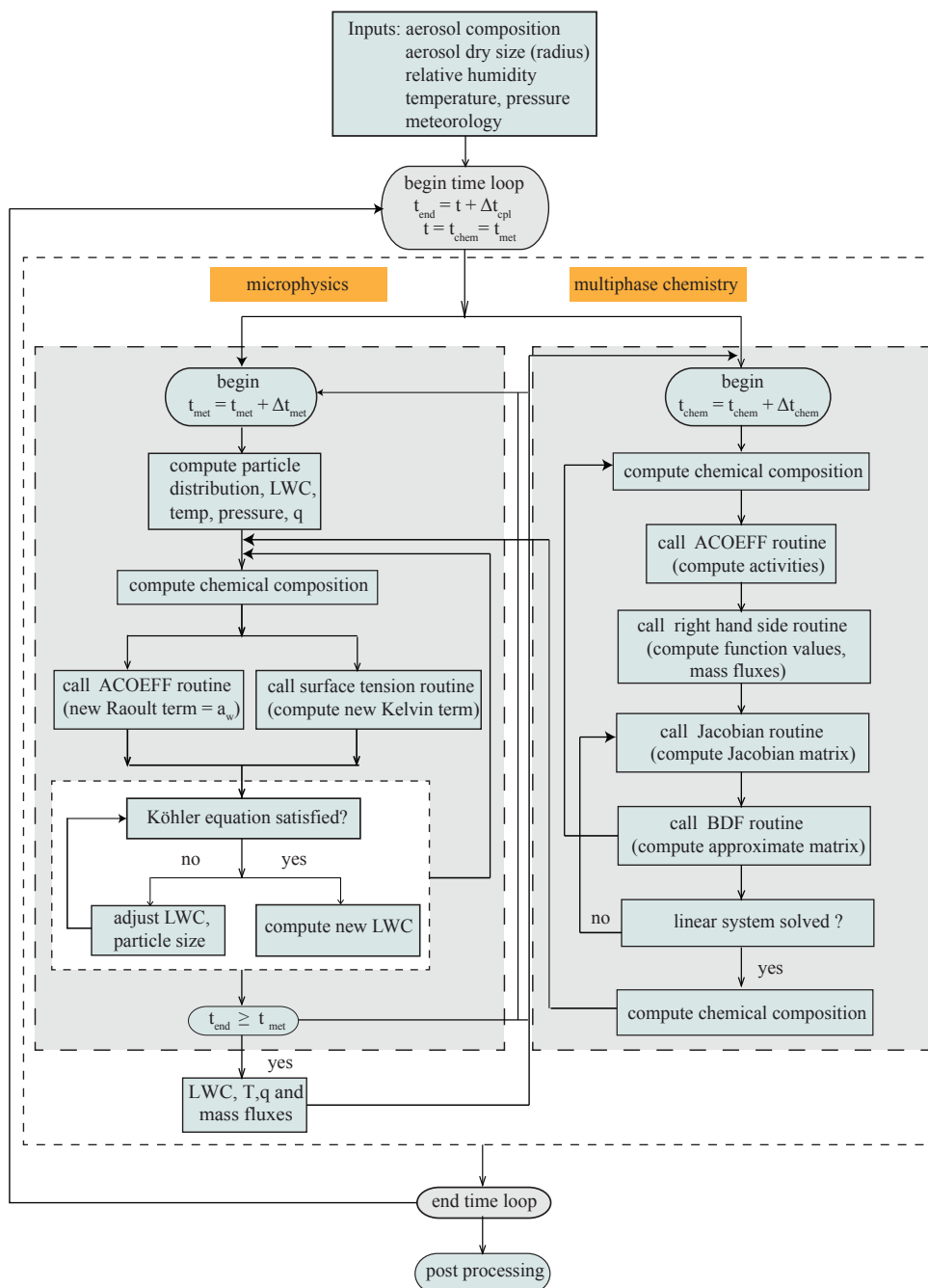


Figure 5.3: Schematic of activity coefficients used in the microphysics and multiphase chemistry models.

5.4.1 Major modifications performed in numerics

Unlike most modules available in the literature, the current implemented activity coefficient and surface tension modules are written to be easily specialized or extended to include new species for instance inorganic ions and organic functional groups for instance ketone and methanol. All of these specifics of the activity coefficient model, surface tension parameterizations and chemical reactions are reading from input files. As a result, updates in interaction parameters, will be easy to incorporate. Besides, the flexibility of the computer code will facilitate changes and future inclusions.

To implement the treatment of non-ideality for aqueous phase chemistry, using the coupled mass balance equations (Eq. 5.1 and Eq. 5.2), the numerical schemes have to be adjusted, mainly (i) time integration scheme, (ii) linear algebra and (iii) the computation of Jacobian matrix apart from the microphysics. Fig. 5.3, shows the implemented scheme and modified numerics along with the utilization of activity coefficient routine in microphysics as well as in multiphase chemistry. To explain the required modifications, the main points of the algorithm presented in detail in Wolke et al. (2005) and Wolke and Knoth (2002) are summarized along with the implementation for non-ideal conditions.

5.4.2 Time integration scheme

The comparison between governing model equations Eq. 4.8 - Eq. 4.9 and Eq. 5.1 - Eq. 5.2 explains the characteristic nonlinearity and interactive coupling of the multiphase chemical system for the ideal and non-ideal approach, respectively. Mainly, the differences between the two approaches consists in the dependence of the reaction and Henry terms on the activities shown in Eq. 5.1 and Eq. 5.2 instead of molalities. Both, molalities and activities, are functions of the mass concentration c . Hence, the abstract formulation for the system Eq. 4.8 - Eq. 4.9 is given as:

$$\left. \frac{dc}{dt} \right|_{ideal} = f_{chem}(t, m(c)) + f_{henry}(t, m(c)) + f_{mphys}(t, c) , \quad (5.27)$$

where $m(c)$ denotes the vector of molalities in aqueous phase. Similarly, in the non-ideal approach, the abstract formulation for the mass balance equation Eq. 5.1 and Eq. 5.2 can be written as:

$$\left. \frac{dc}{dt} \right|_{non-ideal} = f_{chem}(t, a(c)) + f_{henry}(t, a(c)) + f_{mphys}(t, c) , \quad (5.28)$$

where $a(c)$ represent the vector of activities. In both approaches, the resulting ODE systems are integrated by higher order backward differential formula (BDF) schemes (e.g. Hairer et al. (1993)). Thus, the approximations x_{n-k+1}, \dots, x_n to the exact solution of Eq. 5.27 and Eq. 5.28 are known, the derivation of a formula for x_{n+1} needs the consideration of a polynomial $q(t)$ which interpolates the values $\{(t_i, x_i) | i = n - k + 1, \dots, n + 1\}$. The implicit formulas of the BDF scheme are in the form:

$$\sum_{j=0}^k \frac{1}{j} \nabla^j x_{n+1} = h f_{n+1} , \quad (5.29)$$

where ∇^j represents the backward differences

$$\nabla^0 x_n = x_n, \quad \nabla^{j+1} x_n = \nabla^j x_n - \nabla^j x_{n-1}.$$

Accordingly, the use of the BDF implicit multistep method implies the solution of a non-linear equation system

$$F(x_{n+1}) = x_{n+1} - X^n - \beta \Delta t_n f(t_{n+1}, x_{n+1}) = 0, \quad (5.30)$$

where x_{n+1} is the solution vector, $\beta > 0$ a parameter of the integration method which depends on the order of the BDF method and X^n a linear combination of x values at times t_n, t_{n-1}, \dots

Problem Eq. 5.30 is solved by a Newton-like iteration as utilized in [Wolke and Knoth \(2002\)](#). The main task in the algorithm consists in solving linear systems of the form:

$$(I - \beta \Delta t J) \Delta x = b, \quad (5.31)$$

where I denotes the identity matrix and Δt representing the time step size. The matrix J stands for an approximation of the Jacobian $\frac{\partial f(t, x)}{\partial x}$ of the right hand side of the ODE system (the vector b), can be explained as:

$$b = x^n - X^n - \beta \Delta t f(t_n, x^n). \quad (5.32)$$

In the former version, where aqueous phase chemistry is considered as ideal solutions, the exact Jacobian is used as matrix J . Since, only an approximation of the Jacobian is required in the iteration method, J is held constant for several time steps and is recomputed either if the convergence fails or slower (see [Wolke and Knoth \(2002\)](#)).

5.4.3 Linear system solver

Usually, the dimension of the linear system Eq. 5.31 is rather high. Such large systems can be solved with reasonable effort by iteratively or by direct sparse solvers which utilize the special sparse structure of the system. Such solvers are developed and applied in SPACCIM ([Wolke and Knoth, 2002](#); [Wolke et al., 2005](#)). But this effective solvers can only used in the "non-ideal" approach, if the structure remains unchanged. Before this is analyzed, the special structure of the Jacobian is described shortly for the ideal case.

Similar to Eq. 5.27, the Jacobian of the right-hand side ($f(t, m(c))$) can be separated as:

$$J = J_{chem} + J_{henry} + J_{mphys} = \frac{\partial f(t, c)}{\partial c} = \frac{\partial f_{chem}(t, m(c))}{\partial c} + \frac{\partial f_{henry}(t, m(c))}{\partial c} + \frac{\partial f_{mphys}(t, c)}{\partial c}. \quad (5.33)$$

The structure of the Jacobian for two droplet classes is shown in Fig. 5.4. As can be seen, the dots are usually non-zero entries, that means, that the species in the row depends on the species in the column. The diagonal elements of the Jacobian describe the dependence from the species itself. These entries can be caused by chemical reactions and phase transfer, but also by the terms from microphysical fluxes and entrainment.

The block structure in Fig. 5.4 can be explained as follows: the blocks in the diagonal corresponds to the Jacobians of the gas phase and aqueous phase reaction terms, respectively. The upper left block (light blue) represents the gas phase. The other two diagonal blocks (blue) coming

from the aqueous phase chemistry attained to be have the same sparse structure. The green left and upper boundary blocks represent the phase interchange between gas phase species and corresponding liquid species in each class, according to [Schwartz \(1986\)](#). The orange diagonal matrices include the coupling terms resulting from the mass transfer between liquid species and the corresponding species in the other classes.

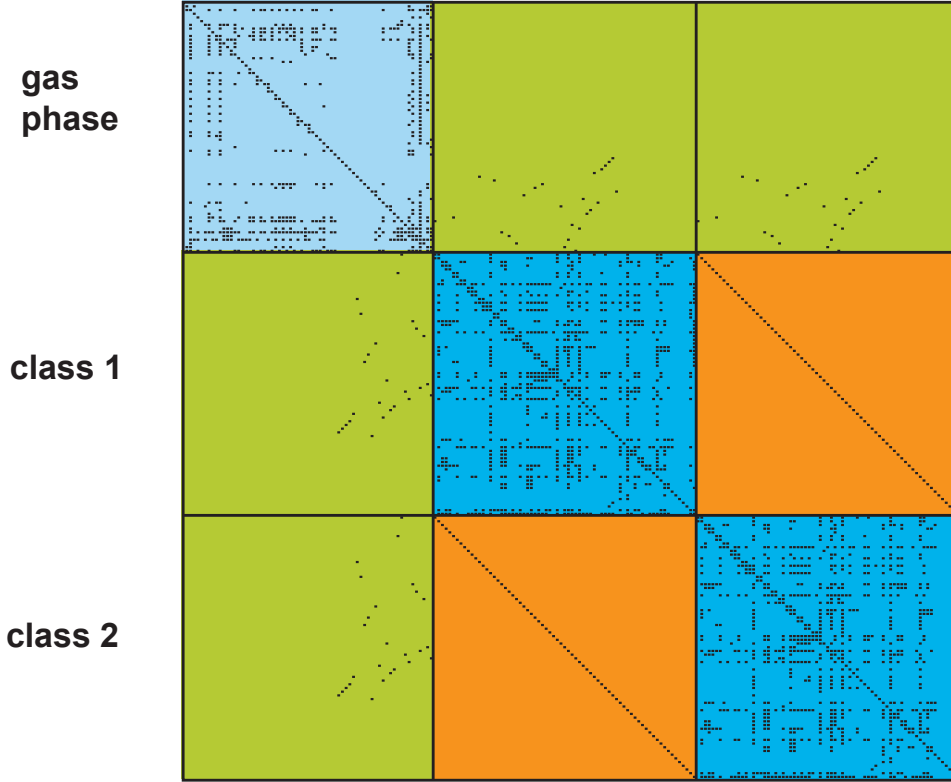


Figure 5.4: Sparse structure of Jacobian and two droplet classes [adapted from [Wolke et al. \(2005\)](#)].

As mentioned before, an efficient solution of the linear system (Eq. 5.31) by direct methods is only possible by utilizing the special properties of the Jacobian (sparsity, block structure, different types of coupling). In SPACCIM, enhanced direct sparse solvers are adjusted to the special structure of the system (see [Wolke and Knoth \(2002\)](#); [Wolke et al. \(2005\)](#)). In the implementation, the sparse block matrices are generated explicitly and stored in a sparse form. The sparse factorization is stored and performed only when the Jacobian J has been recomputed. Consequently, only one LU decomposition is required as utilized in this approach.

5.4.4 Adjustment of Jacobian calculation and linear system solver

While implementing the treatment of non-ideality, the aforementioned numerical schemes are modified, mainly the computation of Jacobian matrix. In the non-ideal approach, the abstract formulation for the mass balance equations is given as Eq. 5.28. Thus, the approximate solution of this linear system involves the Jacobian of the right-hand side of the ODE system:

$$J = J_{chem} + J_{henry} + J_{mphys} = \frac{\partial f(t, c)}{\partial c} = \frac{\partial f_{chem}(t, a(c))}{\partial c} + \frac{\partial f_{henry}(t, a(c))}{\partial c} + \frac{\partial f_{mphys}(t, c)}{\partial c}. \quad (5.34)$$

While adjusting the solver, initially the differences in the Jacobian J of the right hand side of the systems are analyzed. The microphysical fluxes and the entrainment terms shown in Eq. 5.2 are the same as in the ideal approach, which are directly depends on the mass concentrations. Therefore, the derivatives with respect to mass concentrations are utilized as equal to the former version of SPACCIM. In other words, the orange color matrices shown in Fig. 5.4 are unchanged. The further analysis is performed for the chemistry and phase exchange terms. This is realized, while taking into account the dependencies of corresponding molalities (m) and activities (a) from the concentrations, to clarify the differences between model equations.

For the calculation of the derivatives, the chain rule have to be applied. The outer derivatives with respect to m and a , respectively, have the same structure described in Sec. 5.4.3. Obviously, the main difference consists in the dependency of the activities from all species in the class, exactly speaking, from all species used in the activity coefficient module.

Let c^k be the vector of all concentrations in k^{th} droplet class. In the former approach (considering the ideal solutions) the molalities are depend on the corresponding species regard (i.e $m_j^k(c_j^k)$). While prescribing the liquid water content (L_k) from meteorology, the modifications are performed from ideal to non-ideal solutions:

$$m_j^k = m_j^k(c_j^k) = \frac{c_j^k}{L_k}, \quad (5.35)$$

$$a_j^k = a_j^k(c^k) = \gamma_j^k(c^k) \cdot m_j^k = \gamma_j^k \cdot \left(\frac{c_j^k}{L_k}\right) \cdot \frac{c_j^k}{L_k}. \quad (5.36)$$

The gradient with respect to vector c^k is denoted as:

$$\nabla_{c^k} = \left(\frac{\partial}{\partial c_1^k}, \dots, \frac{\partial}{\partial c_{NA}^k} \right). \quad (5.37)$$

With this definition, this gradient of the molalities for the ideal approach can be extended as follows:

$$\nabla_{c^k} m_j^k(c_j^k)|_{ideal} = \frac{1}{L_k} \cdot (0, \dots, 0, 1, 0, \dots, 0). \quad (5.38)$$

In the above formulation the gradient has only one entry in the j^{th} position, which conserves the structure of the "outer" Jacobian. In contrary, while applying the chain rule, the gradient for non-ideal solutions would be:

$$\nabla_{c^k} a_j^k(c^k)|_{non-ideal} = (\nabla_{c^k} \cdot \gamma_j^k(c^k)) \cdot \frac{c_j^k}{L_k} + \frac{1}{L_k} \cdot (0, \dots, 0, \gamma_j, 0, \dots, 0), \quad (5.39)$$

where the gradient $(\nabla_{c^k} \cdot \gamma_j^k(c^k))$ of activity coefficients depends on the vector of concentrations c^k .

The first term in Eq. 5.39 is a vector with entries in several positions depending on the activity coefficient model. This leads to "fill-in" in the corresponding lines of the Jacobian from aqueous phase chemistry (blue blocks) and Henry terms (green blocks). In consequence, the efficient direct sparse solvers are used in SPACCIM for the linear system cannot be utilized. However, since we need only a "good" approximation for the Jacobian we omit the first term shown in Eq. 5.39, while assuming the variability of the activity coefficients from the concentrations can be neglected

over the time step, since the full Jacobian matrix includes the terms involving derivatives of activity coefficients γ_j with respect to molality of that particular species m_j . Although, the derivative of activity coefficients is omitted, the same data structures are obtained as in case of ideal case. The second term in the right hand side of Eq. 5.39 has the same structure as in the right hand side of Eq. 5.38. Only the non-zero entry in the j^{th} position changes from 1 to γ_j^k . This leads to modifications of the non-zero entries in the Jacobians from the chemistry (blue blocks) and Henry terms (green blocks), but the sparse structure of the systems is conserved effectively.

These corresponding changes are implemented in the current version of SPACCIM. In summary, the implemented very efficient sparse solvers can be utilized also in the "non-ideal" approach. Our experience shows that these modifications works well in order to treat the non-ideality for the aqueous phase chemistry.

Chapter 6

Model results and discussions

6.1 Activity coefficient model verification

Several authors have compared, recently, the well established activity coefficient models, for example the study of Raatikainen and Laaksonen (2005) that could be potentially suitable for modeling of hygroscopic properties of organic-electrolyte particles. On contrary, consideration of organic and inorganic compounds in a atmospheric aerosol systems in a single framework are limited. On the contrary, these models can be divided as groups contribution and substance specific methods. However, this broad classification of models and techniques greatly varying with complexity and range of applicability. The substance specific models (e.g. extended UNIQUAC model), requires individual parameterizations for each specific compound, on the other hand, the group contribution approaches (e.g. UNIFAC) were able to estimate the activities of solutions containing a large fraction of organic compounds by splitting them into functional groups. Since the parameterizations for substance specific models, were fitted with respect to specific substances, these models are quite accurate compare with group contribution methods. Due to the lack of experimental data from which the model parameters can be derived for considered mixture, the group contribution approaches are frequently used in practice compare with substance specific models. The predictions using the group contribution methods have been successful when dealing with athermal systems and, to a lesser extent, with polar systems. Furthermore, the combinatorial term in UNIFAC is underestimated, where as residual term is overestimated (Voutsas and Tassios, 1996), when dealing with aqueous mixtures and with increasing polarity of the organic solute. However, the models that can treat the organic-electrolyte mixtures of atmospheric interest are limited.

Hence, this study is aimed to compare existing activity coefficient models that might be suitable for modeling of the hygroscopic properties, physico-chemical multiphase processing of the atmospheric organic-electrolyte particles. The second objective is to select suitable approach that can treat the complex mixtures of aqueous organic-electrolyte solutions of atmospheric interest. However, due to the limitation of interaction parameters and to predict the activity coefficients at different concentration levels, these comparisons have been performed in order to select the best approach with possible extent to treat the multicomponent mixtures. After critical evaluation of model performance the AIOMFAC model interaction parameters were extended with mod. LIFAC as mentioned in Sec. 3.6. Furthermore, the extended model results were compared with original AIOMFAC and mod. LIFAC to validate the current implementation. In addition, the model output was compared with AIM III (Aerosol Inorganic Model), which is a basis for comparison and understanding in the atmospheric community. The evaluated model is used for further investigations i.e. investigation of influence of non-ideality on multiphase chemistry in dynamic gas/particle mass transfer models. The comparisons were performed in a sequential order. At

first the comparison is performed for selected binary aqueous electrolyte solutions, then aqueous organic solutions, followed by mixtures of aqueous organic-electrolyte solutions.

6.1.1 Comparison with published activity coefficient models

In this section the performance of the selected activity coefficient models is examined, by comparing calculated activity coefficients and water activities with literature data. Although, other data types such as growth factors as a function of RH are available, that could potentially use for comparison, the current predictions are focused on water activities and activity coefficients, since considerable uncertainties were also exist in the experimental growth factors. As per the argument of Raatikainen and Laaksonen (2005), in the study of Cruz and Pandis (2000), there seems to be an artifact in the measurements of the 80% glutaric acid-20% $(\text{NH}_4)_2\text{SO}_4$ particles. Furthermore, measurements from Hämeri et al. (2002) and Prenni et al. (2003) are inconsistent for the same mixture at 303.15K at a RH above 85%. As a result, in this PhD thesis, the model comparisons are based primarily on water activity calculations. Furthermore, the focus is to treat the dicarboxylic and hydroxy-carboxylic acids due to their predominance in the atmosphere, and they serve as surrogates for more complex aerosol organic compounds. For all water activity calculations, the organic acids are treated as non-dissociating solutes, and a single liquid phase is assumed with no solid phases present. All calculations are performed at atmospheric pressure (1 atm) and at 298 K.

The aqueous phase of an aerosol contains considerable amount of electrolyte and non-electrolyte ions, a well performing inorganic model part is envious in order to treat the non-ideality in the inorganic aqueous solutions. The group contribution method UNIFAC (Fredenslund et al., 1975), has been widely used for the mixtures of non-electrolytes, including organic compounds and water. As a result, most of the activity coefficient models for mixed electrolyte-organic aqueous solutions, therefore, UNIFAC approach is used for the organic term for SR interactions. Most of these activity coefficient models for mixed electrolyte-organic water systems incorporate existing electrolyte-water or organic-water activity coefficient models, similar to the work of Ming and Russel (2002). Hence, these models typically reduce and usually holds the same accuracy as the electrolyte-water or organic-water activity models in aqueous electrolyte and aqueous organic solutions respectively. Similar to the investigations of Raatikainen and Laaksonen (2005), only predictive models are used for the comparison. Pitzer model which can treat the electrolytes, UNIFAC to treat the organic compounds, the models i.e. LIFAC (Yan et al., 1999), mod. LIFAC (Kiepe et al., 2006), AIOMFAC (Zuend et al., 2008) and the approach of Ming and Russel (2002). In this context the aforementioned models were implemented in this study. Initially, the predicted model results were compared with original model results, in other words the original model results were reproduced. Afterwards, the intercomparison between the models have been performed.

6.1.1.1 Binary aqueous electrolyte solutions

As explained before, all the selected models have the ion \leftrightarrow ion interaction term, that causes deviations from ideality in aqueous-electrolyte solutions. In order to evaluate the flexibility and reliability of the implemented models, all results are compared with the original models. Fig. 6.1 - 6.2 shows the current predicted results for mean ionic activity coefficients of binary electrolyte salts where the salt molalities vary from 0 to 10 (mol kg^{-1}). The x-axis is the amount of salt (in moles) dissolved in 1 kg of the solvent, with respect to completely dissociated salts into cations

and anions. As can be seen from Fig. 6.1 - 6.2, the current predicted mean activity coefficients of various salts were compared with original LIFAC (Yan et al., 1999) shows in general excellent agreement.

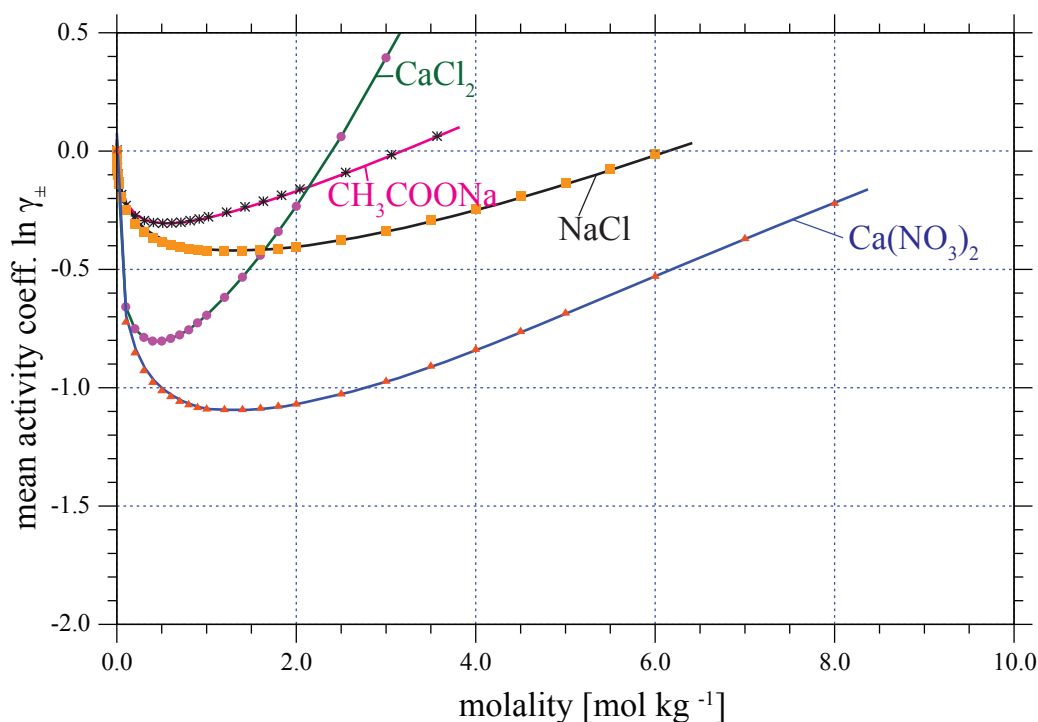


Figure 6.1: Comparison between experimental (symbols) and predicted mean activity coefficients (solid lines) for aqueous electrolyte solutions at 25 °C as a function of molality. Salt molalities 0-10 mol kg⁻¹, γ_{\pm} (————) LIFAC, (\blacktriangle , \bullet , \blacksquare , \star), experimental values from Hamer and Wu (1972).

The current obtained results, from the considered models, where the interaction parameters are fitted to predict the ionic activity coefficients of salts dissolved in water, uses a fixed reference state, that have been seems to rather inaccurate. Moreover, a reliable prediction of LLE using the original LIFAC model is not possible, thus with the variable reference state (see App. B.1) proposed in the work of Kiepe et al. (2006). Furthermore, the prediction of LLE in electrolyte systems have not been considered to be part of the original models. Moreover, it is important when focusing on mean ionic activity coefficient calculations, that are generally not required for the calculation of the VLE. As can be seen from Fig. 6.3 - 6.4, the variable reference state introduced, mean ionic activity coefficients electrolytes in binary non-aqueous mixtures often cannot be described with LIFAC. However, the reliable prediction of activity coefficients with improved reference state calculation, the improved model description of mod. LIFAC (Kiepe et al., 2006) can compute reliable activity coefficients as compare with LIFAC. As can be seen in Fig. 6.3 - 6.4, solely good results were obtained by applying the mod. LIFAC compare with LIFAC. Due to the new normalization of the activity coefficient term for the ion in the MR term as described in Sec. 3.6.2 gives the better accuracy compare with the original LIFAC.

The original LIFAC model is only parameterized up to salt saturation and fails to predict activities of supersaturated solutions. Similar to LIFAC, mod. LIFAC which can able to predict VLE and LLE, cannot predict the deviations from ideality at high salt concentrations. For these reasons the more comprehensive model framework AIOMFAC (Zuend et al., 2008) also

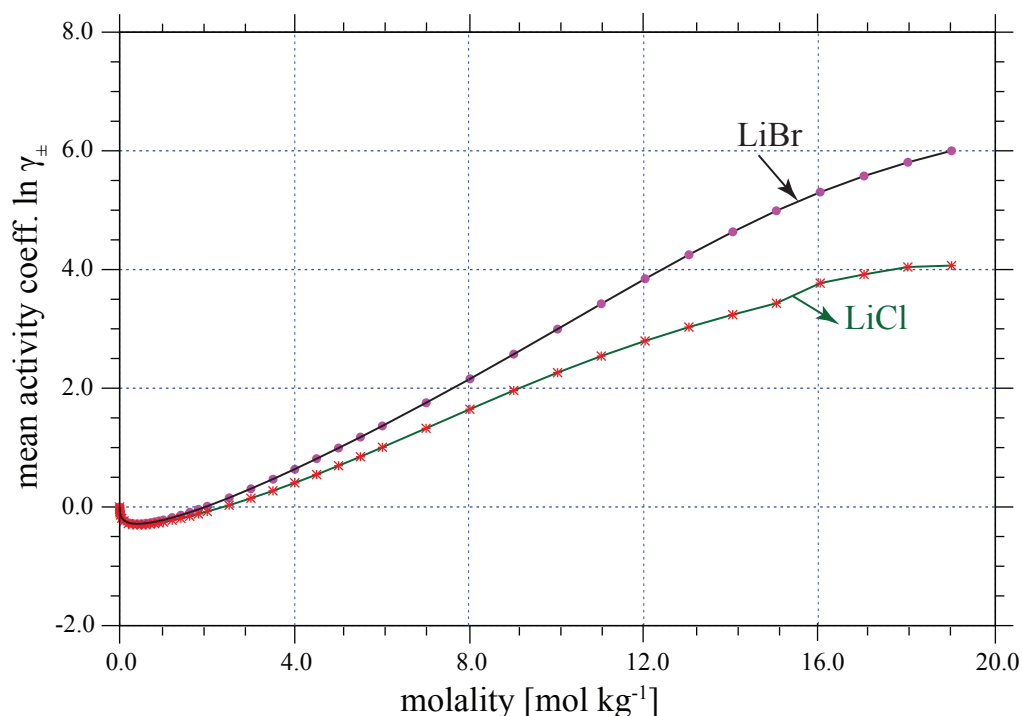


Figure 6.2: Comparison between experimental (symbols) and predicted mean activity coefficients (solid lines) for aqueous electrolyte solutions at 25 °C as a function of molality. Salt molalities 0-20 mol kg⁻¹, γ_{\pm} (—) LIFAC, (\blacktriangle , \bullet , \blacksquare , \star), experimental values from *Hamer and Wu (1972)*.

considered and implemented in this study, which aimed to predict the activities in organic-inorganic multicomponent mixtures up to high ionic strength, since the aqueous phase of an aerosol can contain high amounts of inorganic ions. Fig. 6.5 and Fig. 6.6 shows the comparison between AIOMFAC with current implementation. As can be seen in schematic illustration, barely good results were obtained and the original results were reproduced.

6.1.1.2 Aqueous organic solutions

One disadvantage in this context is the limitation of these group contribution approaches e.g. AIOMFAC to systems at room temperature. In order to describe ion induced liquid-liquid phase separations, models have to explicitly treat the interactions between ions and organics. The occurrence of such phase separations has consequences for the gas/particle partitioning of atmospheric aerosols, because in the case of two liquid phases, partitioning of semi-volatile organics to the particulate phase is enhanced compared with the situation of particles consisting of one liquid phase (*Erdakos and Pankow, 2004*). This increases the amount of particle bound organic mass and decreases the gas phase fraction of semi-volatile components (*Stokes, 1948*).

Besides, we examine the accuracies of the models by comparing experimental and calculated water activities as well as mean activity coefficients. The UNIFAC model is employed to account for organic \leftrightarrow water interactions in all four activity coefficient models. Furthermore, similar sets of UNIFAC interaction parameters (A_{mn} and A_{nm}) was used. However, AIOMFAC and mod.

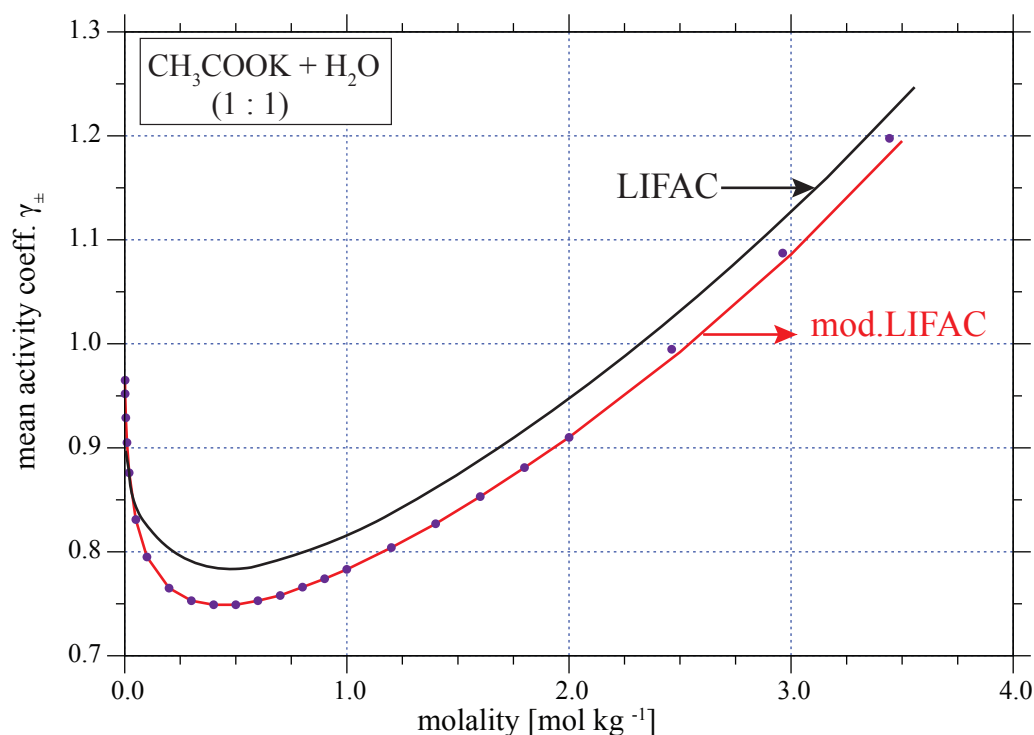


Figure 6.3: Comparison between experimental (symbols) and predicted mean activity coefficients (solid lines) for aqueous electrolyte solutions at 25 °C as a function of molality. Salt molalities 0–4 mol kg⁻¹, γ_{\pm} (—) LIFAC, mod. LIFAC, (●) experimental values from Hamer and Wu (1972).

LIFAC didn't include the COOH functional group. On the other hand, we are aimed to study the behavior of water activities when acids completely dissociated in solutions. Hence, these comparisons were performed with original UNIFAC (Fredenslund et al., 1975) and Ming and Russell approach (Ming and Russel, 2002), which includes the acid group. The sensitivity studies with different data sets are performed by various authors and the resulted predictions are of with comparable accuracy (Tong et al., 2008). Because all the fitted models have the same UNIFAC parameters in non-electrolyte solutions, therefore, the model deviations are compared with those of other UNIFAC-based non-electrolyte models. However, several versions of model interaction parameters are available for the UNIFAC. Hence, the current investigations are aimed to show the deviations between the interaction parameters used in the various studies. Fig. 6.7 - 6.8 shows the comparison between the different interaction parameters. Parameters for the original UNIFAC are adopted from Hansen et al. (1991). The new fitted UNIFAC parameters given by Peng et al. (2001) for OH, H₂O and COOH were also used here for comparison. However, the remaining parameters are the same as in the original UNIFAC. The original UNIFAC and Ming and Russell model interaction parameters have minor differences. However, the current adopted interaction parameters gives the better results as shown in Fig. 6.7 - 6.8.

The present UNIFAC as well as that of Peng et al. (2001) have deviations that are usually less than half of the deviations of the original UNIFAC. The UNIFAC version of Peng et al. (2001) has the smallest deviations. The comparison of predicted water activities and the experimental data were presented in Fig. 6.7 - 6.8. Even though, different data sets are available, all the interaction parameters can be used for atmospheric modeling. However, without fitting of new

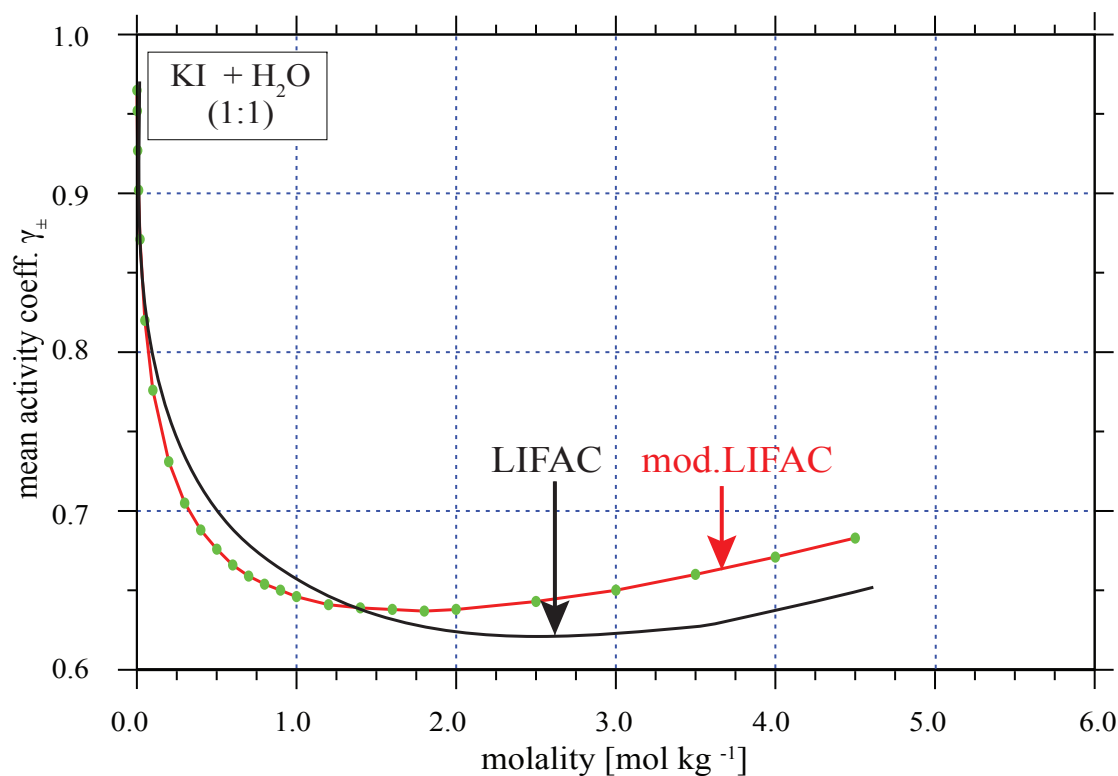


Figure 6.4: Comparison between experimental (symbols) and predicted mean activity coefficients (solid lines) for aqueous electrolyte solutions at 25 °C as a function of molality. Salt molalities 0-6 mol kg⁻¹, γ_{\pm} (—) LIFAC, mod. LIFAC (this work), (●, ★) experimental values from Hamer and Wu (1972).

parameters, few of the non-electrolyte models are actually suitable for atmospheric organics. For instance, the original UNIFAC showed much bigger deviations than the UNIFAC version of Peng et al. (2001) as shown in Fig. 6.8. However, these models have their own advantages to compute the activity coefficients and water activity, with variable reference state calculation. All in all, these models can able to produce the LLE along with VLE behavior, as explained in the previous section. Furthermore, the accuracy to predict the activity coefficients of the organic species will not change by introducing the new organic functional groups.

6.1.2 Intercomparison between activity coefficient models

Considerable effort has been devoted, formerly, in order to parameterize the interaction parameters, for activity coefficient model framework, comprised of either aqueous electrolyte solutions or aqueous organic, electrolyte-free systems. Several authors (e.g. Raatikainen and Laaksonen (2005) and Tong et al. (2008)) have compared the well established activity coefficient models that could potentially suitable for modeling of hygroscopic properties of organic-electrolyte particles as well as prediction of activity coefficients of species and water activities. On the other hand, most of the models can't exploit the estimation of activity coefficients at high electrolyte molalities. Likewise, some of the models have limitations, such as vapor-liquid equilibrium (VLE) only, limited to estimate the activity coefficients at room temperature only and restrictions to the

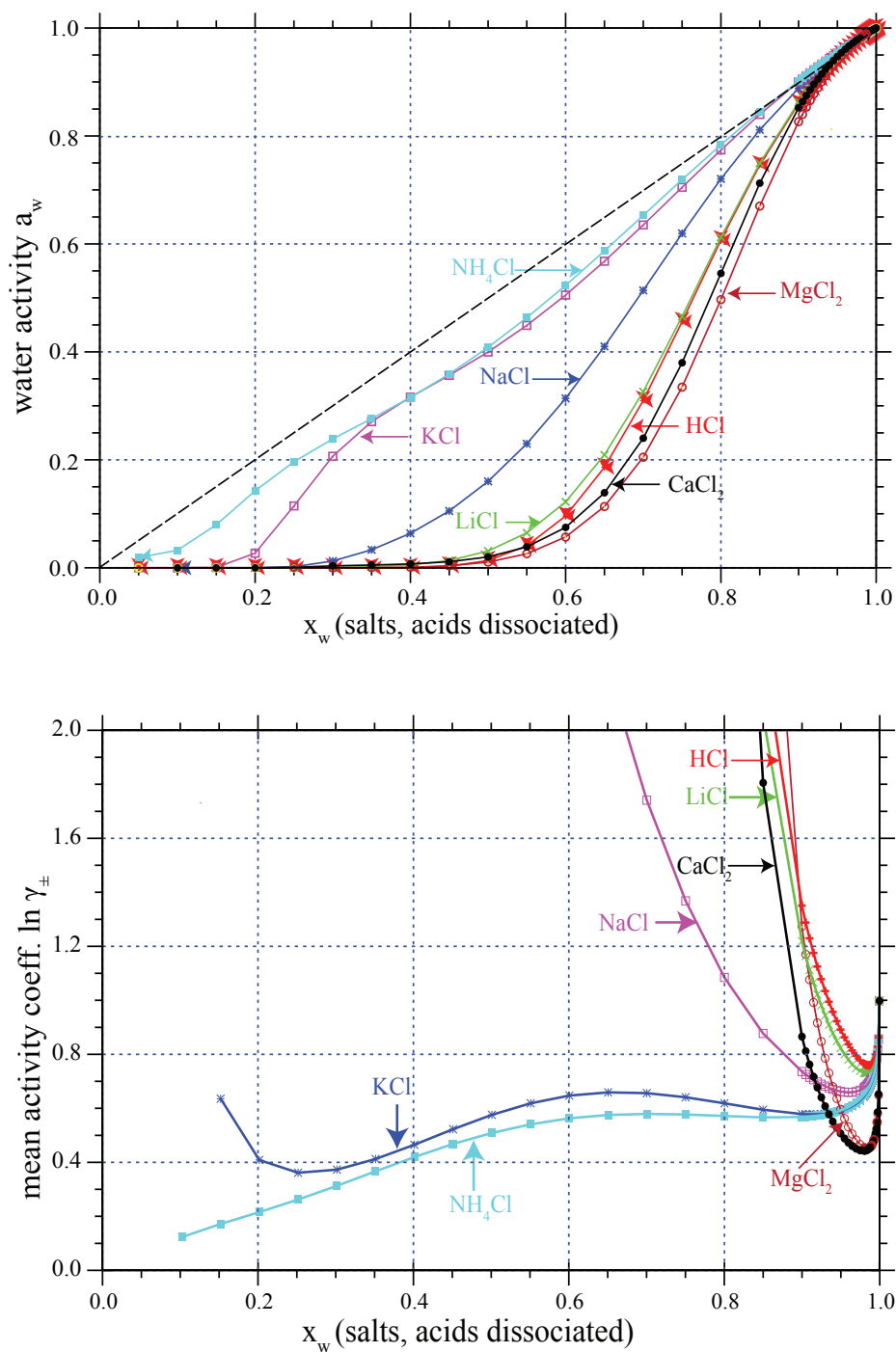


Figure 6.5: Comparison between original AIOMFAC (symbols) and modeled (solid lines, this study) water activities and mean activity coefficients of the Cl^- ions in binary aqueous salt (or acid) solutions at 298 K. The diagonal, dashed line in the upper panels shows the water activity of an ideal mixture.

maximum electrolyte molality. In spite of the models compared by Raatikainen and Laaksonen (2005), AIOMFAC can estimate the activity coefficients of aqueous electrolyte solutions at high ionic strength (low water content/RH). In addition, AIM model (Clegg et al., 1998a,b), which is integrated in the model of Ming and Russel (2002) also offers the good accuracy for the

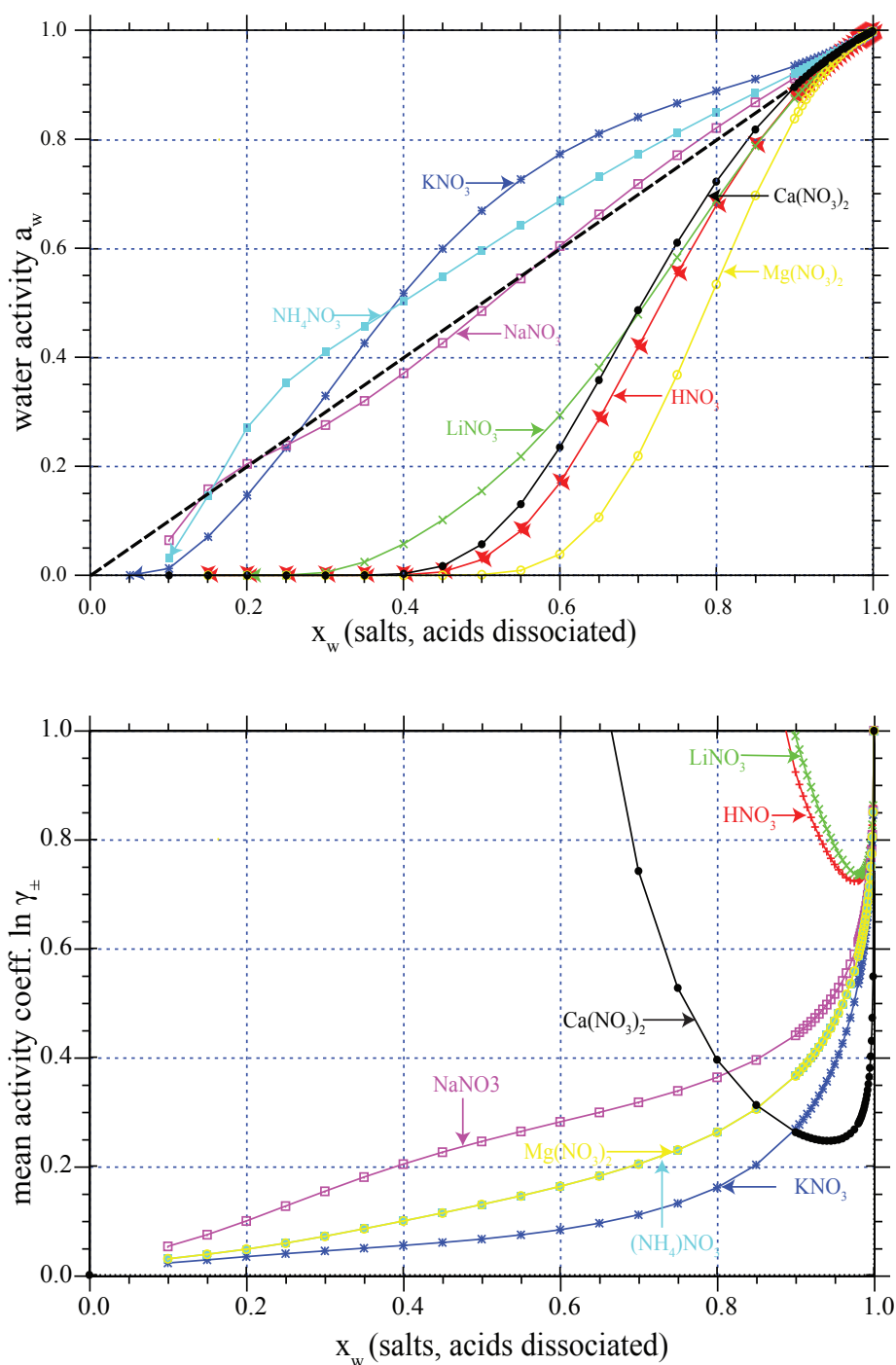


Figure 6.6: Comparison between original AIOMFAC (symbols) and modeled (solid lines, this study) water activities and mean activity coefficients of the NO_3^- ions in binary aqueous salt (or acid) solutions at 298 K. The diagonal, dashed line in the upper panels shows the water activity of an ideal mixture.

aqueous electrolyte representation. Moreover, the another advantage of AIOMFAC can able to predict VLE, LLE, and solid-liquid equilibria (SLE) with the same parameterization. In fact, the models (e.g. LIFAC) selected for the comparison by Raatikainen and Laaksonen (2005) can't able to predict the VLE/LLE/SLE with the the same parameterization similar to AIOMFAC.

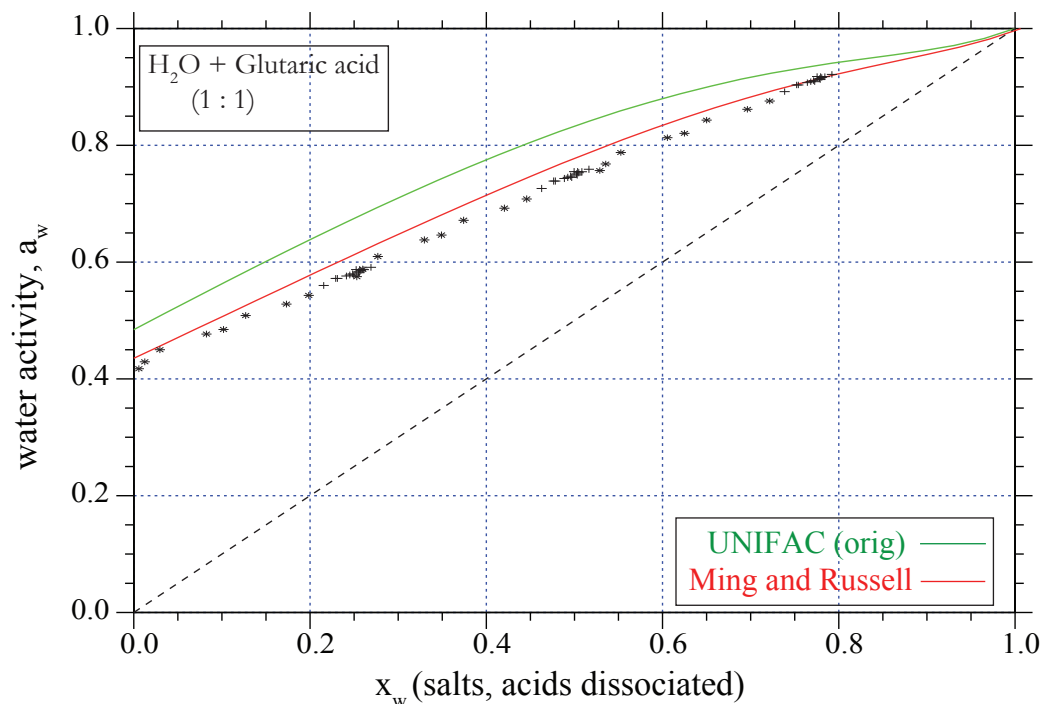


Figure 6.7: Comparison between experimental and calculated water activities (a_w) in aqueous glutaric acid solutions as a function of water fraction (x_w) at 298.15K. Experimental data from Peng et al. (2001).

Besides, an improved and modified version of LIFAC (mod. LIFAC) by Kiepe et al. (2006) can able to predict VLE and LLE. The major difference between these two models relies on the parameterization using the various data sets. While AIOMFAC, which has been parameterized using a variety of data types, including LLE and SLE data, on the other hand organic-inorganic MR interaction parameters of mod. LIFAC have been obtained from VLE, osmotic coefficients, and mean ionic activity coefficient data (Zuend et al., 2008).

Fig. 6.9 shows the comparison between experimental and predicted water activity data of four different aqueous electrolyte solutions at 298 K and corresponding model calculations of AIM III (Aerosol Inorganic Model) (Clegg et al., 1998b), mod. LIFAC, Pitzer approach which is included in Ming and Russell model and AIOMFAC. Fig. 6.9 shows that the water activity differences between all considered models are in good agreement up to moderate salt concentrations ($x_w \approx 0.5$). The predicted water activities at below moderate concentrations ($x_w \approx 0.4$) indicate the formation of a solid salt (or hydrate), when the solution becomes supersaturated as well as the deliquescent point of the particular salt. This is not reproduced by the models, since the formation of solids was not incorporated in the model calculations. As can be seen from Fig. 6.9 - 6.10, at low and moderate concentrations the calculated water activities agree well with each other and the measurements. At high salt concentrations mod. LIFAC strongly deviates from AIOMFAC and shows in Fig. 6.9, a steep increase in a_w and in Fig. 6.10 an increase followed by a sharp decrease, features that have to be rated as artifacts of the mod. LIFAC parameterization, whereas Ming and Russell model, behaves similar to AIOMFAC at medium concentrations and proceed to formation of solids.

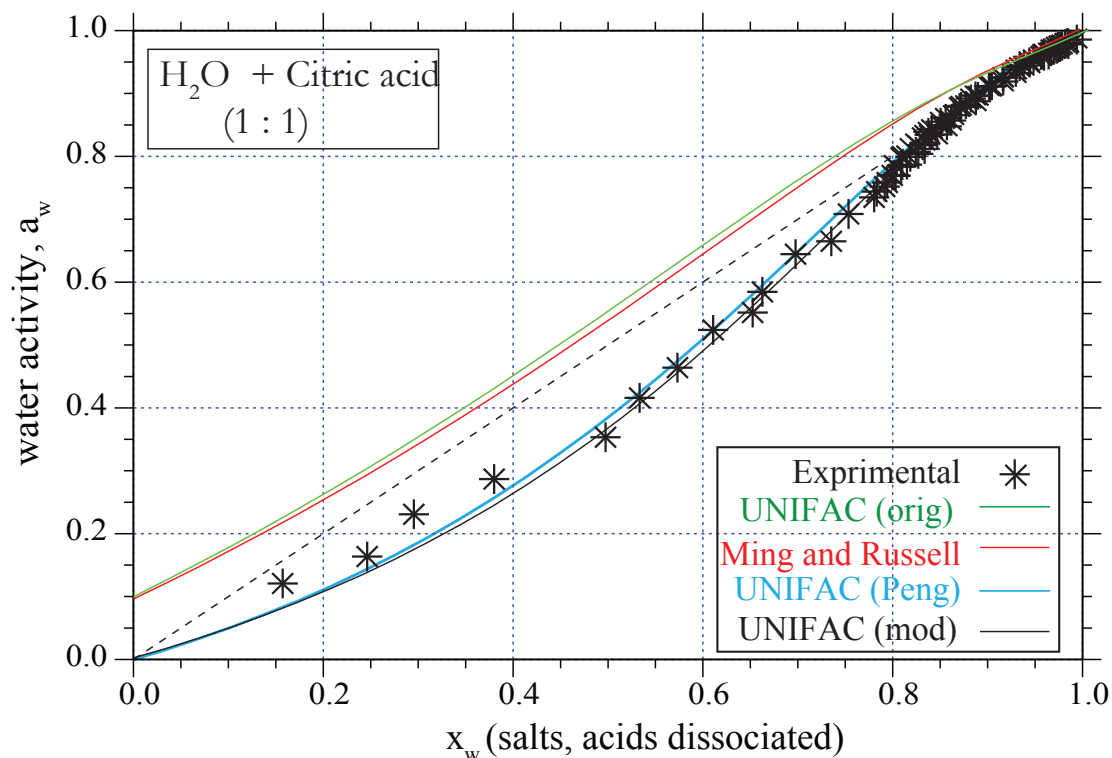


Figure 6.8: Comparison between experimental and calculated water activities (a_w) in aqueous citric acid solutions as a function of water fraction (x_w) at 298.15K. Experimental data from *Maffia and Meirelles (2001)*.

Fig. 6.10 suggests that, for the $\text{Ca}(\text{NO}_3)_2$ parameterization in mod. LIFAC, only water activity data of bulk measurements were used. But, in the AIOMFAC the experimental data covering high solution concentrations and ternary mixtures for the EMF measurements are used (see *Zuend et al. (2008)*) in order to fit the parameters. Hence, the gradient of curve enable much better descriptions and predictions up to high concentrations, even very low water concentration available and at high ionic strength. Apart from the predicted water activities, the calculated mean activity coefficients also have differences with each other. Since, $\text{Ca}(\text{NO}_3)_2$ is not available in the AIM, we show the comparison of VLE mean activity coefficients and water activities for $\text{Ca}(\text{NO}_3)_2$. As can be seen from Fig. 6.10, the predicted mean activity coefficient with the AIOMFAC and Ming and Russell, shows the similar behavior with 5 % of difference, where as the mod. LIFAC shows completely unusual behavior. This is mainly caused by the ion \leftrightarrow organic interactions included in the model. However, all the computed water activities agrees at the high relative humidities and the out put behavior is overall similar. In addition, these examples show the importance of a wide database covering different experimental methods and data types as well as various organic compounds containing the same functional groups to parameterize with accurate selection of reference state, needs to be include in an activity model over a wide composition range of solute and solvents.

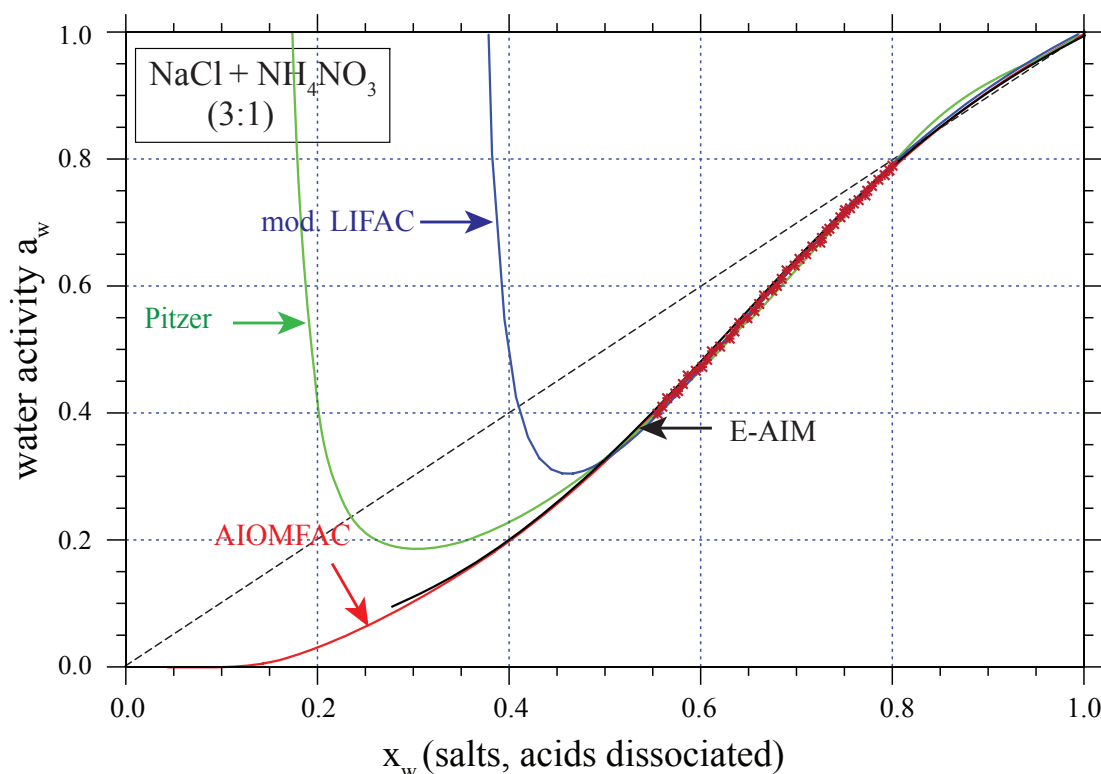


Figure 6.9: Comparison with measurements of aqueous electrolyte solutions (symbols) and corresponding calculations of the models AIM III (Clegg *et al.*, 1998b), mod. LIFAC (Kiepe *et al.*, 2006), Ming and Russell (Ming and Russel, 2002) and AIOMFAC (Zuend *et al.*, 2008) at 298 K for the salt NaCl + NH_4NO_3 at a molar salt mixing ratio of (3:1). Experimental data from Ha *et al.* (2000).

6.1.3 Verification of activity models with water activity measurements

The activity coefficient in a solid-liquid or in a vapor-liquid system, depends on the interaction of the dissolved solute or vapor molecules with the solvent molecules, in the liquid phase. The solid phase or the vapor phase, therefore, does not play an important role in the non-ideality of the solution. Therefore, the experimental vapor-liquid systems can be used in the development or validation of an activity coefficient model. Hence, in this section the performance of the considered activity coefficient models is evaluated by comparing calculated and measured water activities of mixtures of electrolyte and organic system. For all water activity calculations, the organic acids are treated as non-dissociating solutes, and a single liquid phase is assumed with no solid phases present. All calculations are performed at atmospheric pressure (1 atm) and at 298 K. Fig. 6.11 shows the comparison between experimental and predicted water activities for the mixture of $(\text{NH}_4)_2\text{SO}_4$ + Ethanol + Acetic acid [(2:1:1) mole ratio]. All the models strongly agree with the measurements at high relative humidities or at low and moderate salt concentrations ($x_w \approx 0.8$), whereas at the deliquescent phase ($x_w \approx 0.6$), mod. LIFAC and Ming and Russell models strongly deviate from AIOMFAC. Furthermore, it is difficult to determine mixture parameters to represent the thermodynamic properties of aqueous electrolyte \leftrightarrow organic systems to high concentrations. For instance, the mixture terms based on the Pitzer molality-based

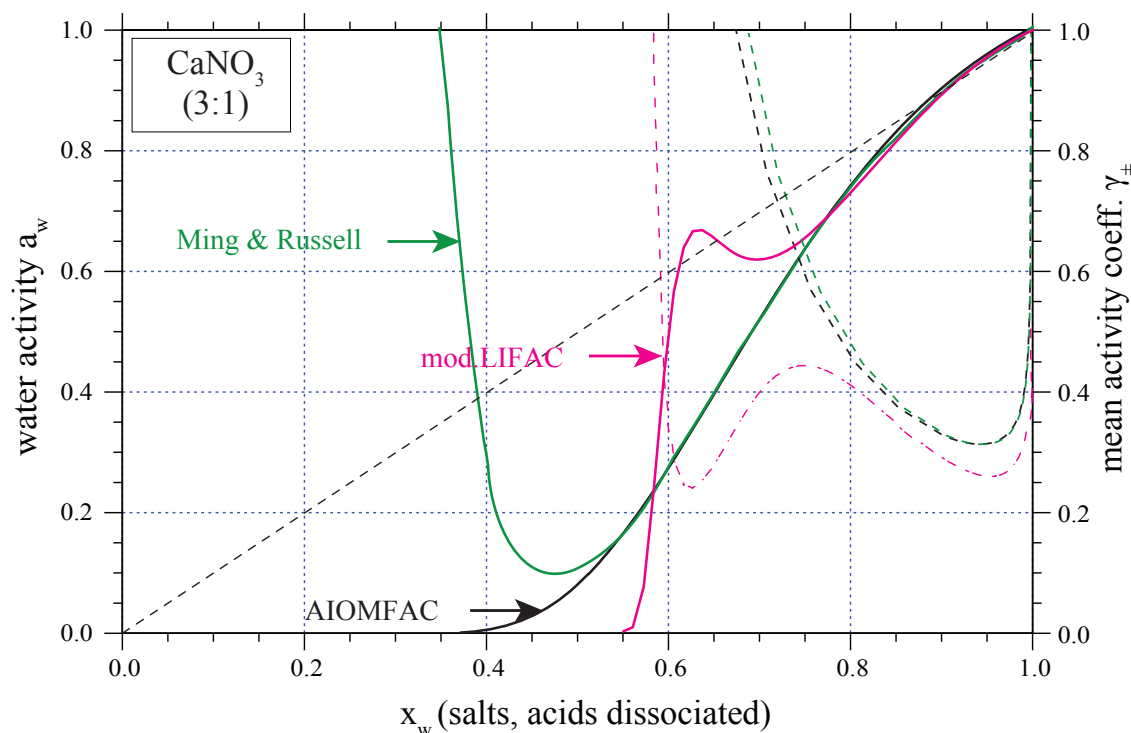


Figure 6.10: Intercomparison between selected models for $\text{Ca}(\text{NO}_3)_2$ salt.

equations, which are included in the Ming and Russell and CSB (Clegg et al., 2001) model, are suitable for low to moderate concentrations only up to about 6 mol/kg.

The unusual behavior does not appear for the pure organic and pure electrolyte mixture predictions, as shown in Fig. 6.1- 6.6. As a result, we extrapolate that the MR interaction term in the model is responsible for atypical shape in the predictions. The main reason is that, in the MR part, the logarithms of activity coefficients are calculated as sums of terms which are proportional to the fitting parameters, ion molalities and ionic strength. Because these terms have quite large numerical values, and a small change in the interaction parameters or molality can cause a very big change to activity coefficients. The MR part and modification of SR part given in the AIOMFAC could be the main reason, since this model can predict the water activities at high salt concentrations as well. Consequently, as can be seen from Fig. 6.11 mod. LIFAC have an increase followed by a sharp decrease, features that have to be rated as artifacts of the mod. LIFAC parameterization, where as Ming and Russell models also have strong increase after the water fraction is about $x_w \approx 0.3$. As mentioned earlier, these artifacts indicate the formation of a solid salt (or hydrate), when the solution becomes supersaturated, since the the formation of solids was not enabled in the model calculations. However, the consideration here, is only a limited set of mixtures of organic-electrolyte compounds. Hence, the presented results should be viewed as a provisional assessment. The scarcity of experimental data for mixtures of atmospheric relevance remains a limitation for testing activity coefficient models. When experimental data become available, further development in the comparison of water activities can be performed in order to validate the models. However, all the interaction parameters in the considered models, were

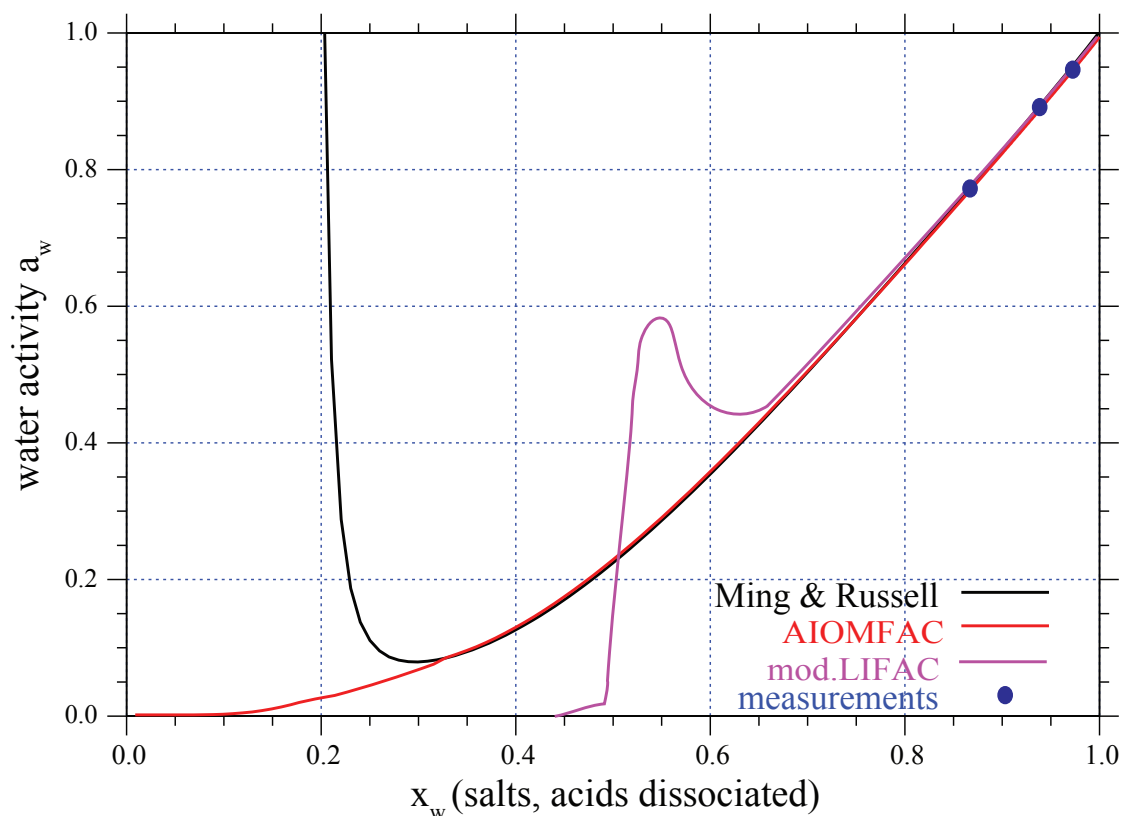


Figure 6.11: Comparison between measured and modeled water activities for the aqueous solution composed of organic-electrolyte mixture: $(\text{NH}_4)_2\text{SO}_4 + \text{Ethanol} + \text{Acetic acid}$ [(2:1:1) mole ratio].

fitted against measurements. Hence, this comparison can be considered as indirect comparison with measurements. All in all, despite the difficulties in determining the ion \leftrightarrow organic mixture parameters, it should be remembered that the ion \leftrightarrow organic interaction parameters can improve model performance (Clegg et al., 2001; Clegg and Seinfeld, 2006a; Tong et al., 2008).

6.1.4 Verification of robustness: extended AIOMFAC

As pointed out in the previous sections, the developed activity coefficient models are suitable for industrial purposes. Field studies reporting that, important individual organic compounds, compound classes, and/or distributions of functional groups found in ambient aerosols, identified as alkyl, carboxyl, hydroxyl, ketone, aldehyde, amines, organosulfates, ether, alkenyl, and aromatic groups (Decesari et al., 2000; Maria et al., 2003; Decesari et al., 2006; Russell et al., 2009; Gilardoni et al., 2009). Hence, many organic aerosol components can be characterized by means of about 10 different kinds of organic functional groups. Consequently, these functional groups were not included in any single framework. From the critical evaluation of the models, we have concluded to extend the ion \leftrightarrow organic interactions along with organic functional groups. Based on the aforementioned sensitivity studies, AIOMFAC, which is based on the group-contribution model LIFAC (Yan et al., 1999)-and yet modified in many respects to better represent relevant species, reference states, and the relative humidity range of the atmosphere,

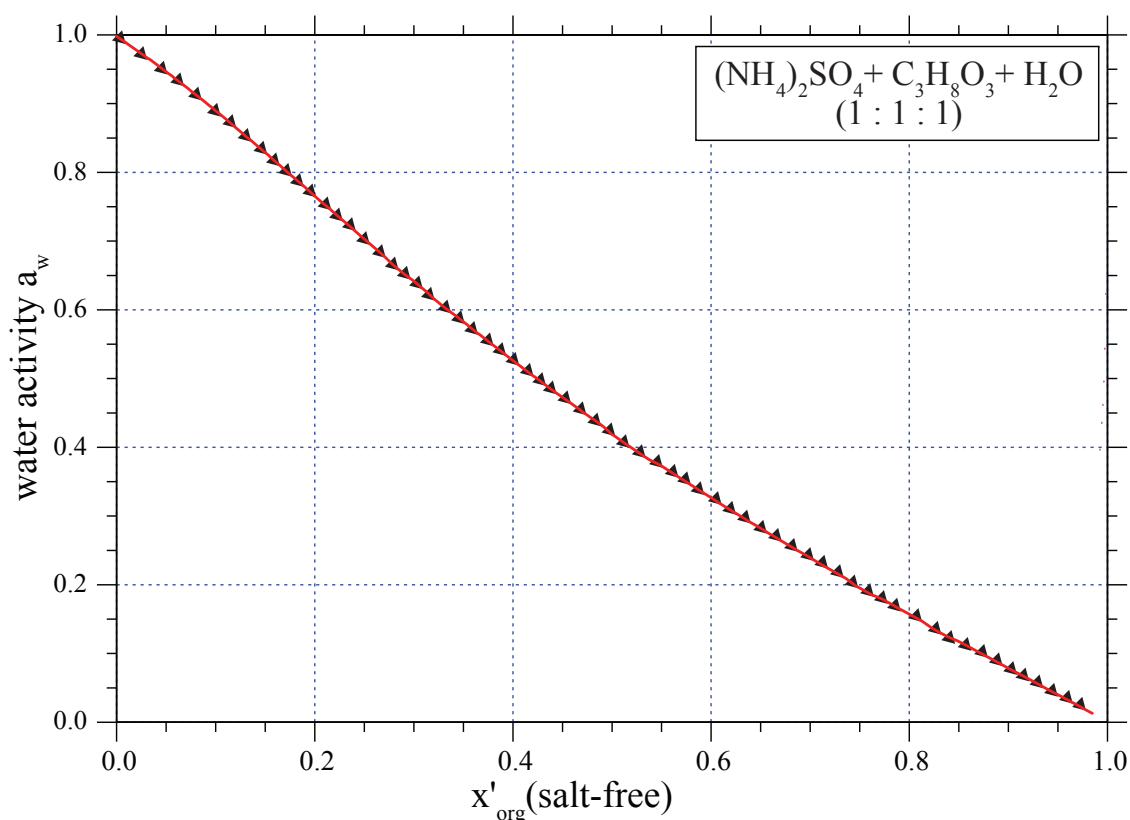


Figure 6.12: Water activities of glycerol- water-ammonium sulphate mixture at 298 K. (\blacktriangle) are original AIOMFAC (Zuend et al., 2008) a_w data, (—) extended AIOMFAC results. The solid line is the extended AIOMFAC a_w of the salt-free solvent mixture with respect to completely dissociated in water.

could potentially give good results. Furthermore, the computation of activity coefficients at high concentrations of salt/organics dissolved in water, was also possible.

Based on this, we have extended the interaction parameters for the different interaction terms, as well as the model equations for the MR part (see Sec. 3.6.2). As concluded by Zuend et al. (2008), the similarity between mod. LIFAC and AIOMFAC facilitates the comparison between the two models as the AIOMFAC framework can be easily adapted to the model equations and parameters given by Kiepe et al. (2006). All compound-specific parameters in the LR and SR parts are already set and non-adjustable, as utilized in the original AIOMFAC Zuend et al. (2008). This includes all interactions among different organic compounds and water, which are treated in the modified UNIFAC model that makes up the AIOMFAC SR part. However, addition of new organic functional groups in the SR and MR parts are possible without altering the model equations as described in Sec. 3.6.2. Likewise, all adjustable AIOMFAC parameters to extend the description of organic functional groups \leftrightarrow ion interactions in mixtures can be implemented in the MR part. Therefore, we are aimed to extend the data base which can be used for full length of aforementioned organic functional groups. Despite to the consideration in original AIOMFAC, with a wide range of alcohols/polyols composed of the alkyl (CH_n , $n = 0, 1, 2, 3$) and hydroxyl (OH) functional groups for the organic \leftrightarrow inorganic interactions. Hence, we extended the AIOMFAC model ion \leftrightarrow organic interactions in MR part as well as organic functional group parameterization in SR part to compute the activity coefficient calculations

of mixtures containing methanol, carboxyl, aldehyde, acetate, formate, ether, acid functional groups, plus water and the inorganic ions (see Fig. 3.4).

After extension of model, sensitivity studies were performed, in order to verify the robustness of the models. Fig. 6.12 - 6.14 shows the comparison between original AIOMFAC and extended version of AIOMFAC. As can be seen, after extension of parameters, the same accuracy has been achieved with respect to original AIOMFAC. As explained in the Sec. 3.6.2, the ion \leftrightarrow organic interaction parameters, for the alkyl (CH_n) and hydroxyl (OH), are considered from the original AOMFAC, for the remaining groups the interaction parameters were considered from mod. LIFAC. Hence, for the system of ions and organic species, which are included in the original AIOMFAC, follows the same computational procedure. However, sensitivity studies were performed in order to verify the disturbances. As can be seen, from the examples of schematic illustrations, the accuracy of the results are unaltered (see Fig. 6.13).

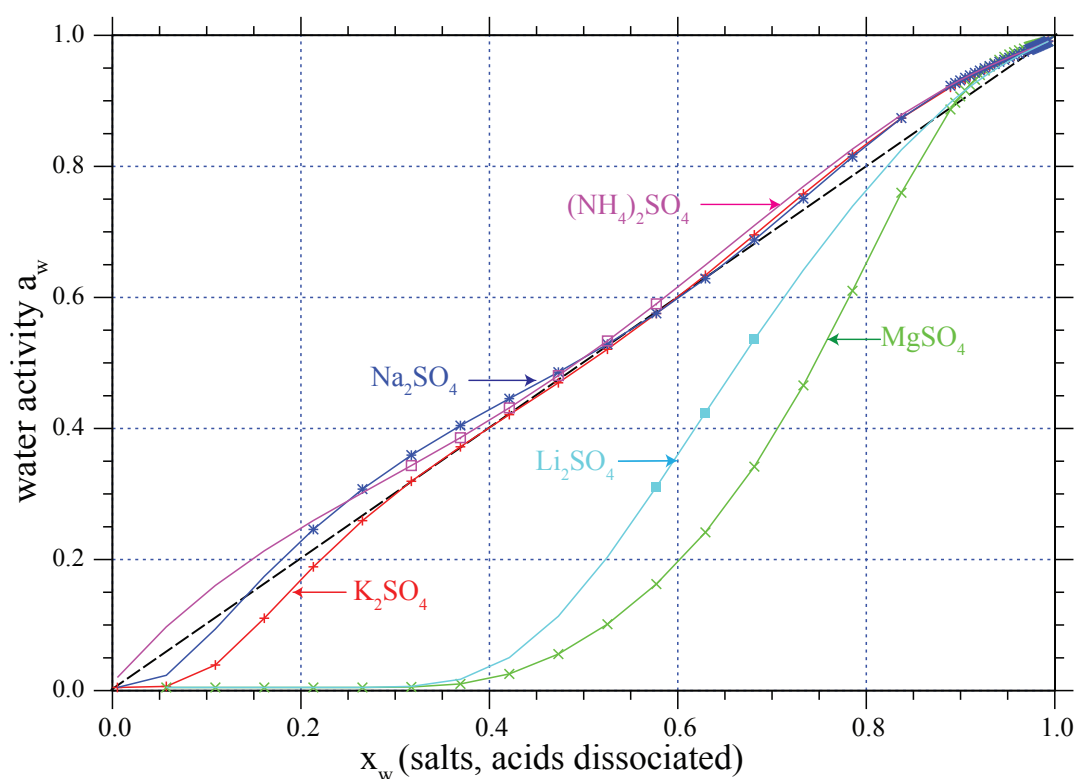


Figure 6.13: Comparison of water activities of the SO_4^{2-} ions in binary aqueous salt (or acid) solutions at 298K from original (symbols) and extended AIOMFAC (solid lines). The diagonal, dashed line in the upper panels shows the water activity of an ideal mixture.

Note that organic acids are treated as undissociated species in all considered activity coefficient models. This is a simplification, as organic acids, e.g., dicarboxylic acids, tend to dissociate at least partially in dilute aqueous solutions. This simplification is justified for moderately to highly concentrated solutions of carboxylic acids and when reactions with strong bases are not considered. The reason for this simplification, and with it the omission of carboxylate ions and salts, in the group-contribution representation. In order to explicitly treat the partial dissociation of organic acids within a group-contribution method, one would need to define a dissociation constant of the carboxyl functional group, but different organic acids have quite

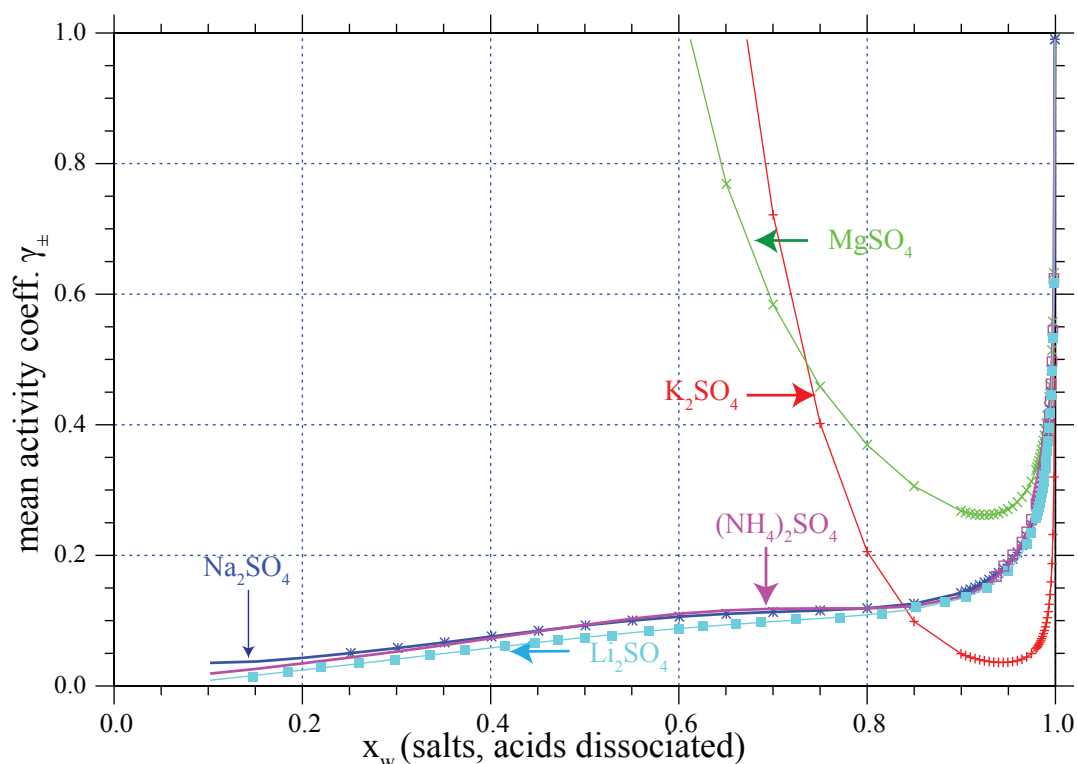


Figure 6.14: Comparison of mean activity coefficients of the SO_4^{2-} ions in binary aqueous salt (or acid) solutions at 298K from original (symbols) and extended AIOMFAC (solid lines).

different dissociation constants (Clegg and Seinfeld, 2006a,b) making it difficult to assign a specific dissociation constant to the COOH group.

Moreover, experimental data to determine interactions between organic anions (e.g. oxalate) and inorganic cations are rather incomplete (Clegg and Seinfeld, 2006a,b). Therefore, we neglect the dissociation of organic acids in aqueous solutions for the extended version of AIOMFAC. However, the effects of partially dissociated carboxylic acids on the non-ideal mixing behavior are to some extent implied by means of the ionic strength dependent $\text{COOH} \leftrightarrow \text{ion}$ interactions. The activity coefficients of dissociated acid ions, are computed from the LR and SR contributions (van der Waals subgroup volume R_i and surface area parameters Q_i), where as in the MR contributions are set to 0 which can have also considerable influence on the computation of total activity coefficients. After critical evaluation the extended version of AIOMFAC is used for the further investigations for the calculation of phase partitioning and compound activities for the computation of reaction rates in detailed multiphase chemistry model SPACCIM.

6.1.5 Importance of interactions

Intermolecular forces or interactions are essential at deliquescent particle phase, where the high solute concentration and low water fraction is available. They are important, however, because they are responsible for many of the physical properties of solids, liquids, and gases. Moreover, these forces become significant at the molecular range of about 1 nanometer or less, but are

much weaker than the forces associated with chemical bonding. The characteristic contribution of different interaction forces from the model development point of view in the solution can be computed using Eq. 3.7. Utilizing this conceptual idea in the computation of activity coefficients, here we address the question- Which intermolecular forces of attraction are important and need be considered for the treatment of non-ideality for organic-electrolyte mixtures. The models to treat the organic-inorganic mixtures can be further categorized into (i) so called decoupled models, where an explicit organic \leftrightarrow ion mixing term is not considered, and (ii) fully coupled models, as described in detail by Tong et al. (2008). Furthermore, Tong et al. (2008), studied the importance of inclusion of a treatment of ion \leftrightarrow organic interactions and states that these interactions would substantially improve the performance of the coupled models over that of the decoupled models. It has been concluded that, decoupled approaches, such as those in CSB (Clegg et al., 2001), ADDEM (Topping et al., 2005a,b), performs well, and in some cases better than the coupled models. Additionally in such cases, the ion \leftrightarrow organic terms do not necessarily lead to improved model predictions. At the same time, models are prerequisite, composed of an aqueous electrolyte term, an (aqueous) organic term, and an organic \leftrightarrow ion mixing term in order to treat the organic-inorganic mixtures. Hence, contrast to the study of Tong et al. (2008) regarding the model performance, the focus of this investigation is to evaluate the importance of different interaction terms in the models, which is necessarily to be considered in the computation of water activities as well as the activity coefficients. In order to answer this question the extended AIOMFAC is used for sensitivity studies.

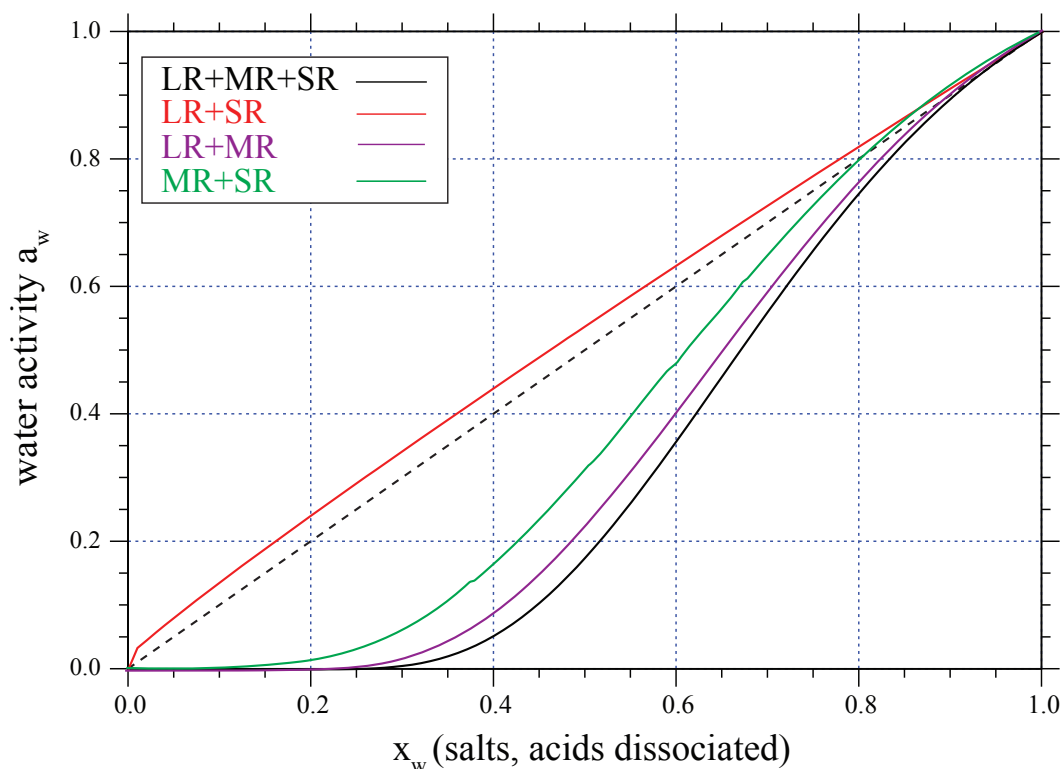


Figure 6.15: Importance of different interactions in the aqueous solution composed of $\text{NaCl} + (\text{NH}_4)_2\text{SO}_4 + \text{Ethanol} + \text{Malonic acid}$ [1:1:1:1 (mole ratio)].

Fig. 6.15 shows the contribution of different interaction forces in the solution for the solution of $\text{NaCl} + (\text{NH}_4)_2\text{SO}_4 + \text{Ethanol} + \text{Malonic acid}$ [1:1:1:1 (mole ratio)] as an example. However

the deviations regarding the different interactions depends on the considered mixture. As can be seen in the Fig. 6.15, the water activity is strongly deviates in absence of MR interaction forces, mainly caused from ion \leftrightarrow ion, ion \leftrightarrow dipole and ion \leftrightarrow induced dipole forces. Thus the MR interactions were found important. Similar to the findings of Tong et al. (2008), it is expected that ion \leftrightarrow organic interactions are of most importance in solutions with high solute concentrations, for which inclusion of ion \leftrightarrow organic parameters would be beneficial. However, the absence of each interaction terms can be seen in Fig. 6.15. The short range interactions also influence in the total contribution of computation of water activity, where the deviations are about 10%. In the case of considering the MR and SR interactions the deviations are about 25%. It should be noted that the ion \leftrightarrow organic interactions are the dominant interaction forces in the solution, however the other interactions forces are need to be consider. The deviations from the total contribution of interaction forces is significant in all ranges of relative humidity as well as the full range of concentration. Nevertheless, the deviations are increasing from lower salt/acid concentration to higher. During the low salt/acid concentration ($x_w \approx 0.9$) the contribution of the considered interactions were found similar.

6.1.6 Conclusions

The selected group contribution models LIFAC (Yan et al., 1999), mod. LIFAC (Kiepe et al., 2006), AIOMFAC (Zuend et al., 2008) and Ming and Russell model (Ming and Russel, 2002) were compared to provide a more complete treatment by including ion \leftrightarrow organic interactions for mixed organic-electrolyte solutions. The model selection was based on the model deviations and the predictive capabilities. However, the accuracy of the model predictions agrees well and reproduced with available measurements and literature data presented in Fig. 6.1 - 6.14. For comparison, deviations were calculated also for some other models (e.g. E-AIM), which are suitable for the atmospheric relevance. Since, AIOMFAC offers the computation of thermodynamic parameters as well as the activity coefficients at low relative humidities and high concentrations, the original model has been extended. Thermodynamic equilibrium data of mixed organic-inorganic systems from the literature are critically assessed and used in combination with mod. LIFAC (Kiepe et al., 2006) to establish a comprehensive database for the extension of AIOMFAC model parameters. Various organic compounds and inorganic ions, representing important species and compound classes found in atmospheric aerosol samples, have been used to extend the model interaction parameters. The new database of extended AIOMFAC achieves generally good agreement with a large number of experimental datasets and also with the original models. The applied methodology and the presented database can efficiently calculate solubility limits of salts and organics and phase compositions of LLE and VLE systems.

Finally, due to lack of experimental data, fitting the ion \leftrightarrow organic interaction parameterization can be challenging. In future, we will extend this database, if the ion \leftrightarrow organic interactions are available. The new extended data base including the various further functional groups can apply to predict the stable phases and thermodynamic behavior for multicomponent mixtures of atmospheric relevance. The evaluated and extended activity coefficient model is valuable in generating predictions of gas/particle partitioning for complex mixtures multicomponent aerosol particles. Water as the fixed reference solvent for inorganic ions allows the prediction and description of multicomponent LLE, VLE, SLE within the AIOMFAC, it can also be possible that the computation of LLE behavior using this extended database. If the two solvents co-exist in the particle phase, this extended version of AIOMFAC also helpful, to treat such situations, since the database has been extended from mod. LIFAC (Kiepe et al., 2006), which considers the variable reference state. Besides, using this extended version of AIOMFAC, it can possible

to compute the bulk to surface partitioning as well as the prediction of activity coefficients at surface and bulk simultaneously. If the surface enriched or film forming organic compounds available at the surface, the computation of activity coefficients can also be performed similar to the bulk calculation using the extended version of AIOMFAC utilizing the extended database.

6.2 Multiphase processing in aqueous particles and clouds

The study of atmospheric chemical reactions is rather difficult. One of the primary obstacles encountered in studying the atmospheric chemistry is that dealing with incredibly low concentrations. Hence, the analysis of reaction products is quite difficult. Furthermore, solid and liquid particles as well as clouds have a strong influence on atmospheric chemistry as sources and sinks for gas-phase species, as sites for surface reactions (solid particles), and as bodies for aqueous-phase reactions (liquid droplets). Within the past decades, several model studies were performed mainly by using permanent and non-permanent cloud conditions. It is often assumed in most multiphase models, that the deliquescent particles, cloud droplets as well as the individual components are not considerably influenced by the presence of the other components, i.e., behave ideally. Due to the mounting interest, regarding aqueous phase chemical modifications, simulations considering the chemistry of deliquescent particles as well as the cloud phase have received great attention. However, similar studies considering non-ideal solutions are more appropriate, to explain the multiphase processing of cloud and deliquescent particle chemistry in detail, since the particles can exhibit non-ideal effects upon varying the relative humidity/concentration levels. As such, the main strength of this modeling study lies in accurate estimation of activity coefficients and their influence on multiphase chemistry. The major outcomes are presented in the succeeding subsections.

6.2.1 Description of microphysical scenarios

For the current simulations, an adequate meteorological scenario has been created with an in-cloud residence time of about 15%, in order to perform the non-permanent cloud simulations similar to the investigations performed in [Tilgner \(2009\)](#) and [Tilgner and Herrmann \(2010\)](#), which are based on the global calculations of [Pruppacher and Jaenicke \(1995\)](#). Indeed, this prescribed value of 15% represents the calculated cloud volume fraction in the lower 6 km of the troposphere (see [Pruppacher and Jaenicke \(1995\)](#)). Consequently, one can assume an average in-cloud residence time of about 4 hours per day for tropospheric air masses or air parcels ([Tilgner, 2009](#)). As a result, in this scenario an air parcel moves along with a predefined trajectory including 4 cloud passages (2 day time (noon) and 2 night time (midnight) clouds) of about 2 hours within 60 hours of modeling time span and an intermediate aerosol state at different relative humidity levels, by modifying the meteorological scenario as shown in [Fig. 6.16](#).

The current model applications, have been performed for three characteristic model scenarios initializing at 90% RH. It should be noted that the simulations were performed without any variation of the input parameters, moreover, the relative humidity levels (i.e. 80% RH, 70% RH) were varied after the second cloud passage as illustrated in [Fig. 6.16](#). Moreover, all the particles are assumed as mono dispersed with a radius of 0.2 μm for the current investigations. As a result, the time evolution of total liquid water content and supersaturation ratio of the parcel were designed to behave similarly for all the simulations performed. These model scenarios were created based on their corresponding upwind velocity and the pressure. The alternating

cycle between day and nighttime cloud conditions with equal time contributions has been used to assure the comparability of all simulations (see [Tilgner \(2009\)](#) and [Tilgner and Herrmann \(2010\)](#)). During this meteorological model scenario the simulated air parcel starts to ascend adiabatically while passing through clouds and becomes supersaturated. The aerosol particles whose radii exceed the critical ones are considered as activated and continue growing. For the clear understanding about the performed simulations along with used acronyms are described in [Table. 6.1](#).

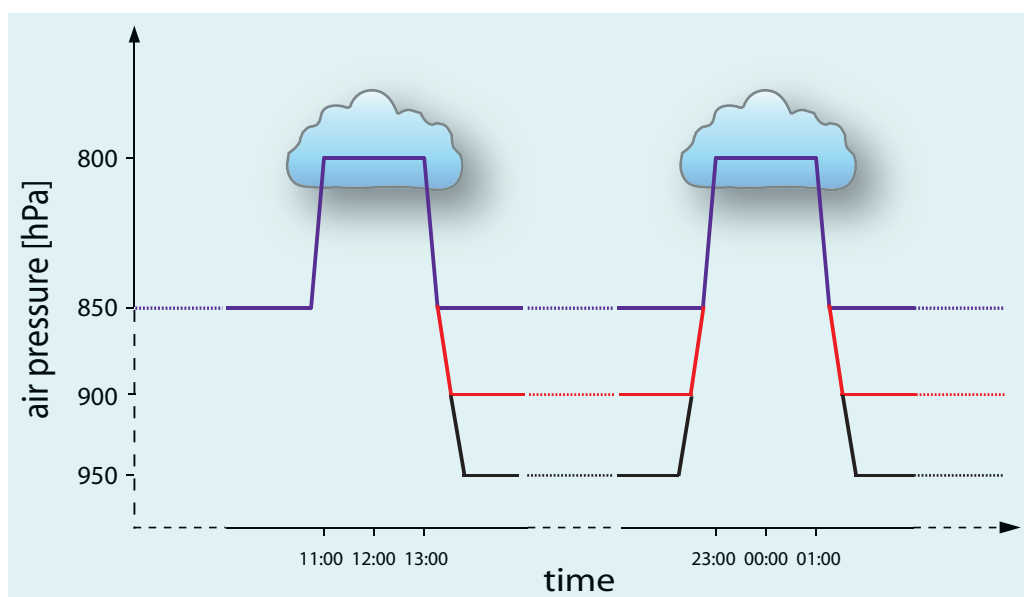


Figure 6.16: Schematic of used model scenarios. (————) Base case (90% RH), (————) 80% RH, (————) 70% RH.

Simulations have been performed with a realistic physical and chemical initialization data, for two different atmospheric scenarios (urban: anthropogenic polluted case, remote: continental background case) beginning at 0:00. The chemical and physical model initialization parameters are taken from [Tilgner \(2009\)](#); [Tilgner and Herrmann \(2010\)](#), time-constant microphysical values are assigned as constant for temperature $T = 298$ K and pressure $p = 1013$ hPa. Simulations have been carried out with complex gas phase and aqueous phase chemistry to investigate the effect of multiphase aerosol-cloud chemistry interactions. Finally, this non-permanent cloud meteorological scenario including more realistic in-cloud and cloud free time periods allows more realistic investigations of the aerosol cloud interactions compared to the former studies i.e. treatment of aqueous phase chemistry as ideal solutions.

The major findings will be presented sequentially. At first, the behavior and pattern of modeled activity coefficients will be discussed. Next, the main differences in the aqueous phase chemistry while considering ideal and non-ideal solutions for the aqueous phase chemistry will be outlined. Later on the performed sensitivity studies, aiming to investigate the influence of treatment of non-ideality at three different relative humidity levels, as shown in [Fig. 6.16](#) and as described in [Table. 6.1](#).

Table 6.1: Description of the microphysical model scenario and its acronym used in this study.

| Scenario | simulated case | scenario | Acronym |
|-------------------|----------------|----------|----------|
| Basecase (90% RH) | Ideal | Remote | 90%-IDR |
| | | Urban | 90%-IDU |
| | Non-ideal | Remote | 90%-NIDR |
| | | Urban | 90%-NIDU |
| 80% RH | Ideal | Remote | 80%-IDR |
| | | Urban | 80%-IDU |
| | Non-ideal | Remote | 80%-NIDR |
| | | Urban | 80%-NIDU |
| 70% RH | Ideal | Remote | 70%-IDR |
| | | Urban | 70%-IDU |
| | Non-ideal | Remote | 70%-NIDR |
| | | Urban | 70%-NIDU |

6.2.2 Applied multiphase chemistry mechanism: RACM-MIM2ext/CAPRAM 2.4+organicExt

In order to investigate the influence of treatment of non-ideality on multiphase processing, it is thus necessary to apply a multiphase chemistry with an adequate complexity. For the current model applications, the existing aqueous phase mechanism CAPRAM 3.0 (Chemical Aqueous Phase Radical Mechanism) is rather complex. Furthermore, other simple mechanisms such as INORG mechanism (see [Sehili et al. \(2005\)](#)), are not able to simulate and can't hold the capability to predict the activity coefficients of organic compounds that might change the multiphase processing, using the UNIFAC group-contribution model. Hence, a reduced chemical mechanism is extracted from the CAPRAM family, which illustrate the broader knowledge on chemical aqueous phase transformations in tropospheric clouds and deliquescent particles. The current employed mechanism consists of CAPRAM2.4 ([Ervens et al., 2003](#)), combined with a reduced organic extension of CAPRAM3.0red ([Deguillaume et al., 2009](#)), along with condensed oxidation scheme of malonic acid and succinic acid based on the CAPRAM3.0red (see [Deguillaume et al. \(2009\)](#) for more details and reduction step 3b).

Schematic illustration of current multiphase mechanism used for this model applications is shown in Fig. 6.17. The current applied multiphase mechanism consists of a extended RACM-MIM2ext gas phase mechanism (see [Tilgner and Herrmann \(2010\)](#) for further details) with about 277 reactions and the aqueous phase mechanism CAPRAM2.4+ organicExt, which contains 395 reactions, including complex implementation of aqueous phase inorganic chemistry and a reaction mechanism for atmospherically relevant organic compounds. The interchange processes between the gas and liquid phases are specified according to the Schwartz approach ([Schwartz, 1986](#)), considering Henry's law solubility, gas phase diffusion and mass accommodation coefficient for 42 soluble species. The developed organic extension contains C₁ to C₄ chemistry, including OH and important NO₃ reaction pathways. Further details and the respective material regarding the

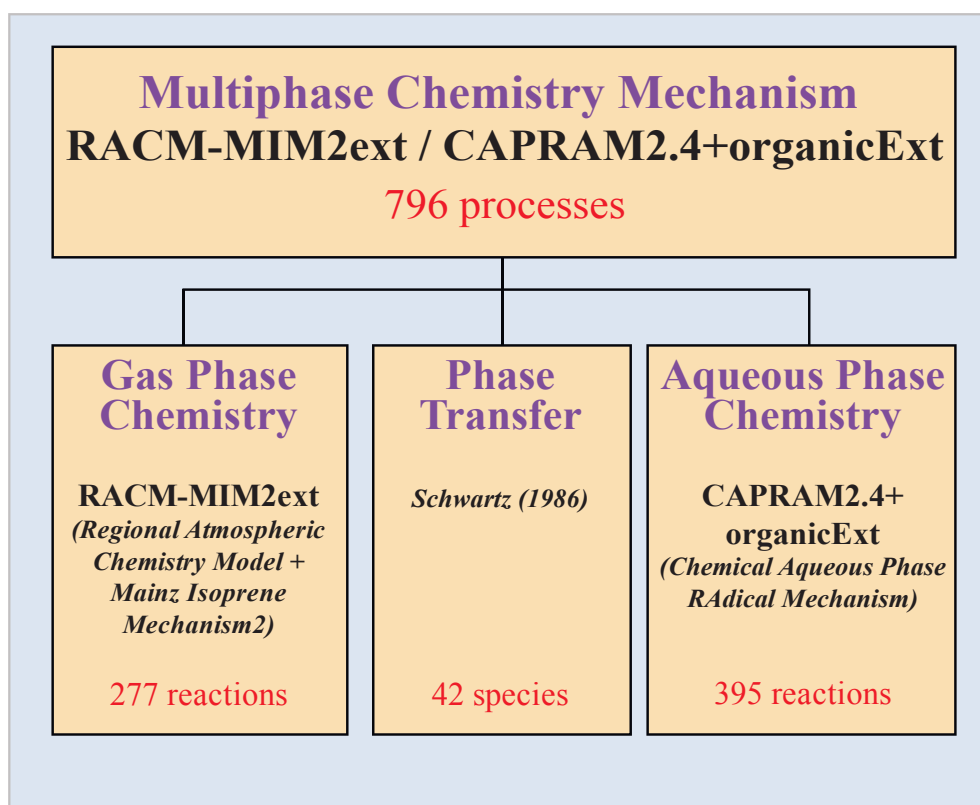


Figure 6.17: Schematic of multiphase mechanism employed in this study including the number of processes, reactions and phase transfer processes (modified from Deguillaume et al. (2009); Tilgner and Herrmann (2010)).

different CAPRAM mechanisms including reaction tables, revisions along with references are available via the [CAPRAM](#) website.

6.2.3 Modeled microphysical conditions

Supersaturation and LWC are the important and decisive microphysical parameters for the multiphase chemistry. As shown in Fig. 6.18, the modeled LWC is varied every 12 hours by about 5 orders of magnitude according to the cloud formation in all environmental cases reaching to total LWC of about 0.5 l m^{-3} . As can be seen, the simulated supersaturation is changed for the simulation while considering the aqueous phase chemistry as non-ideal solutions, in comparison with assumption of ideal solutions (see Fig. 6.18). This is mainly caused by the modification of Raoult term (water activity, a_w) incorporated in the Köhler's theory. Furthermore, the feedback described in Sec. 5.3 is also considered for all of the simulations considering ideal and non-ideal solutions for the aqueous phase chemistry. Hence, it can be expected that, the Raoult term is dominated by the water activity for the simulations performed including the treatment of non-ideality. Whereas, the simulations performed while assuming the ideal solutions, the Raoult term is an approximation of, sum over the molar ratios of all soluble species. Moreover, the gas phase uptake can directly modifies the total dissolved mass, the time rate of change of concentrations due to the phase transfer will also influence the total mass of the particle, so these

deviations are obvious. However, activated CCN can evaporate due to the decreasing water vapor saturation with increasing cloud life time. These effects are noticeable in some of the following concentration profiles as well as mass flux depictions and will be explicitly mentioned there.

The notable differences are also observed for the LWC during deliquescence particles as shown in Fig. 6.19. Since, the presented simulations are performed at 90% RH level, the difference between the ideal solutions and non-ideal solutions are not so large. Furthermore, it is thus obvious that the solution is becoming more concentrated (deliquescent phase) after the could evaporation and the deviations between the simulations 90%-IDU and 90%-NIDU are increasing gradually until the air parcel reached to 60 hours (see Fig. 6.19 right). Furthermore, due to the incorporation of treatment of non-ideality the mass of the total system is also modified due to the incorporation of real solutions instead of ideal solutions for the aqueous phase chemistry.

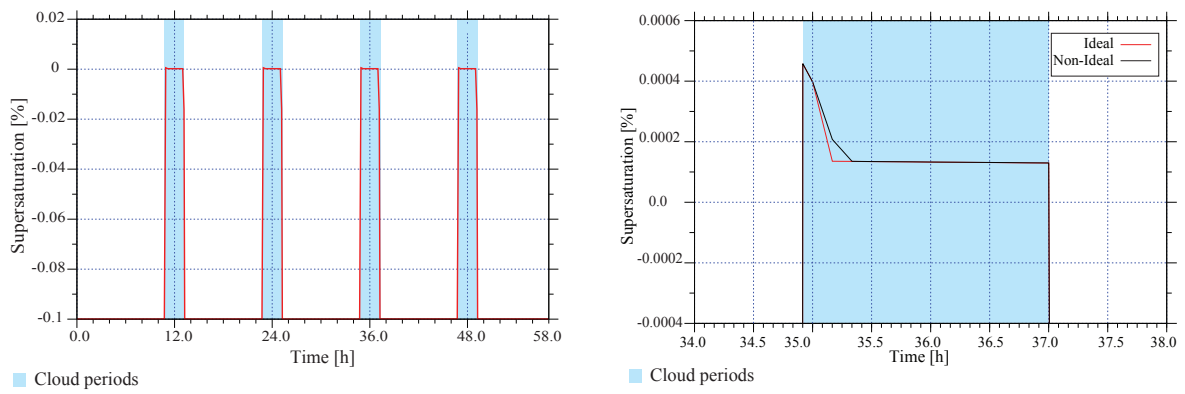


Figure 6.18: Evolution of Supersaturation during the meteorological scenario at 90%RH (left). Closer look during the activation period for selected period of time (right).

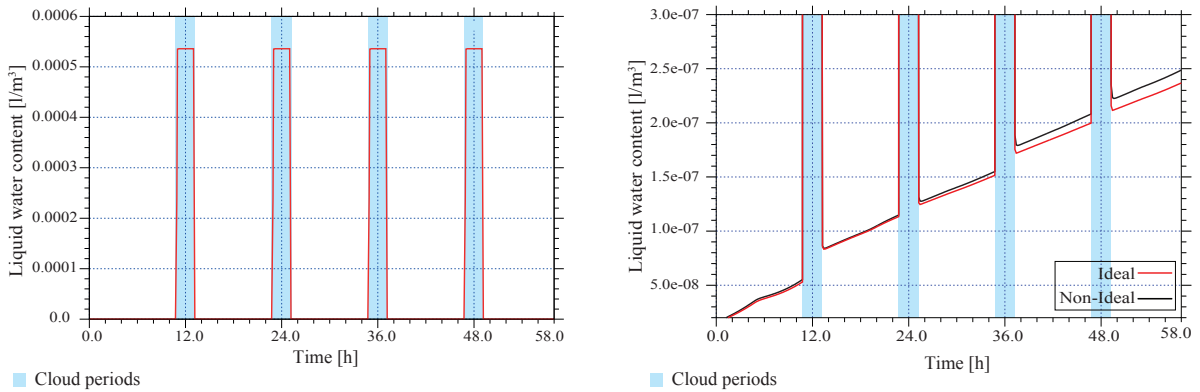


Figure 6.19: Evolution of LWC during the meteorological scenario for the simulations 90%-IDU vs. 90%-NIDU. Closer look during the deliquescence particle phase (right).

6.2.4 Modeled activity coefficients

The behavior of modeled activity coefficients is discussed in detail in this section. As explained earlier, the time evolution of activity coefficients were computed according to the extended AIOMFAC (see Sec. 3.6). Furthermore, the activity coefficients for the radicals as well as the

solids were treated as unity, as described in Table. 5.1. The description of the modeled activity coefficients for the key compounds that might have impact on the multiphase processing is presented in the proceeding subsections.

6.2.4.1 Inorganic compounds

The predicted activity coefficient values for key inorganic ions computed for urban and remote environmental conditions during the day time (at 27 hours of modeling time) and night time (at 38 hours of modeling time) are tabulated in the Table. 6.2. As enumerated, the predicted activity coefficients are presented separately for inorganic anions and inorganic cations. These results implicate that the activity coefficients of the mono charged ions (cations and anions) as well as the double charged ions for inorganics, behaves similarly due to the charge number utilized in the computation of ionic strength. Furthermore, the numerical values of activity coefficients computed for the inorganic ions, implicate that the inorganic multiphase processing is expected to be declined since the activity coefficients are less than unity ($\gamma < 1$). The expected behavior is observed with the comparison between aqueous phase concentrations of the ionic species in mol m^{-3} (see Sec. 6.2.6.1 - 6.2.6.2). As tabulated in Table. 6.2, the behavior or pattern of activity coefficient values for the mono anion or mono cation have same range of activity coefficient. Moreover, the value of dianion and dications are also in the range. Apart from this, the computed numerical values of activity coefficients suggest that the activity coefficient is decreased while increasing the charge number.

This is mainly caused due to the consideration of ionic strength of the solution. The dependency of charge of ions is vital in the computation of ionic strength (see Eq. 3.12, which is a important parameter in the Debye-Hückel theory for the computation of activity coefficients. As a result, these differences in the activity coefficients are obtained. Moreover, the influences of activity coefficients are observed as strongly dependent on the salt and water contents of mixtures. The dependency or influence of non-ideality is observed to decrease with an increase of the salt content in a mixture, especially, if the water content is decreased at the same time. However, the activity coefficient values for the ions, which are parametrized from the original AIOMFAC, (e.g. SO_4^{2-} , HSO_4^-etc) found to be dissimilar, due to their corresponding interaction coefficients incorporated in the computation of activity coefficients. Simultaneously, as shown in Table. 6.2, the ions, those interaction parameters are adopted from mod.LIFAC also found to be dissimilar with each other. However, for those ions, whose interaction parameters, are assigned to be zero, the predicted activity coefficients are same. All in all, the observed pattern for the activity coefficients of inorganic ions are less than unity and the activity coefficient values are strongly depends on the charge number. Moreover, while increasing the charge number the activity coefficient values are decreased.

Apart from the molar concentrations the predicted activity coefficients have strong influence on the reaction equilibrium constant. For instance, according to the incorporation of treatment of non-ideality for the equilibrium reactions shown in Sec. 5.1.2 (see Eq. 5.8 and Eq. 5.9) the equilibrium constant can be computed as the ratio of activities (whereas $\gamma = 1$ for ideal solutions) between products to reactants. Due to the predicted activity coefficients obtained as less than unity, the equilibrium constraint will be decreased, when considering the non-ideal solutions in comparison with ideal solutions. Hence, the equilibrium will be shifted from backward to forward, depending on the activity coefficients. As shown in Sec. 5.1.2, the computational procedure for the rate of the reaction (see Eq. 5.3 and Eq. 5.4), the rate of the reaction would be decreased, since the predicted activity coefficients are less than unity for inorganic ions, while

considering the non-ideal solutions in comparison with ideal solutions. For increasing the charge number of the ions, the activity coefficients are decreased ($\gamma^{+/-} > \gamma^{2+/2-} \dots > \gamma^{n+/n-}$, see Table. 6.2). Subsequently, the rate of reaction for irreversible reactions and equilibrium constant for the equilibrium reactions will be decreased due to the incorporation of treatment of non-ideality for the aqueous phase chemistry.

Table 6.2: Predicted activity coefficients of the selected ions and water activity in the deliquescent particles for the simulations 90%-NIDR and 90%-NIDU.

| Species | Remote | | Urban | |
|---------------------------------|--------|-------|-------|-------|
| | Day | Night | Day | Night |
| <i>Inorganic anions</i> | | | | |
| SO ₄ ²⁻ | 0.33 | 0.33 | 0.26 | 0.26 |
| HSO ₄ ⁻ | 0.59 | 0.59 | 0.52 | 0.51 |
| NO ₃ ⁻ | 0.65 | 0.66 | 0.59 | 0.59 |
| OH ⁻ | 0.73 | 0.73 | 0.65 | 0.64 |
| F ⁻ | 0.85 | 0.84 | 0.73 | 0.75 |
| Cl ⁻ | 0.85 | 0.84 | 0.73 | 0.75 |
| Br ⁻ | 0.63 | 0.63 | 0.56 | 0.52 |
| I ⁻ | 0.60 | 0.63 | 0.53 | 0.52 |
| <i>Inorganic cations</i> | | | | |
| H ⁺ | 0.74 | 0.74 | 0.68 | 0.68 |
| NH ₄ ⁺ | 0.67 | 0.69 | 0.63 | 0.62 |
| Na ⁺ | 0.71 | 0.71 | 0.67 | 0.66 |
| K ⁺ | 0.69 | 0.69 | 0.65 | 0.64 |
| Mg ²⁺ | 0.45 | 0.45 | 0.39 | 0.38 |
| Ca ²⁺ | 0.38 | 0.38 | 0.39 | 0.38 |
| Fe ²⁺ | 0.33 | 0.33 | 0.33 | 0.28 |
| Mn ²⁺ | 0.33 | 0.33 | 0.33 | 0.33 |
| Cu ²⁺ | 0.36 | 0.35 | 0.37 | 0.36 |
| Fe ³⁺ | 0.12 | 0.11 | 0.13 | 0.12 |
| Mn ³⁺ | 0.12 | 0.12 | 0.13 | 0.12 |
| <i>water activity</i> | 1.53 | 1.51 | 1.62 | 1.60 |

In the current performed simulations, the influence of activity coefficients for the inorganic ions might be small, probably due to the dominance of organic compounds in the simulated aerosol at 90% RH. This influence on the multiphase processing of the inorganic compounds can be more in absence of organic chemistry (i.e. the multiphase mechanism comprises only inorganic chemistry). Furthermore, the influence can be expected more, for high concentrated solutions when the RH range is $\leq 80\%$. In order to understand the behavior and pattern of modeled activity coefficients comparisons have been performed for the simple multiphase mechanism like INORG mechanism (see [Sehili et al. \(2005\)](#)). Interestingly, the results were observed approximately about 2% difference with the CAPRAM2.4+organicExt. Hence, it was clear that organic scheme incorporated in the multiphase mechanism CAPRAM2.4+organicExt, itself have influences in the predication of activity coefficient values. Furthermore, it has been observed that the predicted

activity coefficients are in good agreement for the INORG mechanism with the AIM model (Clegg et al., 1998a,b).

In spite, the computation of activity coefficients for the remaining ions (those experimental interaction parameters are not available, yet included in the system, for instance succinate, glycolate...etc.), mainly performed from the Pitzer-like part implemented in the extended AIOMFAC. However, concerning the conceptual model uncertainties as well as the limited experimental data sets, it is clear that the extended AIOMFAC cannot predict the activity coefficients of multicomponent organic-electrolyte mixtures, with same high level of accuracy as the Pitzer-like part of AIOMFAC (since most of the MR interaction parameters are assigned to zero) or other detailed thermodynamic models, such as the AIM model (Clegg et al., 1998a,b), as attained for aqueous electrolyte solutions (organic-free). Apart from these, the water activity, which is obtained as greater than unity (see Table. 6.2) might change the both microphysics (to find the new equilibrium and critical radius, critical supersaturation) and multiphase chemistry (see Fig. 5.3).

The partitioning between gas to liquid phase is also found differences due to the incorporation of treatment of non-ideality for the aqueous phase chemistry. However, the observed influence is not eminent due to the aforementioned reasons (i.e. for moderate concentrated solutions and consideration of organic compounds). Moreover, equilibrium partial pressures of the inorganic gases HNO_3 , lead to be different for the non-ideal solutions compare with ideal solutions. The gas/liquid equilibrium of HNO_3 is described, on the molality scale, as: $K_{H(\text{HNO}_3)} = a_{\text{H}^+} \cdot a_{\text{NO}_3^-} / p_{\text{HNO}_3} = m_{\text{H}^+} \gamma_{\text{H}^+} \cdot m_{\text{NO}_3^-} \gamma_{\text{NO}_3^-} / p_{\text{HNO}_3}$, where the $K_{H(\text{HNO}_3)}$ is the molality based Henry's law constant of HNO_3 will be modified by the consideration of activity coefficients. Thus, it is clear from the above equation that the differences between the ideal and non-ideal solutions will be mainly caused by differences in γ_{H^+} and $\gamma_{\text{NO}_3^-}$.

6.2.4.2 Organic compounds

Similar to the inorganic compounds, the predicted activity coefficient values for the key organic compounds are tabulated in the Table. 6.3. As can be seen, the pattern of the predicted activity coefficients are >1 for alcohols, some of the dialdehydes and for the dicarboxylic acids. In addition, the activity coefficients of some of the aldehydes and mono carboxylic acids are less than unity. Non-unity activity coefficients for aerosol components have been previously inferred from other measurements (Jang et al., 1997; Mukherji et al., 1997); however, it has generally been asserted that non-unity γ 's arise from mixing together very dissimilar materials and are usually $\gamma > 1$. For the organics, the computation of activity coefficients, strongly depends on the composition of corresponding species (i.e. $\gamma_{org} = f(C_{org})$). Furthermore, apart from the chemical composition, the functional subgroups have substantial contribution regarding the computation of activity coefficients. For instance, malonic acid have two functional subgroups ($2 \times \text{COOH}$ and $1 \times \text{CH}_2$). The activity coefficients are computed for each subgroup included in the corresponding compound for the residual part described in the SR contribution. Hence, the computed activity coefficient for the each functional subgroup (see Eq. 3.38) have a substantial contribution in the calculation of total compound activity coefficient. If one of the functional subgroup has the activity coefficient as greater than unity, the activity coefficient of the total compound will be greater than unity, since the subgroup activity coefficients are multiplied with each other. Finally, as explained in Sec. 3.6, the activity coefficients obtained from the different interaction contributions are the product of individual interactions (see Eq. 3.49). This gives the total activity coefficient as greater than or less than unity for the corresponding species. This is

the main reason in order to obtain the activity coefficients greater than unity for some of the compounds and less than unity for some of the compounds shown in Table. 6.3.

The values of the activity coefficients for some of the compounds were obtained very large for the polluted environmental scenario (≈ 1.2 to 50) during the sensitivity studies (not shown here), while investigating the influence of non-ideality for aqueous phase for smaller particles. Such a large values were also observed while estimation of infinite dilution activity coefficients of organic compounds in water with neural classifiers (see Giralt et al. (2004)). Similar large values (≈ 1.2 to almost 2500) were also observed during the dynamic gas/partitioning calculations using UCD-CACM model (see Clegg et al. (1998a)) in spectral distribution of aerosol particles. As a result, it has been clear that the range of activity coefficients can be high for smaller particles (even at 90% RH) due to the available amount of LWC in the deliquescent particles. Furthermore, the central factor affecting the partitioning of the organic compounds, are consideration of chemical reactions and gas/particle mass exchange, and their corresponding activity coefficients in the aqueous phase. The dissociation of organic acids in the aqueous phase has the potential affect on both, mass of the compounds included in the system, and also aerosol pH. The observed magnitude of this influence, mainly depends on the activity coefficients calculated for, or assigned to, the undissociated organic acid molecule and organic acid anions as well as the pH controlled by the inorganic electrolytes present.

Even the activity coefficients for the organic ions are also less than unity, for the dissociation of organic compounds the the backward reaction proceeds slowly since the activity coefficient for the organic ions are found as less then unity. However, the forward reaction is proceeds faster compare with backward reaction (see the discussion in Sec. 6.2.4.1). In such a way, it is become prominent, that the multiphase processing of organic chemistry can also be declined. The predicted activity coefficients for these compounds in the multicomponent mixture were observed to be quite variable even though they are chemically very similar and differ only with the functional subgroups (for instance $-\text{CH}_2$, OH and/or COOH).

Table 6.3: Predicted activity coefficients of the selected organic compounds in the deliquescent particles for the simulations 90%-NIDR and 90%-NIDU.

| Species | Remote | | Urban | |
|--|--------|-------|-------|-------|
| | Day | Night | Day | Night |
| <i>Alcohols</i> | | | | |
| Methanol | 1.04 | 1.04 | 1.19 | 1.09 |
| Ethanol | 1.17 | 1.15 | 1.14 | 0.92 |
| <i>Aldehydes</i> | | | | |
| <u>Formaldehyde</u> | | | | |
| CH ₂ OH ₂ | 0.82 | 0.82 | 0.38 | 0.38 |
| HCHO | 0.83 | 0.83 | 0.75 | 0.74 |
| <u>Acetaldehyde</u> | | | | |
| CH ₃ CHO | 0.79 | 0.79 | 0.77 | 0.72 |
| CH ₃ CHOH ₂ | 1.26 | 1.246 | 1.08 | 1.02 |
| Propionaldehyde | 1.07 | 1.07 | 1.19 | 1.06 |
| Butyraldehyde | 1.34 | 1.32 | 1.83 | 1.58 |
| <i>Substituted carbonyl compounds</i> | | | | |
| <u>Glycolaldehyde</u> | | | | |

Table 6.3: Predicted activity coefficients of the selected organic compounds in the deliquescent particles for the simulations 90%-NIDR and 90%-NIDU(Continued)

| Species | Remote | | Urban | |
|---|--------|-------|-------|-------|
| | Day | Night | Day | Night |
| OHCCH ₂ OH | 0.73 | 0.72 | 0.45 | 0.45 |
| OH ₂ CHCH ₂ OH | 1.42 | 1.39 | 1.22 | 1.17 |
| <u>Glyoxal</u> | | | | |
| CHOH ₂ CHOH ₂ | 1.08 | 1.05 | 0.59 | 0.57 |
| GLY | 0.49 | 0.49 | 0.37 | 0.35 |
| CH ₃ COCHOH ₂ | 1.02 | 1.09 | 0.72 | 0.74 |
| OHCCHCHCHO | 1.05 | 0.87 | 1.07 | 0.86 |
| 2-hydrody 3-oxo butanedial | 0.28 | 0.28 | 0.16 | 0.15 |
| <u>Monocarboxylic acids</u> | | | | |
| <u>Formic acid</u> | | | | |
| HCOOH | 0.90 | 0.90 | 0.85 | 0.85 |
| HCOO ⁻ | 0.65 | 0.65 | 0.59 | 0.59 |
| <u>Acetic acid</u> | | | | |
| CH ₃ COOH | 0.86 | 0.85 | 0.82 | 0.80 |
| CH ₃ COO ⁻ | 0.74 | 0.74 | 0.68 | 0.68 |
| Propanoic acid | 1.13 | 1.12 | 1.41 | 1.26 |
| Butyric acid | 1.47 | 1.45 | 2.17 | 1.86 |
| <u>Glycolic acid</u> | | | | |
| CH ₂ OHCOOH | 0.80 | 0.79 | 0.55 | 0.53 |
| CH ₂ OHCOO ⁻ | 0.72 | 0.72 | 0.67 | 0.67 |
| <u>Glyoxylic acid</u> | | | | |
| CHOH ₂ COOH | 0.75 | 0.73 | 0.67 | 0.67 |
| CHOH ₂ COO ⁻ | 0.72 | 0.72 | 0.33 | 0.33 |
| <u>Pyruvic acid</u> | | | | |
| CH ₃ COCOOH | 0.87 | 0.86 | 0.91 | 0.85 |
| CH ₃ COCOO ⁻ | 0.72 | 0.72 | 0.67 | 0.67 |
| <u>Dicarboxylic acids</u> | | | | |
| <u>Oxalic acid</u> | | | | |
| H ₂ C ₂ O ₄ | 0.59 | 0.59 | 0.51 | 0.50 |
| C ₂ O ₄ ²⁻ | 0.37 | 0.37 | 0.33 | 0.33 |
| HC ₂ O ₄ ⁻ | 0.72 | 0.72 | 0.67 | 0.67 |
| Fe(C ₂ O ₄) ₂ ⁻ | 0.72 | 0.72 | 0.67 | 0.67 |
| Fe(C ₂ O ₄) ⁺ | 0.72 | 0.72 | 0.67 | 0.67 |
| Fe(C ₂ O ₄) ₃ ³⁻ | 0.12 | 0.12 | 0.10 | 0.10 |
| <u>Malonic acid</u> | | | | |
| HOOCCH ₂ COOH | 1.38 | 1.31 | 1.22 | 1.08 |
| HOOCCH ₂ COO ⁻ | 0.65 | 0.65 | 0.59 | 0.58 |

Table 6.3: Predicted activity coefficients of the selected organic compounds in the deliquescent particles for the simulations 90%-NIDR and 90%-NIDU(Continued)

| Species | Remote | | Urban | |
|--|--------|-------|-------|-------|
| | Day | Night | Day | Night |
| OOCCH ₂ COO ²⁻ | 0.36 | 0.36 | 0.33 | 0.33 |
| <u>Succinic acid</u> | | | | |
| C ₂ H ₄ (COOH) ₂ | 1.38 | 1.31 | 1.22 | 1.08 |
| HOCC ₂ H ₄ COO ⁻ | 0.65 | 0.65 | 0.59 | 0.58 |
| OOCCH ₂ CH ₂ COO ²⁻ | 0.36 | 0.36 | 0.33 | 0.33 |
| <u>Keto malonic acid</u> | | | | |
| HOCCOCO ^{OH} | 0.89 | 0.89 | 0.84 | 0.84 |
| HOCCOCO ^{O-} | 0.65 | 0.65 | 0.67 | 0.67 |
| OCCOCO ^{O2-} | 0.36 | 0.36 | 0.33 | 0.33 |
| <u>Malic acid</u> | | | | |
| HOOCCHOHCH ₂ COOH | 1.13 | 1.08 | 0.94 | 0.88 |
| HOOCCHOHCH ₂ COO ⁻ | 0.65 | 0.65 | 0.67 | 0.67 |
| OOCCHOHCH ₂ COO ²⁻ | 0.36 | 0.36 | 0.33 | 0.33 |

Similar to the current predicted activity coefficients for diacids as, $2 > \gamma_i \geq 1$, the same range of activity coefficients were reported using UNIFAC group contribution approach (see Cappa et al. (2008)). The values of predicted activity coefficients, shown in Table. 6.3, that are less than unity are some how unexpected, especially because it will lead to increased partitioning of these compounds (e.g. glycolic and glyoxylic acid) to the particle phase. As argued by Cappa et al. (2008) in their investigations, the vapor pressures of individual components show strong, identity-dependent deviations from ideality (i.e. Raoult's Law), with the vapor pressures of the smaller, more volatile compounds decreased significantly in the mixtures. In addition, they found in their experimental investigations, that the activity coefficients for some of the organic compounds are also in the range of less than unity, as this model results were obtained. Furthermore, based on the obtained numerical values, it can be expected that, this non-ideal behavior of these compounds can modify their gas-particle partitioning, much more for the larger, lower vapor pressure compounds. Moreover, it can be possible that the physical properties such as vapor pressure of these more abundant, lower-molecular-weight components in organic/inorganic mixtures are apparently lower than those of the pure compounds, probably lead to this behavior (i.e., $\gamma < 1$). Evidently, the addition of an inorganic salt, for instance NaCl, NaNO₃ and (NH₄)₂SO₄ influences the nature of the intermolecular interactions in compound specific ways, where the MR interactions found to be important. As for these simulations, the (NH₄)₂SO₄ particles are initialized, hence the total interactions between the organic compounds and the inorganic compounds, caused for this behavior, where the activity coefficient values are less than unity.

6.2.5 Particle acidity

Particle acidity is important determining indicator for the physico-chemical processing of multi-phase chemistry. Thus, the determination of pH variations were investigated during the cloud droplets as well as deliquescent particles while considering the aqueous phase as non-ideal solution in comparison with ideal solutions. The H⁺ concentration is initialized in the SPACCIM by means

of a charge balance, afterwards the time evolution of pH was computed dynamically throughout the simulation time (see [Sehili et al. \(2005\)](#)). As a result, it can be expected that the particle acidity will be affected, both of the changes in chemical processing as well as microphysical conditions. Mainly, the pH is obstructed by the microphysical aspects, such as liquid water content. The resulting evolution of pH from the simulations during the whole simulation time is shown in [Fig. 6.20](#) for the urban environmental conditions (corresponding illustration for remote scenario is presented in [Fig. C.5](#)). As shown in [Fig. 6.20](#), the predicted value of pH is, initially about 3 for the performed simulations while assuming the aqueous phase chemistry as ideal and non-ideal solutions. During the first cloud period (day time cloud) the pH is increased up to 5 (solution becomes basic). Interestingly, the value of pH is decreased and the solution becomes acidic during the aqueous deliquescent particles. However, the value of pH is constantly decreasing during the cloud periods as well as in the deliquescent particles. Moreover, the difference in the pH for the simulations performed while assuming the aqueous phase chemistry as ideal and non-ideal solutions in the deliquescent particles is approximately about 10%. However, the predicted pH at the end of simulation time is about 0.4 when treatment of non-ideality was incorporated for the aqueous phase chemistry. Whereas the pH is about 0.6 at the end of the simulation time, when the aqueous phase chemistry was considered as ideal solutions. Due to the continuous mass feedback, the pH is gradually decreased after the cloud periods.

As mentioned in [Sec. 6.2.4.1](#), when the ionic strength increases, the activity coefficient of ions decreases. This has an effect of lowering the activity of hydrogen ion ([Suryanarayana, 2002](#)), which is seen as an decrease in pH (more acidic). Moreover, the presence of other ions (such as Na^+ , SO_4^{2-} , Ca^{2+}) in solution tends to limit the mobility of the hydrogen ion, thereby decreasing the activity of H^+ . Furthermore, in the cloud droplets, the acidity is interrupted by the microphysical LWC. This is due to the large quantity of LWC in the cloud droplets, the solution act as ideal solution. However, after the cloud evaporation the differences be more or less prominent. Due to the availability of LWC, the pH of cloud droplets doesn't shown any deviations for the simulations 90%-IDU and 90%-NIDU. Furthermore, the inorganic and organic components of the aerosol affect each other mainly through the liquid water content, which controls the partitioning of the water soluble semi-volatile compounds, and to a lesser extent through the pH.

Interestingly, under polluted conditions, the differences in the particle acidity is noteworthy, since the availability of acid forming precursors such as SO_2 and, especially due the available NO_3 in the particle phase. This tendency to lower pH (more acidic) implicates, that the chemical processes such as dissociation of organic compounds that can produce more H^+ ions, may probably act as more important medium during the deliquescence period compare with cloud droplets. On the whole, the modeled average pH values of the deliquescent particles are around 1.2 and 1.4 (on the average over whole simulation period) in the urban and remote environmental conditions respectively. This is significantly smaller than the simulation 90%-IDU and 90%-IDR. All in all, the current results admits the acidification of aqueous particles becomes obvious by cloud processing. Furthermore, pH changes lead to differences in cloud chemistry and gas uptake, as well. As illustrated in [Fig. 6.20](#) the evolution of pH is gradually decreased from first cloud period to last cloud period. In spite of urban scenario, the deviations in the evolution of pH for the remote environmental conditions are mainly caused due to the S(VI) production (see [Fig. C.5](#)). Moreover, the similar pattern (particles becoming acidic) is observed for both environmental conditions. As mentioned earlier, this simulations are performed with the 90% RH level. Despite, the evolution of pH would be notable for the sensitivities, while reducing the relative humidity, which are commonly encounter in the atmosphere. Furthermore, only a limited data available for the pH measurements for continental aerosol particles considering the treatment of non-ideality

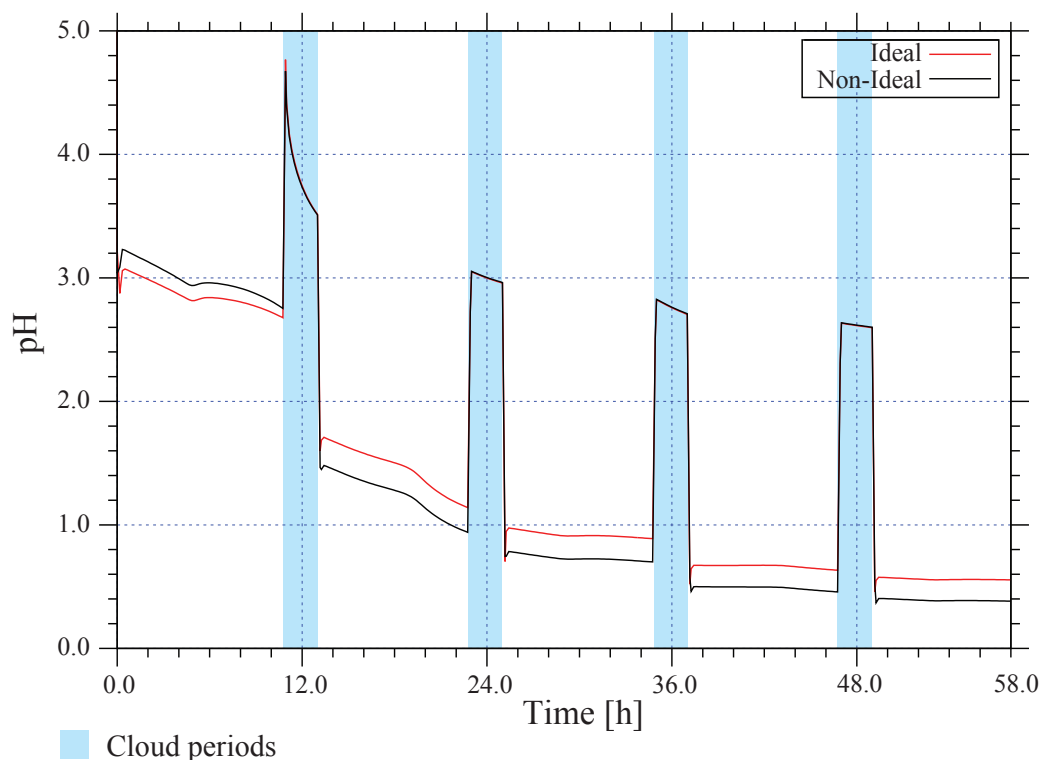


Figure 6.20: Modeled *pH* value as a function of time for the urban environmental scenario for the simulations 90%-IDU vs. 90%-NIDU.

for the aqueous phase chemistry. Hence, comparisons between predicted and measured *pH* was not examined in this study.

6.2.6 Multiphase processing of inorganics

The gas/aerosol partitioning of water-soluble organic semi-volatile compounds links to the thermodynamics of the inorganic fraction of the aerosol particles mainly via the amount of aerosol water, dissociation to $\text{H}^+_{(aq)} \leftrightarrow$ organic anions, and interactions between inorganic ions \leftrightarrow organic molecules that lead to changes in the activity coefficients. Based on the behavior and range of the modeled activity coefficients for the inorganic ions (see Table. 6.2), the influence of treatment of non-ideality on multiphase processing of inorganic compounds will be discussed in the following subsections.

6.2.6.1 Sulphur processing

Sulphur dioxide (SO_2) can be oxidized in both gas phase by the OH radical and in the cloud phase by several ways. However, it is evident with various model studies that the S(VI) in-cloud oxidation pathways are more favored, due to their higher efficiency. Aiming to investigate the

behavior of S(VI) oxidation, the current models simulations were performed while considering the ideal and non-ideal solutions for the aqueous phase chemistry. Fig. 6.21 shows the modeled aqueous phase S(VI) concentration in $\text{mol m}_{(air)}^{-3}$ as a function of the modeling time for the urban environmental conditions. As shown in Fig. 6.21, the S(VI) is effectively produced in the cloud droplets. Furthermore, the production is higher in the day time clouds, compare with night time cloud periods. This production is about 2.5×10^{-7} in the first noon cloud and about 4.3×10^{-7} in the consequent noon clouds, where as the production in the deliquescent particles is all most constant during the day and night times. At the same time, the production in the first night time is about 2.8×10^{-7} and about 4.8×10^{-7} in the alternative night time cloud period. In summary, the production is all most all similar in the cloud periods, for the simulations 90%-IDU and 90%-NIDU. As, it is clear that cloud periods are behaves like ideal solutions. Hence, it can be argued that, the implemented model works well. However, the contribution of reaction pathways for S(VI) are decreased approximately about 50% during the night time cloud periods in comparison with noon clouds. Very small differences are observed in the deliquescent particles. However, these small differences are most likely caused by the change in pH.

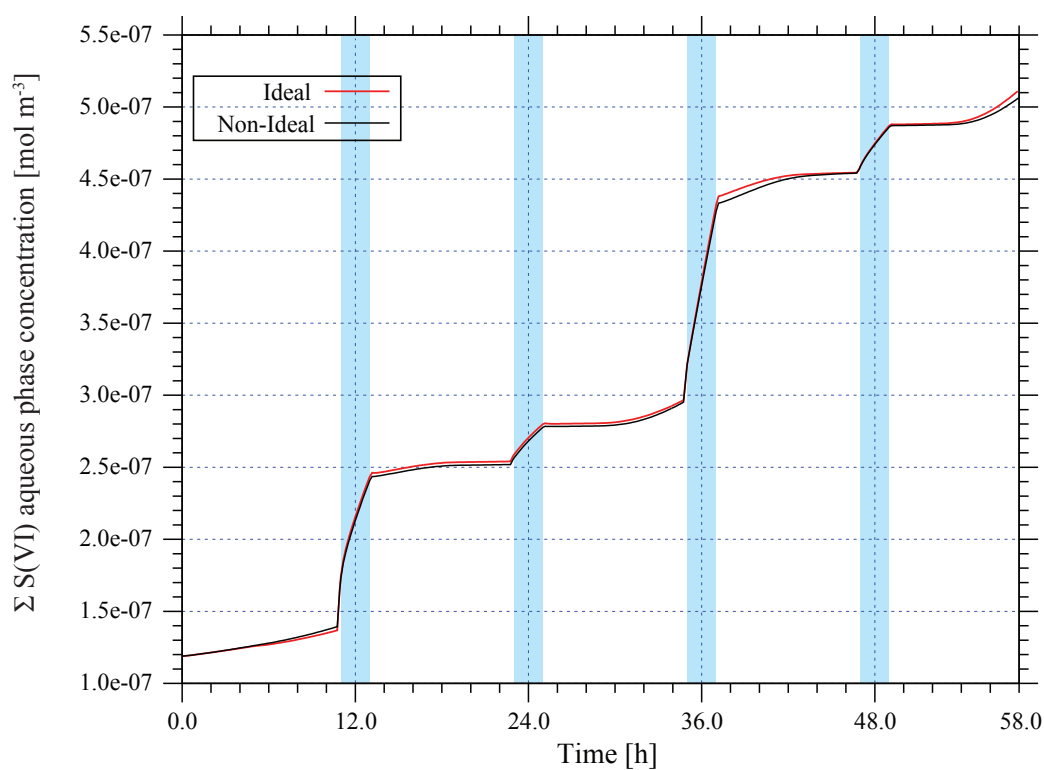


Figure 6.21: Modeled S(VI) aqueous phase concentration in mol m^{-3} vs. modeling time for the urban scenario for the simulations 90%-IDU vs. 90%-NIDU.

6.2.6.2 Iron chemistry

It has been indicated by several authors (for instance [Deguillaume et al. \(2005\)](#) and references therein) that iron is the most abundant TMI in the tropospheric particles, which play a vital role in the atmospheric chemistry of fog and droplets. Furthermore, the behavior of time dependent chemical processing of iron in clouds and deliquescent particles under non-ideal conditions is quite important to investigate, since the iron speciation and redox-cycling is responsible for several chemical interactions, for instance HO_x/HO_y processing ([Tilgner, 2009](#)). Furthermore, [Deguillaume et al. \(2005\)](#) argued in their review that still large uncertainties of TMI chemistry within cloud droplets, since the iron speciation is an indicator for the atmospheric oxidation and reduction as well as reactivity of the aqueous phase radical chemistry. However, the uncertainties are small in the cloud droplets compare with aqueous deliquescent particles. [Tilgner and Herrmann \(2010\)](#) have shown, quite strong relevance for the processing of iron chemistry in deliquescent particles. In light of this, thus, this study aimed to bridge the gap between the uncertainties explained in the former studies, by incorporating the treatment of non-ideality. Fig. 6.22, illustrates the aqueous phase concentration of Fe(II) in mol m^{-3} vs. total simulation time along with the time evolution of corresponding activity coefficient for the whole simulation time.

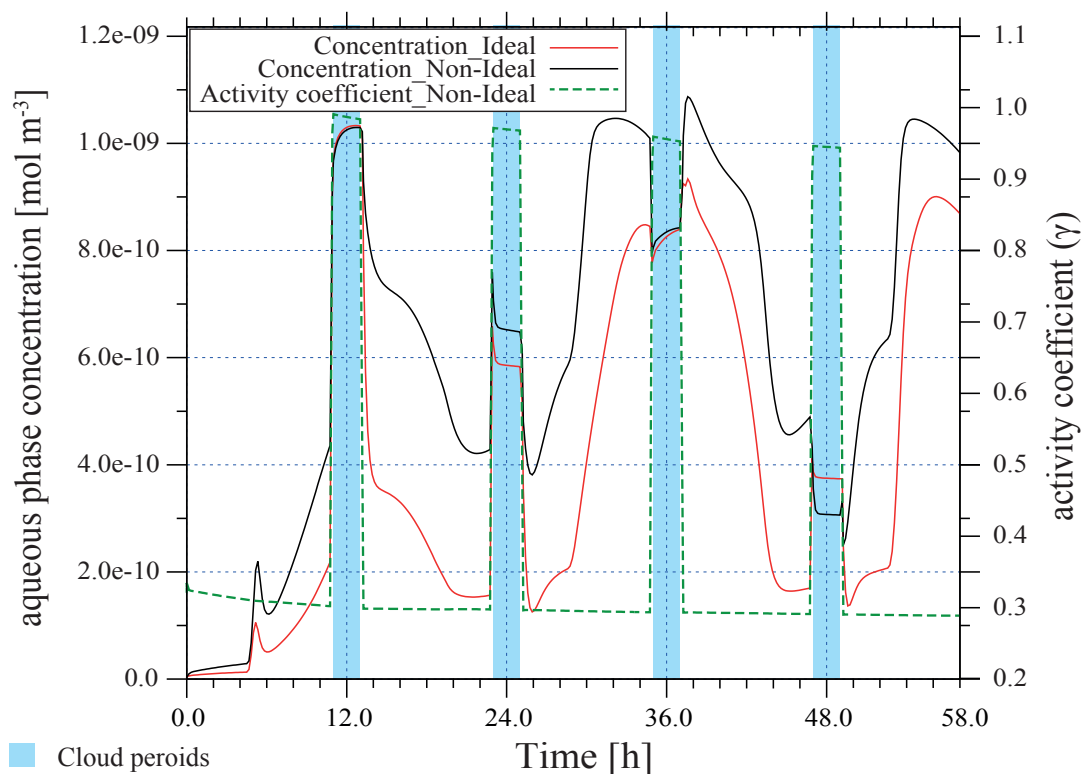


Figure 6.22: Modeled Fe(II) aqueous phase concentration in mol l^{-1} vs. modeling time for the urban scenario for the simulations 90%-IDU vs. 90%-NIDU.

The corresponding, total sinks and sources of Fe(II) in the aqueous phase against a selected interval of the modeling time is shown in Fig. 6.22. The corresponding plots for remote case is also presented in the Appendix (see Fig. C.2). As can be seen from Fig. 6.22, the aqueous phase concentration is higher while considering the aqueous phase chemistry as non-ideal solutions in

comparison with ideal solutions during the deliquescent particle phase. However, in the night time clouds the aqueous phase concentrations are approximately about 45% of the concentrations in the noon clouds. Significant differences, can be seen from this plot in the aqueous phase concentrations in the night cloud periods. Due to the implemented scheme of chemistry (mass) feedback of aqueous phase particle chemistry on the cloud chemistry, the differences are obvious in the aqueous phase concentrations for the simulations performed for the simulations 90%-IDU vs. 90%-NIDU. One can explain this, as the photochemistry which is inactive during the night time, might be the main reason for these discrepancies. Furthermore, the concentration profile is declined for the simulation 90%-NIDU compare with 90%-IDU. As shown in the evolution of activity coefficient which is less than unity is the main reason to obtain these deviations in aqueous deliquescent particles. However, the aqueous phase concentrations are increased for 90%-NIDU to 90%-IDU with approximately about 20%. The Fe(II) sources are dominating than sinks, hence the total aqueous phase concentrations are higher for 90%-IDU than 90%-NIDU (see Fig. 6.23).

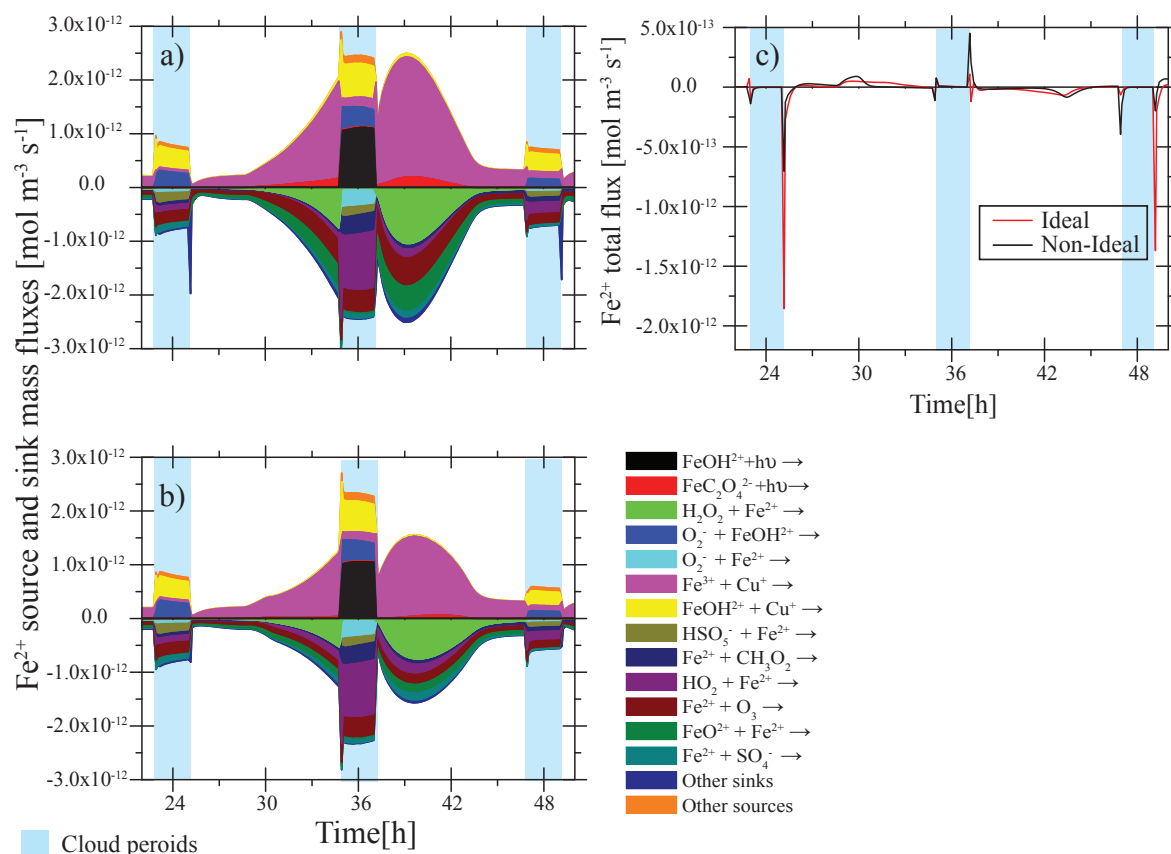


Figure 6.23: Modeled chemical sink and source mass fluxes of Fe(II) in aqueous phase in $\text{mol m}^{-3} \text{s}^{-1}$ for the second day of modeling time for the urban scenario for the simulations 90%-IDU vs. 90%-NIDU. a) ideal solutions (90%-IDU), b) non-ideal solutions (90%-NIDU), c) corresponding total fluxes. Only sinks and sources with a contribution larger than $\pm 1\%$ presented.

However, due to the activity coefficient which is less than unity, influences the whole processing of Fe(II). For instance, the Fenton reaction which acts as sink for the Fe(II) processing, the contribution is reduced for 90%-NIDU compare with 90%-IDU. In this reaction, the activity coefficients for the OH radical and H_2O_2 are treated as unity. Hence, the rate of the reaction

would be decreased (see the discussion in Sec. 6.2.4.1). As shown in the Table. 6.2, the activity coefficients for all the ions are less than unity. Hence, the rate of the reaction would be decreased depending on the corresponding activity coefficients, as a result the sources and sink fluxes are decreased as shown in the Fig. 6.23 and Table. 6.4. Furthermore, the influence of treatment of non-ideality can be obtained from Fig. 6.23, where the interconversion reaction between Fe^{3+} and Cu^+ act as a major source for the Fe^{2+} .

As described earlier, the corresponding activity coefficients of the ions modifies the reaction rate for the production of Fe(II). Subsequently, it has been clear that, the predicted activity coefficients would decide the multiphase processing of Fe(II) chemistry. The deviations and advantages by incorporating the treatment of non-ideality for aqueous phase chemistry can be obtained from the integrated percentage contributions. Table. 6.4 shows the important reaction pathways along with integrated percentage contributions of the main sinks and sources reactions for Fe(II), caused for the deviations between the simulations 90%-IDU and 90%-NIDU.

Table 6.4: Integrated percentage contributions of the most important Fe(II) sources and sinks reactions for the urban case classified regarding to the various microphysical conditions during the simulation time considering ideal and non-ideal solutions for aqueous phase chemistry (Total = Total contributions throughout the simulation time, Total clouds = Contribution throughout all cloud events, Aqueous aerosol particles = Contribution throughout the deliquescent particle conditions, Δ Difference = Difference between the aqueous phase particle fluxes (90%-NIDU - 90%-IDU), only sinks and sources with a contribution larger than \pm % presented for 90%-IDU vs. 90%-NIDU).

| Reaction | Ideal | | Non-ideal | | Δ Difference |
|---|---------|----------------|-----------|----------------|---------------------|
| | Total | Aqueous clouds | Total | Aqueous clouds | |
| $\text{Fe}(\text{OH})_2^+ + h\nu \rightarrow \text{Fe}^{2+} + \text{OH}^-$ | 13.8% | 32.8% | 16.2% | 33.1% | 1.5% |
| $\text{Fe}(\text{C}_2\text{O}_4)_2^- \rightarrow$ | 4.8% | 0.6% | 3.0% | 0.8% | -2.2% |
| $\text{H}_2\text{O}_2 + \text{Fe}^{2+} \rightarrow \text{Fe}^{3+} + \text{OH}^- + \text{OH}^-$ | -24.6% | -0.5% | -25.1% | -0.5% | -3.0% |
| $\text{O}_2^- + \text{Fe}^{3+} \rightarrow \text{Fe}^{2+} + \text{O}_2$ | 1.1% | 3.5% | 1.3% | 3.6% | 0.0% |
| $\text{HO}_2 + \text{Fe}(\text{OH})_2^+ \rightarrow$ | 0.4% | 1.2% | 0.4% | 1.2% | 0.0% |
| $\text{O}_2^- + \text{Fe}(\text{OH})_2^+ \rightarrow \text{Fe}^{2+} + \text{O}_2 + \text{OH}^-$ | 5.9% | 21.7% | 7.4% | 23.1% | 0.2% |
| $\text{O}_2^- + \text{Fe}(\text{OH})_2^+ \rightarrow$ | 0.3% | 1.2% | 0.3% | 1.1% | 0.0% |
| $\text{O}_2^- + \text{Fe}^{2+} \rightarrow$ | -4.2% | -15.4% | -5.2% | -16.5% | -0.1% |
| $\text{Fe}^{3+} + \text{Cu}^+ \rightarrow \text{Fe}^{2+} + \text{Cu}^{2+}$ | 55.3% | 6.6% | 51.9% | 6.1% | -0.4% |
| $\text{Fe}(\text{OH})_2^+ + \text{Cu}^+ \rightarrow \text{Fe}^{2+} + \text{Cu}^+ + \text{OH}^-$ | 17.6% | 30.0% | 18.6% | 28.9% | 0.7% |
| $\text{Fe}(\text{OH})_2^+ + \text{Cu}^+ \rightarrow$ | 0.4% | 1.5% | 0.4% | 1.2% | 0.0% |
| $\text{Fe}^{2+} + \text{Mn}^{3+} \rightarrow \text{Fe}^{3+} + \text{Mn}^{2+}$ | -1.3% | 0.0% | -0.7% | 0.0% | 0.8% |
| $\text{HSO}_5^- + \text{Fe}^{2+} \rightarrow \text{SO}_4^- + \text{Fe}(\text{OH})_2^+$ | -4.1% | -15.5% | -4.9% | -15.4% | 0.2% |
| $\text{Fe}^{2+} + \text{CH}_3\text{O}_2 \rightarrow \text{Fe}(\text{CH}_3\text{O}_2)_2^+$ | -5.2% | -8.8% | -6.7% | -8.8% | -1.1% |
| $\text{HO}_2 + \text{Fe}^{2+} \rightarrow$ | -11.42% | -25.0% | -16.1% | -25.5% | -5.1% |
| $\text{OH} + \text{Fe}^{2+} \rightarrow \text{Fe}(\text{OH})_2^+$ | -1.2% | -0.1% | -0.8% | -0.1% | 0.4% |
| $\text{Fe}^{2+} + \text{O}_3 \rightarrow \text{FeO}^{2+} + \text{O}_2$ | -20.9% | -18.9% | -15.9% | -18.6% | 6.7% |
| $\text{FeO}^{2+} + \text{Fe}^{2+} \rightarrow \text{Fe}^{3+} + \text{OH}^-$ | -14.0% | -1.2% | -8.8% | -1.8% | 6.0% |
| $\text{FeO}^{2+} + \text{Fe}^{2+} \rightarrow$ | -1.4% | -0.1% | -0.9% | -0.1% | 0.6% |
| $\text{SO}_5^- + \text{Fe}^{2+} \rightarrow$ | -1.2% | -4.8% | -1.3% | -4.5% | 0.0% |
| $\text{Fe}^{2+} + \text{SO}_4^{2-} \rightarrow$ | -6.6% | -9.5% | -7.5% | -9.0% | -1.2% |
| $\text{Cl}_2^- + \text{Fe}^{2+} \rightarrow \text{Cl}^- + \text{Fe}^{3+}$ | -1.1% | 0.0% | -1.7% | 0.0% | -0.9% |
| $\text{Br}_2^- + \text{Fe}^{2+} \rightarrow \text{Br}^- + \text{Fe}^{3+}$ | -1.8% | 0.0% | -3.5% | 0.0% | -2.5% |

Table 6.4: Integrated percentage contributions of the most important Fe(II) source and sink reactions for the urban case (Continued)

| Reaction | Ideal | | Non-ideal | | Δ Difference in Aqueous particle fluxes |
|---------------|-------|-----------------------------|-----------|-----------------------------|--|
| | Total | Aqueous clouds particles | Total | Aqueous clouds particles | |
| Total sources | 100% | 100% | 100% | 100% | 100% |
| Total sinks | -100% | -100% | -100% | -100% | -100% |

The main differences can also be obtained between cloud droplets and deliquescent particles by integrated percentage contributions of sources and sinks, as shown in Table. 6.4. The major and total contribution for the production of Fe^{2+} is the reaction of Fe^{3+} with Cu^+ contributing in the urban (remote) case about 55% (25%) and 52% (25%) for the simulations 90%-IDU and 90%-NIDU. Furthermore, $\text{Fe}(\text{OH})^{2+}$ photolysis and reaction of $\text{Fe}(\text{OH})^{2+}$ with Cu^{2+} plays a major role as source contributing with 14% (9%) and 18% (10%) for the simulation 90%-IDU although, these reactions are contributing about 16% (9%) and 19% (8%) for the simulation 90%-NIDU. Accordingly, the photolysis of $\text{Fe}(\text{OH})^{2+}$, reaction of Fe^{3+} and $\text{Fe}(\text{OH})^{2+}$ with Cu^+ contributes approximately 32.8% (11%), 7% (0.13%) and 30% (6%) for the simulation 90%-IDU, 33.1% (11%), 6% (0.12%) and 29% (6%) while including the treatment of non-ideality for aqueous phase chemistry in the cloud droplets. However, the same reactions are contributing approximately 8% (6%), 71% (49%) and 14% (13%) for the simulation 90%-IDU and about 10% (7%), 70% (49%) and 15% (11%) for the simulation 90%-NIDU in the deliquescent particles phase.

Moreover, the Fenton reaction seems to be more important sink for the Fe(II) with the total contribution in urban (remote) case is about 24% (53%) and 25% (52%) for the simulations while treating the multiphase chemistry for the simulations 90%-IDU and 90%-NIDU respectively. On the other hand, this reaction contributes approximately 32% (62%) and 35% (61%) in the particle phase for the simulations 90%-IDU and 90%-NIDU respectively. Although, the reaction of Fe^{2+} with ozone also plays a vital role while contributing in the total mass fluxes with about 21% and 16% for the simulations 90%-IDU and 90%-NIDU. Similar behavior was observed with the percentage contribution approximately about 22% and 15% for the simulations 90%-IDU and 90%-NIDU respectively in the particle phase. Interestingly, this reaction of Fe(II) with ozone contributes approximately about 1% in the remote case. Another important reaction which act as the one of the major sink during the particle phase is the reaction with FeO^{2+} , which contributes approximately 18% and 12% for the simulations 90%-IDU and 90%-NIDU respectively in the particle phase, whereas the total contribution is about 14% and 9%, for the simulations 90%-IDU and 90%-NIDU respectively, especially in polluted environmental scenario.

Finally, reaction of Fe^{2+} with sulphur radicals (SO_4^- , HSO_5^-) as well as the reactions of the ferryl ion (FeO_2^+) and formate contributes to a significant amount for the simulations 90%-IDU and 90%-NIDU, besides Fenton reaction. However, the contribution of these reaction pathways are observed as declined for 90%-NIDU compare with 90%-IDU (see Table. 6.4). Furthermore, it has been observed that the oxidation is rather slow for the simulation 90%-NIDU compare with 90%-IDU. However, notable differences can be obtained if, one consider the more concentrated particle phase, since the intermolecular forces are expected to be high during such conditions.

6.2.7 Multiphase processing of radicals

Atmospheric radicals are important oxidants and play a decisive role for the self-cleaning capability of the troposphere. However, the complexity with which one calculates their interactions within the clouds and deliquescence particles, and of course by presence of inorganic and organic species complicates the multiphase radical processing greatly, especially while incorporating the treatment of non-ideality for aqueous phase chemistry. Hence, it is the purpose of these investigations, to study the chemical multiphase processing of radicals while assuming the non-ideal solutions for aqueous phase chemistry in detail. In this respect, it will be able to assess our ability to model these atmospherically important systems to challenge the former studies performed while treating the aqueous phase chemistry assuming the ideal solutions. However, these investigations

are aiming to clarify the main impact of the multiphase interactions and the fate of radicals in the aqueous phase.

6.2.7.1 OH radical

The OH radical has been proven to be one of the important reactive intermediate oxidant in atmospheric chemical processes (Stumm and Morgan, 1996). The characterisation of interaction of hydroxyl radicals with its aqueous environment is particularly important for atmospheric chemistry, as many atmospheric chemical reactions occur in or on aqueous atmospheric aerosols, cloud droplets, and in particles. Hence, it is needed to study the behavior of OH radical in non-ideal solutions. As can be seen from Fig. 6.24, the concentration of OH for urban case in aqueous phase for the simulations 90%-IDU and 90%-NIDU are plotted vs. simulated time, are significantly differed. The corresponding plot for remote case is presented in Fig. C.4. It has been already mentioned that the activity coefficients for the radicals are treated as unity (see Table. 5.1). The aqueous phase concentrations presented here are depends on both the available water, in other words, the microphysical parameters and on the chemical sources as well as sink fluxes of the species, apart from the activity coefficients of the species which are reacting with OH radical. As shown in Fig. 6.24, the lower concentrations are obtained in the urban environmental scenario due to the possible sink fluxes are larger. Furthermore, reduction of OH budget in the aqueous phase can be observed after the cloud evaporation. This reflects the effective oxidation within the cloud. However, the difference between deliquescent particle and cloud droplet conditions are in the range of about two orders of magnitude, and of course lower than the range of the LWC variation of about five orders of magnitude. Hence, sources of OH in the aqueous phase are rather important. It has been observed from the aqueous phase concentrations, the solution effect is more dominating in the nighttime clouds, whereas the in-situ sources of OH radical act more effectively under daytime conditions.

Furthermore, it has been observed that, the aqueous phase concentration is declined during night time clouds for the simulation 90%-NIDU, whereas the concentration is found similar during day time clouds. Since, the in-situ sources of OH radical act more effectively under day-time conditions, similar behavior is observed for both simulations i.e. 90%-NIDU and 90%-IDU. Even though, the activity coefficients for the radicals are considered as unity, the influence of non-ideality has been considered for the computation of reaction rates, when the radicals reacting with other organic/inorganic compounds. As a result, the differences in the concentrations are obtained. In order to find the influence of non-ideality on multiphase processing of OH radical, the flux diagnosis also performed for the both 90%-NIDU and 90%-IDU simulation cases. This results can also be obtained from the flux diagnosis of the most important sinks and sources of the OH radical in the aqueous phase (see Fig. 6.25). As mentioned earlier, apart from the microphysical variables which are designed as similar for 90%-IDU and 90%-NIDU, the activity coefficients have strong influence on the aqueous phase concentrations of OH radical. As shown in the Table. 6.2 and Table. 6.3, for the activity coefficients of key inorganic ions and organic compounds, the processing of OH radical is strongly depends on the behavior of activity coefficients. It can be expected that, if the activity coefficients are less than unity, the processing can be declined. Simultaneously, the processing can be increased, if the activity coefficients are greater than unity.

The flux diagnosis for the most important sinks and sources of the OH radical in the aqueous phase are plotted vs. a selected time interval of the modeling time (2nd day) for urban conditions is shown in Fig. 6.25. The similar plot for the remote case is shown in Fig. C.6. The color

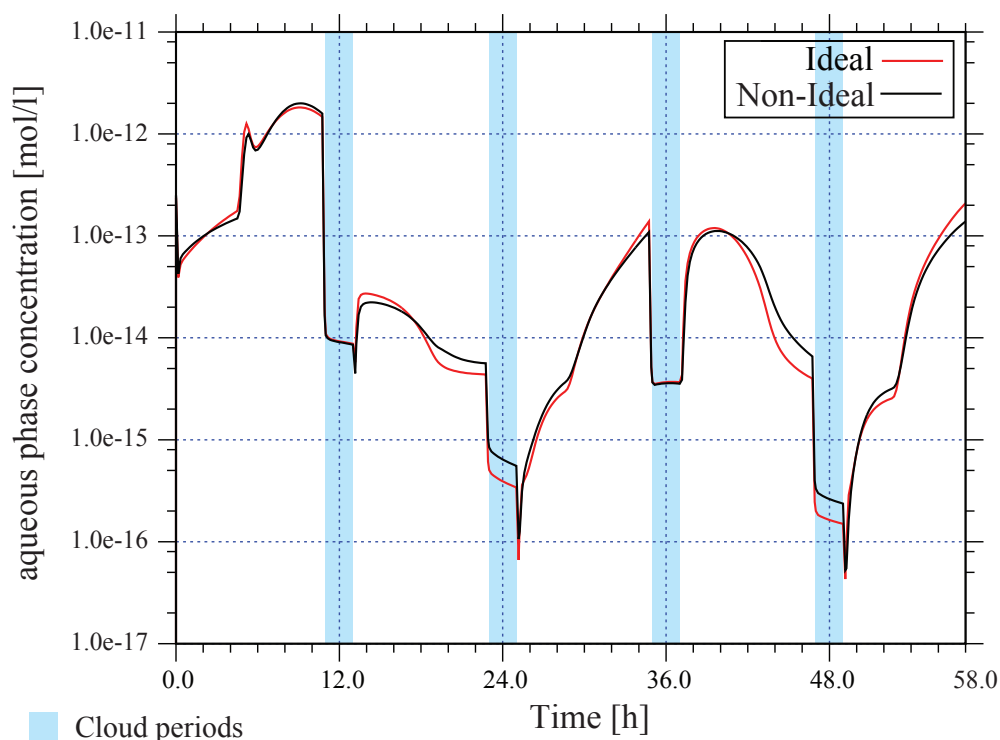


Figure 6.24: Modeled OH aqueous phase concentration in mol l^{-1} vs. modeling time for the urban scenario for the simulations 90%-IDU vs. 90%-NIDU.

changes in the reaction flux plots show significant differences in the sinks and sources between deliquescent aerosol conditions and cloud conditions for the simulations 90%-IDU and 90%-NIDU. This is mainly caused by the phase transfer of soluble compounds into the droplets that can act as additional sinks and sources. The contribution of different reaction pathways will further provides the required information regarding the behavior and differences between the simulations 90%-IDU and 90%-NIDU. The integrated percentage contributions for the most important OH sources and sinks for the urban case are summarized in Table. 6.5. The similar calculations were presented in Table. C.2 for the remote case.

Incorporated over all cloud periods, the mass transfer of OH radical from the gas phase to the aqueous phase for the urban (remote) environmental scenario in the deliquescent particle phase contributes for the simulations 90%-IDU (90%-IDR) and 90%-NIDU (90%-NIRD) about 2.8%(15.6%) and 3.6%(17.0%) respectively. It further, demonstrates that the gas to particle phase transfer is increased 0.8% (1.4%) due to the incorporation of treatment of non-ideality for the aqueous phase chemistry. Hence, due to the treatment of non-ideality for the aqueous phase chemistry, the gas phase OH compensated the other sources to enter into the particles. On the other hand, the OH formation is dominated by the Fenton reaction of Fe(II) with H_2O_2 in the deliquescent particles. The aqueous $\text{Fe}(\text{OH})^{2+}$ photolysis and the Fenton reaction are contributing for the simulation 90%-IDU in the deliquescent particle phase about 16.6% (6.4%) and 68.8%(63%), whereas, these contributions were found to be for the simulation 90%-NIDU about 18% (6.9%) and 66.9% (58.8%). As evident to the Fig. 6.25 and Fig. C.6, the contribution

of Fenton reaction, which is a one of the major source for the OH radical is decreased about 1.8% (3.8%), by incorporating the treatment of non-ideality for the aqueous phase chemistry, since the activity coefficient of Fe^{2+} is about 0.33 (see Table. 6.2). Moreover, the contribution of NO_3^- photolysis is observed for the urban environmental conditions for the simulations 90%-IDU and 90%-NIDU about 10.3% and 9.1%.

Table 6.5: Integrated percentage contributions of the most important OH radical source and sink reactions for the urban case classified regarding to the various microphysical conditions during the simulation time ($Total = Total\ contributions\ throughout\ the\ simulation\ time$, $Total\ clouds = Contribution\ throughout\ all\ cloud\ events$, $Aqueous\ aerosol\ particles = Contribution\ through\ out\ the\ deliquescent\ particle\ conditions$, $\Delta\ Difference = Difference\ between\ the\ aqueous\ phase\ particle\ fluxes\ (90\%-NIDU - 90\%-IDU)$, only sinks and sources with a contribution larger than $\pm\%$ presented).

| Reaction | Ideal | | Non-ideal | | Δ Difference |
|---|--------|----------------|-----------|----------------|---------------------|
| | Total | Aqueous clouds | Total | Aqueous clouds | |
| phase transfer: $OH_g \leftrightarrow OH_{aq}$ | 4.9% | 11.0% | 5.8% | 10.9% | 0.8% |
| $Cl^- + HO \leftrightarrow ClOH^-$ | -13.3% | 6.9% | -16.7% | 11.9% | -8.5% |
| $Br^- + HO \leftrightarrow BrOH^-$ | -7.8% | 0.0% | -9.1% | 0.1% | -2.6% |
| $Fe(OH)^{2+} + h\nu \rightarrow Fe^{2+} + OH$ | 28.8% | 65.0% | 30.6% | 60.4% | 1.4% |
| $NO_3 + h\nu \xrightarrow{H_2O} NO_2 + OH + OH^-$ | 10.1% | 9.6% | 9.2% | 9.4% | -1.2% |
| $H_2O_2 + Fe^{2+} \rightarrow$ | 51.7% | 0.3% | 47.4% | 1.0% | -1.8% |
| $H_2O_2 + Cu^+ \rightarrow$ | 0.62% | 0.05% | 0.82% | 0.06% | 0.3% |
| $Cu^+ + O_3 \xrightarrow{H^+} Cu^{2+} + OH + O_2$ | 0.6% | 1.6% | 0.8% | 1.6% | 0.1% |
| $CH_2OHCOOH + HO \rightarrow$ | -2.4% | -1.0% | -1.9% | -0.1% | 0.4% |
| $OH + OHCCHCHO \rightarrow$ | -10.9% | -27.8% | -12.4% | -27.7% | -0.6% |
| $OH + CH_2OHCH_2OH \rightarrow$ | -12.1% | -8.6% | -13.3% | -8.7% | -1.9% |
| $OH + OHCCH_2OH \rightarrow$ | -0.7% | -1.9% | -0.8% | -1.9% | -0.0% |
| $OH + OH_2CHCH_2OH \rightarrow$ | -2.2% | -5.5% | -2.4% | -5.6% | -0.0% |
| $OH + Fe^{2+} \rightarrow Fe(OH)^{2+}$ | -2.5% | -0.3% | -1.4% | -0.1% | 1.2% |
| $HO_3 \rightarrow OH + O_2$ | 0.9% | 2.9% | 1.1% | 3.0% | 0.1% |
| $HO + CH_3OH \rightarrow$ | -0.4% | -1.3% | -0.5% | -1.3% | -0.2% |
| $HO + CH_3CH_2OH \rightarrow$ | -1.3% | -3.6% | -1.5% | -3.7% | -0.1% |
| $HO + CH_2OH_2 \rightarrow$ | -11.7% | -32.4% | -13.4% | -32.7% | -0.4% |
| $OH + HCOO^- \rightarrow$ | -0.7% | -2.5% | -0.8% | -2.3% | -0.0% |
| $OH + CHO_2CHOH_2 \rightarrow$ | -3.7% | -8.9% | -4.2% | -9.0% | -0.2% |
| $OH + CHO_2COOH \rightarrow$ | -8.2% | -0.2% | -4.1% | -0.3% | 5.1% |

Table 6.5: Integrated percentage contributions of the most important OH radical source and sink reactions for the urban case (Continued)

| Reaction | Ideal | | Non-ideal | | Δ Difference |
|---|---------|--------------------------|-----------|--------------------------|---------------------|
| | Total | Aqueous clouds particles | Total | Aqueous clouds particles | |
| OH + CH ₃ COCHOH ₂ → | -0.6% | -1.8% | -0.7% | -1.8% | -0.0% |
| OH + HOOCCH ₂ COO ⁻ → | -1.1% | 0.0% | -1.3% | 0.0% | -0.4% |
| OH + OHCCHOHCOCHO → | -4.2% | -0.3% | -2.3% | -0.4% | 2.5% |
| OH + HOCCCHOHCOCHO → | -2.5% | -0.0% | -0.9% | -0.0% | 1.9% |
| OH + OHCCCHOHCHOHCHO → | -3.9% | -0.3% | -3.1% | -0.4% | 0.9% |
| OH + HOCCCHOHCHOHCHO → | -2.1% | -0.0% | -0.9% | -0.0% | 1.6% |
| Total sources | 100.0% | 100.0% | 100.0% | 100.0% | 100.0% |
| Total sinks | -100.0% | -100.0% | -100.0% | -100.0% | -100.0% |

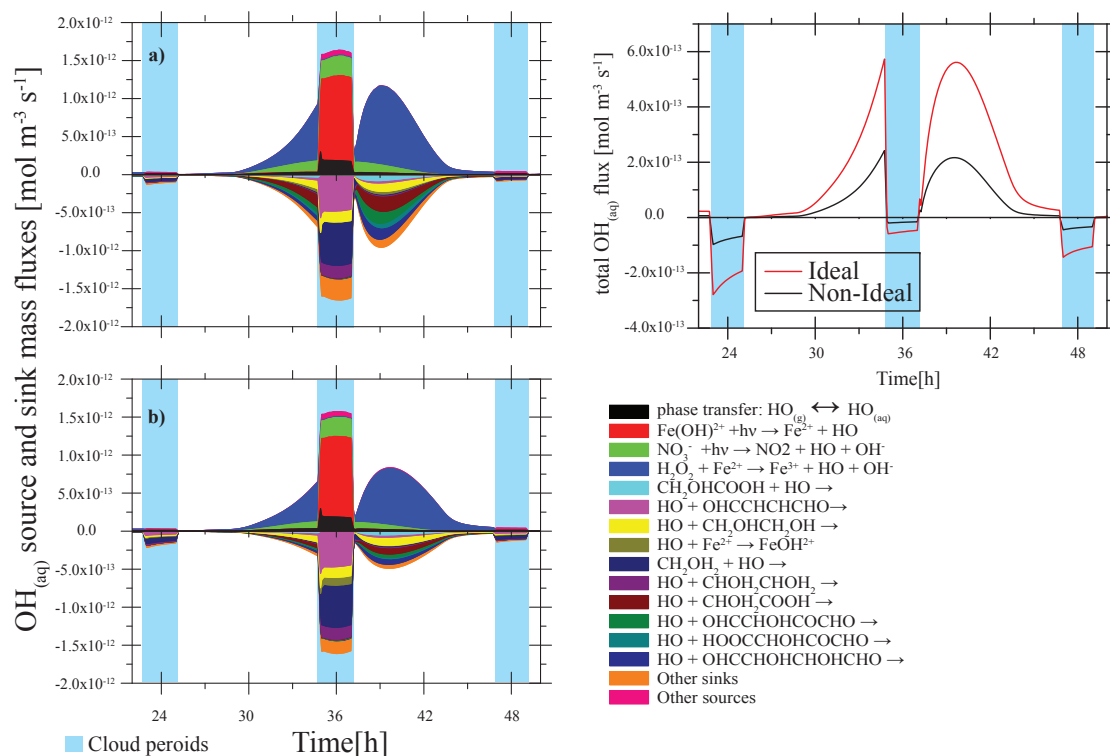


Figure 6.25: Modeled chemical sink and source mass fluxes of OH in aqueous phase in mol m⁻³ s⁻¹ for the second day of modeling time for the urban scenario for the simulations 90%-IDU vs. 90%-NIDU. a) ideal solutions (90%-IDU), b) non-ideal solutions (90%-NIDU), c) corresponding total fluxes. Only sinks and sources with a contribution larger than ± 1% presented.

However, this contribution is observed as < 1% for both of the simulations 90%-IDU and 90%-NIDU for the remote environmental conditions. Furthermore, the HO₃ decomposition contributes about 0.2% (2.4%) and 0.3% (2.7%) for the simulations 90%-IDU and 90%-NIDU respectively, with the percentage contribution increase about 0.1% (0.3%) due to the incorporation of treatment of non-ideality for the aqueous phase chemistry. Moreover, as illustrated in Fig. 6.25, the oxidation in the deliquescent particle phase, is somewhat delayed compare for the simulation 90%-IDU. The computed model results shows that in-situ OH production under wet aerosol particle conditions strongly depends on TMI concentration especially on H₂O₂ concentration. As shown in Fig. 6.25, the OH sinks are also varied during the cloud phase as well as the deliquescent particle phase. The equilibriums between OH with Cl and Br radicals plays a role as sinks with the percentage contributions about 20.2% (31.6%) and 10.4% (3.8%) for the simulation 90%-IDU. At the same time these reaction contributions are about 28.7% (31.2%) and 13% (2%) for the simulation 90%-NIDU. Furthermore, reaction of OH radical with organic compounds are acting as major sinks for the OH radical. The reaction of OH radical with 2-butene 1,4 dial, ethylene glycol, formaldehyde, glyoxylic acid, 2-hydroxy 3-oxo butandial and 2,3 hydroxy 4-oxo butyraldehyde contributes for the simulation 90%-IDU about 5.3%, 13.3%, 4.8%, 10.8%, 5.5% and 5.2%. Whereas, these reaction contributions are found to be for the simulation 90%-NIDU about 5.9%, 15.2%, 5.2%, 5.7%, 3.0% and 4.2% respectively, particularly in the deliquescent particle phase. Moreover, the processing of OH radical has been modified in the cloud phase also, due to the incorporation of treatment of non-ideality and of course the activity coefficients of the compounds, with which OH radical is reacting. Since, the focus is to reveal the differences

between the particle phase while employing the treatment of non-ideality for the aqueous phase chemistry, in comparison with former studies, performed considering the aqueous phase chemistry as ideal solutions, this discussion more focused on particle phase rather than cloud phase.

Fig. 6.25, shows the comparison between total turnovers processing of OH radical, for the simulations 90%-IDU and 90%-NIDU, in the aqueous phase. As shown in this illustration, the mass fluxes were observed as smaller for the simulation where the non-ideal solutions were assumed for aqueous phase chemistry compare with ideal solution. The differences are observed as approximately about 15% in the cloud phase and approximately about 40% in the deliquescence particle phase. Similar deviations were also observed in the remote case, yet, the differences are smaller compare with urban scenario. Furthermore, the activity coefficients computed for organics as well as inorganics have a strong impact on the overall processing of OH radical. Hence, it can be expected that the multiphase processing of OH radical is declined due to the incorporation of treatment of non-ideality for the aqueous phase chemistry.

6.2.7.2 NO₃ radical

NO₃ radical is one of the most important radical during the night time. The differences between the aqueous phase NO₃ concentrations for the simulations 90%-IDU and 90%-NIDU can be obtained in Fig. 6.26. The corresponding plot for remote case is shown in Fig. C.4. As can be seen, the aqueous phase concentrations are rather affected by their aqueous phase sinks and in-situ sources for both of the simulations 90%-IDU and 90%-NIDU. The urban concentrations are relatively stable in both simulations 90%-IDU and 90%-NIDU, due to the remarkable continuous uptake flux into droplets, due to the advantages of solution effect in the cloud formation particularly during the night time clouds. The phase transfer from the gas phase is only the source for the NO₃ radical in the aqueous phase for the remote and urban environmental conditions. Other in-situ sources are only of minor importance apart from the first day of the simulation, where they act as relevant sinks and sources for NO₃ radical in the deliquescent particles. In particular, the radical interconversion reactions with Cl and Br radicals act as important NO₃ sink as well as source in the deliquescent particles depending on the time of day for the simulations 90%-IDU and 90%-NIDU. The total in-cloud oxidation fluxes (see Fig. 6.27) of the two main radical oxidants OH and NO₃ are in the same order in considered in the simulations 90%-IDU and 90%-NIDU.

Fig. 6.27 illustrates that the in-cloud oxidation of methylglyoxal and its oxidation products pyruvic acid are the efficient sources for the NO₃ radical for the simulations 90%-IDU and 90%-NIDU, particularly under urban environmental conditions. The most important urban NO₃ sinks and sources including their integrated percentage contributions are summarized in Table. 6.6. Similar results are presented for the remote conditions in Table. C.3. In contrast to the behavior of OH radical budget that have pervasive influence by C₁ - C₄ organic compounds, the NO₃ budget is almost influenced by C₃ organic compounds due to their considerable reactivity with NO₃ radical (see Tilgner (2009)). However, the differences in the predicted activity coefficient values were mentioned earlier (see Table. 6.3) can alter the multiphase processing of NO₃ radical, due to the incorporation of treatment of non-ideality. Similar to the results presented earlier the major profound differences between the simulations 90%-IDU and 90%-NIDU for the urban (remote) environmental conditions will be discussed below.

The uptake of NO₃ contributes to 28% (11.3%) for the simulation 90%-IDU (90%-IDR), whereas this contribution is observed with the percentage contribution about 1.7% (26.2%) for the simulation 90%-NIDU (90%-NIDR). Interestingly, the gas to particle mass transfer is decreased

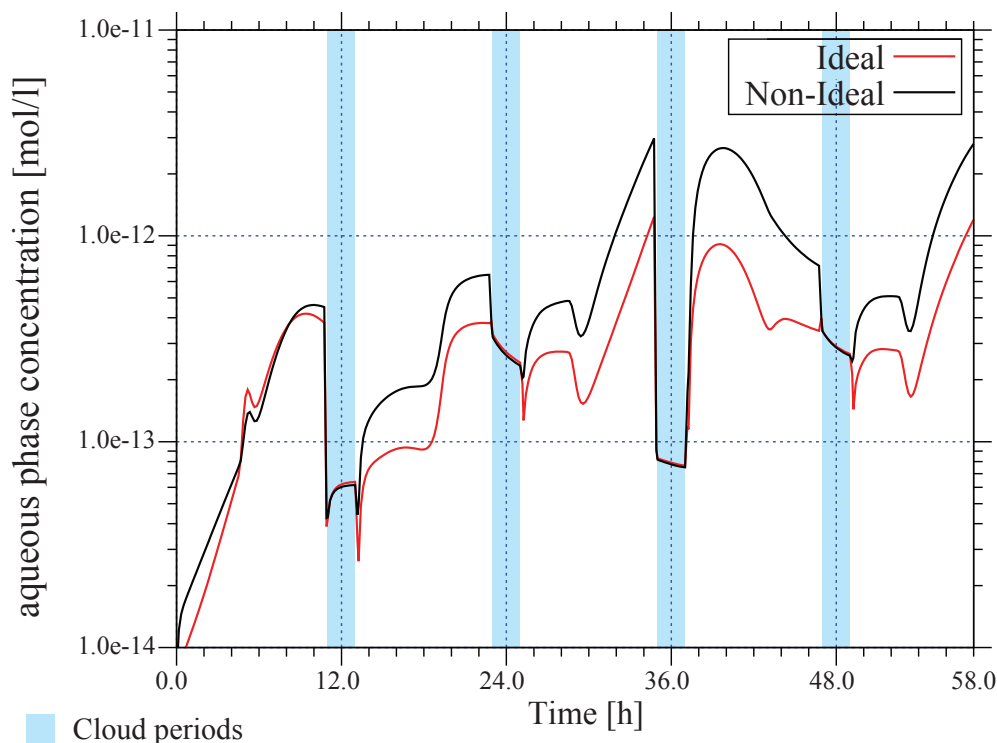


Figure 6.26: Modeled NO_3 aqueous phase concentration in mol l^{-1} vs. modeling time for the urban scenario for the simulations 90%-IDU vs. 90%-NIDU.

approximately about 27% (15%) due to the incorporation of treatment of non-ideality for the aqueous phase chemistry. The equilibrium is attained quite earlier for the simulation 90%-NIDU (90%-NIDR) in comparison with 90%-IDU (90%-IDR), in other words the source fluxes are reduced. Moreover, the radical interconversion reactions with Cl and Br were contributed for the simulations 90%-IDU (90%-IDR) approximately about 59% (86.5%) and 7% (11.7%), whereas these reactions contributes about 72.7% (91.3%) and 7.3% (5.7%) for the simulation 90%-NIDU (90%-NIDR), respectively.

Moreover, reactions with NO_3 radical appear to be important in the deliquescent particle. As a result, the mass fluxes shown in Fig. 6.27 are appears mainly in the cloud phase. However, the sink fluxes are increased during the deliquescent particle phase due to the incorporation of treatment of non-ideality, accordingly the pattern of change in concentrations are observed, with significant difference between the two simulations 90%-IDU and 90%-NIDU. Furthermore, the reaction of NO_3 radical with HSO_3^- and HSO_4^- also acts as important sink fluxes for the NO_3 radical. Especially, NO_3 reacts with HSO_4^- is observed as major sink in the deliquescent particles for the urban (remote) environmental conditions for the simulations 90%-IDU (90%-IDR) and 90%-NIDU (90%-NIDR) about 39% (46%) and 38% (41%) respectively. Moreover, NO_3 reacts with methylglyoxal, 2,3 dihydroxy 4-oxo1-butanoic acid and 3-oxo pyruvic acid anion contributes for the simulation 90%-IDU about 4.2%, 3.6% and 11.8%, whereas these reaction fluxes contributes for the simulation 90%-NIDU about 3.6%, 2.2% and 5.2%. Moreover, these

reactions are contributing in total approximately about 20%, 1.8% and 10% for the simulation 90%-IDU, 17%, 1.3% and 6.1% for the simulation 90%-NIDU.

Table 6.6: Integrated percentage contributions of the most important NO_3 radical source and sink reactions for the urban case classified regarding to the various microphysical conditions during the simulation time ($\text{Total} = \text{Total contributions throughout the simulation time}$, $\text{Total clouds} = \text{Contribution throughout all cloud events}$, $\text{Aqueous particles} = \text{Contribution throughout the deliquescent particle conditions}$, $\Delta \text{Difference} = \text{Difference between the aqueous phase particle fluxes (90\%-NIDU - 90\%-IDU)}$, only sinks and sources with a contribution larger than $\pm 1\%$ presented for 90\%-IDU vs. 90\%-NIDU)

| Reaction | Ideal | | Non-ideal | | $\Delta \text{Difference}$ |
|---|--------|----------------|-----------|-------------------|----------------------------|
| | Total | Aqueous clouds | Total | Aqueous particles | |
| phase transfer: $\text{NO}_3(g) \rightleftharpoons \text{NO}_3(aq)$ | 66.3% | 99.5% | 48.8% | 99.6% | -26.1% |
| $\text{NO}_3 + \text{Cl}^- \rightleftharpoons \text{NO}_3^- + \text{Cl}$ | 22.4% | -9.3% | 29.8% | -16.65% | 13.6% |
| $\text{NO}_3 + \text{Fe}^{2+} \rightarrow \text{NO}_3^- + \text{Fe}^{3+}$ | -1.1% | -0.2% | -0.9% | -0.2% | 0.6% |
| $\text{NO}_3 + \text{HSO}_3^- \rightarrow \text{NO}_3^- + \text{H}^+ + \text{SO}_3^-$ | -10.0% | -17.6% | -8.4% | -16.4% | 0.3% |
| $\text{NO}_3 + \text{HSO}_4^- \rightarrow \text{NO}_3^- + \text{H}^+ + \text{SO}_4^-$ | -18.2% | -0.3% | -19.8% | -0.3% | 1.0% |
| $\text{NO}_3 + \text{SO}_4^{2-} \rightarrow \text{NO}_3^- + \text{SO}_4^-$ | -1.8% | -1.2% | -1.27% | -1.1% | 1.1% |
| $\text{SO}_4^- + \text{NO}_3^- \rightarrow$ | 0.6% | 0.2% | 0.5% | 0.2% | 0.3% |
| $\text{NO}_3 + \text{HC}_2\text{O}_4^- \rightarrow$ | -0.5% | -0.2% | -1.2% | -0.2% | -1.2% |
| $\text{Br}^- + \text{NO}_3 \rightarrow \text{NO}_3^- + \text{Br}$ | -3.4% | -0.1% | -4.0% | -0.49% | -0.3% |
| $\text{NO}_3 + \text{CH}_3\text{C}(\text{O})\text{CH}(\text{OH})_2 \rightarrow$ | -19.4% | -32.4% | -16.6% | -30.7% | 0.6% |
| $\text{NO}_3 + \text{CH}_3\text{C}(\text{O})\text{COO}^- \rightarrow$ | -6.0% | -7.7% | -5.5% | -7.1% | 0.0% |
| $\text{NO}_3 + \text{CH}_2(\text{OH})\text{COO}^- \rightarrow$ | -1.9% | -3.0% | -2.0% | -3.4% | 0.1% |
| $\text{NO}_3 + \text{HOCCCH}(\text{OH})\text{C}(\text{O})\text{CHO} \rightarrow$ | -1.0% | -0.2% | -0.7% | -0.1% | 0.9% |
| $\text{NO}_3 + \text{OHCCH}(\text{OH})\text{CH}(\text{OH})\text{CHO} \rightarrow$ | -1.2% | -0.2% | -1.8% | -0.4% | -0.6% |
| $\text{NO}_3 + \text{HOCCCH}(\text{OH})\text{CH}(\text{OH})\text{CHO} \rightarrow$ | -1.8% | -0.3% | -1.3% | -0.2% | 1.4% |
| $\text{NO}_3 + \text{OOCCH}(\text{OH})\text{CH}(\text{OH})\text{CHO}^- \rightarrow$ | -0.9% | -1.3% | -0.6% | -1.0% | 0.1% |
| $\text{NO}_3 + \text{CH}(\text{OH})_2\text{CH}_2(\text{OH}) \rightarrow$ | -5.1% | -8.1% | -4.4% | -7.7% | 0.1% |
| $\text{NO}_3 + \text{HOCH}_2\text{C}(\text{O})\text{COO}^- \rightarrow$ | -2.9% | -3.4% | -1.4% | -2.1% | 1.6% |
| $\text{NO}_3 + \text{CHOC}(\text{O})\text{COO}^- \rightarrow$ | -10.2% | -8.9% | -6.1% | -7.1% | 6.6% |
| $\text{CH}_2(\text{OH})_2 + \text{NO}_3 \rightarrow$ | -1.2% | -2.0% | -1.1% | -1.9% | 0.1% |
| $\text{HCOO}^- + \text{NO}_3 \rightarrow$ | -1.0% | -1.7% | -0.8% | -1.6% | 0.0% |
| $\text{NO}_3 + \text{CH}(\text{OH})_2\text{COOH} \rightarrow$ | -0.6% | -0.1% | -0.7% | -0.1% | 0.2% |
| Total sources | 100% | 100% | 100% | 100% | |
| Total sinks | -100% | -100% | -100% | -100% | |

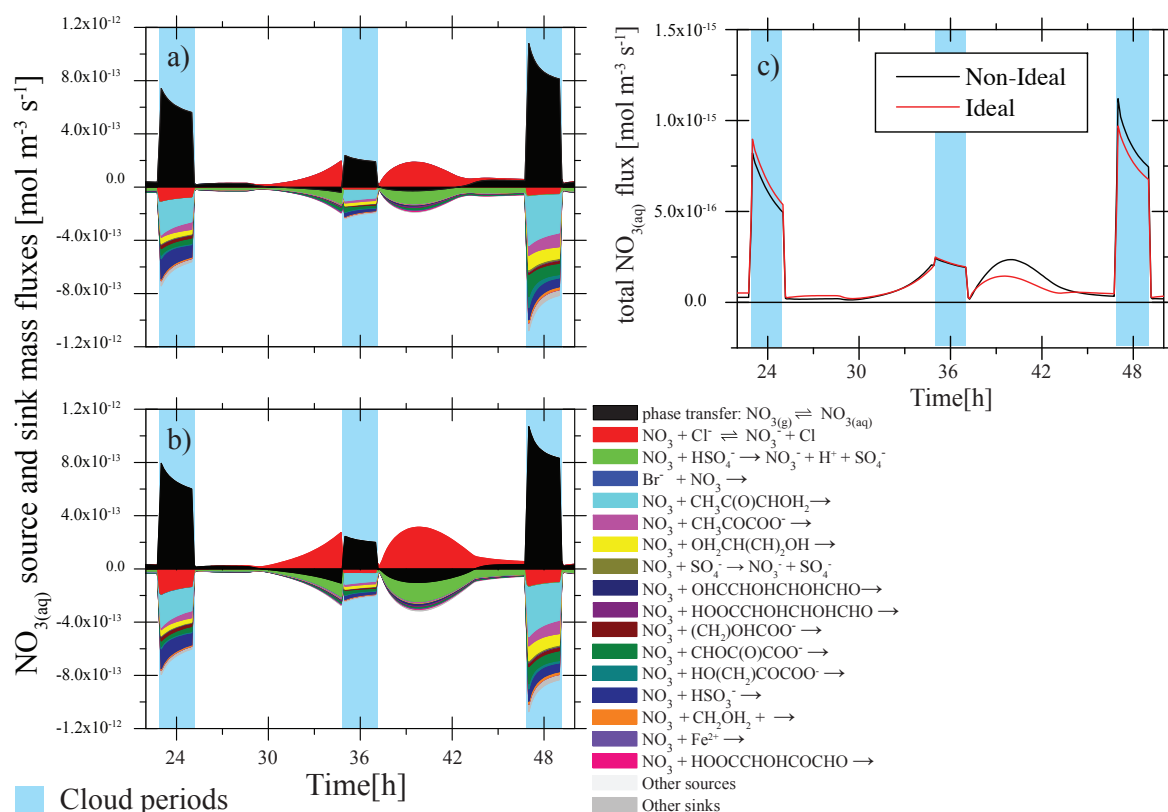


Figure 6.27: Modeled chemical sink and source mass fluxes of NO_3 in aqueous phase in $\text{mol m}^{-3} \text{s}^{-1}$ for the second day of modeling time for the urban scenario for the simulations 90%-IDU vs. 90%-NIDU. a) ideal solutions (90%-IDU), b) non-ideal solutions (90%-NIDU), c) corresponding total fluxes. Only sinks and sources with a contribution larger than $\pm 1\%$ presented.

Notable differences can also be obtained in the total turnover of the NO_3 radical from the Fig. 6.27. As can be seen, the NO_3 radical degradation is more compare with production during the deliquescence phase. Eventually, there is small amount of production is observed in the cloud droplets as well, even though the production and destruction more when the treatment of non-ideality employed for the aqueous phase chemistry. In the cloud phase, the differences are observed as increase with about 10% and about 25% in the deliquescence particles.

6.2.7.3 Multiphase HO_2/O_2^- radical processing

As explained earlier in Sec. 6.2.7.1, the multiphase processing of OH radical is strongly connected to the hydrogen radical HO_2 . In the current applied multiphase chemical mechanism, the in-cloud reductions of the HO_2 concentration was more favored to the day time (noon) cloud conditions. Similar to the OH and NO_3 radical, the aqueous HO_2/O_2^- aqueous phase concentration highlights the deviations throughout the simulation time. One should note that, the aqueous phase concentration of HO_2/O_2^- is about 5 orders of magnitude higher than the respective OH concentration for both of the cases considering ideal and non-ideal solutions. The aqueous phase concentration profile for HO_2/O_2^- is shown in Fig. 6.28. As can be seen, the daytime concentrations are higher than nighttime time during the cloud phase. The concentration profiles for the 90%-IDU and 90%-NIDU are obtained similar during the first two cloud periods. During the cloud period of 2nd day the aqueous phase concentrations are obtained a minor differences. It

has been already mentioned that, the aqueous particle chemistry have a continuous feedback on the cloud chemistry. As shown in Fig. 6.28, the aqueous phase concentrations are obtained about $1.5 \times 10^{-9} \text{ mol l}^{-1}$ from the simulation 90%-NIDU and $3.4 \times 10^{-10} \text{ mol l}^{-1}$ from the simulation 90%-IDU. The integrated mass fluxes for the processing of HO_2/O_2^- for the urban environmental conditions is shown in Fig. 6.29 for the selected period of modeling time.

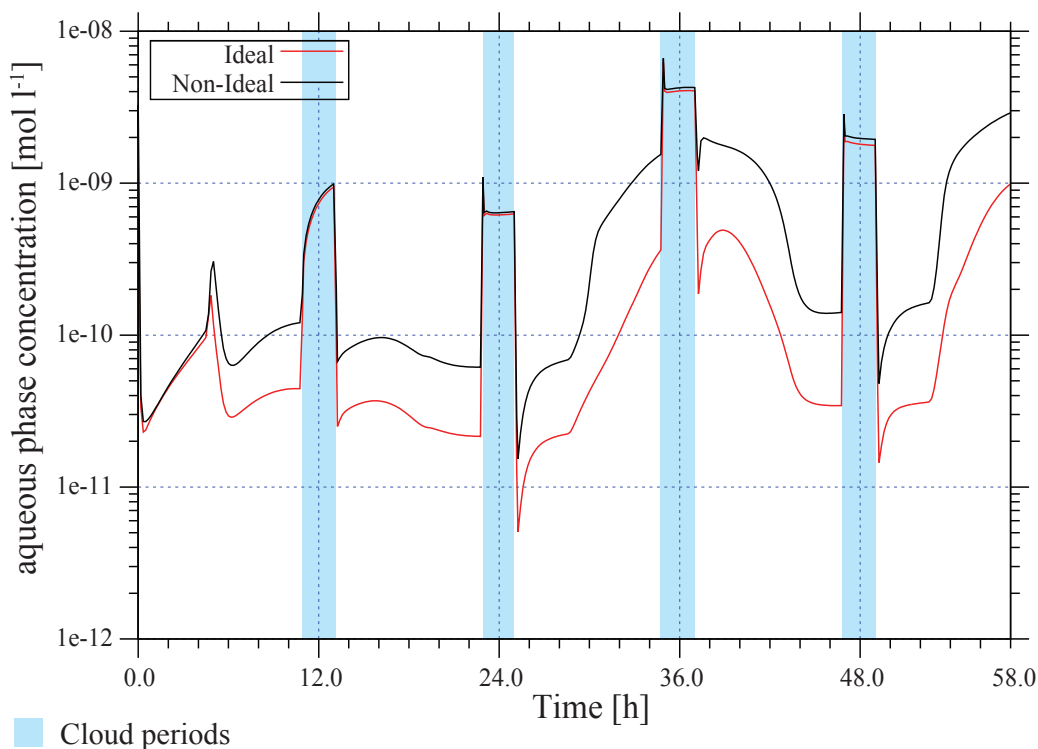


Figure 6.28: Modeled HO_2/O_2^- aqueous phase concentration in $\text{mol m}^{-3} \text{ s}^{-1}$ vs. modeling time for the urban scenario for the simulations 90%-IDU vs. 90%-IDU.

Furthermore, the aqueous phase concentrations are observed as same for the simulations 90%-IDU and 90%-NIDU in the night time clouds, whereas slight changes are observed during day time clouds. It has been observed that the concentrations are higher while treating the aqueous phase chemistry as non-ideal solutions. Especially, in the deliquescent particles, the uptake is dominating source besides the available in-situ sources. Subsequently, the obtained model results explores that the concentrations are higher while assuming the aqueous chemistry as non-ideal solutions in comparison with ideal solutions. The day time (noon) concentrations at the end of the simulation time (60 h) shows the considerable reduction of factor about 3 for the simulation 90%-IDU compared with 90%-NIDU. Furthermore, the specific deviations from ideal conditions were quantified by comparing the observed direct phase transfer contribution for the urban (remote) environmental conditions approximately about 68% (76%) and 66%(73%) in total, for the simulations 90%-IDU (90%-IDR) and 90%-NIDU (90%-IDR), respectively. However, the uptake is more dominant in the deliquescent particles, with the percentage contribution about 76%(72%) and 74% (72%) for the simulations 90%-IDU (90%-IDR) and 90%-NIDU (90%-NIDR), respectively. The hydrated form of acetyl proxy radical acts as sources for the total processing of HO_2/O_2^- , which contributed about 10% (8.4%) for the simulation 90%-IDU (90%-IDR), however,

this reaction pathway is contributes for the simulation 90%-NIDU(90%-NIDR) about 8.6% (8.2%).

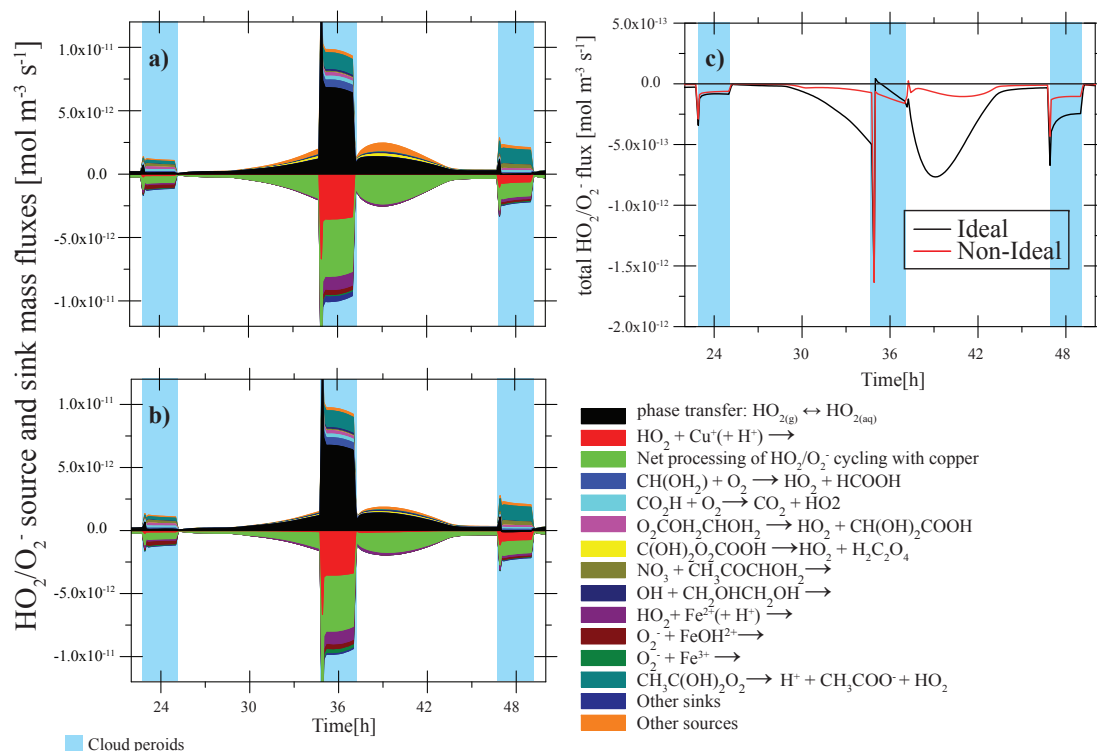


Figure 6.29: Modeled chemical sinks and source mass fluxes of HO_2/O_2^- in aqueous phase in $\text{mol m}^{-3} \text{s}^{-1}$ for the second day of modeling time for the urban scenario for the simulations 90%-IDU vs. 90%-NIDU. a) ideal solutions (90%-IDU), b) non-ideal solutions (90%-NIDU), c) corresponding total fluxes. Only sinks and sources with a contribution larger than $\pm 1\%$ presented.

The decomposition of formaldehyde is contributing to produce HO_2 about 7.3% (5.3%) and 6.4% (5.1%) for the simulations 90%-IDU and 90%-NIDU respectively. As shown in Fig. 6.29, the net processing, which includes the net effect of HO_2/O_2^- cycling with copper and its backward cycling, acts as major sink in the particles, and this processing is declined due to the incorporation of treatment of non-ideality for the aqueous phase chemistry. The total net processing contributes about 71% (64%) and 67% (63%) for the simulations 90%-IDU and 90%-NIDU respectively. Furthermore, reaction between HO_2 and Cu^+ which acts as sinks for the total processing of HO_2/O_2^- budget, contributes about 20.4% (17%) in the particle phase for the simulation 90%-NIDU, whereas this reaction contributes about 16% (15%) for the simulation 90%-IDU. Moreover, the O_2^- reacts with metal ions such as Fe^{2+} and Fe^{3+} also acts as sink fluxes for the total processing of HO_2/O_2^- . However, due to the increasing the charge number of ions, the activity coefficients are observed as decreasing (see Table. 6.2). Since, the original AIOMFAC and mod. LIFAC didn't included the interaction parameters for the metal ions, like Fe^{2+} , Fe^{3+} and O_2^- , but due to the interest to treat these ions, the activity coefficients are computed mainly from the LR and SR contributions as explained in Sec. 3.6, which is one of the main limitation in order to explain the processing of HO_2/O_2^- .

All in all, the activity coefficient module implanted in SPACCIM, can able to compute the activity coefficients of the ions which are included in the system. Hence, based on the predicted activity coefficients of ions (both cations and anions), the multiphase processing can be determined. However, the multiphase processing of HO_2/O_2^- is observed as declined for the simulations 90%-IDU and 90%-NIDU, due to the incorporation of treatment of non-ideality for the aqueous phase chemistry. The total mass fluxes shown in Fig. 6.29, gives the total relative change of the processing of HO_2/O_2^- in the aqueous phase particles. The differences are found to be declined approximately about 35% for the simulations 90%-IDU and 90%-NIDU, which further illustrate the influence of treatment of non-ideality on multiphase processing of radicals. Although, the accurate prediction of activity coefficients for the ions, is not performed yet in this study, however, these studies will throw light on the issues for the multiphase processing of radicals.

6.2.8 Aqueous multiphase processing of organic compounds

As explained in Tilgner (2009) and Tilgner and Herrmann (2010) the studies of aqueous multiphase chemical processing of organics is not only limited to in-cloud conditions but also proceeds in deliquescent particle phase with significant mass fluxes. Furthermore, it has been argued that in their model studies, that aqueous radical conversions of carbonyl compounds and its oxidation products can contribute potentially to the formation of functionalised organic acids. Aiming to reveal the understanding about the influence of non-ideality on multiphase organic processing, current model results are presented in the succeeding subsections for the selected species of C_2 and C_3 chemistry considering treatment of non-ideality for aqueous phase chemistry in comparison with the former studies performed while assuming the aqueous phase chemistry as ideal solutions.

6.2.8.1 C_2 aqueous phase processing

The in-cloud oxidations of semi-volatile C_2 organic compound glyoxal lead to the formation oxalic acid which represents the most abundant diacid and an important organic component of the organic particulate matter. However, the results explaining the influence of non-ideality for these kind of processes proceeding in the atmosphere are scarce. Fig. 6.30 shows the modeled aqueous phase concentrations of oxalic acid and its precursors, glyoxylic and glycolic acid, along with corresponding activity coefficients vs. simulated time for the urban environmental conditions. Initially, the oxalic acid precursors are effectively produced under day time cloud conditions as shown in Fig. 6.30, later on the degradation proceeds almost in deliquescent particles during the day in urban environmental conditions. However, the overall production of glycolic acid and glyoxylic acid was observed as declined for the simulation 90%-NIDU due to the incorporation of treatment of non-ideality. The computed activity coefficients have substantial influence while obtaining this behavior. However, the deviations from ideal behavior are markedly dependent on the species regarded. For instance, the differences for glycolic acid ($\text{CH}_2\text{OHCOOH}+\text{CH}_2\text{OHCOO}^-$) are more pronounced than for glyoxylic acid ($\text{CH}(\text{OH})_2\text{COOH}+\text{CH}(\text{OH})_2\text{COO}^-$).

As shown in Table. 6.3, the activity coefficient of dissociated and undissociated forms of these acids are different (see also Fig. 6.30). Furthermore, the dissociation reaction of these compounds have impact on the pH, as well as the processing of the compounds it self. Due to the differences in the activity coefficients of dissociated and undissociated forms of these acids, the concentration profiles are expected to be different for the simulations 90%-IDU and 90%-NIDU. Moreover, both of these dissociated and undissociated forms have the tendency to modify the over all sink

and source mass fluxes (turnovers), therefore, the sum of dissociated and undissociated aqueous phase concentrations of these compounds were plotted, as shown in Fig. 6.30.

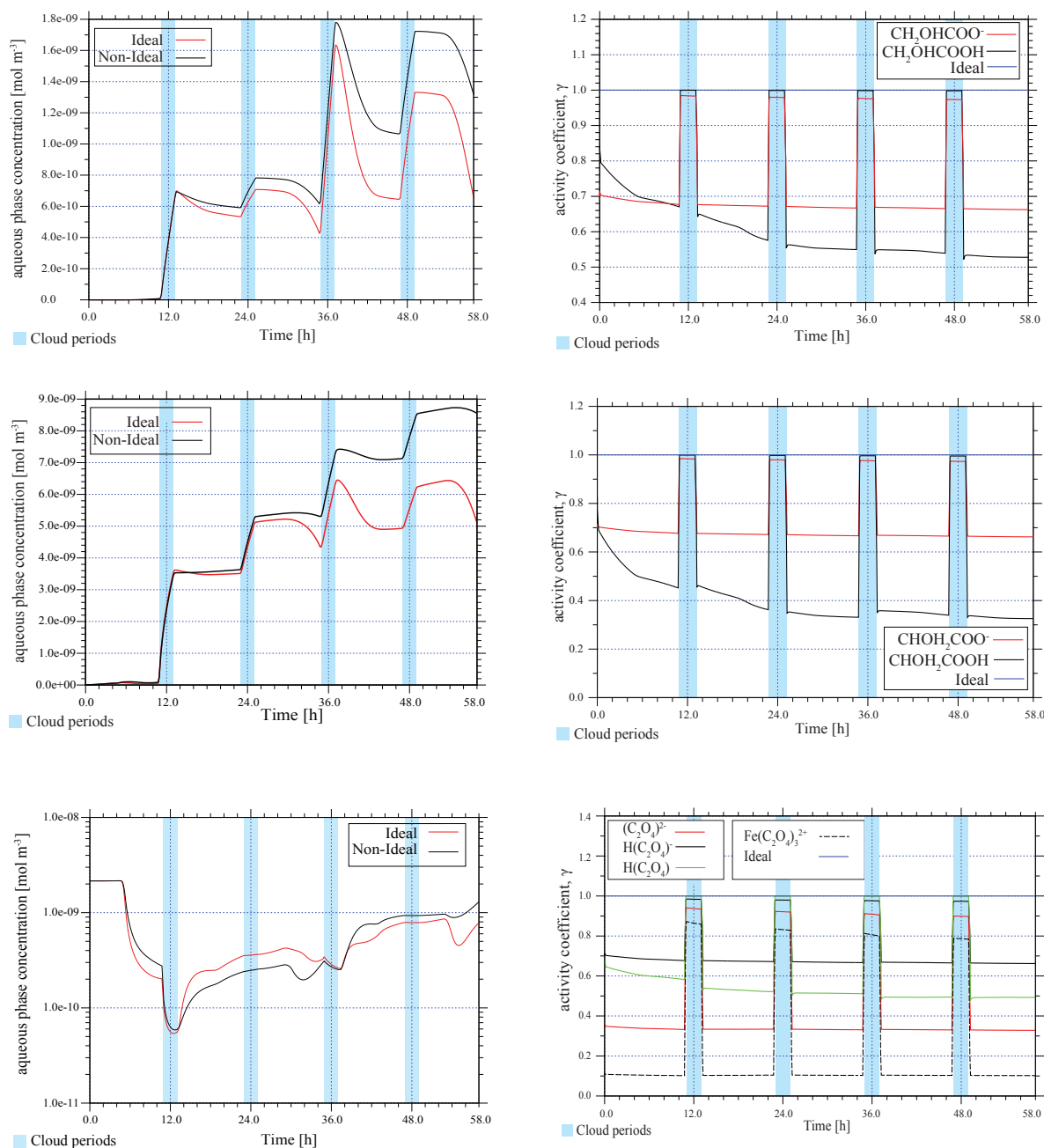


Figure 6.30: Modeled aqueous phase in $\text{mol m}^{-3}_{(\text{air})}$ and corresponding activity coefficients for the most important C_2 oxidation products for the urban scenario for the simulations 90%-IDU vs. 90%-NIDU, Glycolic acid (top), Glyoxylic acid (center), Oxalic acid (bottom).

Fig. 6.30 shows the computed activity coefficients of dissociated and undissociated forms of organic compounds. It has been observed that the activity coefficients of the species shown here are less than unity. However, in the deliquescent phase the differences are about 20% between the dissociated and undissociated forms. The change or differences in the particle phase might have strong influence on multiphase processing of these compounds shown here.

As can be seen, for instance glycolic acid due to the incorporation of activity coefficients, the degradations are lower for 90%-NIDU compare with 90%-IDU. Furthermore, the production is also not similar in the particles phase. Even though the production is increasing in the particle phase, during the whole simulation period, the deviations are also increasing with the simulation time, for 90%-IDU and 90%-NIDU. The reaction of OH radical with glycolaldehyde, is decreased in the particle phase, (see Table. C.4), due to the incorporated activity coefficients. Even the activity coefficients of radicals are prescribed as unity, the influence of activity coefficients of organic compounds are obvious. As described in Sec. 6.2.7.1, the multiphase processing of organic compounds are strongly liked with OH radical processing. While computing the rate of reaction, where the reactants (hydrated and unhydrated glycolaldehyde) varies, due to the aqueous phase concentrations along with the correction factors i.e., activity coefficients. As a result, the production of glycolic acid is decreased, from these reaction pathways for the simulation 90%-NIDU compare with the simulation 90%-IDU. The similar principles will be applied for all the C₂ products shown here. Based on the numerical values obtained for the activity coefficients, the multiphase processing is proceeds as declined since, the activity coefficients are obtained as less than unity.

It has been evident from the former studies that, for polluted conditions, glycolic acid is formed mainly by reacting the glycolaldehyde with OH radical (see Tilgner (2009)). As soon as the glycolic acid is produced, it will further react with other radical oxidants, which can have the tendency to change the sink and source mass fluxes (turnovers) of the glycolic acid. All in all, the departure from the ideal behavior caused mainly due to the reaction with OH with the total contribution in the urban (remote) case in total is approximately 82% (95%) and 73% (96%) for the simulations 90%-IDU and 90%-NIDU respectively. Whereas this reaction contributing in particle phase for urban (remote) environmental cases with 97% (97%) and 94% (96%) for the simulations 90%-IDU and 90%-NIDU respectively. Furthermore, the OH reacts with glycolaldehyde (both hydrated and unhydrated forms) to produce the glycolic acid contributing in total with about 68% (98%), 66% (97%) for the computations 90%-IDU and 90%-NIDU respectively. As mentioned earlier, the production of glycolic acid in the deliquescent particles, is observed as declined while employing the treatment of non-ideality for aqueous phase chemistry in comparison with ideal solutions for the aqueous phase chemistry. Subsequently, the reaction of glycolaldehyde with OH radical in the particle phase contributes with about 84% (93%), 79% (97%) for the computations 90%-IDU and 90%-NIDU. This strong deviation from ideal behavior expands our ability to access the specific impact of treatment of non-ideality combined to the aqueous phase chemistry (see Table. C.4). In contrast with OH radical, the reaction of glycolaldehyde with NO₃ radical to produce the glycolic acid contributes about 32% (74%), 35% (73%) in total, whereas this production in the particles is about 15% (75%), 21% (73%) for the simulations 90%-IDU and 90%-NIDU respectively. As explained before the undissociated form also have significant impact under non-ideal conditions, it can be observed when CH(OH)₂COO⁻ reacting with NO₃ radical contributing in total approximately 18% (24%) and 27% (23%), whereas this reaction contributes in the particle phase is about 3% (5%), 6% (3%) for the computations carried out while considering ideal and non-ideal solutions for aqueous phase chemistry. Aside from the particle phase, the glycolate reacts with NO₃ radical in the cloud conditions contributing approximately 90% (9%) and 94% (5%), for the simulations 90%-IDU (90%-IDR) and 90%-NIDU (90%-NIDR), respectively.

Glyoxal oxidation: The aqueous reaction pathway of glyoxal to produce glyoxylic acid, is the major source for the glyoxylic acid. The contribution of this reaction pathway is observed in total about 69% (36%) and 73% (36%) for the simulations 90%-IDU (90%-IDR) and 90%-NIDU (90%-NIDR), respectively. Moreover, the production of glyoxylic acid mainly proceeds in the

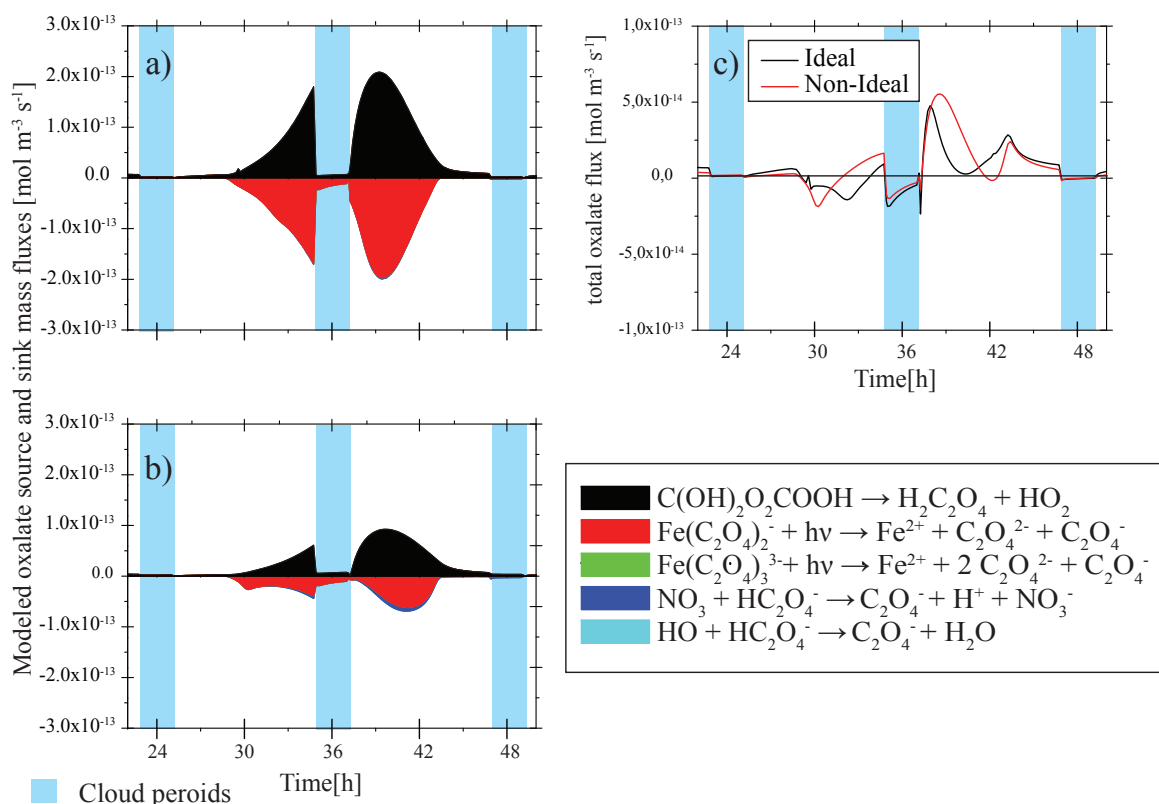


Figure 6.31: Modeled chemical sinks and source mass fluxes of oxalic acid/oxalate for the second day of modeling time for 90% RH for the urban scenario in aqueous phase in $\text{mol m}^{-3} \text{s}^{-1}$. a) ideal solutions, b) non-ideal solutions, c) corresponding total fluxes. Only sinks and sources with a contribution larger than $\pm 1\%$ presented.

cloud phase. However, the production in the cloud phase is observed as only the minor difference with 93% (63%) and 92% (63%) obtained from the simulations 90%-IDU and 90%-NIDU. However, significant increase ($\approx 6\%$) was observed for the production of glyoxylic acid in the particle phase with the contribution of 35% (10%) and 41% (10%) during the simulations 90%-IDU and 90%-NIDU respectively. Besides, reaction of OH radical with glycolic acid to produce glyoxylic acid seems also play a decisive role during the particle phase, with the contribution of 39% (71%) and 34% (71%) for the simulations 90%-IDU (90%-IDR) and 90%-NIDU (90%-NIDR), respectively. Furthermore, the decomposition of ketomalonic acid to produce glyoxylic acid is also decreased, during the 90%-IDU (90%-IDR) and 90%-NIDU (90%-NIDR) simulated case, with the contribution of 25% (12%) and 21% (11%). Although the difference is small, it explores the importance of treatment of non-ideality with the help of activity coefficient computation. The reaction of glyoxylic acid with OH radical is the important sink for the glyoxylic acid, contributing with 96% (71%) and 90% (67%) for the both simulations with the difference of ($\approx 6\%$). Whereas this reaction contributes with 95% (74%) and 91% (70%) in the particle phase for the simulations 90%-IDU (90%-IDR) and 90%-NIDU (90%-NIDR), respectively.

Furthermore, the degradation is observed as declined approximately about 4% (3%), in the aqueous particles while employing the treatment of non-ideality for aqueous phase chemistry. However this process contributes in the cloud droplets about 79% (68%) and 76% (63%) for the

simulations 90%-IDU (90%-IDR) and 90%-NIDU (90%-NIDR), respectively. On the other hand, the reaction of glyoxylic acid with SO_4^- radical plays a role as sink, mainly in the cloud phase with 15% and 17% in the urban environmental conditions for the simulations 90%-IDU and 90%-NIDU. Moreover, it has been observed that this reaction plays a minor role in the remote environmental conditions. Hence, these results explore, that the production is increased during the particles, and the degradations are decreased, when combining treatment of non-ideality in the aqueous phase chemistry. Although, strong deviations were not observed during the cloud droplets, yet the impact is noteworthy.

Oxalic acid formation: As discussed earlier, the oxalic formation taking place preferably in the aqueous phase of the deliquescent particles. Fig. 6.31 shows the modeled aqueous phase chemical sinks and source mass fluxes of oxalic acid/oxalate in the urban environmental scenario. As shown in Fig. 6.31, oxalic acid is effectively produced by the oxidation of glyoxylic acid during the day especially in the deliquescent particles. However, the computed mass fluxes (turnovers) were decreased by factor of 2 for the simulation 90%-NIDU compared to the simulation 90%-IDU. As discussed in Sec. 6.3.5 the single charged ions (cations and anions) behaves similarly. Hence, only some of the ions were plotted in Fig. 6.30, even though, all the dissociated forms (i.e. $(\text{C}_2\text{O}_4)^{2-}$, $\text{H}(\text{C}_2\text{O}_4)^-$, $\text{H}_2(\text{C}_2\text{O}_4)$, $\text{Fe}(\text{C}_2\text{O}_4)_2^-$, $\text{Fe}(\text{C}_2\text{O}_4)^+$, $\text{Fe}(\text{C}_2\text{O}_4)_3^{3-}$) are considered for the computation of concentrations for the simulations 90%-IDU and 90%-NIDU. Moreover, the degradation reactions with inorganic radicals such as OH are not favorable, as the importance of photolytic decay. As can be seen from Fig. 6.31 and Fig. 6.2.8.1, the oxalate is photolysed under day time conditions, whenever it produced. The differences in the aqueous phase concentrations are completely effected by the predicted activity coefficients. The corresponding activity coefficients of the oxalic acid and the oxalate forms (see Fig. 6.2.8.1), changed the complete turnovers of the oxalic acid/oxalate. As shown in Table. 6.3, the activity coefficients of ions are strongly depends on the charge number. Based on the corresponding charge number, the computed activity coefficients for the oxalate and the iron complexes are differed with each other (see Fig. 6.2.8.1 for activity coefficients of oxalic acid/oxalate). These differences in the activity coefficients are, influenced the production and degradation of the oxalic acid/oxalate based on the obtained activity coefficients.

6.2.8.2 C₃ aqueous phase processing

In the considered multiphase mechanism, methylglyoxal is effectively oxidized under cloud conditions to produce C₃ organic mass production. In Fig. 6.32 the aqueous phase concentration of the main aqueous oxidation products such as pyruvic acid, 3-oxo pyruvic acid and finally ketomalonic acid, along with corresponding activity coefficients are plotted vs. the simulated time. As can be seen, pyruvic acid is effectively produced in the model clouds. Moreover, night time clouds are acting as more effective medium for the production of pyruvic acid than corresponding day time clouds in the urban case. It can be reasonable, that especially during the night, important gas phase methylglyoxal sinks such as the photolytic decay and the OH reaction are irrelevant so that the aqueous NO_3 radical oxidation represents the exclusive sink. Hence, the in-cloud oxidation of methylglyoxal and its oxidation products such as pyruvic acid is not only an efficient sink of the NO_3 radical in the aqueous phase, but also an important oxidative sink for themselves as explained in Sec. 6.2.7.2.

As can be seen from Fig. 6.2.8.2, the activity coefficients for the dissociated and undissociated forms of these organic compounds acid plays a central role in the total turnovers as observed in earlier section. As shown in Fig. 6.2.8.2, the activity coefficients are reduced for the both dissociated and undissociated forms of these organic compounds are less than unity. As discussed

earlier, the major contribution to produce pyruvic acid is the reaction of NO_3 radical with methylglyoxal. As shown in Table. 6.3, the activity coefficients for the both dissociated and undissociated forms of the pyruvic acid are less than unity. Furthermore, the activity coefficients for the organic and inorganic ions also less than unity. However, the activity coefficient values for the methylglyoxal and pyruvic acid are in the same range (see Table. 6.3). During the reaction of NO_3 radical with methylglyoxal, due to the activity coefficients are found to be less than unity, the reaction rate would be smaller for the simulation 90%-NIDU in comparison with 90%-IDU, thus, the corresponding aqueous phase concentrations are also observed as declined for the simulation 90%-NIDU compare to the simulation 90%-IDU.

The NO_3 reaction with methylglyoxal contributes to produce pyruvic acid in urban (remote) conditions in total about 89% (5%) and 90% (5%) for the simulations 90%-IDU and 90%-NIDU. Subsequently, this reaction becomes more important in the cloud phase with 96% (6%) and 90% (6%) for the simulations 90%-IDU and 90%-NIDU respectively. Similarly, in the particle phase this reaction contributes about 77% (1%) and 82% (1%) for the two simulated cases 90%-IDU and 90%-NIDU. At the same time, the reaction of OH radical with methylglyoxal contributes in total about 10% (95%) and 9% (95%) during the simulations 90%-IDU and 90%-NIDU respectively. However, it has been observed that this reaction pathway plays a minor role in the cloud phase, while contributing about 4% (94%) for the simulation 90%-IDU, 9% (94%) for the simulation 90%-NIDU. The similar contribution in the particle phase is reduced for the simulation 90%-NIDU compare with 90%-IDU, with the contribution of 18% (98%) and 23% (98%).

As pointed out earlier, about the importance of dissociated and undissociated forms of organic acids, accordingly the reaction of NO_3 with $\text{CH}_3\text{COCOO}^-$ is act as important sink, with the contribution in total 65% (38%) and 73% (44%) with the remarkable increase ($\approx 8\%$) under non-ideal conditions. Furthermore, the same reaction contributes 92% (15%) and 98% (16%) for the simulations while treating the multiphase chemistry under ideal and non-ideal solution conditions in the cloud phase. Similar to the aforementioned reaction of OH with pyruvic acid undissociated form also plays a role as sink with the total contribution in total of 30% (25%) and 22% (24%) for the simulations 90%-IDU (90%-IDR) and 90%-NIDU (90%-NIDR) respectively. Moreover, this reaction highlights the influence of non-ideality with the difference in integrated percentages contribution of $\approx 6\%$, when it contributes approximately 6% (0.5%) and 0.1% (0.5%) for the simulations 90%-IDU (90%-IDR) and 90%-NIDU (90%-NIDR) in the cloud phase. Similarly, the contribution of this reaction in the particle phase is with 55% (31%) and 43% (30%), with the decrease in the percentages about 12% for the computation carried out while employing the treatment of non-ideality for the aqueous phase chemistry in comparison with the assumption of ideal solutions under deliquescent particle conditions.

As implemented in the mechanism, the pyruvic acid further oxidized to oxo-pyruvic acid, finally produce the ketomalonic acid. In order to produce the oxo-pyruvic acid the treatment of non-ideality have strong impact as shown in the Fig. 6.32. The reaction of NO_3 with $\text{CH}_3\text{COCOO}^-$ is an important source to produce the CHOCOCOO^- with the total contribution of 29% (27%) and 48% (33%) with the simulations 90%-IDU (90%-IDR) and 90%-NIDU (90%-NIDR). Furthermore, this reaction also act as important source for the dissociated form of oxo-pyruvic acid with 53% (12%) and 63% (24) for both of the simulations while treating the multiphase chemistry while considering ideal and non-ideal solutions for the aqueous phase chemistry in the cloud phase. At the same time, this reaction contributes to 14% (30%) and 35% (37%) with the simulations 90%-IDU (90%-IDR) and 90%-NIDU (90%-NIDR), respectively in the particle phase. Furthermore, 3-hydroxy 2-oxo propanoic acid reacts with NO_3 radical also plays a vital role to produce CHOCOCOO^- contributes in total about 24% (13%) and 22% (14%). The similar

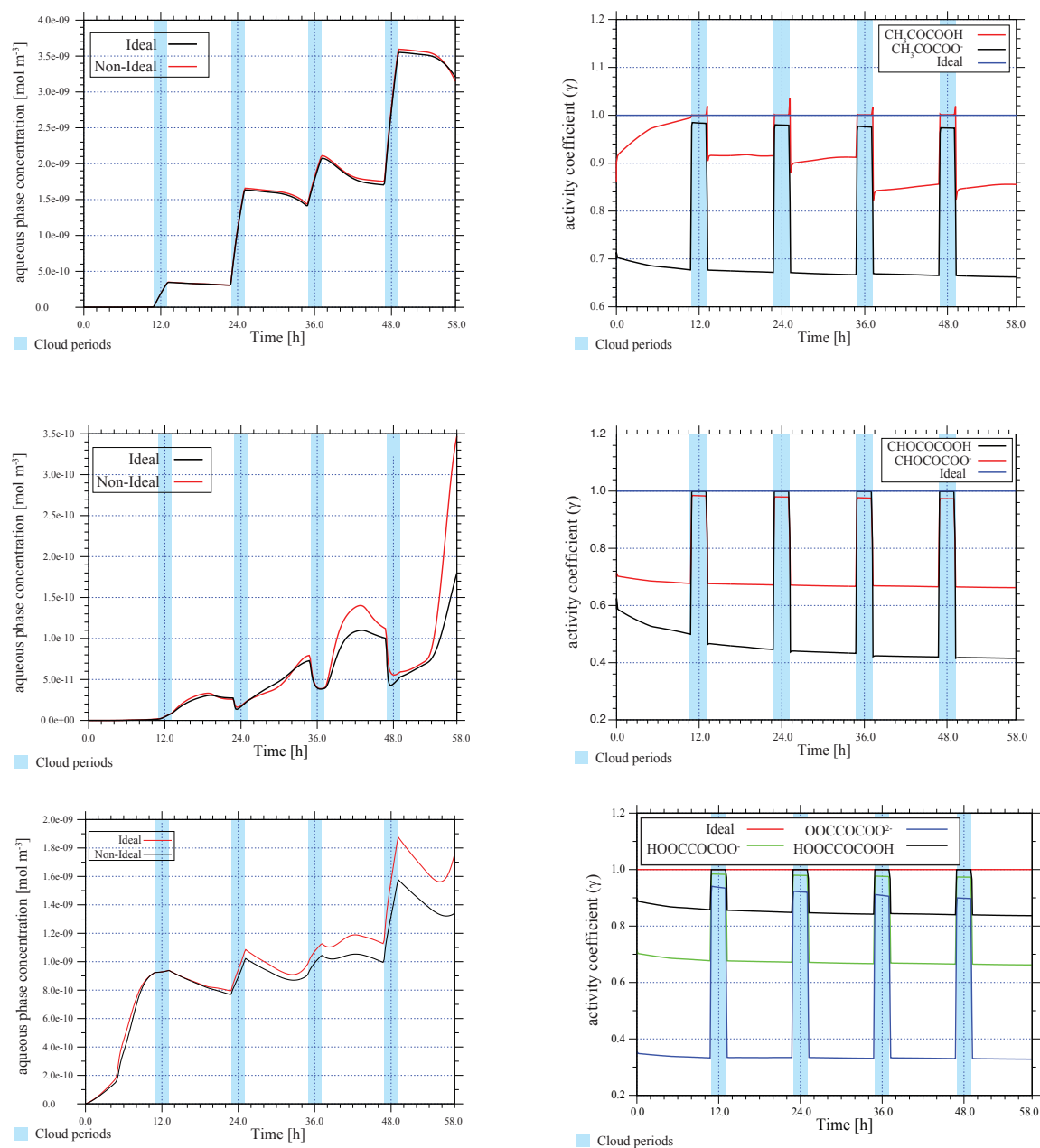


Figure 6.32: Modeled aqueous phase concentrations in $\text{mol m}^{-3}_{(\text{air})}$ for the most important C_3 oxidation products for the urban scenario for the simulations 90%-IDU vs. 90%-NIDU, Pyruvic acid (top), Oxopyruvic acid (center), Ketomalonic acid (bottom).

reaction contribution was observed in the cloud phase about 41% (5%) and 33% (12%) in the cloud phase while considering the ideal and non-ideal solutions for aqueous phase chemistry, respectively. At the same time, this reaction contributes about 14% (14%) and 11% (15%) in particle phase for 90%-IDU (90%-IDR) and 90%-NIDU (90%-NIDR) simulation cases. It has been observed, that the reaction of OH radical reacts with undissociated form of pyruvic acid acts as one more important source during the particle phase about 21% (21%) and 28% (21%)

for both of the simulations 90%-IDU (90%-IDR) and 90%-NIDU (90%-NIDR). Subsequently, 3-hydroxy 2-oxo propanoic acid reacts with OH radical appears to be important in the particle phase while contributing with 16% (9%) and 4% (7%). Furthermore, the reaction of OH with un-dissociated form of pyruvic acid seems to be act as source for the oxo-pyruvic acid, especially in the particle phase contributing about 21%(21%) and 28% (21%). All in all, these deviations are obtained due to the incorporation of treatment of non-ideality. As these results, shown that the predicted activity coefficients changed the multiphase processing as well as the turnovers of these products.

Furthermore, CHOCOCOO^- reacts with NO_3 radical to produce HOCCOCOO^- acts as a sink for the total budget of oxo-pyruvic acid, about 87% (86%) and 94% (89%) over the total simulation time period with the simulations 90%-IDU (90%-IDR) and 90%-NIDU (90%-NIDR). Besides, this reaction seems very important sink in the cloud phase also while contributing with 99% (60%) and 99% (80%) for both simulated cases. At the same time, this reaction contributed to 79% (89%) and 89% (92%) in the particle phase for the two cases of simulations 90%-IDU (90%-IDR) and 90%-NIDU (90%-NIDR). It has been observed by the help of these percentage differences that, the degradation is high for the simulation performed while considering the treatment of non-ideality for aqueous phase chemistry. Furthermore, the oxo-pyruvic acid reacts with OH radical producing ketomalonic acid, also plays a significant role in the particle phase with 13% (7%) and 6% (5%).

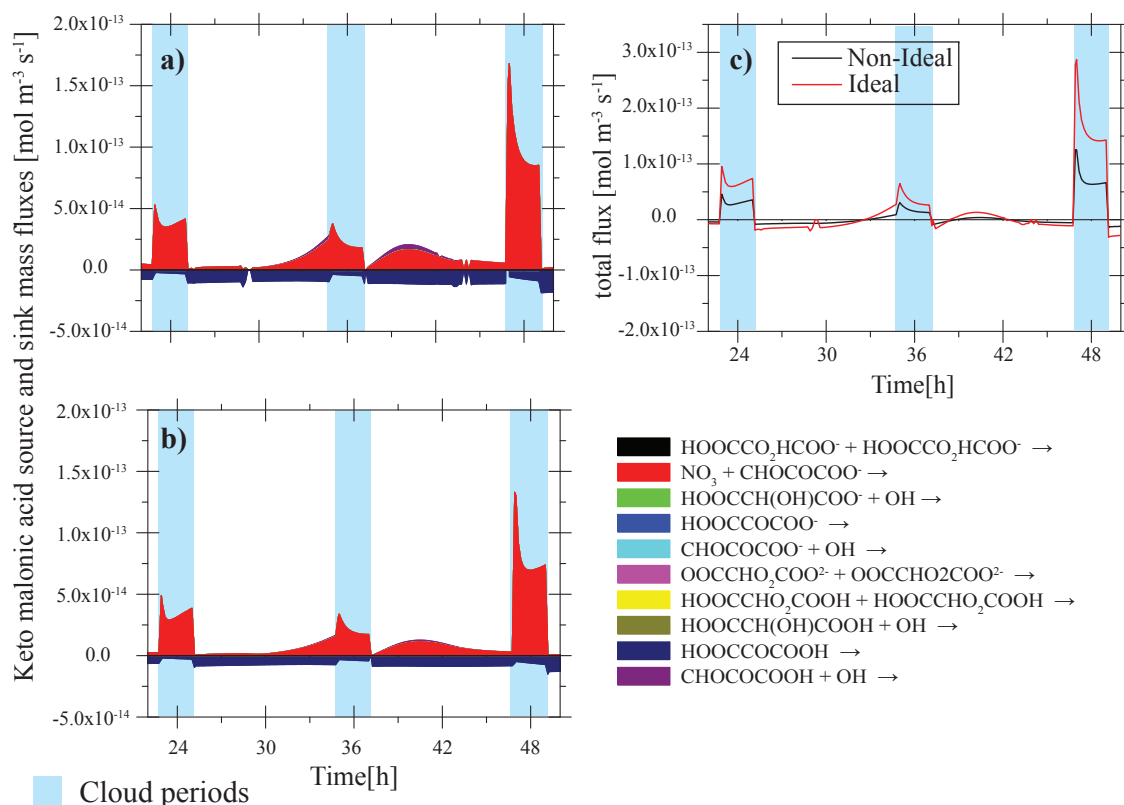


Figure 6.33: Modeled chemical sinks and source mass fluxes of keto malonic acid in aqueous phase for the second day of modeling time for the urban scenario in $\text{mol m}^{-3} \text{s}^{-1}$. a) ideal solutions, b) non-ideal solutions, c) corresponding total fluxes. Only sinks and sources with a contribution larger than $\pm 1\%$ presented.

Along the oxidation chain, the less volatile oxidation products of pyruvic acid are further oxidized to ketomalonic acid in the deliquescent particles particularly during the day time. Ketomalonic acid is a keto-dicarboxylic acid which is the final C₃ product in the reaction chain. The obtained accumulation and the quite high concentration levels of ketomalonic acid might be artificial because of the missing and underestimated sinks in the current state of the mechanism, respectively. However, the NO₃ radical reacts with oxo-pyruvate is the major source for the keto malonate. This reaction contributes in total for the urban (remote) case about 71% (78%) and 67% (81%) under ideal and non-ideal conditions respectively. At the same time, this reaction contributes about 99% (55%) and 99% (61%) in the cloud phase for both of the simulated cases 90%-IDU (90%-IDR) and 90%-NIDU (90%-NIDR), respectively. Moreover, in the particle phase, the same reaction contributing with 57% (81%) and 48% (83%) when assuming the aqueous phase chemistry as ideal and non-ideal solutions for urban (remote) environmental conditions, respectively. Furthermore, ketomalonic acid acts as source for glyoxylic acid for both urban and remote conditions. This reaction contributes in total about 98% (98%) and 97% (98%) with the simulated cases 90%-IDU (90%-IDR) and 90%-NIDU (90%-NIDR). Interestingly, this reaction contributes at the similar range in the cloud phase with 82% (31%) and 83% (30%) in both of the simulations while treating the aqueous phase chemistry as ideal and non-ideal solutions, respectively. Although this reaction contributed to 99% (99%) and 99% (99%) during the particle phase with the simulations 90%-IDU (90%-IDR) and 90%-NIDU (90%-NIDR), respectively.

6.2.9 Summary: Processing of multiphase chemistry under non-ideal conditions

Simulations with the parcel model SPACCIM were performed for urban and remote environmental conditions considering ideal and non-ideal solutions for the aqueous phase chemistry. A detailed microphysical model is coupled with multiphase chemistry in order to investigate the influence of non-ideality on multiphase chemical processing of tropospheric aerosol particles and trace gases using a substantial meteorological scheme. The present model studies have provided a closer insight into the chemical multiphase processing of important atmospheric radicals, inorganic compounds and organic compounds while treating the aqueous phase chemistry as non-ideal solutions in comparison with former studies assuming ideal solutions, in cloud droplets and aqueous particles.

The activity coefficients of the inorganic ions are observed as <1. The predicted activity coefficients strongly depends on the charge number of corresponding ion. The computed activity coefficients are observed as decreasing with increasing the charge number. For mono-ions, the predicted activity coefficients are in the range of 0.50 - 0.85, whereas the activity coefficients of double-charged ions are observed in the range of 0.30 - 0.40. However, the activity coefficients of triple-charged ions are found to be in the range of 0.10 - 0.20. The activity coefficients of organic compounds are depends on the nature of intermolecular interactions in compound specific ways. Mainly, the activity coefficients for the dialdehydes, dicarboxylic acids and alcohols are observed as >1, whereas aldehydes and mono carboxylic acids are observed as <1. The computation of activity coefficients strongly depends on functional groups of organic comprising with corresponding organic compounds. The current simulations have shown for the simulations performed at 90% RH, the aerosol particle pH becomes more acidic for the simulation considering the treatment of non-ideality for the aqueous phase chemistry, comes from the inorganic fraction/components of the aerosol. The pH value is observed in the average over the whole simulation period for the ideal solutions is about 1.4 and for the non-ideal solutions it has been obtained around 1.2. The

implemented model robustness is obtained good, since the total S(VI) processing is found to be same over the whole period of simulation time.

Mainly, S(VI) produced in the cloud phase, the aqueous phase concentrations are obtained same for the simulations performed while assuming the aqueous phase chemistry as ideal and non-ideal solutions respectively. Moreover, it is clear that the activity coefficients in the cloud phase are almost equal to unity, and the same has been obtained in these studies, which demonstrate the model performance. The multiphase processing of inorganic compounds are observed as declined, since the corresponding activity coefficients of ions are obtained as less than unity. During the Fe(II) processing, the Fenton reaction is decreased about 3% for the simulation performed, while assuming the non-ideal solutions in comparison with ideal solutions. Although, the aqueous phase concentrations are obtained higher, for the simulation considering the non-ideal solutions, the turnovers are observed as reduced. The current model studies have shown considerable effects of multiphase interactions becomes more important in the radical oxidation budget while treating the aqueous chemistry as non-ideal solutions. Furthermore, the multiphase processing of OH radical is observed as declined and the turnovers of the NO₃ radical is obtained as increasing in the deliquescent particles. The phase transfer of OH and NO₃ radicals are reduced about 0.8 % and 26 % in the deliquescent particles while employing the treatment of non-ideality for the aqueous phase chemistry. At the same time, the Fenton reaction is also decreased about 1.8%, to produce the OH radical for the simulation performed while assuming the aqueous phase chemistry as non-ideal solutions. All in all, the multiphase processing of OH radical is decreased about 40 % in the deliquescent particles while incorporating the treatment of non-ideality.

The turnovers of NO₃ radical are increased in the particle phase. The interconversion reaction between NO₃ and Cl⁻, acts as one of the source for NO₃ radical, and the contribution of this reaction is increased about 13.6% for the urban environmental conditions, while employing the treatment of non-ideality for the aqueous phase chemistry. Similar to OH radical the aqueous phase concentrations are increased for the HO₂/O₂⁻ radical processing. Furthermore, the OH radical have a feedback on processing of HO₂/O₂⁻. Although, the turnovers are decreased for the simulation performed while considering the aqueous phase chemistry as non-ideal solutions, the aqueous phase concentrations are observed as higher.

As mentioned earlier the multiphase processing of organic compounds strongly connected to the nature of the intermolecular forces between the compounds. The comprising functional subgroups have substantial contribution, in order to predict the activity coefficient of the corresponding organic compounds. The differences in the organic functional subgroups give the different values for the activity coefficients for the organic compounds. Although, the activity coefficients are obtained as less than unity for the C₂ organic compounds, the aqueous phase concentrations are observed as higher while incorporating the treatment of non-ideality. But, the turnovers are reduced, due to the treatment of non-ideality. Moreover, the dissociated and undissociated forms of organic acids, are observed as equally important in order to investigate the influence of treatment of non-ideality on multiphase chemistry. The production and losses are reduced for the oxalic acid in the urban environmental scenario is reduced about the factor of 2 due to the incorporation of treatment of non-ideality. Similarly, the reaction of glyoxylic acid with OH radical is reduced about 6% due to the treatment of non-ideality. The gas to particle mass transfer doesn't seem to be affected by the treatment of non-ideality. However, the oxidation is observed as rather slow for the organic compounds due to the treatment of non-ideality.

Since the activity coefficients are obtained as less than unity, the backward reaction proceeds slowly compare with forward reaction in the equilibriums. The rate coefficient is modified, depends on the activity coefficients of the corresponding species, hence the multiphase processing is

observed as declined. The dissolved salts in the aqueous phase solution modify the intermolecular forces between electrolytes, organics and water. Hence, the corresponding activity coefficients of electrolytes and organics are observed as dissimilar. As a result, the multiphase processing of organic compounds is decreased. Furthermore, it seems likely that in these simulations at 90% of relative humidity, the values of the activity coefficients are varying very little. Hence, for such cases the activity coefficients could be determined just once at the beginning of the simulation rather than multiple times during every gas/aerosol partitioning calculation.

6.3 Chemical sensitivity studies

Aiming to investigate the influence of non-ideality on multiphase chemistry in more detail, the sensitivity studies were performed at different relative humidity levels as described in Table. 6.1. This has been realized by modifying the meteorological scenario as shown in Fig. 6.16. The comparisons have been performed for the three characteristic model scenarios, initializing at same relative humidity level. While obtaining the same particle number concentrations, the relative humidity is varied for all the simulations after second cloud period (see Fig. 6.34). It should be noted that the simulations were performed without any variation of the input parameters. In the succeeding subsections the observed differences will be presented. Although the sensitivity studies were performed for urban and remote environmental scenarios, the current results from the sensitivity studies are focused mainly for urban environmental scenario, since, the aqueous solution is more likely to be concentrate under urban environmental conditions compared to the remote conditions.

6.3.1 Modeled activity coefficients

As explained in the Sec. 3.6, the time evolution of activity coefficients were computed according to the extended AIOMFAC. Upon varying the relative humidity, particles are expected to become more concentrated. Hence, the behavior of modeled activity coefficients during such concentrated solutions will be outlined at first which can directly influence the multiphase chemistry. Similar to the presentation in Sec. 6.2.4, the behavior of computed activity coefficients for the inorganic compounds will be discussed at first, later the behavior of predicted activity coefficient values for the organic compounds will be presented.

6.3.2 Inorganic compounds

The predicted activity coefficient values for key inorganic ions for urban and remote environmental conditions are tabulated in Table. 6.7, under various relative humidity conditions. As enumerated, the predicted activity coefficients are characterized into inorganic anions, inorganic cations similar to Table. 6.2. Similar to the observations discussed in Sec. 6.2.4.1, the current resulting output, implicate that the activity coefficients of the single charged ions (cations and anions) as well as the double charged ions for inorganic species, behaves similarly even varying the relative humidity. As shown in Table. 6.7, with the increase in the concentration the activity coefficients are approaching towards zero. Furthermore, the values of the computed activity coefficients are decreased with decreasing the relative humidity (γ_i 90%-NIDU > γ_i 80%-NIDU > γ_i 70%-NIDU). However, the predicted values of activity coefficients at different concentration levels are less than unity, as observed for the simulation performed for 90%-NIDU. As shown in Table. 6.2, the

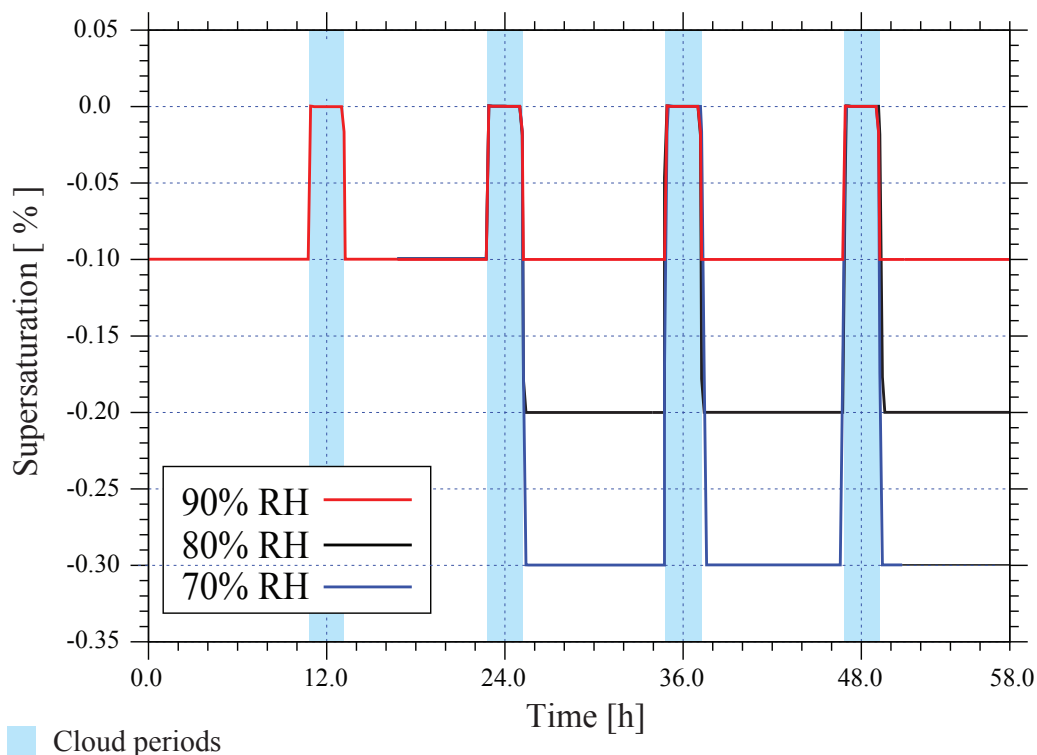


Figure 6.34: Schematic of used model scenarios for sensitivity studies. Basecase (—), 80% RH (—), 70% RH (—).

difference between the activity coefficient values for day time and night time is small. Hence, Table 6.7 shows the computed activity coefficient values during the day time at 32 hours of simulation time.

Interestingly, the values of activity coefficients are reduced approximately about 20% from 90%-NIDU simulated case to 70%-NIDU simulated case. Hence, it can be expected that the multiphase processing of inorganic compounds still decrease in comparison with base case. The deviations from the base case to the 70% of RH level is also observed as decreasing with increasing the charge number (see Fig. C.3). In fact, the ratio of available soluble mass to the total mass in side of the box plays a crucial role for these deviations. This is can be observed, from the values of activity coefficients in the cloud phase, which are not exactly equal to unity. As argued by Clegg and Seinfeld (2006a) and Clegg and Seinfeld (2006b), the current fitted interaction parameters available in the various models, were assumed the pure compounds, which are infinitely diluted in the solution. However, the parameters, considering the dissociating equilibria as well as the data for supersaturated solutions are still scarce. This is possibly one of the reason to obtain the non-unity activity coefficients during the clouds for activated particles, even the clouds have large liquid water content.

Table 6.7: Predicted activity coefficients of ions and water activity in the particles for the remote and urban scenario at three different RH levels, $\Delta\gamma$ = Differences (increase/decrease) in the activity coefficient values between 90% RH vs. 70% RH.

| Species | Remote | | | | Urban | | | |
|---------------------------------|--------|------|------|----------------|-------|------|------|----------------|
| | 90% | 80% | 70% | $\Delta\gamma$ | 90% | 80% | 70% | $\Delta\gamma$ |
| <i>Inorganic anions</i> | | | | | | | | |
| SO ₄ ²⁻ | 0.32 | 0.25 | 0.21 | 0.11 | 0.26 | 0.18 | 0.13 | 0.13 |
| HSO ₄ ⁻ | 0.59 | 0.45 | 0.36 | 0.23 | 0.51 | 0.35 | 0.26 | 0.25 |
| NO ₃ ⁻ | 0.66 | 0.54 | 0.45 | 0.21 | 0.59 | 0.46 | 0.36 | 0.23 |
| OH ⁻ | 0.73 | 0.69 | 0.68 | 0.05 | 0.64 | 0.55 | 0.50 | 0.14 |
| F ⁻ | 0.84 | 0.71 | 0.62 | 0.22 | 0.75 | 0.68 | 0.59 | 0.16 |
| Cl ⁻ | 0.65 | 0.53 | 0.45 | 0.20 | 0.59 | 0.44 | 0.35 | 0.24 |
| Br ⁻ | 0.63 | 0.50 | 0.41 | 0.22 | 0.56 | 0.41 | 0.32 | 0.24 |
| I ⁻ | 0.61 | 0.47 | 0.37 | 0.24 | 0.53 | 0.37 | 0.27 | 0.26 |
| <i>Inorganic cations</i> | | | | | | | | |
| H ⁺ | 0.75 | 0.69 | 0.65 | 0.10 | 0.69 | 0.61 | 0.55 | 0.14 |
| NH ₄ ⁺ | 0.68 | 0.57 | 0.49 | 0.19 | 0.62 | 0.50 | 0.41 | 0.21 |
| Na ⁺ | 0.71 | 0.62 | 0.55 | 0.16 | 0.66 | 0.56 | 0.47 | 0.19 |
| K ⁺ | 0.69 | 0.59 | 0.52 | 0.17 | 0.64 | 0.52 | 0.43 | 0.21 |
| Mg ²⁺ | 0.44 | 0.37 | 0.32 | 0.12 | 0.39 | 0.35 | 0.30 | 0.09 |
| Ca ²⁺ | 0.38 | 0.34 | 0.32 | 0.06 | 0.35 | 0.29 | 0.26 | 0.09 |
| Fe ²⁺ | 0.33 | 0.25 | 0.20 | 0.13 | 0.29 | 0.21 | 0.16 | 0.13 |
| Mn ²⁺ | 0.33 | 0.25 | 0.20 | 0.13 | 0.29 | 0.21 | 0.16 | 0.13 |
| Cu ²⁺ | 0.36 | 0.29 | 0.24 | 0.12 | 0.33 | 0.26 | 0.21 | 0.12 |
| Fe ³⁺ | 0.12 | 0.08 | 0.06 | 0.06 | 0.10 | 0.07 | 0.05 | 0.05 |
| Mn ³⁺ | 0.12 | 0.08 | 0.06 | 0.06 | 0.10 | 0.07 | 0.05 | 0.05 |
| <i>water activity</i> | 1.12 | 1.16 | 1.20 | 0.08 | 1.10 | 1.13 | 1.15 | 0.05 |

As shown in Table. 6.7, the differences in the activity coefficient values between the simulations 90%-NIDU and 70%-NIDU, are also reducing with increasing the charge number. The differences for the mono anions in the urban (remote) environmental scenario are approximately around 0.25 (0.22), for dianions the difference is observed around 0.13 (0.11). Interestingly, the differences are observed for mono cations are also behaves similar to anions. The observed differences for mono cations for urban (remote) environmental scenario are approximately about 0.20 (0.18). However, as explained in Sec. 3.6, the interaction parameters which are prescribed as zero for the ions, have the same value of activity coefficients and the differences are obtained same for the urban (remote) as 0.05 (0.06). Apart from the ions, the water activity is increased while decreasing the relative humidity. Since, the particles are more concentrated in the urban environmental conditions, the differences in the water activity is observed as smaller in the urban case compared with remote case. Subsequently, the obtained water activity will further influence the microphysics, to find the new equilibrium and critical values (i.e. radius and saturation ratio). As a result, it will influence the multiphase chemistry from the microphysics. The time-interpolated mass fluxes will changed along with the ratio of soluble fraction to total fraction available in the particles.

As argued in Sec. 6.2.4.1, the pattern or behavior of lower values of activity coefficients for the simulations performed while decreasing the relative humidity, for 90%-NIDU to 70%-NIDU, is mainly caused due to the consideration of ionic strength of the solution. It is thus, obvious since the charge of an ion is of great importance for the magnitude of the ion interaction coefficient. Moreover, it has been observed that the ionic strength is greater than the molar concentration, since the solution contains ions with multiple charges. Hence, this magnitude of the electrolyte effect is strong dependent on the charges of the species in which may undergone for chemical reaction. For instance, if only neutral species are involved chemical equilibrium reactions, the equilibrium position is basically independent of electrolyte concentration, simultaneously, for the charged species, the magnitude of the electrolyte effect increases with charge. This electrolyte effect results from the electrostatic attractive and repulsive forces that exist between the ions of an electrolyte and the ions involved in an equilibrium. This effect seems to be dominant in the computation of activity coefficients of the ions in the multicomponent solution. All in all, the activity coefficient of the ions are obtained as less than unity for all the simulations performed. Furthermore, due to the availability of small LWC, it is thus obvious that, the ionic strength in the solution increases (8.6 mol kg^{-1} for 90% RH case and 14.3 mol kg^{-1} for 70% RH case), as observed here. The lower values attained due to the changes in the liquid water content available in the particles. Furthermore, in these simulations the influence from the microphysics also plays a decisive role for attaining the smaller values.

6.3.3 Organic compounds

The behavior of the modeled activity coefficient values for the key organic compounds are summarized in this section. Similar to Table. 6.3, the activity coefficient values for the key organic compounds are tabulated in Table. 6.8, obtained from the sensitivity studies at three relative humidity levels. The major reasons behind the computation of activity coefficients and their expected impact on the multiphase processing of organic compounds was explained in Sec. 6.2.4.2.

Similar to the behavior noted for 90%-NIDU, the computed activity coefficient values for the dissociated organic compounds are less than unity, at different relative humidity levels also. Moreover, the organic ions are behave similar to the inorganic ions similar to 90%-NIDU. The resulting deviations for the simulated case 90%-NIDU case to 70%-NIDU are approximately about 30%. In contrast to the dissociated form, the undissociated form have also exhibited similar behavior for the predicted time evolution of activity coefficients at three relative humidity levels. Furthermore, it has been observed that the activity coefficient values are linearly increasing with respect to the time. This is mainly caused due to the chemical composition available in the solution. As explained earlier, the chemical composition have continuous feedback on the computation of activity coefficients (i.e. $\gamma_{org} = f(x_{org})$). During the lower humidity levels ($\leq 85\%$) the aqueous solution expected to attain liquid-liquid phase separations (Zuend et al., 2008), as well as the salt formation (crystallization), however, such conditions are not considered in these simulations. While assuming the aqueous phase as a single phase, the activity coefficients are computed in the present studies.

As can be seen from Table. 6.8, the activity coefficients for the organic compounds in dissociated form are less than unity for all the simulations performed while varying the relative humidity. Similar to the 90%-NIDU simulated case, the activity coefficient values for the alcohols are larger than unity for the 80%-NIDU and 70%-NIDU simulated case. The increasing behavior of the activity coefficient is attained with decreasing with the relative humidity. It is thus obvious,

that the particle concentration is higher with decreasing the relative humidity. Hence, these results implicate that the multiphase processing of alcohols might be increased with decreasing the relative humidity similar to 90%-NIDU simulated case. However, depending on the activity coefficients shown in Table. 6.8, the multiphase processing of organics are expected to increase if the activity coefficients are greater than unity. At the same time, it would be decreasing, if the activity coefficients are less than unity.

Notable differences are observed, between the predicted activity coefficients while decreasing the relative humidity. Interestingly, the activity coefficients as greater than unity, was obtained for the simulations 90%-NIDR to 70%-NIDR for glyoxal, whereas the activity coefficients are obtained as less than unity for the simulations 90%-NIDU to 70%-NIDU. Moreover, the pattern of computed activity coefficients are observed as increasing while decreasing the relative humidity. The deviations in the activity coefficients are mainly caused from the available concentrations in the particles. The aqueous phase concentrations are obtained higher in the urban case compare with remote case. Hence, depending on the concentrations at corresponding simulation time, the activity coefficients are computed. Moreover, it has been observed that, for increasing the concentration the corresponding activity coefficients are decreased. Furthermore, the activity coefficient values for the C₄ organic oxidation products are obtained even less than the inorganic ions (see Table. 6.8 for 2-hydroxy 3-oxo butandial). Apart from the chemical composition, the functional groups used to compute the activity coefficients have strong dependence. The functional subgroups involved in 2-hydroxy 3-oxo butandial are 3×CHO, 1×OH and 1×C. Hence, in order to calculate the total activity coefficient for the 2-hydroxy 3-oxo butandial, based on the model equations described in Sec. 3.6, the activity coefficient of these each functional subgroup are multiplied with the associated subgroup. As a result, the corresponding functional subgroups, which are contributing to computation of total activity coefficients are caused to obtain such a small values. Mainly, it has been observed that, the alkane group involved in the organic products have the lower values, which directly influences the total activity coefficients.

Furthermore, the activity coefficient values for the succinic acid are obtained higher than malic acid for the simulations 80%-NIDR and 70%-NIDR (see Table. 6.8). In these two products the main difference is the functional subgroup CH₂, which causes the lower value for the succinic acid. The alkane subgroup (CH₂) multiplied twice, in the calculation of total activity coefficients for the succinic acid. As mentioned earlier, the alkane functional subgroup have lower activity coefficients, which further decreasing the total compound activity coefficients as obtained for these compounds. All in all, the activity coefficient values are increased while decreasing the relative humidity. However, for the organic ions, the activity coefficients are decreased similar to the behavior observed for the inorganic ions, while decreasing the relative humidity. Moreover, the smallest diacids and mono carboxylic acids can easily evaporate from the multicomponent mixture, since they become more concentrated at lower relative humidity and constantly changes the composition due to the possibility of evaporating the higher-volatility compounds. Accordingly, the evaporation of higher-volatility, which might be the reason, that calculated activity coefficients for these compounds are closer to unity as shown in Table. 6.8. Subsequently, the low-volatile compounds are apparently be present in the particle phase, hence the corresponding chemical composition is high, as a result the computation of activity coefficients strongly depends on this composition, which gives the different activity coefficient values.

Table 6.8: Predicted activity coefficients of key organic compounds in the particles for the remote and urban scenario at three different RH levels, $\Delta\gamma$ = Differences (increase/decrease) in the activity coefficient values between 90% RH vs. 70% RH.

| Species | Remote | | | | Urban | | | |
|--|--------|------|------|----------------|-------|------|------|----------------|
| | 90% | 80% | 70% | $\Delta\gamma$ | 90% | 80% | 70% | $\Delta\gamma$ |
| <u>Alcohols</u> | | | | | | | | |
| Methanol | 1.04 | 1.15 | 1.33 | 0.29 | 1.19 | 1.23 | 1.59 | 0.40 |
| Ethanol | 1.16 | 1.57 | 2.33 | 1.17 | 1.10 | 1.21 | 1.77 | 0.67 |
| <u>Aldehydes</u> | | | | | | | | |
| <u>Formaldehyde</u> | | | | | | | | |
| CH ₂ OH ₂ | 0.82 | 0.82 | 0.78 | 0.04 | 0.41 | 0.32 | 0.22 | 0.19 |
| HCHO | 0.83 | 0.71 | 0.62 | 0.21 | 0.75 | 0.59 | 0.48 | 0.27 |
| <u>Acetaldehyde</u> | | | | | | | | |
| CH ₃ CHO | 0.79 | 0.69 | 0.66 | 0.13 | 0.72 | 0.56 | 0.51 | 0.21 |
| CH ₃ CHOH ₂ | 1.25 | 1.81 | 2.83 | 1.58 | 1.04 | 1.44 | 2.24 | 1.20 |
| Propionaldehyde | 1.02 | 1.21 | 1.64 | 0.62 | 1.06 | 1.25 | 2.04 | 0.98 |
| Butyraldehyde | 1.32 | 2.11 | 4.04 | 2.72 | 1.55 | 2.64 | 3.41 | 1.86 |
| <u>Substituted carbonyl compounds</u> | | | | | | | | |
| <u>Glycolaldehyde</u> | | | | | | | | |
| OHCCH ₂ OH | 0.73 | 0.63 | 0.58 | 0.15 | 0.46 | 0.33 | 0.25 | 0.21 |
| OH ₂ CHCH ₂ OH | 1.40 | 2.27 | 3.93 | 2.53 | 1.18 | 1.84 | 3.17 | 1.99 |
| <u>Glyoxal</u> | | | | | | | | |
| CHOH ₂ CHOH ₂ | 1.06 | 1.42 | 2.00 | 0.94 | 0.61 | 0.67 | 0.74 | 0.13 |
| CHOCHO | 0.49 | 0.27 | 0.16 | 0.33 | 0.36 | 0.16 | 0.08 | 0.28 |
| CH ₃ COCHOH ₂ | 1.02 | 1.25 | 1.70 | 0.68 | 0.75 | 0.82 | 1.12 | 0.37 |
| OHCCHCHCHO | 0.97 | 1.11 | 1.47 | 0.50 | 0.95 | 1.02 | 1.56 | 0.61 |
| OHCCHOHCOCHO | 0.28 | 0.09 | 0.04 | 0.24 | 0.16 | 0.04 | 0.02 | 0.14 |
| <u>Monocarboxylic acids</u> | | | | | | | | |
| <u>Formic acid</u> | | | | | | | | |
| HCOOH | 0.90 | 0.82 | 0.75 | 0.15 | 0.85 | 0.74 | 0.66 | 0.19 |
| HCOO ⁻ | 0.65 | 0.53 | 0.45 | 0.20 | 0.59 | 0.46 | 0.38 | 0.21 |
| <u>Acetic acid</u> | | | | | | | | |
| CH ₃ COOH | 0.86 | 0.79 | 0.68 | 0.17 | 0.82 | 0.73 | 0.67 | 0.15 |
| CH ₃ COO ⁻ | 0.74 | 0.68 | 0.52 | 0.22 | 0.68 | 0.60 | 0.52 | 0.16 |
| CH ₃ CH ₂ COOH | 1.12 | 1.39 | 1.76 | 0.64 | 1.24 | 1.62 | 2.43 | 1.19 |
| CH ₃ CH ₂ CH ₂ COOH | 1.45 | 2.42 | 4.34 | 2.89 | 1.82 | 3.40 | 4.53 | 2.71 |
| <u>Glycolic acid</u> | | | | | | | | |
| CH ₂ OHCOOH | 0.79 | 0.72 | 0.61 | 0.18 | 0.58 | 0.43 | 0.30 | 0.28 |
| CH ₂ OHCOO ⁻ | 0.72 | 0.63 | 0.56 | 0.16 | 0.67 | 0.56 | 0.48 | 0.19 |
| <u>Glyoxylic acid</u> | | | | | | | | |
| CHOH ₂ COOH | 0.74 | 0.65 | 0.53 | 0.21 | 0.36 | 0.24 | 0.13 | 0.23 |

Table 6.8: Predicted activity coefficients of key organic compounds at three different relative humidity levels (Continued)

| Species | Remote | | | | Urban | | | |
|---|--------|------|------|----------------|-------|------|------|----------------|
| | 90% | 80% | 70% | $\Delta\gamma$ | 90% | 80% | 70% | $\Delta\gamma$ |
| CHOH ₂ COO ⁻ | 0.72 | 0.63 | 0.56 | 0.16 | 0.67 | 0.56 | 0.48 | 0.19 |
| <u>Pyruvic acid</u> | | | | | | | | |
| CH ₃ COCOOH | 0.86 | 0.79 | 0.64 | 0.22 | 0.85 | 0.77 | 0.72 | 0.15 |
| CH ₃ COCO ⁻ | 0.72 | 0.63 | 0.56 | 0.16 | 0.67 | 0.56 | 0.48 | 0.19 |
| <u>Dicarboxylic acids</u> | | | | | | | | |
| <u>Oxalic acid</u> | | | | | | | | |
| H ₂ C ₂ O ₄ | 0.59 | 0.36 | 0.19 | 0.40 | 0.48 | 0.27 | 0.12 | 0.36 |
| C ₂ O ₄ ²⁻ | 0.37 | 0.29 | 0.25 | 0.12 | 0.33 | 0.26 | 0.21 | 0.12 |
| HC ₂ O ₄ ⁻ | 0.72 | 0.63 | 0.56 | 0.16 | 0.66 | 0.55 | 0.47 | 0.19 |
| Fe(C ₂ O ₄) ₂ ⁻ | 0.72 | 0.63 | 0.56 | 0.16 | 0.66 | 0.55 | 0.47 | 0.19 |
| Fe(C ₂ O ₄) ⁺ | 0.72 | 0.63 | 0.56 | 0.16 | 0.66 | 0.55 | 0.47 | 0.19 |
| Fe(C ₂ O ₄) ₃ ³⁻ | 0.12 | 0.08 | 0.06 | 0.06 | 0.10 | 0.07 | 0.05 | 0.05 |
| <u>Malonic acid</u> | | | | | | | | |
| HOOCCH ₂ COOH | 1.05 | 1.11 | 1.15 | 0.10 | 1.06 | 1.20 | 1.39 | 0.33 |
| HOOCCH ₂ COO ⁻ | 0.65 | 0.53 | 0.45 | 0.20 | 0.58 | 0.45 | 0.36 | 0.22 |
| OOCCH ₂ COO ²⁻ | 0.36 | 0.29 | 0.25 | 0.11 | 0.33 | 0.26 | 0.21 | 0.12 |
| <u>Succinic acid</u> | | | | | | | | |
| C ₂ H ₄ (COOH) ₂ | 1.12 | 1.30 | 1.47 | 0.35 | 1.24 | 1.38 | 1.63 | 0.39 |
| HOOCCH ₂ H ₄ COO ⁻ | 0.65 | 0.53 | 0.44 | 0.21 | 0.59 | 0.45 | 0.36 | 0.23 |
| OOCCH ₂ CH ₂ COO ²⁻ | 0.36 | 0.29 | 0.25 | 0.11 | 0.33 | 0.26 | 0.21 | 0.12 |
| <u>Keto malonic acid</u> | | | | | | | | |
| HOCCOCOOH | 0.89 | 0.80 | 0.73 | 0.16 | 0.84 | 0.72 | 0.62 | 0.22 |
| HOCCOCOO ⁻ | 0.72 | 0.63 | 0.56 | 0.16 | 0.67 | 0.56 | 0.48 | 0.19 |
| OCCOCOO ²⁻ | 0.36 | 0.29 | 0.25 | 0.11 | 0.33 | 0.26 | 0.21 | 0.12 |
| <u>Malic acid</u> | | | | | | | | |
| HOOCCHOHCH ₂ COOH | 1.12 | 1.45 | 1.85 | 0.73 | 1.18 | 1.38 | 1.63 | 0.45 |
| HOOCCHOHCH ₂ COO ⁻ | 0.72 | 0.63 | 0.56 | 0.16 | 0.67 | 0.56 | 0.48 | 0.19 |
| OOCCHOHCH ₂ COO ²⁻ | 0.36 | 0.29 | 0.25 | 0.11 | 0.33 | 0.26 | 0.21 | 0.12 |

6.3.4 Particle acidity

The importance of particle acidity as well as the computational procedure was discussed earlier (see Sec. 6.2.5). The time evolution of pH for the simulations performed at three different relative humidity levels for the urban environmental scenario is shown in Fig. 6.35. As shown in this plot, the calculated pH was decreased with increasing the relative humidity for all the simulations performed while considering the aqueous phase chemistry as ideal and non-ideal solutions. Interestingly, the deviation between 70%-IDU to 70%-NIDU is higher than 80% and 90% relative humidity cases while assuming the aqueous phase chemistry as ideal and non-ideal

solutions. The tendency has been observed that the deviations from ideal to non-ideal solutions is more obvious, while decreasing the relative humidity. The experimental determination of pH in the particles is rather difficult since, the particle water contents are usually small for direct pH measurements. However, the model studies were performed while varying the relative humidity were concentrated mainly for marine environmental conditions (see Fridlind and Jacobson (2000)), similar studies for the remote and urban environmental conditions were still scarce to compare the current results.

For instance, Chameides and Stelson (1992) observed a decrease (become basic) in sea salt aerosol pH with decreasing the relative humidity in their box model. von Glasow and Sander (2001) argued, that the results and the explanation of given by Chameides and Stelson (1992), are by means of effects of activity coefficients were shown to be insufficient, since the microphysical variables also have certain influence on the particle acidity (see von Glasow and Sander (2001)). Moreover, Fridlind and Jacobson (2000) used the equilibrium model EQUISOLV II for analyzing the pH of sea salt aerosol for the data obtained from Aerosol Characterization Experiment (ACE1) campaign. Their results also shows the aqueous phase aerosol particle pH, is less acidic, with decreasing relative humidity. Although, these results explained the behavior of particle pH for marine aerosol particles, similar results are achieved in the sensitivity studies for all the simulations for urban environmental conditions.

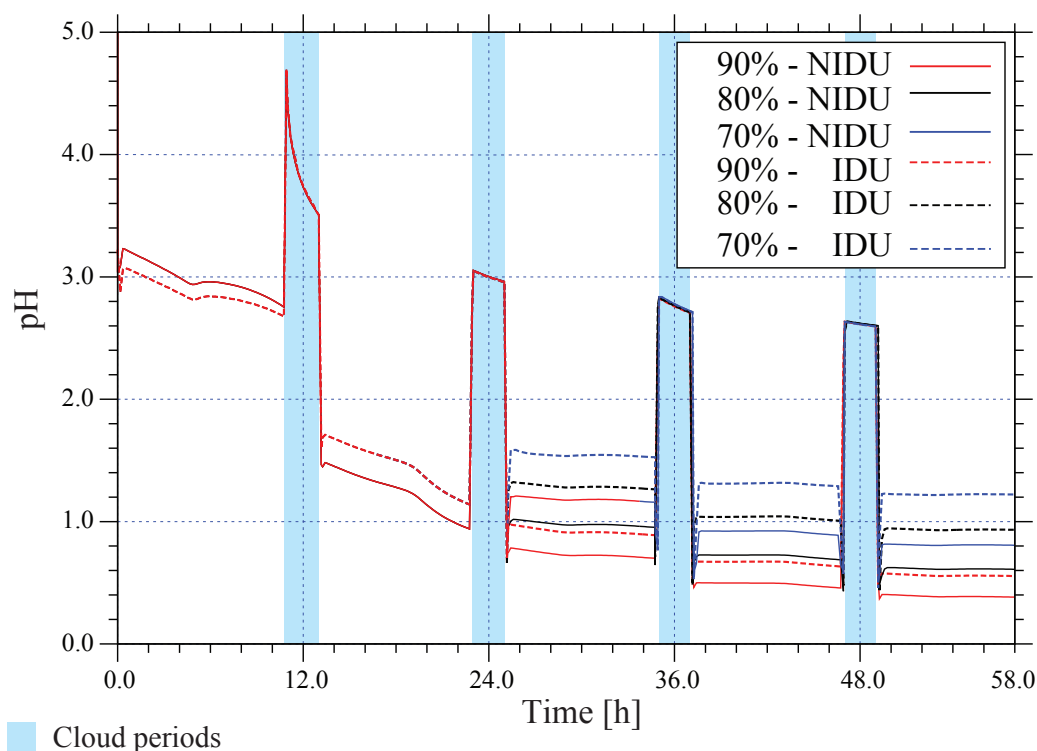


Figure 6.35: Modeled pH value as a function of time for the urban environmental conditions at three different relative humidity levels.

As mentioned earlier, at low liquid water contents, possibly the more volatile acids stay in the gas phase. Interestingly, the differences in the gas phase concentrations are observed as the same range between the 90% relative humidity case to 70% relative humidity case. Since, the gas phase concentrations didn't change significantly, the relative changes in the partial and saturated

vapor pressure for these acids are also negligible. Hence, the deviations are expected mainly from the microphysical variables such as LWC. Hence, whenever, particle liquid water content increases, the dissociated ionic content in the aqueous solutions would be decrease due to the dilution/ solubility effect. One possible reason could be when the concentrations of inorganic anions and organic anion concentration decreases, the corresponding H^+ concentration must increase to keep the product as constant. As a result, the pH of the solution decreases (see the analytical solution in [von Glasow and Sander \(2001\)](#)). According to this analytical solution, both inorganic anions as well as the dissociating organic compounds and H^+ increase in units of $\text{mol}/\text{m}_{air}^3$ but the relative increase of both inorganic anions as well as the organic anions, to keep the equilibrium constant, may be probably negligible, whereas the same increase in H^+ might have apparently large effect to exhibit this behavior.

6.3.5 Multiphase processing of inorganics

It has been already explained, that the gas/aerosol partitioning of aqueous phase particles is modified, mainly via the amount of liquid water content, particle acidity and interactions between inorganic ions \leftrightarrow organic molecules that lead to changes in the activity coefficients. Based on the predicted activity coefficients for the inorganic compounds, the impact of treatment of non-ideality on multiphase processing of inorganic chemistry (Fe(II) chemistry) at three relative humidity levels will be discussed in the following subsection.

The profound differences while considering the aqueous phase chemistry as ideal and non-ideal solutions for 90%-NIDU simulated case was discussed earlier (see Sec. 6.2.6.2). The sensitivity studies with different relative humidity levels and their impact on multiphase processing of Fe(II) will be outlined in this subsection. Fig. C.3, illustrates the aqueous phase concentration of Fe^{2+} in mol m^{-3} vs. total simulation time at three relative humidity levels. As shown in this plot, the aqueous phase concentrations while considering the aqueous phase chemistry as ideal solutions at three different simulated cases differ significantly. The aqueous phase concentrations are decreased while decreasing the relative humidity. Since, the liquid water content is small for the 70% relative humidity case, the mass concentrations as well as the ionic strength ($\approx 14.3 \text{ mol kg}^{-1}$) are higher inside of the particles. In such a way, this behavior is promising. Whereas the simulations performed with the aqueous phase chemistry assuming the non-ideal solutions, the deviations are rather lower while decreasing the relative humidity. In the cloud phase, the mass concentrations are observed as higher with decreasing the relative humidity. Due to the inactivity of photochemistry during the night time, the aqueous phase concentration of Fe^{2+} is remains unchanged, for the simulations while considering the ideal and non-ideal solutions. Interestingly, soon after the droplets are evaporated, mainly in night time the total budget of the Fe(II) remains same during the treatment of non-ideality for the aqueous phase chemistry. The similar behavior is observed for the simulations performed at 80%-NIDU and 70%-NIDU.

Furthermore, the aqueous phase mass concentrations are overlapping during the 80% and 70% relative humidity levels after the cloud evaporation. One possible reason could be, both microphysical and dilution effects are dominating than the treatment of non-ideality. Due to the non-linear coupling of microphysics and multiphase chemistry, the change in mass with respect to change in liquid water content is less than the change in molalities ($\Delta c/\Delta LWC < \Delta m/\Delta LWC$), with decreasing the relative humidity. The simultaneous dissociations and the reaction pathways considered in the aqueous phase as well as the treatment of non-ideality makes the reactions slower, since the activity coefficients are less than unity, whenever the particles become more concentrated. Moreover, the formation of Fe^{2+} might be faster during the cloud evaporation, so

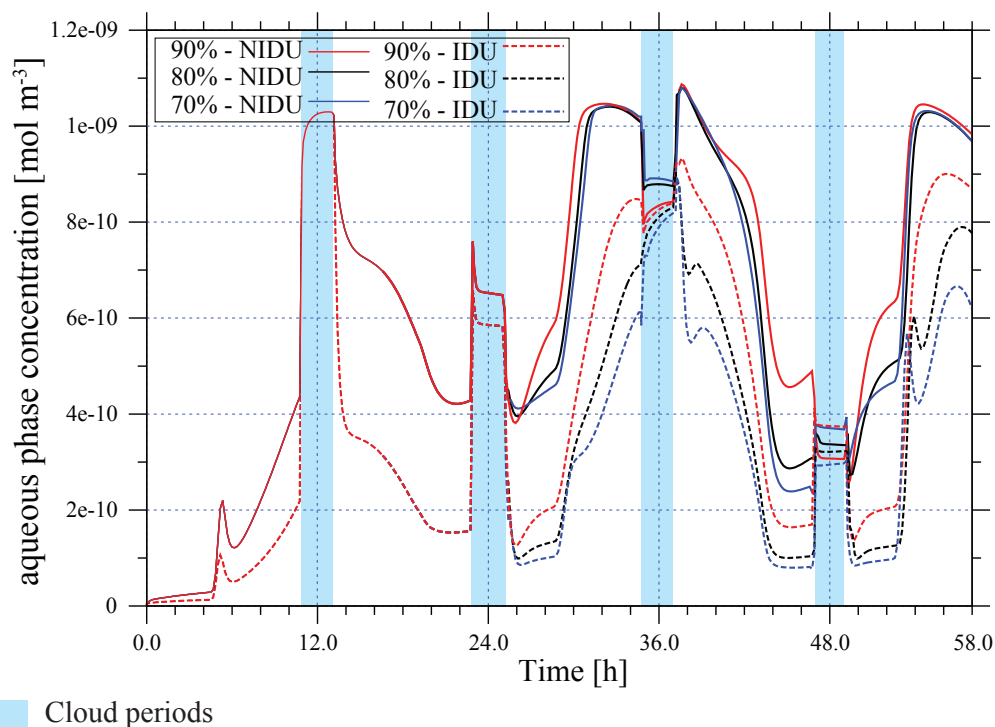


Figure 6.36: Modeled $Fe(II)$ aqueous phase concentration in $mol\ m^{-3}$ vs. modeling time for the urban scenario at three different relative humidity levels.

the mass concentrations are differed at all three simulated cases considering ideal and non-ideal solutions for aqueous phase chemistry.

For instance, in the reaction of Fe^{3+} and Cu^+ , the rate of the reaction would decrease due to the obtained activity coefficients, which are less than unity. Hence the contribution of this reaction during the total processing of Fe^{2+} would be decreased in the aqueous deliquescent particles (see Table. 6.4). Furthermore, the activity coefficients are observed as decreasing with decreasing the relative humidity. Hence the processing of $Fe(II)$ can be further decreased while decreasing the relative humidity (see Fig. C.3). As can be seen from this schematic, the difference in the activity coefficients is approximately about 20% between base case to 80% of relative humidity level. At the same time this value deviates approximately about 35% from 90% to 70% of relative humidity level (see Fig. C.3). Subsequently, the processing of $Fe(II)$ will be decreasing with decreasing of relative humidity or whenever the particles are become more concentrated.

6.3.6 Multiphase OH radical processing

In this section, the influence of treatment of non-ideality for the radical processing will be outlined by varying the relative humidity during the deliquescent particle phase. The influence of treatment of non-ideality was described in detail for the key species (i.e. OH, NO_3 and HO_2/O_2^-). In light of this, similar to the former presented results Sec. 6.3.6, the influence of non-ideality on

multiphase processing of radicals will be explained only for the OH radical in the proceeding subsection, since the OH radical is one most important reactive radical oxidant in tropospheric chemical processes.

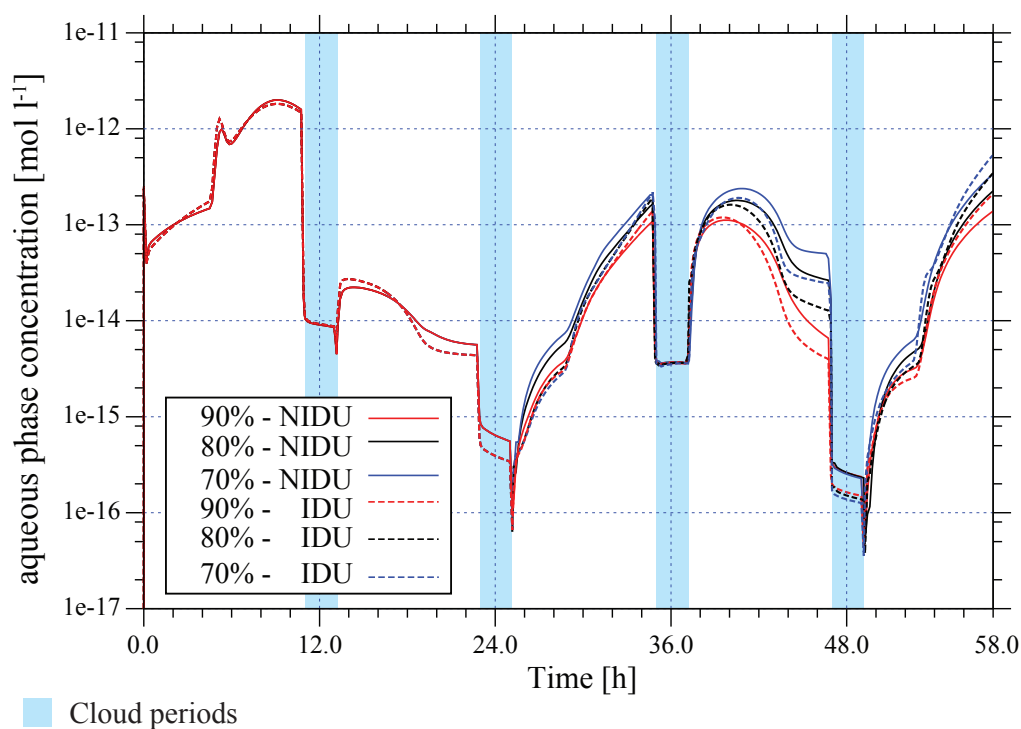


Figure 6.37: Modeled OH aqueous phase concentration in mol l⁻¹ vs. modeling time for the urban scenario at three different RH levels.

The aqueous phase concentrations of OH radical for urban environmental conditions, while varying the relative humidity levels plotted vs. simulated time, in Fig. 6.37, while assuming the aqueous phase chemistry as ideal and non-ideal solutions. As can be seen, the aqueous phase concentrations are increasing during the particle phase, during the day time after cloud evaporation, with decreasing the relative humidity. At the same time, the aqueous phase concentrations are observed as decreasing with decreasing the relative humidity at night time. Interestingly, different pattern of concentrations are obtained different during the noon and night time clouds. The concentrations are found same for all the simulations at noon clouds, whereas, the concentrations are higher in the simulations performed, while assuming the non-ideal solutions for aqueous phase chemistry in comparison with the assumption of ideal solutions. Moreover, the concentrations are found to be same for the simulations performed, while incorporating the treatment of non-ideality.

Fig. 6.37 shows the aqueous phase concentrations are slightly increased during treatment of non-ideality. Moreover, the increasing behavior of aqueous phase concentrations are observed in all three relative humidity levels, when the aqueous phase chemistry was assumed as ideal and non-ideal solutions. During the noon cloud periods, the aqueous phase concentrations are equal, while treating the aqueous phase chemistry as ideal and non-ideal solutions at all three different relative humidity levels. However, due to the change in the ratio of soluble mass to the total

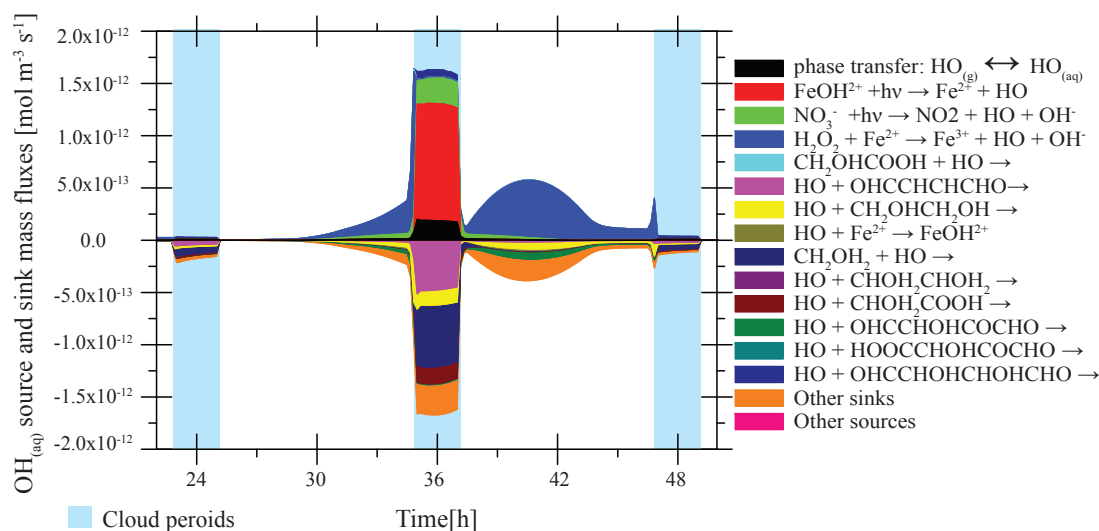


Figure 6.38: Modeled chemical sinks and source mass fluxes of OH radical in aqueous phase in mol m⁻³ s⁻¹ for the second day of modeling time for the urban scenario for the simulation 70%-NIDU. Only sinks and sources with a contribution larger than ± 1% presented.

mass, the particles are not attained to unity activity coefficient for the inorganic ions. Depending on the charge, the most ions have lower value even at cloud phase. As shown in Fig. 6.25 for the simulation performed at 90% relative humidity case the total sink fluxes are higher in the ideal case compared with the non-ideal case. The same behavior can be expected for the all three cases while varying the relative humidity. Moreover, the turnovers for the OH radical with various reaction pathways are different but the total budget is same. Since, the continuous feedback of concentrations and masses from the deliquescent particles on cloud phase, these differences are obvious. However, due to the combined modifications in microphysics as well as from the multiphase chemistry, apart from the treatment of non-ideality it is difficult to determine, that the differences are obtained from microphysics or from multiphase chemistry, respectively.

However, noticeable differences are observed during the deliquescent particle phase at three different relative humidity levels when treating the aqueous phase chemistry as ideal and non-ideal solutions. The concentrations are increasing with decreasing the relative humidity. As shown in Fig. 6.37, for the simulations while assuming the aqueous phase chemistry as ideal and non-ideal solutions have higher concentrations during the deliquescent particle phase. As shown in Fig. 6.25 for the base case the sources are higher during the deliquescent particles. Furthermore, the deviations are higher during the day time compared to night time. The contribution of various reaction pathways, to obtain these differences are explained in Sec. 6.2.7.1. Furthermore, it has been observed that the concentrations are increasing gradually and then start to decrease during the all simulations with decreasing the relative humidity.

Noticeable differences can be obtained for the simulation performed at 70% relative humidity level. As mentioned in Sec. 6.2.7.1, the Fenton reaction is more dominant in the deliquescent particle phase. Hence, it is thus obvious due to the contribution of Fenton reaction, the aqueous

phase concentrations are varied at all three different relative humidity levels. The contribution of organic chemistry also enhances the concentration during the deliquescent particle phase. Similar to the simulations performed at 90% relative humidity level and the contribution of reaction pathways described in Table. 6.5, the fluxes can further decreased due to the consideration of treatment of non-ideality for the aqueous phase chemistry. Fig. 6.38 shows the turnovers for the OH radical for the simulation 70%-NIDU. As can be seen the multiphase processing of OH radical is decreased compare with 90%-NIDU (see Fig. 6.25). All in all, it can be expected that the multiphase processing of radicals is decreased with decreasing the relative humidity while treating the aqueous phase chemistry as non-ideal solutions.

6.3.7 Aqueous multiphase processing of organic compounds

The importance of multiphase processing of organic compounds was described in detail for the key species in Sec. 6.2.8. In this section, the performed sensitivity studies while varying the relative humidity and their impact on multiphase processing of organic compounds in the aqueous phase will be discussed for C₂ organic compounds similar to the discussion presented in Sec. 6.2.8.

The modeled aqueous phase concentrations of oxalic acid and its precursors, glycolic acid and glyoxylic acid, along with corresponding computed activity coefficients vs. simulated time for the urban environmental conditions, is shown in Fig. 6.39 from the simulations performed at three different relative humidity levels. Similar to the aqueous phase concentrations obtained from the simulations performed at 90% relative humidity, the in-cloud production is increasing with decreasing the relative humidity levels due to the lower OH processing (see Fig. 6.39). Moreover, the differences are increasing with decreasing the relative humidity. As explained earlier (see Sec. 6.2.8.1), the oxalic acid precursors are effectively produced primarily under day time cloud conditions and degraded mostly in deliquescent particles during the day time, due to the availability of OH radicals in the aqueous phase as pointed out in the Sec. 6.2.8.1. However, in the deliquescent particles, the degradation is delayed with decreasing the relative humidity. This deviation is increasing with decreasing the relative humidity. Since, the activity coefficients of dissociated and undissociated forms of glycolic acid are found to be less than unity, thus, the multiphase processing of the glycolic acid is decreased similar to simulation 90%-NIDU (see Fig. 6.39). Furthermore, the activity coefficients are found to be lower values compare with 90%-NIDU simulated case, the activities are reduced due to the incorporation of activity coefficients, hence the production will be decreased with decreasing the relative humidity. Moreover, it has been observed that, for 80%-NIDU and 70%-NIDU, the in cloud production is same. At the same time, the deviations for 90%-NIDU to 80%-NIDU and 80%-NIDU to 70%-NIDU are large. However, the combined microphysical and multiphase chemistry effects apart from the activity coefficients are strongly plays a role for the obtained differences in aqueous phase concentrations. Similar to the simulation performed at 90% relative humidity, the oxidation is probably proceeds longer, for the three simulations while varying the relative humidity, apart from the treatment of non-ideality.

Similar behavior is also observed for the glyoxylic acid while performing the simulations at different relative humidity levels. As shown in Fig. 6.39, the aqueous phase concentrations of glyoxylic acid are increased with decreasing the relative humidity. The production rate is increased with decreasing the relative humidity. The differences between the simulations performed, while considering the aqueous phase chemistry as ideal and non-ideal solutions are increased with decreasing the relative humidity (i.e. ΔC - 90% > ΔC - 80% > ΔC - 70%, where ΔC represents the differences between the concentrations, when the simulations performed while

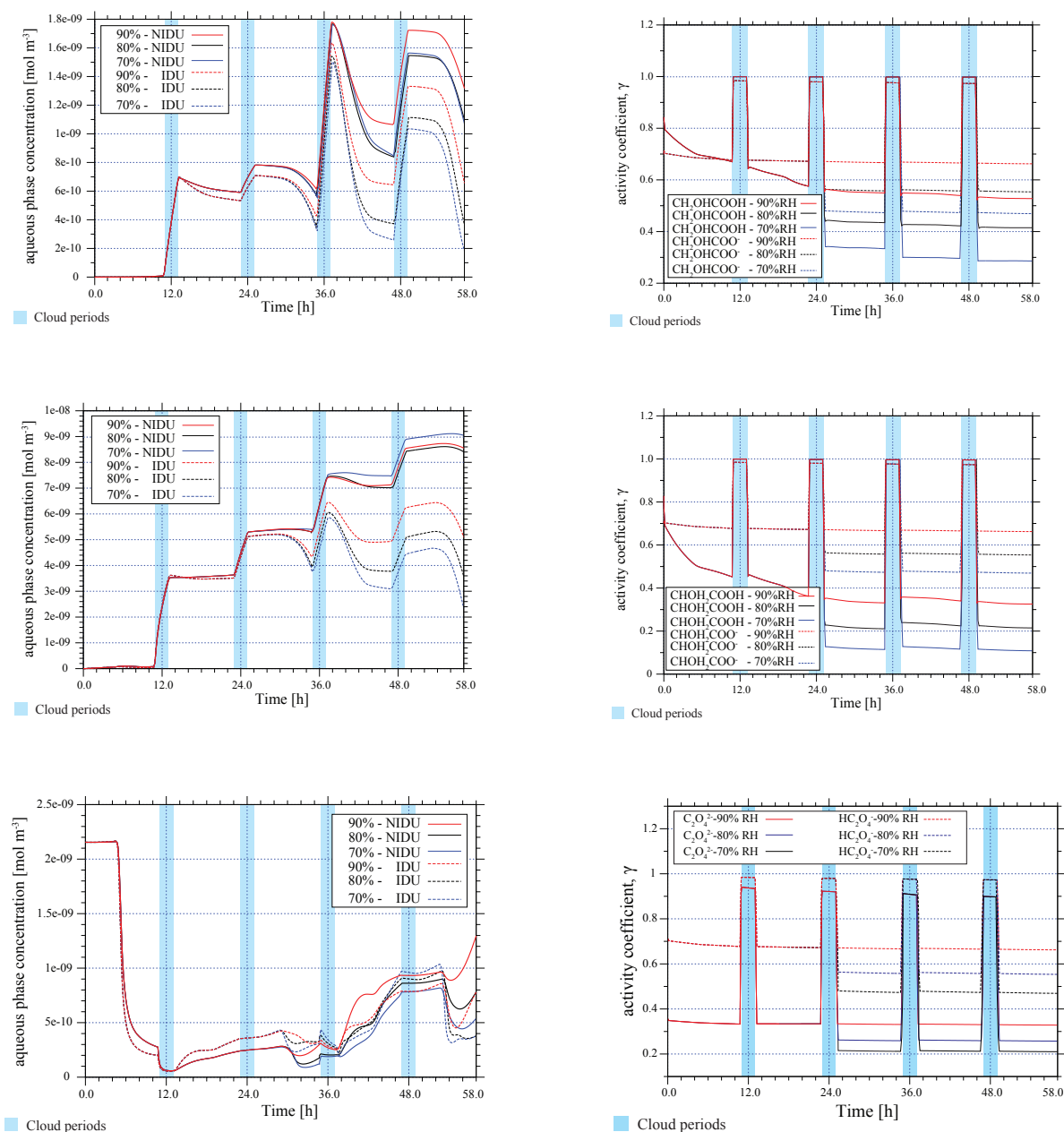


Figure 6.39: Modeled aqueous phase $\text{mol m}^{-3}_{(\text{air})}$ and corresponding activity coefficients for the most important C_2 oxidation products at three different relative humidity levels, Glycolic acid (top), glyoxylic acid (center) and Oxalic acid (bottom).

considering the aqueous phase chemistry as non-ideal and ideal solutions). The differences in the production of glyoxylic acid between the 90%-NIDU to 70%-NIDU is same during the night time cloud periods. Whereas, small differences are observed for the simulations 90%-IDU to 70%-IDU, are mainly due to the domination of microphysical differences and chemistry effects. However, in the night time clouds the differences between the concentrations are increasing while decreasing the relative humidity. Even, the differences are noteworthy, between 90%-IDU to 70%-IDU. This deviation is decreasing with decreasing of relative humidity. However, due to the

non-linear coupling between microphysics and multiphase chemistry and the impact from the activity coefficients the differences between the 90%-NIDU to 70%-NIDU are small. Due to the activity coefficient values, which are less than unity for both dissociated and undissociated forms, the oxidation is proceeds longer (since the glycolic acid activity coefficients are less than unity, which contributes in the formations of glyoxylic acid) for the simulations when aqueous phase chemistry was assumed as non-ideal solutions compare with ideal solutions (see Fig. 6.39 for the activity coefficients of glyoxylic acid).

For instance, the reaction of glycolic acid reacts with OH radical to produce glyoxylic acid. However, as shown in Fig. 6.39, the activity coefficients of the glycolic acid and glyoxylic acid are still decreasing with decreasing the relative humidity, with the same percentage range. Although, the activity coefficients are decreasing with decreasing the relative humidity, the aqueous phase concentrations are observed as nearly same in the aqueous particles. It should be noted that, the reaction pathways (see Table. C.5 for the simulation 90%-NIDU) might have substantial contribution, while acting as sources and sinks for the glyoxylic acid. Due to the change in the relative humidity, the microphysics (LWC, soluble and total mass) is more dominating than the multiphase chemistry during the simulations performed while considering the aqueous phase chemistry as ideal solutions. Whereas the combined consideration of microphysics (LWC and water activity) and multiphase chemistry along with incorporation of the treatment of non-ideality leads to small changes in the aqueous phase concentrations for the glyoxylic acid for the simulations 90%-NIDU to 70%-NIDU. Interestingly, the oxidation is reduced due to the calculated activity coefficient, which is less than unity.

As described earlier, the in-cloud oxidations of volatile C₂ organic compounds such as glycolaldehyde and glyoxal lead to the formation of oxalic acid which is the most abundant diacid and important organic component of the organic particulate mater. Furthermore, as discussed in Sec. 6.2.8.1, the production or formation of oxalic acid takes place preferably in the aqueous phase of deliquescent particles. As shown in Fig. 6.39, the aqueous phase concentrations of oxalic acid are decreased while decreasing the relative humidity, in other words the turnovers are decreased if the particles become more concentrated. The activity coefficients for the C₂O₄²⁻, HC₂O₄⁻, H₂C₂O₄, Fe(C₂O₄)₂⁻, Fe(C₂O₄)⁺ and Fe(C₂O₄)₃³⁻ also influence on turnovers of the oxalic acid. As shown in Fig. 6.30, the activity coefficients of the ions as well as the undissociated form of oxalic acid, are found to be less than unity. Hence, the total mass fluxes are reduced while employing the treatment of non-ideality for the aqueous phase chemistry in comparison with ideal solutions. Similarly, as shown in Table. 6.8, the activity coefficients for the aforementioned ions and the undissociated form of oxalic acid including the iron oxalates, are reduced while decreasing the relative humidity. As a result, the total turnovers, for the oxalic acid can be reduced while decreasing the relative humidity. As depicted in Fig. 6.39, the aqueous phase concentrations are decreased initially and then effectively produced in the aqueous phase deliquescent particles. The aqueous phase concentration of oxalic acid is increasing until the end of simulation time in all the simulated cases while assuming the aqueous phase chemistry as ideal and non-ideal solutions, with varying the relative humidity. However, the production is reduced while decreasing the relative humidity. The pattern observed for these differences, are same for the simulations performed with and without treatment of non-ideality for the aqueous phase chemistry. The differences in the aqueous concentrations for the simulations performed at 90%-NIDR to 70%-NIDR are observed as declined (i.e. ΔC- 90% > ΔC- 80% > ΔC- 70%, where ΔC represents the differences between the concentrations, when the simulations performed, while considering the aqueous phase chemistry as non-ideal and ideal solutions). Moreover, the differences in the aqueous phase concentrations are noticeable while incorporating the treatment of non-ideality for the aqueous phase chemistry. The influence of treatment of non-ideality on the multiphase processing of

oxalic acid/oxalate plays a vital role. Due to the decrease in the activity coefficient of the oxalic acid/oxalate, the turnovers are expected to decrease, while decreasing the relative humidity. As tabulated in Table. 6.8, the activity coefficients for the oxalic acid and glyoxylic acid are still decreased while decreasing the relative humidity. Hence, the production fluxes can be expected as declined, when decreasing the relative humidity compare with the simulation performed at 90% relative humidity level, and also compared with the simulations performed while considering the aqueous phase chemistry as ideal and non-ideal solutions.

6.3.8 Summary: Influence of treatment of non-ideality on multiphase chemistry at different relative humidity levels

Sensitivity studies are performed with the parcel model SPACCIM for urban and remote environmental conditions while varying the relative humidity. The current results shown that the activity coefficients for the inorganic and organic ions are less than unity. The activity coefficients of alcohols, some of the aldehydes (acetaldehyde), substitute carbonyl compounds (glyoxal), dicarboxylic acids (malonic acid, succinic acid, malic acid) are obtained as greater than unity and these values are increased with decreasing the relative humidity. However, the observed differences are related to both microphysics and treatment of non-ideality for the aqueous phase chemistry. However, the computation of activity coefficients is strongly depend on the aqueous phase concentrations. Since, the intermolecular forces are high due to the available LWC, the ionic strength is found to be about 14.3 mol kg^{-1} . Due to the high ionic strength the particles becomes more concentrated, hence the activity coefficients are decreased.

The activity coefficients are observed for the inorganic ions in the range of 0.30 - 0.70 for the mono-ions, 0.10 - 0.25 for the double charged ions and 0.05 - 0.10 for the triple charged ions at 70% relative humidity for the urban and remote environmental conditions, respectively. Furthermore, the activity coefficients of inorganic ions are decreased about 15% - 20% with decreasing the relative humidity depends on the charge number. The obtained activity coefficient values for the organic compounds are depending the functional subgroups comprised in the corresponding species. Activity coefficients of organic ions also decreasing with decreasing the relative humidity. Some of the aldehydes, are observed as increasing in the activity coefficients while decreasing the relative humidity. Based on the obtained activity coefficient values at three different levels of relative humidities, the current results suggest that the processing of multiphase chemistry might be declined with decreasing the relative humidity, due to the incorporation of treatment of non-ideality. The particle pH becomes less acidic while decreasing the relative humidity. The multiphase processing of Fe(II) is also observed as declined while decreasing the relative humidity.

Performed comparisons, shown that lower aqueous phase concentrations are attained for the OH radical in the deliquescent particles. The aqueous phase concentrations of glycolic acid is also observed as declined while decreasing the relative humidity, since the corresponding activity coefficients of the dissociated and undissociated forms are found to be less than unity. Furthermore, due to this behavior of predicted activity coefficients, the oxidation is reduced and it proceeds longer in the deliquescent particles. The concentration profiles of glyoxylic acid, shows the increasing behavior with reducing the relative humidity.

Chapter 7

Summary and outlook

The complexity of organic fraction in the tropospheric aerosols requires the analysis of appropriate prognostic tools, in order to improve our current ability to model the tropospheric aerosols from different environments. The influence of organic or inorganic compounds on droplet growth and behavior is understood, but the deeper understanding on mixed organic/inorganic systems is limited. Thus, a detailed modeling framework is required in order to bridge the gap between the current understanding of multiphase multicomponent mass transfer under non-ideal conditions to the former studies performed with ideal conditions. Hence, accurate prediction of condensation rates during the droplet activation process including complex multiphase chemistry and non-ideal interactions are utmost essential to the successful formulation of this new model framework. Aiming to improve the understanding about the multiphase chemical processing of tropospheric aerosols, an extended description of treatment of non-ideality for the aqueous chemistry by means of activity coefficient models are implemented in the context of air parcel model SPACCIM. Precisely, the model framework was extended by functions and algorithms to calculate activity coefficients (e.g., UNIFAC, (Fredenslund et al., 1975), Pitzer model, (Pitzer, 1973), Ming and Russel (2002) and (Zuend et al., 2008)), surface tension (e.g., approaches given by Facchini et al. (1999) and Ervens et al. (2004)). The process studies were performed to clarify the influence of treatment of non-ideality on multiphase chemistry. Finally, these studies has provided the valuable insight of the processing cloud and deliquescent particles while incorporating the treatment for aqueous phase chemistry. For the model studies, a complex multiphase mechanism considering a complex multiphase mechanism RACM-MIM2ext/CAPRAM2.4+OrganicExt, which comprises a detailed inorganic and organic chemistry of tropospheric aerosols. In the following, the profound results from the activity coefficient model verification and extended model robustness will be presented. Later on, the influence of treatment of non-ideality on multiphase chemistry will be summarized.

Activity coefficient model extension and verification

Most of the published activity coefficient models are implemented for industrial processes, where organic solvents, which are not common for the atmospheric application. Nevertheless, these models doesn't hold the same accuracy to compute the activity coefficients, as seen here, when these models were compared with experimental data and compared with each other. Therefore, in Chapter.3, an extended description of robust method was presented, for calculating the activity coefficients in aqueous particles comprised of a multicomponent mixture of organic compounds, inorganic salts, and water. This extended model framework, is predictive, regarding the computation of activity coefficients at high ionic strength and holds the same accuracy as the original models. The model selection was based on the model deviations, in addition to the predictive capabilities, to compute the activity coefficients at high ionic strength, concentrations and at low water content available in the aqueous particles. This

thermodynamically consistent modeling framework enables the reliable computation of activity coefficients in binary, ternary and multicomponent organic-inorganic mixtures with a set of limitations. This extended description of group-contribution concept provides the capability for simulating multicomponent organic-inorganic mixtures, consisting of the functional groups and ions, commonly found in the atmosphere.

However, concerning the conceptual model uncertainties as well as the limited experimental data sets, it is clear that the extended AIOMFAC cannot predict the activity coefficients of multicomponent organic \leftrightarrow electrolyte mixtures, with same high level of accuracy as the Pitzer-like part of AIOMFAC (since most of the MR interaction parameters are assigned to zero) or other detailed thermodynamic models, such as the AIM model (Clegg et al., 1998a,b), as attained for aqueous electrolyte solutions (organic-free). However, important issues regarding limitations of database, uncertainties of experimental data, and extended model uncertainties along with sensitivities are discussed. Indeed, the activity coefficient predictions for complex multifunctional organic compounds are less accurate, because the group-contribution concept offers only very limited means to account for intramolecular interactions between neighboring functional groups - a liquid phase is basically treated as a solution of individual functional groups (solution-of-groups concept). However, structural complexity of individual organic compounds should not be confused with number of components in a mixture. Mixtures consisting of tens to many hundreds of compounds do not need to become less accurate with increasing number of components. In fact, the solution-of-groups concept implies that extended AIOMFAC results are unaffected by the number of different components a set of functional groups belongs to. Therefore, extended AIOMFAC is well suited for computations of activity coefficients in multicomponent organic/inorganic mixtures, such as atmospheric aerosol mixtures, expected to contain up to a few hundreds of different organic compounds exhibiting a wide spectrum in terms of molecular structure and polarity.

All in all, the current model results, indicate that the parameters fitted by various authors are strongly deviating with other. This is mainly because, the interaction parameters were fitted, considering the pure compound properties. Consideration of dissociation constants and dissociation equilibria can improve the accuracy to predict the activity coefficients in a multicomponent system. In order to treat organic compounds, non-electrolyte models such as UNIFAC are apparently suitable, without fitting of parameters and simply extending the parameters. The complexity, with the computation of activity coefficients for organic compounds, was observed as, it is greatly depends on the size and the functional groups. Hence, the accuracy of predicting the activity coefficients are decreased with increasing structural behavior of organic compounds. Furthermore, the prediction of activity coefficients for the complex multifunctional organic compounds don't get the same level of accuracy. This is mainly, due to the intermolecular forces between neighboring functional groups bonded with each other, since the aqueous phase solution is generally considered to be solution of individual groups. However, three types of contributions to activity coefficient computation were considered, for ion-organic-water mixtures. The current shown that, at moderate concentrations ($x_w = 0.4$) considered activity coefficient models gives relatively good results. Whereas, at low concentrations the accuracy of activity coefficient models differed with each other. Concerning the longstanding debate regarding the consideration of ion \leftrightarrow organic interactions, it was shown that these interactions are necessary to hold the accuracy of predicted activity coefficients. This robust module coupled with gas/particle partitioning of multicomponent tropospheric multiphase chemistry model SPACCIM.

Influence of treatment of non-ideality on multiphase chemistry

A robust and detailed model framework is developed and implemented in order to treat the aqueous phase chemistry as non-ideal solutions, in the context of multiphase model SPACCIM. This activity coefficient module is written to be easily specialized or extended to include new species e.g. non-electrolytes. Indeed, of the activity coefficient model and chemical reactions are read from input files. As a result, updates in interaction parameters, will be easily incorporated. Besides, the flexibility of the computer code will facilitate changes and future inclusions. The implemented model architecture uses a simple bisection approach to find a solution to the Köhler equation, which is included in the microphysics model, in which a variety of surface tension approaches and activity coefficient models can be employed easily. The implemented numerical schemes merely gives good computational efficiency. Due to the limitations regarding the lack of experimental data, and the ability to treat the organic-electrolyte mixtures of atmospheric relevance at various complexity, predictions are improved considerably while using extended interaction parameters.

Finally, simulations with the parcel model SPACCIM were performed for urban and remote environmental conditions, considering ideal and non-ideal solutions for the aqueous phase chemistry. The activity coefficients are computed, using the extended AIOMFAC model. The predicted activity coefficients of the mono charged ions (cations and anions) as well as the double charged ions for inorganics, behaves similarly due to the charge number utilized in the computation of ionic strength. Furthermore, the activity coefficients of inorganic ions are decreasing while increasing the charge number. All in all, the activity coefficients of inorganic ions are observed as less than unity ($\gamma < 1$). Ionic strength of the solution plays a substantial role in order to compute the activity coefficients. The accuracy of obtained activity coefficients varies with the composition of the solution. For the simple inorganic chemistry the prediction of activity coefficients is possible with high level of accuracy compare with the mixtures of organic/inorganic components. The partitioning of gas to liquid phases is not influenced due to the treatment of non-ideality. However, the observed influence is not eminent due to the aforementioned reasons (i.e. for moderate concentrated solutions and consideration of organic compounds). Moreover, equilibrium partial pressures of the inorganic gases HNO_3 , lead to be different for the non-ideal solutions compare with ideal solutions. Since, the influence of inorganic-electrolyte content on aerosol partitioning of the semi-volatile compounds is exerted mainly via available aerosol water content. The relation between water activity (in other words RH) and concentration of the mixture at moderate to high RH probably leading to the such deviations.

Similar to the inorganic ions, the activity coefficients of the organic ions also exhibits the same behavior and the activity coefficients are obtained as less than unity. However, the activity coefficients of organic compounds strongly depends on the composition of the corresponding species. Due to the non-linear change of activity coefficients in terms of the molality due to the different types of interactions in the solution, the activity coefficients doesn't change linearly. These determine the organic contribution to the total water content of the aerosol which is relatively small, the deviations from the ideality have small influences on the partitioning between aerosol and gas phases. In contrast to our predictions with extended AIOMFAC, the sensitivity studies with UNIFAC predicts $2 > \gamma_i \geq 1$ for the compounds incorporated in the multiphase chemistry mechanism. These results therefore suggest that the total interactions between these are currently not adequately represented as sums of parameterized binary interaction parameters between the functional groups of the molecules, in this case particularly $-\text{COOH}$ and $-\text{CH}_2$ groups. Moreover, the interactions between $\text{CHO} \leftrightarrow$ ions are considered as zero. Although it have significant impact, the resulting activity coefficients are less than unity. Further development of estimation methods that consider other interactions, for instance, binary, ternary interactions,

may be necessary to accurately represent interactions of organic \leftrightarrow inorganics, in the current available models. Moreover, it can be possible that the physical properties (for instance vapor pressure) of these more abundant, lower-molecular-weight components in organic/inorganic mixtures are apparently lower than those of the pure compounds, will thus lead to unexpected behavior (i.e., $\gamma < 1$).

The current simulations shown that the pH of the particles becomes more acidic, due to the treatment of non-ideality. The modeled average pH values of the deliquescent particles are around 1.2 and 1.4 (on the average over whole simulation period) in the urban and remote environmental conditions respectively, for the simulations performed when the aqueous phase chemistry is assumed as non-ideal solutions, whereas the average pH is about 1.0 and 1.2 for the ideal solutions. Due to the increase in the ionic strength of the solution, the activity coefficient of ions decreases, hence this has an effect of lowering the activity of hydrogen ion, which is seen as an decrease in pH (more acidic).

The multiphase processing of inorganic compounds are observed as declined, since the corresponding activity coefficients of ions are obtained as less than unity. During the Fe(II) processing, the Fenton reaction is decreased about 3% for the simulation performed, while assuming the non-ideal solutions in comparison with ideal solutions. Although, the aqueous phase concentrations are obtained higher, for the simulation considering the non-ideal solutions, the turnovers are observed as reduced. The current model studies have shown considerable effects of multiphase interactions becomes more important in the radical oxidation budget while treating the aqueous chemistry as non-ideal solutions. Furthermore, the multiphase processing of OH radical is observed as declined and the turnovers of the NO_3 radical is obtained as increasing in the deliquescent particles. The phase transfer of OH and NO_3 radicals are reduced about 0.8 % and 26 % in the deliquescent particles while employing the treatment of non-ideality for the aqueous phase chemistry. At the same time, the Fenton reaction is also decreased about 1.8%, to produce the OH radical for the simulation performed while assuming the aqueous phase chemistry as non-ideal solutions. All in all, the multiphase processing of the OH radical is decreased about 40 % in the deliquescent particles while incorporating the treatment of non-ideality. Similar to OH radical the aqueous phase concentrations are increased for the HO_2/O_2^- radical processing. Furthermore, the OH radical have a feedback on processing of HO_2/O_2^- . Although, the turnovers are decreased for the simulation performed while considering the aqueous phase chemistry as non-ideal solutions, the aqueous phase concentrations are observed as higher. The turnovers of NO_3 radical are increased in the particle phase. The interconversion reaction between NO_3 and Cl^- , acts as one of the source for NO_3 radical, and the contribution of this reaction is increased about 13.6% for the urban environmental conditions, while employing the treatment of non-ideality for the aqueous phase chemistry.

As mentioned earlier the multiphase processing of organic compounds strongly connected to the nature of the intermolecular forces between the compounds. The comprising functional subgroups have substantial contribution, in order to predict the activity coefficient of the corresponding organic compounds. The differences in the organic functional subgroups give the different values for the activity coefficients for the organic compounds. Although, the activity coefficients are obtained as less than unity for most of the C_2 organic compounds, the aqueous phase concentrations are observed as higher while incorporating the treatment of non-ideality. But, the turnovers are reduced, due to the treatment of non-ideality. Moreover, the dissociated and undissociated forms of organic acids, are observed as equally important in order to investigate the influence of treatment of non-ideality on multiphase chemistry. The production and losses are reduced for the oxalic acid in the urban environmental scenario is reduced about the factor of 2 due to the incorporation of treatment of non-ideality. Similarly, the reaction of glyoxylic acid

with OH radical is reduced about 6% due to the treatment of non-ideality. The gas to particle mass transfer doesn't seem to be affected by the treatment of non-ideality. However, the oxidation is observed as rather slow for the organic compounds due to the treatment of non-ideality.

Since the activity coefficients are obtained as less than unity, the backward reaction proceeds slowly compared with forward reaction in the equilibria. The rate coefficient is modified, depends on the activity coefficients of the corresponding species, hence the multiphase processing is observed as declined. The dissolved salts in the aqueous phase solution modify the intermolecular forces between electrolytes, organics and water. Hence, the corresponding activity coefficients of electrolytes and organics are observed as dissimilar. As a result, the multiphase processing of organic compounds is decreased. These results provide important modeling support for a conceptual framework in which activity coefficients of partitioned compounds may differ significantly from unity. This can occur in complex mixtures of similar compounds, and may therefore influence organic aerosol formation in the atmosphere.

The dissociation of organic acids in the aerosol aqueous phase can potentially affect both the total amount/mass of the compounds available in the aerosol phase, and also aerosol pH. The magnitude of this influence depends upon (i) the dissociation constants of the organic compounds; (ii) the activity coefficients calculated for, the undissociated organic acid molecule and organic acid anions, and (iii) the degree to which pH is controlled by the inorganic electrolytes present. For the current simulations, the RH does not exceed 90% and it is found that, the aerosol pH becomes more acidic for the simulation considering the non-ideality for the aqueous phase chemistry, comes from the inorganic fraction/components of the aerosol, in compare with ideal solutions. It seems likely that in these simulations the values of the activity coefficients will therefore vary little, and in such cases could be determined just once at the beginning of the simulation rather than multiple times during every gas/aerosol partitioning calculation. Finally, the current developed model framework can be applicable to the more realistic atmospheric processes for instance the current implemented activity coefficient module can integrate with regional and large atmospheric models.

Future directions

In the current model studies, liquid-liquid phase separations as well as the salt formation (crystallization) were not considered adequately. However, these separations can occur in mixtures of two or more immiscible or partially miscible components, and while decreasing the relative humidity. Furthermore, the non-ideal molecular interactions between the different mixture components can cause for phase separations. Hence, the molecules with dissimilar functional groups, coexisting in aqueous phases differ typically in the degree of solution as well as polarity of the corresponding components (permanent dipoles, ions vs. uncharged, non-polar species). Thus, such a realistic processes can be included in this modeling framework. Indeed, in order to investigate the influence of non-ideality on multiphase chemistry, the realistic spectral particle-droplet discretization should be considered. Furthermore, focusing on a more appropriate description of the phase transfer processes for different type of particles, consideration of surface processes (e.g., organic films) in multiphase particles are also equally important. Therefore, a kinetic compartment model approach should be realized, which allows the consideration of surface effects and transport processes inside of particles/drops by dividing a single particle/drop in several compartments similar to the two-layer approach of Pöschl et al. (2007). The influence of non-ideality in different compartments on chemistry as well as life cycles of species should be investigated. For that, a realistic surface chemistry is also needed to study these kind of influences.

Furthermore, the current implemented surface tension parameterizations into the SPACCIM's microphysics model, were developed based on the specific compounds available in the solution. The aforementioned parameterizations or mixing rules were implemented, based on the the semi-empirical Szyszkowski-Langmuir equation (Szyszkowski, 1908), which is used in various studies, for instance Facchini et al. (1999) and Ervens et al. (2004). One can derive, similar mixing rules for the robust multiphase mechanism like CAPRAM, while prescribing the water activity, and to fit the new parameterization, in order to obtain the reliable consideration of surface tension depression, from the water soluble organic compounds available in the mechanism. In this way the current model framework can be extended.

Bibliography

- Abdul-Razzak, H. and Ghan, S.: Parameterization of the influence of organic surfactants on aerosol activation, *J. Geophys. Res.-Atmos.*, 109, 2004.
- Abdul-Razzak, H. and Ghan, S.: Influence of slightly soluble organics on aerosol activation, *J. Geophys. Res.-Atmos.*, 110, 2005.
- Abrams, D. and Prausnitz, J.: Statistical thermodynamics of liquid mixtures: a new expression for the Gibbs energy of partly or completely miscible systems, *AIChE*, 21, 116–128, 1975.
- Achard, C., Dussap, C., and Gros, J.: Representation of vapour-liquid equilibria in water-alcohol-electrolyte mixtures with a modified UNIFAC-group-contribution method, *Fluid Phase Equilibria*, 98, 71–89, 1994.
- Adkins, C.: *Equilibrium Thermodynamics*, Cambridge University Press., 285 pp., 1983.
- Ansari, A. S. and Pandis, S. N.: Response of Inorganic PM to Precursor Concentrations, *Environ Sci. & Tech.*, 32, 2706–2714, 1998.
- Anttila, T. and Kerminen, V.: Influence of organic compounds on the cloud droplet activation: A model investigation considering the volatility, water solubility, and surface activity of organic matter, *J. Geophys. Res.-Atmos.*, 107, 2002.
- Antypov, D. and Holm, C.: Osmotic coefficient calculations for dilute solutions of short stiff-chain polyelectrolytes, *Macromolecules*, 40, 731–738, 2007.
- Atkins, P. and de Paula, J.: *Atkins' Physical Chemistry*, Oxford, 7 edn., 2002.
- Aznar, M. and Telles, A.: Prediction of electrolyte vapor-liquid equilibrium by UNIFAC-Dortmund, *Brazilian Journal of Chemical Engineering*, 18, 127 – 137, 2001.
- Bassett, M. and Seinfeld, J.: Atmospheric equilibrium model of sulfate and nitrate aerosols, *Atmos. Environ*, 17, 2237–2252, 1983.
- Bassett, M. and Seinfeld, J.: Atmospheric equilibrium model of sulfate and nitrate aerosols. 2. particle-size analysis, *Atmos. Environ.*, 18, 1163–1170, 1984.
- Binkowski, F. S. and Shankar, U.: The Regional Particulate Matter Model .1. Model description and preliminary results, *J. Geophys. Res. Atmos*, 100, 26 191–26 209, 1995.
- Bromley, L. A.: Thermodynamic properties of strong electrolytes in aqueous solutions, *AIChE Journal*, 19, 313–320, 1973.
- Capaldo, K. P., Pilinis, C., and Pandis, S. N.: A computationally efficient hybrid approach for dynamic gas/aerosol transfer in air quality models, *Atmos. Environ.*, 34, 3617 – 3627, 2000.
- Cappa, C. D., Lovejoy, E. R., and Ravishankara, A. R.: Evidence for liquid-like and nonideal behavior of a mixture of organic aerosol components, *Proc. Natl. Acad. Sci. U. S. A.*, 105, 18 687–18 691, 2008.

- Chameides, W. and Stelson, A.: Aqueous-Phase Chemical Processes in Deliquescent Sea-Salt Aerosols: A Mechanism That Couples the Atmospheric Cycles of S and Sea Salt, *J. Geophys. Res.-Atmos.*, 97, 20 565–20 580, 1992.
- Chang, E. I. and Pankow, J. F.: Prediction of activity coefficients in liquid aerosol particles containing organic compounds, dissolved inorganic salts, and water - Part 2: Consideration of phase separation effects by an X-UNIFAC model, *Atmos. Environ.*, 40, 6422–6436, 2006.
- Charlson, R., Schwartz, S., Hales, J., Cess, R., Coakley, J., Hansen, J., and Hofmann, D.: Climate forcing by anthropogenic aerosols, *Science*, 255, 423–430, 1992.
- Chiavone, O. and Rasmussen, P.: Modeling of salt solubilities in mixed solvents, *Brazilian Journal of Chemical Engineering*, 17, 117–131, 2000.
- Chuang, P., Charlson, R., and Seinfeld, J.: Kinetic limitations on droplet formation in clouds, *Nature*, 390, 594–596, 1997.
- Clegg, S. and Brimblecombe, P.: Application of a multicomponent thermodynamic model to activities and thermal properties of 0D40 mol kg⁻¹ aqueous sulfuric acid from 200 to 328 K, *J. Chem. Eng. Data*, 40, 43–64, 1995.
- Clegg, S. and Pitzer, K.: Thermodynamics of Multicomponent, Miscible, Ionic Solutions: Generalized Equations for Symmetrical Electrolytes, *J. Phys. Chem.*, 96, 3513–3520, 1992.
- Clegg, S., Pitzer, K., and Brimblecombe, P.: Thermodynamics of Multicomponent, Miscible, Ionic Solutions. II. Mixtures including Unsymmetrical Electrolytes, *J. Phys. Chem.*, 96, 9470–9479, 1992.
- Clegg, S., Brimblecombe, P., and Wexler, A.: Thermodynamic Model of the System H⁺ - NH₄⁺ - SO₄²⁻ - NO₃⁻ - H₂O at Tropospheric Temperatures, *J. Phys. Chem. A*, 102, 2137–2154, 1998a.
- Clegg, S., Brimblecombe, P., and Wexler, A.: A thermodynamic model of the system H⁺ - NH₄⁺ - Na⁺ - SO₄²⁻ - NO₃⁻ - Cl⁻ - H₂O at 298.15 K, *J. Phys. Chem. A*, 102, 2155–2171, 1998b.
- Clegg, S. L. and Seinfeld, J. H.: Thermodynamic Models of Aqueous Solutions Containing Inorganic Electrolytes and Dicarboxylic Acids at 298.15 K. 1. The Acids as Nondissociating Components, *The J. Phys. ChemA*, 110, 5692–5717, 2006a.
- Clegg, S. L. and Seinfeld, J. H.: Thermodynamic Models of Aqueous Solutions Containing Inorganic Electrolytes and Dicarboxylic Acids at 298.15 K. 2. Systems Including Dissociation Equilibria, *The J. Phys. ChemA*, 110, 5718–5734, 2006b.
- Clegg, S. L., Seinfeld, J. H., and Brimblecombe, P.: Thermodynamic modelling of aqueous aerosols containing electrolytes and dissolved organic compounds, *Journal of Aerosol Science*, 32, 713 – 738, 2001.
- Clegg, S. L., Kleeman, M. J., Griffin, R. J., and Seinfeld, J. H.: Effects of uncertainties in the thermodynamic properties of aerosol components in an air quality model - Part 1: Treatment of inorganic electrolytes and organic compounds in the condensed phase, *Atmos. Chem. Phys.*, 8, 1057–1085, 2008.
- Cruz, C. and Pandis, S.: Deliquescence and hygroscopic growth of mixed inorganic-organic atmospheric aerosol, *Environ. Sci. Tech.*, 34, 4313–4319, 2000.

- Dassios, K. G. and Pandis, S. N.: The mass accommodation coefficient of ammonium nitrate aerosol, *Atmos. Environ.*, 33, 2993 – 3003, 1999.
- Davidovits, P., Kolb, C., Williams, L., Jayne, J., and Worsnop, D.: Mass accommodation and chemical reactions at gas-liquid interfaces, *Chem. Rev.*, 106, 1323–1354, 2006.
- Debye, P. and Hückel, E.: Zur Theorie der Elektrolyte, *Physikalische Zeitschrift*, 24, 185–206, 1923.
- Decesari, S., Facchini, M., Fuzzi, S., and Tagliavini, E.: Characterization of water-soluble organic compounds in atmospheric aerosol: A new approach, *J. Geophys. Res.-Atmos.*, 105, 1481–1489, 2000.
- Decesari, S., Fuzzi, S., Facchini, M., Mircea, M., Emblico, L., Cavalli, F., Maenhaut, W., Chi, X., Schkolnik, G., Falkovich, A., Rudich, Y., Claeys, M., Pashynska, V., Vas, G., Kourtschev, I., Vermeylen, R., Hoffer, A., Andreae, M., Tagliavini, E., Moretti, F., and Artaxo, P.: Characterization of the organic composition of aerosols from Rondonia, Brazil, during the LBA-SMOCC 2002 experiment and its representation through model compounds, *Atmos. Chem. Phys.*, 6, 375–402, 2006.
- Deguillaume, L., Leriche, M., Desboeufs, K., Mailhot, G., George, C., and Chaumerliac, N.: Transition metals in atmospheric liquid phases: Sources, reactivity, and sensitive parameters, *Chem. Rev.*, 105, 3388–3431, 2005.
- Deguillaume, L., Tilgner, A., Schroedner, R., Wolke, R., Chaumerliac, N., and Herrmann, H.: Towards an operational aqueous phase chemistry mechanism for regional chemistry-transport models: CAPRAM-RED and its application to the COSMO-MUSCAT model, *J. Atmos. Chem.*, 64, 1–35, 2009.
- Demaret, J. and Gueron, M.: Composite cylinder models of DNA - Application of the electrostatics of the B-Z transition, *Biophys. J.*, 65, 1700–1713, 1993.
- Erdakos, G. and Pankow, J.: Gas/particle partitioning of neutral and ionizing compounds to single- and multi-phase aerosol particles. 2. Phase separation in liquid particulate matter containing both polar and low-polarity organic compounds, *Atmos. Environ.*, 38, 1005–1013, 2004.
- Ervens, B., George, C., Williams, J., Buxton, G., Salmon, G., Bydder, M., Wilkinson, F., Dentener, F., Mirabel, P., Wolke, R., and Herrmann, H.: CAPRAM 2.4 (MODAC mechanism): An extended and condensed tropospheric aqueous phase mechanism and its application, *J. Geophys. Res.-Atmos.*, 108, 2003.
- Ervens, B., Feingold, G., Clegg, S., and Kreidenweis, S.: A modeling study of aqueous production of dicarboxylic acids: 2. Implications for cloud microphysics, *J. Geophys. Res. Atmos.*, 109, 2004.
- Ervens, B., Feingold, G., and Kreidenweis, S.: Influence of water-soluble organic carbon on cloud drop number concentration, *J. Geophys. Res.-Atmos.*, 110, 2005.
- Facchini, M., Mircea, M., Fuzzi, S., and Charlson, R.: Cloud albedo enhancement by surface-active organic solutes in growing droplets, *Nature*, 401, 257–259, 1999.
- Facchini, M., Mircea, M., Fuzzi, S., and Charlson, R.: Cloud albedo enhancement by surface-active organic solutes in growing droplets, *NATURE*, 401, 257–259, 1999.

- Feingold, G. and Chuang, P. Y.: Analysis of the Influence of Film-Forming Compounds on Droplet Growth: Implications for Cloud Microphysical Processes and Climate, *J. Atmos. Sci.*, 59, 2006–2018, 2002.
- Fowler, R. H. and Guggenheim, E. A.: *Statistical Thermodynamics: A Version of Statistical Mechanics for Students of Physics and Chemistry.*, Cambridge, England: University Press, 1949.
- Franks, F.: *Water - A Comprehensive Treatise*, , vol. 2, Plenum Press, New York, 1973.
- Fredenslund, A., Jones, R., and Prausnitz, J.: Group-contribution estimation of activity coefficients in non-ideal liquid mixtures, *AIChE J.*, 21, 1086–1098, 1975.
- Fridlind, A. and Jacobson, M.: A study of gas-aerosol equilibrium and aerosol pH in the remote marine boundary layer during the First Aerosol Characterization Experiment (ACE 1), *J. Geophys. Res.-Atmos.*, 105, 17 325–17 340, 2000.
- Friedlander, S.: *Smoke, dust, and haze: fundamentals of aerosol behavior*, *Topicals in chemical engineering*, John Wiley & Sons, New York, 1977.
- Fukuta, N. and Walter, L.: Kinetics of hydrometeor growth from a vapor-spherical model, *J. Atmos. Sci.*, 27, 1160–1172, 1970.
- Gibbs, J.: *The Collected Works of J. Willard Gibbs Vol I*, New York: Longmans, Green and Co., 1928.
- Gilardoni, S., Liu, S., Takahama, S., Russell, L. M., Allan, J. D., Steinbrecher, R., Jimenez, J. L., De Carlo, P. F., Dunlea, E. J., and Baumgardner, D.: Characterization of organic ambient aerosol during MIRAGE 2006 on three platforms, *Atmos. Chem. Phys.*, 9, 5417–5432, 2009.
- Giralt, F., Espinosa, G., Arenas, A., Ferre-Gine, J., Amat, L., Girones, X., Carbo-Dorca, R., and Cohen, Y.: Estimation of infinite dilution activity coefficients of organic compounds in water with neural classifiers, *AIChE J.*, 50, 1315–1343, 2004.
- Gmehling, J.: Present status and potential of group contribution methods for process development, *J. Chem. Thermodyn.*, 41, 731–747, 2009.
- Gregoire, P., Chaumerliac, N., and Nickerson, E.: Impact of cloud dynamics on tropospheric chemistry- Advances in modeling the interactions between microphysical and chemical processes, *J. Atmos. Chem.*, 18, 247–266, 1994.
- Gros, J. and Dussap, C.: Estimation of equilibrium properties in formulation or processing of liquid foods, *Food Chem.*, 82, 41–49, 2003.
- Ha, Z., Choy, L., and Chan, C.: Study of water activities of supersaturated aerosols of sodium and ammonium salts, *J. Geophys. Res.-Atmos.*, 105, 11 699–11 709, 2000.
- Hairer, E., Nørsett, S., and Wanner, G.: *Solving Ordinary Differential Equations: Stiff and differential-algebraic problems*, Springer series in computational mathematics, Springer-Verlag, 1993.
- Hamer, W. J. and Wu, Y.-C.: Osmotic Coefficients and Mean Activity Coefficients of Uni-univalent Electrolytes in Water at 25[degree]C, *Journal of Physical and Chemical Reference Data*, 1, 1047–1100, 1972.

- Hämeri, K., Charlson, R., and Hansson, H.-C.: Hygroscopic properties of mixed ammonium sulfate and carboxylic acids particles, *AIChE Journal*, 48, 1309–1316, 2002.
- Hansen, H., Rasmussen, P., Fredenslung, A., Schiller, M., and Gmehling, J.: Vapor-liquid equilibria by UNIFAC group contribution. 5. Revision and extension., *Ind. Eng. Chem. Res.*, 30, 2352–2355, 1991.
- Hanson, D. and Ravishankara, A.: Uptake of HCl and HOCl onto sulfuric acid: Solubilities, diffusivities, and reaction, *J. Phys. Chem.*, 97, 12 309–12 319, 1993.
- Hudischewskyj, A. B. and Seigneur, C.: Mathematical modeling of the chemistry and physics of aerosols in plumes, *Environ Sci. & Tech.*, 23, 413–421, 1989.
- Iliuta, M., Thomson, K., and Rasmussen, P.: Extended UNIQUAC model for correlation and prediction of vapour-liquid-solid equilibria in aqueous salt systems containing non-electrolytes. Part A. Methanol-water-salt systems, *Chem. Eng. Sci.*, 55, 2673–2686, 2000.
- IPCC: Climate Change 2007, Tech. rep., Cambridge University Press., 2007.
- Jacobson, M.: Fundamentals of atmospheric modeling, Cambridge University Press, 1999.
- Jacobson, M. Z.: Development and application of a new air pollution modeling system .Part II. Aerosol module structure and design , *Atmos. Environ.*, 31, 131–144, 1997a.
- Jacobson, M. Z.: Development and application of a new air pollution modeling system .Part III. Aerosol-phase simulations , *Atmos. Environ.*, 31, 587–608, 1997b.
- Jacobson, M. Z., Tabazadeh, A., and Turco, R. P.: Simulating equilibrium within aerosols and nonequilibrium between gases and aerosols, *J. Geophys. Res.*, 101(D4), 9071 – 9091, 1996.
- Jang, M., Kamens, R., Leach, K., and Strommen, M.: A thermodynamic approach using group contribution methods to model the partitioning of semivolatile organic compounds on atmospheric particulate matter, *Environ. Sci. Technol.*, 31, 2805–2811, 1997.
- Karl, M., Dorn, H. P., Holland, F., Koppmann, R., Poppe, D., Rupp, L., Schaub, A., and Wahner, A.: Product study of the reaction of OH radicals with isoprene in the atmosphere simulation chamber SAPHIR, *J. Atmos. Chem.*, 55, 167–187, 2006.
- Kiepe, J., Noll, O., and Gmehling, J.: Modified LIQUAC and Modified LIFACA Further Development of Electrolyte Models for the Reliable Prediction of Phase Equilibria with Strong Electrolytes, *Ind. Eng. Chem. Res.*, 45, 2361–2373, 2006.
- Kikic, I., Fermeglia, M., and Rasmussen, P.: Unifac prediction of vapor-liquid equilibria in mixed solvent-salt systems, *Chem. Eng. Sci.*, 46, 2775 – 2780, 1991.
- Kim, Y. P., Seinfeld, J. H., and Saxena, P.: Atmospheric Gas-Aerosol Equilibrium I. Thermodynamic Model, *Aerosol Sci. Technol.*, 19, 157 – 181, 1993.
- Kiriukhin, M. and Collins, K.: Dynamic hydration numbers for biologically important ions, *Biophys. Chem.*, 99, 155–168, 2002.
- Kleeman, M., Cass, G., and Eldering, A.: Modeling the airborne particle complex as a source-oriented external mixture, *J. Geophys. Res. Atmos*, 102, 21 355–21 372, 1997.
- Knopf, D., Luo, B., Krieger, U., and Koop, T.: Thermodynamic dissociation constant of the bisulfate ion from Raman and ion interaction modeling studies of aqueous sulfuric acid at low temperatures, *J. Phys. Chem. A*, 107, 4322–4332, 2003.

- Köhler, H.: The nucleus in and the growth of hygroscopic droplets, *Trans. Faraday Soc.*, 32, 1152–1161, 1936.
- Kokkola, H., Romakkaniemi, S., Kulmala, M., and Laaksonen, A.: A cloud microphysics model including trace gas condensation and sulfate chemistry, *Boreal Env. Res.*, 8, 413–424, 2003.
- Krishna, R. and Wesselingh, J.: The Maxwell-Stefan approach to mass transfer, *Chem. Eng. Sci.*, 52, 861–911, 1997.
- Kulmala, M., Laaksonen, A., Carlson, R. J., and Korhonen, P.: Clouds without supersaturation, *Nature*, 388, 336–337, 1997.
- Kusik, C. and Meissner, H.: Electrolyte activity coefficients in inorganic processing, *AIChE Symp. Series*, 4, 14–20, 1978.
- Lewis, G.: *Outlines of a New System of Thermodynamic Chemistry*, *Proceedings of the American Academy of Arts and Sciences*, 43(7), 259–293, 1907.
- Lewis, G. N. and Randall, M.: *Thermodynamics*, McGraw-Hill Book Co., New York, USA, 2nd edn., 285 pp., 1961.
- Li, J., Polka, H., and Gmehling, J.: A G^E model for single and mixed solvent electrolyte systems .1 . Model and results for strong electrolytes, *Fluid Phase Equilibria*, 94, 89–114, 1994.
- Lohmann, U. and Feichter, J.: Global indirect aerosol effects: A review, *Atm. Chem. Phys.*, 5, 715–737, 2005.
- Lurmann, F. W., Wexler, A. S., Pandis, S. N., Musarra, S., Kumar, N., and Seinfeld, J. H.: Modelling urban and regional aerosols—II. Application to California’s South Coast Air Basin, *Atmos. Environ.*, 31, 2695 – 2715, 1997.
- Maffia, M. C. and Meirelles, A. J. A.: Water Activity and pH in Aqueous Polycarboxylic Acid Systems, *Journal of Chemical & Engineering Data*, 46, 582–587, 2001.
- Marcolli, C. and Peter, T.: Water activity in Polyol/water systems: new UNIFAC parametrization, *Atmos. Chem. Phys.*, 5, 1545–1555, 2005.
- Margules, M.: Über die Zusammensetzung der gesättigten dämpfe von Mischungen, *Sitz. Akad. Wiss. Vienna*, 104, 1293, 1895.
- Maria, S., Russell, L., Turpin, B., Porcja, R., Campos, T., Weber, R., and Huebert, B.: Source signatures of carbon monoxide and organic functional groups in Asian Pacific Regional Aerosol Characterization Experiment (ACE-Asia) submicron aerosol types, *J. Geophys. Res.-Atmos.*, 108, 2003.
- McQuarrie, D. and Simon, J.: *Physical Chemistry: A Molecular Approach*, University Science Books, Sausalito, CA, USA, 1360 pp., 1997.
- Meng, Z. and Seinfeld, J.: Time scales to achieve atmospheric gas-aerosol equilibrium for volatile species, *Atmos. Environ.*, 30, 2889–2900, 1996.
- Meng, Z., Dabdub, D., and Seinfeld, J.: Size-resolved and chemically resolved model of atmospheric aerosol dynamics, *J. Geophys. Res. Atmos.*, 103, 3419–3435, 1998.
- Metzger, S.: *Gas/aerosol partitioning: a simplified method for global modelling*, Ph.D. thesis, University Utrecht, Netherlands, 2000.

- Ming, Y. and Russel, L.: Thermodynamic equilibrium of organic-electrolyte mixtures in aerosol particles, *AIChE*, 48, 1331–1348, 2002.
- Moya, M., Pandis, S. N., and Jacobson, M. Z.: Is the size distribution of urban aerosols determined by thermodynamic equilibrium?: An application to Southern California, *Atmos. Environ.*, 36, 2349 – 2365, 2002.
- Mukherji, S., Peters, C., and Weber, W.: Mass transfer of polynuclear aromatic hydrocarbons from complex DNAPL mixtures, *Environ. Sci. Technol.*, 31, 416–423, 1997.
- Myhre, G., Stordal, F., Berglen, T., Sundet, J., and Isaksen, I.: Uncertainties in the radiative forcing due to sulfate aerosols, *J. Atmos. Sci.*, 61, 485–498, 2004.
- Nenes, A., Pandis, S. N., and Pilinis, C.: ISORROPIA: A New Thermodynamic Equilibrium Model for Multiphase Multicomponent Inorganic Aerosols, *Aquatic Geochemistry*, 4, 123–152, 1998.
- Nenes, A., Pandis, S. N., and Pilinis, C.: Continued development and testing of a new thermodynamic aerosol module for urban and regional air quality models, *Atmos. Environ.*, 33, 1553 – 1560, 1999.
- Nenes, A., Ghan, S., Abdul-Razzak, H., Chuang, P., and Seinfeld, J.: Kinetic limitations on cloud droplet formation and impact on cloud albedo, *Tellus Ser. B*, 53, 133–149, 2001.
- Peng, C., Chan, M., and Chan, C.: The hygroscopic properties of dicarboxylic and multifunctional acids: Measurements and UNIFAC predictions, *Env. Sci. Technol.*, 35, 4495–4501, 2001.
- Pilinis, C.: Modeling atmospheric aerosols using thermodynamic arguments - A Review, *Global Nest: The International Journal*, 1, 5–13, 1999.
- Pilinis, C. and Seinfeld, J. H.: Continued development of a general equilibrium model for inorganic multicomponent atmospheric aerosols, *Atmos. Environ.* (1967), 21, 2453 – 2466, 1987.
- Pilinis, C., Capaldo, K. P., Nenes, A., and Pandis, S. N.: MADM-A New Multicomponent Aerosol Dynamics Model, *Aerosol Sci. Technol.*, 32, 482–502, 2000.
- Pitzer, K.: Thermodynamics of Electrolytes I: Theoretical Basis and General Equations, *J. Phys. Chem.*, 77, 268–277, 1973.
- Pitzer, K.: Activity coefficients in electrolyte solutions, 2 edn, CRC Press, 1991.
- Pitzer, K. and Mayorga, G.: Thermodynamics of Electrolytes II. Activity and Osmotic Coefficients for Strong Electrolytes with One or Both Ions Univalent, *J. Phys. Chem.*, 77, 19, 1973.
- Pöschl, U.: Atmospheric aerosols: Composition, transformation, climate and health effects, *Angew. Chem.-Int. Edit.*, 44, 7520–7540, 2005.
- Pöschl, U., Rudich, Y., and Ammann, M.: Kinetic model framework for aerosol and cloud surface chemistry and gas-particle interactions - Part 1: General equations, parameters, and terminology, *Atmos. Chem. and Phys.*, 7, 5989–6023, doi:10.5194/acp-7-5989-2007, 2007.
- Prausnitz, J. M., Lichtenthaler, R. N., and De Azevedo, E. G.: *Molecular Thermodynamics of Fluid-Phase Equilibria*, Prentice-Hall Inc., Englewood Cliffs, New Jersey, USA, 2nd edn., 1986.
- Prausnitz, J. M., Lichtenthaler, R. N., and De Azevedo, E. G.: *Molecular Thermodynamics of Fluid-Phase Equilibria*, Prentice-Hall Inc., Englewood Cliffs, New Jersey, USA, 3rd edn., 1999.

- Prenni, A., De Mott, P., and Kreidenweis, S.: Water uptake of internally mixed particles containing ammonium sulfate and dicarboxylic acids, *Atmos. Environ.*, 37, 4243–4251, 2003.
- Pruppacher, H. and Jaenicke, R.: The processing of water-vapor and aerosols by atmospheric clouds, A global estimate, *Atmos. Res.*, 38, 283–295, 1995.
- Pruppacher, H. R. and Klett, J. D.: *Microphysics of Clouds and Precipitation*, Dordrecht, The Netherlands, Kluwer Academic Publishers, 1997.
- Raatikainen, T. and Laaksonen, A.: Application of several activity coefficient models to water-organic-electrolyte aerosols of atmospheric interest, *Atmospheric Chemistry and Physics Discussions*, 5, 3641–3699, 2005.
- Redlich, O. and Kister, A.: Algebraic representation of thermodynamic properties and the classification of solutions, *Ind. Eng. Chem.*, 40, 345–348, 1948.
- Rogers, R. and Yau, M.: *A short course in cloud physics*, International series in natural philosophy, Pergamon Press, 1989.
- Russell, L. M., Takahama, S., Liu, S., Hawkins, L. N., Covert, D. S., Quinn, P. K., and Bates, T. S.: Oxygenated fraction and mass of organic aerosol from direct emission and atmospheric processing measured on the R/V Ronald Brown during TEXAQS/GoMACCS 2006, *J. Geophys. Res.-Atmos.*, 114, 2009.
- Saxena, P. and Hildemann, L.: Water-soluble organics in atmospheric particles: a critical review of the literature and application of thermodynamics to identify candidate compounds, *J. Phys. Chem.*, 24, 57–109, 1996.
- Saxena, P., Hudischewskyj, A. B., Seigneur, C., and Seinfeld, J. H.: A comparative study of equilibrium approaches to the chemical characterization of secondary aerosols, *Atmos. Environ.* (1967), 20, 1471 – 1483, 1986.
- Schwartz, S. and Freiberg, J.: Mass-transport limitation to the rate of reaction of gases in liquid droplets: Application to oxidation of SO₂ in aqueous solutions, *Atmos. Environ.*, 15, 1129–1144, 1981.
- Schwartz, S. E.: Mass transport considerations pertinent to aqueous phase reactions of gases in liquid water clouds, *Chemistry of Multiphase Atmospheric Systems*, NATO ASI Series, vol. G6. Springer, Berlin, p. 415–471, 1986.
- Sehili, A., Wolke, R., Knoth, O., Simmel, M., Tilgner, A., and Herrmann, H.: Comparison of different model approaches for the simulation of multiphase processes, *Atmos. Environ.*, 39, 4403–4417, 2005.
- Seigneur, C., Wu, X., Constantinou, E., Gillespie, P., Bergstrom, R., Sykes, I., Venkatram, A., and Karamchandani, P.: Formulation of a second-generation reactive flume and visibility model, *J. Air Waste Manage. Assoc.*, 47, 176–184, 1997.
- Seinfeld, J. H. and Pandis, S. N.: *Atmospheric Chemistry and Physics- From Air Pollution to Climate Change*, John Wiley & Sons, Inc., New York, USA, 285 pp., 1998.
- Seinfeld, J. H. and Pandis, S. N.: *Atmospheric Chemistry and Physics- From Air Pollution to Climate Change*, 2 edition, John Wiley & Sons, Inc., New York, USA, 1232 pp., 2006.

- Shi, Q., Li, Y. Q., Davidovits, P., Jayne, J. T., Worsnop, D. R., Mozurkewich, M., and Kolb, C. E.: Isotope Exchange for Gas-Phase Acetic Acid and Ethanol at Aqueous Interfaces: A Study of Surface Reactions, *The Journal of Physical Chemistry B*, 103, 2417–2430, 1999.
- Shulman, M. L., Jacobson, M. C., Carlson, R. J., Synovec, R. E., and Young, T. E.: Dissolution behavior and surface tension effects of organic compounds in nucleating cloud droplets, *Geophys. Res. Lett.*, 23, 1996.
- Simmel, M. and Wurzler, S.: Condensation and activation in sectional cloud microphysical models, *Atmos. Environ.*, 80, 218–236, 2006.
- Simmel, M., Trautmann, T., and Tetzlaff, G.: Numerical solution of the stochastic collection equation - comparison of the Linear Discrete Method with other methods, *Atmos. Environ.*, 61, 135–148, 2002.
- Simmel, M., Diehl, K., and Wurzler, S.: Numerical simulation of the microphysics of an orographic cloud: Comparison with measurements and sensitivity studies, *Atmos. Environ.*, 39, 4365–4373, 2005.
- Smith, J. M., Ness, V., and Abbott, M. M.: *Introduction to Chemical Engineering Thermodynamics*. 5, ed, McGraw-Hill, 1996.
- Solomon, S., Qin, D., Manning, M., Alley, R. B., Berntsen, T., Bindo, N. L., Chen, Z., Chidthaisong, A., Gregory, J. M., Hegerl, G. C., Heimann, M., Hewitson, B., Hoskins, B. J., Joos, F., Jouzel, J., Kattsov, V., Lohmann, U., Matsuno, T., Molina, M., Nicholls, N., Overpeck, J., Raga, G., Ramaswamy, V., Ren, J., Rusticucci, M., Somerville, R., Stocker, T. F., Whetton, P., Wood, R. A., and Wratt, D.: Technical Summary. In: *Climate Change 2007: The Physical Science Basis. Contribution of Working Group I to the Fourth Assessment Report of the Intergovernmental Panel on Climate Change*, Tech. rep., Cambridge, United Kingdom and New York, NY, USA., 2007.
- Stockwell, W., Kirchner, F., Kuhn, M., and Seefeld, S.: A new mechanism for regional atmospheric chemistry modeling, *J. Geophys. Res.-Atmos.*, 102, 25 847–25 879, 1997.
- Stokes, R. H.: A thermodynamic study of bivalent metal halides in aqueous solution. Part XVII—revision of data for all 2 : 1 and 1 : 2 electrolytes at 25°, and discussion of results, *Trans. Faraday Soc.*, 44, 295–307, 1948.
- Stumm, W. and Morgan, J.: *Aquatic chemistry: chemical equilibria and rates in natural waters*, Environmental science and technology, John Wiley & Sons, Inc., New York, USA, 1996.
- Sun, Q. and Wexler, A.: Modeling urban and regional aerosols - Condensation and evaporation near acid neutrality, *Atmos. Environ.*, 32, 3527–3531, 1998a.
- Sun, Q. and Wexler, A.: Modeling urban and regional aerosols near acid neutrality - Application to the 24-25 June SCAQS episode, *Atmos. Environ.*, 32, 3533–3545, 1998b.
- Suryanarayana, A.: *Mass Transfer Operations*, New Age International (P) Ltd., Publishers, 2002.
- Szyszkowski, B.: Experimental studies on capillary properties of aqueous solutions of fatty acids, *Z. Phys. Chem.*, 64, 385–414, 1908.
- Tester, J. and Modell, M.: *Thermodynamics and Its Applications*, 3rd ed., Prentice Hall, 936 pp., 1997.

- Thomsen, K., Iliuta, M., and Rasmussen, P.: Extended UNIQUAC model for correlation and prediction of vapor-liquid-liquid-solid equilibria in aqueous salt systems containing non-electrolytes. Part B. Alcohol (ethanol, propanols, butanols)-water-salt systems, *Chem. Eng. Sci.*, 59, 3631–3647, 2004.
- Thomson, K.: Aqueous electrolytes: model parameters and process simulation, Ph.D. thesis, Technical University of Denmark, Lyngby, Denmark, 1997.
- Tilgner, A.: Modeling of physico-chemical multiphase processing of tropospheric aerosols, PhD dissertation, University of Leipzig, Leipzig, Germany, 2009.
- Tilgner, A. and Herrmann, H.: Radical-driven carbonyl-to-acid conversion and acid degradation in tropospheric aqueous systems studied by CAPRAM, *Atmos. Environ.*, 44, 5415 – 5422, 2010.
- Tong, C., Clegg, S. L., and Seinfeld, J. H.: Comparison of activity coefficient models for atmospheric aerosols containing mixtures of electrolytes, organics, and water, *Atmos. Environ.*, 42, 5459–5482, 2008.
- Topping, D., McFiggans, G., and Coe, H.: A curved multi-component aerosol hygroscopicity model framework: Part 1 - Inorganic compounds, *Atmos. Chem. Phys.*, 5, 1205–1222, 2005a.
- Topping, D., McFiggans, G., and Coe, H.: A curved multi-component aerosol hygroscopicity model framework: Part 2 - Including organic compounds, *Atmos. Chem. Phys.*, 5, 1223–1242, 2005b.
- Treybal, R.: Mass-transfer operations, McGraw-Hill chemical engineering series, McGraw-Hill, 1980.
- Van Laar, J.: The vapor pressure of binary mixtures, *J. Phys. Chem.*, 72, 723–751, 1910.
- Vaslow, G.: Water and Aqueous Solutions; Structure, Thermodynamics, and Transport Processes, John Wiley & Sons, Inc., New York, USA, 1972.
- von Glasow, R. and Sander, R.: Variation of sea salt aerosol pH with relative humidity, *Geophys. Res. Lett.*, 28, 247–250, 2001.
- Voutsas, E. and Tassios, D.: Prediction of infinite-dilution activity coefficients in binary mixtures with UNIFAC. A critical evaluation, *Ind. Eng. Chem. Res.*, 35, 1438–1445, 1996.
- Wexler, A. S. and Seinfeld, J. H.: The distribution of ammonium salts among a size and composition dispersed aerosol, *Atmos. Environ.* Part A. General Topics, 24, 1231 – 1246, 1990.
- Wilson, G.: Vapour-liquid equilibrium. XI. A new expression for the excess free energy of mixing., *J. Am. Chem. Soc.*, 86, 127–130, 1964.
- Wolke, R. and Knuth, O.: Time-integration of multiphase chemistry in size-resolved cloud models, *Appl. Numer. Math.*, 42, 473–487, 2002.
- Wolke, R., Sehili, A., Simmel, M., Knuth, O., Tilgner, A., and Herrmann, H.: SPACCIM: A parcel model with detailed microphysics and complex multiphase chemistry, *Atmos. Environ.*, 39, 4375 – 4388, 2005.
- Yan, W., Topphoff, M., Rose, C., and Gmehling, J.: Prediction of vapor-liquid equilibria in mixed-solvent electrolyte systems using the group contribution concept, *Fluid Phase Equilibria*, 162, 97–113, 1999.

- Zaveri, R. A., Easter, R. C., Fast, J. D., and Peters, L. K.: Model for Simulating Aerosol Interactions and Chemistry (MOSAIC), *J. Geophys. Res.-Atmos.*, 113, 2008.
- Zhang, Y., Seigneur, C., Seinfeld, J., Jacobson, M., and Binkowski, F.: Simulation of aerosol dynamics: A comparative review of algorithms used in air quality models, *Aerosol Sci. Technol.*, 31, 487–514, 1999.
- Zhang, Y., Pun, B., Vijayaraghavan, K., Wu, S., Seigneur, C., Pandis, S., Jacobson, M., Nenes, A., and Seinfeld, J.: Development and application of the model of aerosol dynamics, reaction, ionization, and dissolution (MADRID), *J. Geophys. Res. Atmos.*, 109, 2004.
- Zuend, A., Marcolli, C., Luo, B. P., and Peter, T.: A thermodynamic model of mixed organic-inorganic aerosols to predict activity coefficients, *Atmos. Chem. Phys.*, 8, 2008.

Appendix A

Thermodynamics of phase equilibria in multicomponent systems

A.1 Phase equilibria in heterogeneous system

The term "equilibrium" refers to a balance between two opposing actions. When applied to chemistry one can say that a condition of equilibrium is reached in a system when two opposing changes occur simultaneously at the same rate. In the context of vapor-liquid equilibrium, it refers to a case when 'two or more phases reach a state of equilibrium wherein all tendency for further change has ceased' (Prausnitz et al., 1986). A heterogeneous closed system is made up of two or more phases with each phase considered as an open system within the overall closed system. Reactions (changes) between or among phases are driven by energy manifested in temperature of chemical potentials. When there is no net change in a closed system among the phases, the system is said to have reached an equilibrium condition. A phase in a closed system has a certain tendency to change at a definite temperature, such a tendency is called "Activity" of the phase. Until, the concentrations disappears from one phase to another, its tendency or activity remains constant. However, the activities of substances in a gas phase are proportional to their partial pressures or concentrations. For a solution, their activities are proportional to their concentrations. Thus, their partial pressures or concentrations are indicators of their tendency to change, where the activity coefficients are the proportional constants.

During the equilibrium conditions, these tendencies of changes reach certain proportion such that the forward and reverse changes are balanced. Similar to the equilibrium conditions of homogeneous systems, heterogeneous systems also tend to reach equilibrium conditions. Furthermore, one can describe the equilibrium conditions of heterogeneous systems by the help of "Equilibrium constants". It has been clear that heterogeneous, closed systems are made up of different phases, considered as homogeneous, open systems, within an overall closed system. Thus, one can be formulate the thermodynamic equilibrium as a state or a system tends to reach and no further changes while given enough time. For instance, a system at constant temperature ($dT = 0$) and pressure ($dp = 0$), using Eq.(2.6) one can obtain as follows while keeping the composition constant as well i.e. ($dn_1 = 0$), it follows ($dG = 0$), or the system has constant Gibbs energy:

$$dG = \sum_i \mu_i dn_i, \tag{A.1}$$

This illustrates, that for an actual, irreversible process ($d^2G = 0$), means that G is minimum at equilibrium, which comes from the second law of thermodynamics, can be stated as "a system will try to increase its entropy and when the entropy reaches its maximum value, the system will

be at equilibrium". That means, at thermodynamic equilibrium, $dG = 0$, in contrast with the process that at isobaric, isothermal conditions, which is known as chemical equilibrium.

$$\sum_i \mu_i dn_i = 0. \quad (\text{A.2})$$

The general result for a closed, heterogeneous system consisting of κ phases and m components, is that at equilibrium with respect to the processes described earlier, at constant T and p , with respect to a small change of species i from any two phases α to β can be written as given by Prausnitz et al. (1986): $n_i^\alpha - dn_i = n_i^\beta + dn_i$. Hence, applying Eq. A.2 to the two phase system, it follows that $\mu_i^\alpha = \mu_i^\beta$. Therefore Eq. A.2 is the basic equation to formulate phase equilibria in isobaric, isothermal heterogeneous systems.

$$\begin{aligned} T^\alpha = T^\beta = \dots\dots\dots = T^\kappa & : \textit{thermal equilibrium} \\ P^\alpha = P^\beta = \dots\dots\dots = P^\kappa & : \textit{mechanical equilibrium} \\ \mu^\alpha = \mu^\beta = \dots\dots\dots = \mu^\kappa & : \textit{chemical equilibrium} \end{aligned} \quad (\text{A.3})$$

where the number of phases is k , and $i = 1, 2, \dots, k$ goes over all system components.

A.2 The Gibbs-Duhem relation

One can characterise, the intensive state of each phase present in heterogeneous system at internal equilibrium by its temperature and pressure, and the chemical potential of each component present. For instance, having n components, this would mean $n+2$ variables to characterise the phase. However, these are not all independent variables. The Gibbs-Duhem relation shows how the variables are linked. Recall the fundamental Eq. A.5 in terms Gibbs energy for a particular phase and upon, integrating this equation from a state of zero mass ($U = S = V = n_i = \dots = n_m = 0$) to finite mass (U, S, V, n_i, \dots, n_m) at constant T, p , as well as the composition, the change in Gibbs energy is according to Euler's equation (Pruppacher and Klett, 1997; Smith et al., 1996):

$$G = \sum_i \mu_i n_i, \quad (\text{A.4})$$

which explains, that the Gibbs energy is the value computed by summation over the products of the chemical potentials and the number of moles of each component (Smith et al., 1996). As defined in the chemical potential as the partial molar derivative of the Gibbs energy this also follows from the same definition.

$$dG = -SdT + Vdp + \sum_i \mu_i dn_i, \quad (\text{A.5})$$

Both, Eq. A.5 and Eq. A.4 are generally used, although p and T do not explicitly appear in Eq. A.4. Based on this, the total change in the G obtained from Eq. A.4 as:

$$dG = \sum_i \mu_i dn_i + \sum_i n_i d\mu_i, \quad (\text{A.6})$$

with the chemical potential μ of species i :

$$\mu_i = \left(\frac{\partial U}{\partial n_i} \right)_{S, V, n_{j \neq i}}. \quad (\text{A.7})$$

while, comparing with Eq. A.5, the following equation can be obtained:

$$-SdT + Vdp - \sum_i n_i d\mu_i = 0. \quad (\text{A.8})$$

This generic expression is called as the Gibbs-Duhem relation, a fundamental equation in the thermodynamics of solutions. However, one can get benefit from this, that, when a change in temperature and pressure of a system, simultaneously there is also a corresponding change of the chemical potentials of the various system species. Thus, in general, only $n + 1$ intensive variables of the $n + 2$ variables per phase are independent variables ($n + 1$ degrees of freedom). Furthermore, during the constant temperature and pressure, there is also a dependency between the chemical potentials. Hence

$$\sum_i n_i d\mu_i = 0. \quad (\text{A.9})$$

However, Eq. A.4 shows, $k - 1$ chemical potentials of the species of a phase at isobaric, isothermal conditions, completely describe the phase behavior. At the same time, one can then measure and/or compute the chemical potential of k^{th} species and, the consistency of the measurements/model can be checked (see Smith et al. (1996)).

A.3 Gibbs excess energy

The aforementioned intermolecular interactions, which can cause the non-ideal contributions to the total Gibbs energy, as well as they can separate the system deviating from ideal solutions. Hence, the Gibbs energy can therefore need to be considered as the sum of "ideal" and so called "excess" contributions (Smith et al., 1996). For instance, if constant system temperature and pressure come across, the expression based on the corresponding mole fraction for the Gibbs energy, while denoting as (x) is:

$$G = \sum_q n_q \left(\mu_q^{o,(x)} + RT \ln a_q^{(x)} \right) = \sum_q n_q \left(\mu_q^{o,(x)} + RT \ln x_q \gamma_q^{(x)} \right). \quad (\text{A.10})$$

However, it has been clear that, the activity coefficients in the ideal solutions are equal to unity, as a result one can write for the ideal Gibbs energy, $G^{\text{id},(x)}$

$$G^{\text{id},(x)} = \sum_q n_q \mu_q^{o,(x)} + \sum_q n_q RT \ln x_q. \quad (\text{A.11})$$

So, the excess Gibbs energy, $G^{\text{ex},(x)}$, is then calculated from the difference $G^{\text{id},(x)}$

$$G^{\text{ex},(x)} = \sum_q n_q RT \ln \gamma_q^{(x)}. \quad (\text{A.12})$$

From the mathematical point of view, the chemical potential Eq. A.7 follows for the ideal chemical potential of substance i :

$$\begin{aligned} \left(\frac{\partial G^{\text{id},(x)}}{\partial n_i} \right)_{p,T,n_{q \neq i}} &= \mu_i^{o,(x)} + \frac{\partial}{\partial n_i} \left[\sum_q n_q RT \ln x_q \right] \\ &= \mu_i^{o,(x)} + RT \ln x_i \end{aligned} \quad (\text{A.13})$$

$$+n_i RT \left(\frac{1}{n_i} - \frac{1}{\sum_q n_q} \right) - RT \sum_{q \neq i} x_q, \quad (\text{A.14})$$

and since $\sum_q \frac{n_q}{\sum_t n_t} = \sum_q x_q = 1$, the contribution from the ideal solution part of the chemical potential is:

$$\left(\frac{\partial G^{id,(x)}}{\partial n_i} \right)_{p,T,n_{q \neq i}} = \mu_i^{id,(x)} = \mu_i^{o,(x)} + RT \ln x_i. \quad (\text{A.15})$$

Thus, one can write the corresponding partial derivative of $G^{ex,(x)}$ is:

$$\left(\frac{\partial G^{id,(x)}}{\partial n_i} \right)_{p,T,n_{q \neq i}} = RT \left(\ln \gamma_i^{(x)} + \sum_q \left(n_q \frac{\partial \ln \gamma_q^{(x)}}{\partial n_i} \right) \right), \quad (\text{A.16})$$

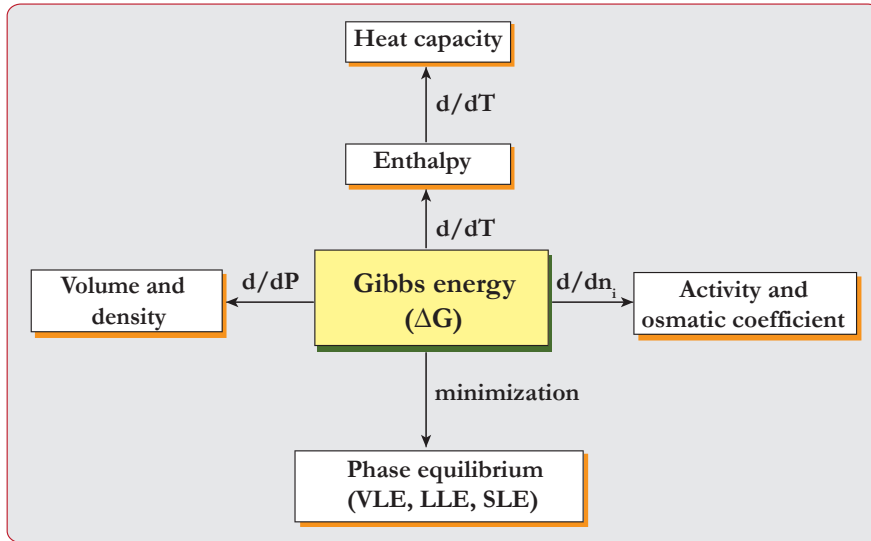


Figure A.1: Thermodynamic relationships between Gibbs energy and other measurable quantities.

at the same time the partial derivative on the right side is according to the Gibbs-Duhem relation is expected to be equal to 0. So, the excess chemical potential is reduced to following generic expression as:

$$\left(\frac{\partial G^{id,(x)}}{\partial n_r} \right)_{p,T,n_{q \neq r}} = \mu_r^{ex,(x)} = RT \ln \gamma_r^{(x)}. \quad (\text{A.17})$$

Furthermore, one can usually describe the the non-ideal thermodynamic behavior in mixtures by an expression similar to Eq. A.17 for the excess Gibbs energy $G^{ex}(p, T, n_j)$, as the characteristic state variables of experiments are usually pressure p and temperature T . Hence, the corresponding

activity coefficients γ_j of the species with amount of moles n_i in the mixture, are related to G^{ex} by:

$$\ln \gamma_j = \left(\frac{\partial G^{ex}/RT}{\partial n_j} \right)_{T,p,n_{j' \neq j}}. \quad (\text{A.18})$$

This derivation explained that an expression for the excess Gibbs energy of a mixture can be used to derive the corresponding expressions for the activity coefficients of the substances involved. Nevertheless, one can compute the Gibbs energy of a specified composition based on the expression for the activity coefficients as contrariwise. Thus, this Gibbs energy can be considered as a generating function to estimate other thermodynamic quantities as shown in Fig. A.1.

The similar kind of expressions for the Gibbs energy can be obtained from the molality based chemical potential expressions. Since, it is too complicated (see Thomson (1997)), another definition for the ideal Gibbs energy was therefore used and introduced (see Pitzer (1991)), to obtain explicit terms for $\ln \gamma_i^{(m)}$ from the partial derivatives of the excess Gibbs energy in the molality basis (Pitzer, 1991). At the same time, for the mixed solvent electrolyte systems (organic-inorganic mixtures), the simpler form of the mole fraction based Gibbs energy expressions is most often used. Mole fraction based activity coefficients of ions are then converted to the molality basis which is conventional approach in the computation of activity coefficients.

A.4 Multi-component reaction equilibria

Chemical reaction equilibria usually can calculate in terms of the equilibrium constant. In general, the equilibrium constant, which is defined in terms of the change in Gibbs free energy at the standard state and hence is a function of temperature only, is equated to the ratio of the activities of the products over the activities of the reactants of the system. However, calculation of the activity of a specific compound requires an accurate estimation of the deviation from ideality, to be precise the measure of non-ideality i.e. activity coefficients of the system.

If a simple chemical reaction is expressed in terms of the following expression:



where $|\nu_i|$ is a stoichiometric coefficient and A_i stands for the reactants and products. The $|\nu_i|$ themselves are called stoichiometric numbers. For the general case of a multi-reaction equilibrium, where M chemical reactions occur simultaneously, one can describe these reactions, by the following equations:

$$\sum_k \nu_{k,j} R_{k,j} \rightleftharpoons \sum_i \nu_{i,j} P_{i,j}, \quad (j = 1, \dots, M) \quad (\text{A.20})$$

where R^k denotes reactant k , P_i denotes product i , and $\nu_{i,j}$ stands for the stoichiometric coefficient of species i in reaction j . At equilibrium, the following equation results from classical thermodynamics

$$\sum_i \nu_{i,j} \mu_i = 0, \quad (\text{A.21})$$

where μ_i is the chemical potential of species i and the summation is over all the reactants and products. In Eq. A.20 and in all the subsequent equations, the stoichiometric coefficients $\nu_{i,j}$ have positive values for the products and negative values for the reactants. The chemical potential of a component i can be written as

$$\mu_i = g_i^o + RT \ln \widehat{a}_i, \quad (\text{A.22})$$

where g_i^o is the standard Gibbs free energy of component i in the system and \widehat{a} is the activity of component i . Substituting Eq. A.21 in to Eq. A.20, one obtains

$$\ln \prod_i \widehat{a}_i^{\nu_{i,j}} = -\frac{\sum_i \nu_{i,j} g_i^o}{RT}, \quad (j = 1, \dots, M). \quad (\text{A.23})$$

By definition, the equilibrium constant of the j^{th} reaction is given by the expression

$$K_j = \exp\left(-\frac{\sum_i \nu_{i,j} g_i^o}{RT}\right) = \exp\left(-\frac{\Delta g_j^o}{RT}\right), \quad (j = 1, \dots, M) \quad (\text{A.24})$$

where, Δg_j^o is the standard Gibbs free energy of the j^{th} reaction, and so

$$K_j = \prod_i \widehat{a}_i^{\nu_{i,j}}. \quad (\text{A.25})$$

In applying Eq. A.24, one has to define the standard state. Consider as standard state of component i the ideal-gas state of pure i at unity pressure. In this case, the activity of i is equal to the fugacity of i and

$$\widehat{f}_i = x_i \phi_i P, \quad (\text{A.26})$$

where \widehat{f}_i is the fugacity of component i , x_i the mole fraction of i , and ϕ_i the fugacity coefficient of i . Therefore, Eq. A.24 can be written as

$$K_j = \prod_i (x_i \phi_i P)^{\nu_{i,j}} = \left(\prod_i x_i^{\nu_{i,j}}\right) \left(\prod_i \phi_i^{\nu_{i,j}}\right) P^{\sum_i \nu_{i,j}}, \quad (j = 1, \dots, M) \quad (\text{A.27})$$

For the case of an ideal mixture, the fugacity coefficients are unity and so Eq. A.26 simplifies considerably. However, for the case of non-ideal mixtures, the fugacity coefficients are not unity and they must be evaluated from classical thermodynamics as shown later. For each reaction j , the extent of reaction ϵ_j is a measure of the progress of the reaction. A simple material balance for component i at equilibrium gives

$$n_i = n_i^o + \sum_j \nu_{i,j} \epsilon_j, \quad (\text{A.28})$$

where n_i is the number of moles of i and superscript o denotes the initial value of the variable. The mole fraction x_i is accordingly

$$x_i = \frac{n_i}{\sum_i n_i} = \frac{n_i}{n}. \quad (\text{A.29})$$

Appendix B

Description of activity coefficient models

B.1 Concentration scales and reference states

If we consider the aqueous electrolyte solutions or mixture of organic-inorganic compounds, the components are need to characterize into ions either anion or cation, organics in dissociated or undissociated forms dissolved in the water. Hence, the estimation of activity coefficients of different components with varying the each component concentration is rather difficult. This further gives the confusion to decide the (Pitzer, 1991). For instance, if any neutral substances, dissolved in the system, always the reference state is commonly chosen to be the pure substance at particular temperature and pressure. As a result, for water: $\gamma_w \rightarrow 1$, for $x_w \rightarrow 1$. At the same time, pure cation or anion is available in the system, a different reference and standard state have to be defined (Prausnitz et al., 1999).

Normally, the reference state for ions are defined to be an infinitely dilute solution of ions in a neutral solvent or solvent mixture. In the technical chemistry and the chemical engineering, the solvents can be vary depends on the process, where is in the atmospheric science, water is always preferable reference solvent, the droplet composition depends on the amount of water also. Thermodynamic models often utilize to illustrate the concentration scale in molality molality (moles of substance / kg of solvent) or mole fractions (moles / total amount of moles in solution) which are most useful than.

From a theoretical point of view, concentration scales like the molality and mole fractions are often used to inter compare the data of different substances than mass fractions (Smith et al., 1996). The chemical properties of, for example, ions either cation or anion, dissolved in an aqueous solution, one cannot use the mass of the compare with mole fractions, since, the physicochemical properties much better described with ions-comparing the amount of moles . Experimental data in the literature (see Pitzer (1991); Chiavone and Rasmussen (2000); Iliuta et al. (2000); Gros and Dussap (2003) and Thomsen et al. (2004)) is often listed in one of the following concentration scales:

$$x_t = \frac{n_t}{\sum_k n_k + \sum_j n_j}; \quad m_t = \frac{n_t}{\sum_k n_k M_k}; \quad mf_t = \frac{n_t M_t}{\sum_k n_k M_k + \sum_j n_j M_j} \quad (\text{B.1})$$

where t is a solvent or solute substance, k denotes solvents, j solutes (ions), n_t are moles of substance, and M_t is the molar mass (kg mol^{-1}). The three concentration measures are then, the mole fraction of t , x_t , the molality of t , m_t (mol kg^{-1}), and the mass fraction of t , mf_t . For the solutes, the molality is in practice to define the concentration scale where as for the mixture components the mole fraction and mass fraction is offer used. Nevertheless, the relation in terms of mathematical expression describing the molality is also used some times for solvent

components as well. If one should try to convert the concentrations from one scale to another (mole to mass or mole to volume), it is sometimes helpful, to express at first also the solvent concentrations in the molality scale.

Due to this, it makes more complicated, if one define the concentration scale for reference states, (Pitzer, 1991). This phenomena is called as symmetric convention. It is only used if all mixture components are related to pure substance reference and standard states. There is the opposite phenomena called unsymmetric conversion. The can be defined for the solvents neutral mixture substances) with respect to the pure reference and standard states. In such situations, the solutes (ions) are defined with respect to an infinitely dilute solution in a reference solvent and the unsymmetric convention depends on the concentration scale. Using the symmetric convention on a mole fraction basis, the reference states for both, ions i and solvents s , are:

$$\gamma_s \rightarrow 1 \text{ as } x_s \rightarrow 1 \quad \text{and} \quad \gamma_i \rightarrow 1 \text{ as } x_i \rightarrow 1 \quad (\text{B.2})$$

The unsymmetric convention for the ions on the molality basis, dissolved in the reference solvent water, refers to the following definitions:

$$\gamma_i \rightarrow 1 \text{ as } m_i \rightarrow 1 \quad \left(\sum_j m_j \rightarrow 0 \right), \quad x_w \rightarrow 1 \quad \text{and} \quad \sum_{s \neq w} x_s = 0, \quad (\text{B.3})$$

where w refers to the reference solvent water. Fig. B.1 shows the solute activity plotted against solute molality. Here the corresponding standard state for the ions is the hypothetical ideal aqueous solution of unit molality ($\mu_i^{o,(m)} = \mu_i(m_i = m_i^o, \gamma_i = 1)$), with $m_i^o = 1 \text{ mol (kgH}_2\text{O)}^{-1}$

Furthermore, the chemical potentials for the solvent and solute are given in Eq. 2.13 in mole scale. By introducing the molal concentration, the chemical potential for the solute is related as

$$\mu_j = \mu_j^\nabla(T, P, x_s) + RT \ln(x_j \gamma_j^\nabla) = \mu_j^*(T, P, x_s) + RT \ln(m_j \gamma_j^\nabla), \quad (\text{B.4})$$

where superscript $*$ indicates the molality scale and infinite diluted reference state. For the solute species, the activity against the molality is shown in Fig. B.1. The hypothetical ideal solution is shown by straight dashed line and that goes through the coordinates (0,0) and (1,1) with a unity slope, which represents the activity coefficient of the solute. The point A, which, implies that the chemical potential of the ideal solution is defined as the standard state for the real solution. The standard state activity is given by A corresponding to unit molality. If one can arbitrary chose the molality of 2.0, the activity of the solute in the real solution is given by C, while that in the hypothetical ideal solution is given by B. In the hypothetical ideal solution the activity of the solute is equal to molality because, in that ideal solution, $\gamma_{ideal}^{(m)} = 1$ for all solute concentrations. Therefore, the activity coefficient of the real solution, $\gamma_i^{(m)} = a_i/m_i$, is given by the ratio CD/BD. However, the real solution has the same properties with the ideal solution, where (origin of coordinate), and $\gamma \rightarrow 1$ as $m_i \rightarrow 0$ (origin of coordinate), which implies the infinite dilution reference state. The specific definition can be obtained from the book of Prausnitz et al. (1999).

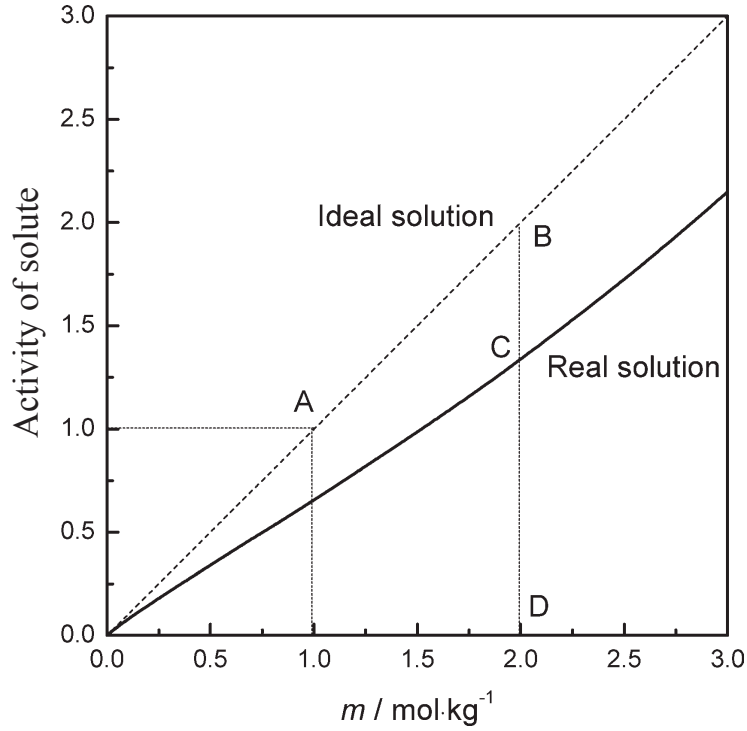


Figure B.1: Schematic of the activity of a non-dissociating solute as a function of its molality (Prausnitz *et al.*, 1999).

B.2 PITZER approach

The first model implemented in this PhD thesis is Pitzer activity coefficient model (Pitzer, 1973; Pitzer and Mayorga, 1973; Pitzer, 1991). The Pitzer activity coefficient model is based on the general equation of the excess Gibbs energy expressed in as a series of terms in increasing powers of molality, m_i , whereas the Debye-Hückel term appears as the limiting law in the first term of the Eq. B.5:

$$\frac{G^{ex}}{RT} = f(I) + \sum_i \sum_j m_i m_j \lambda_{ij}(I) + \sum_i \sum_j \sum_k m_i m_j m_k \mu_{ijk}(I) + \dots, \quad (\text{B.5})$$

The equations of the osmotic coefficient, ϕ , and the activity coefficients of cations (M), anions (X), and the neutrals (N) are derived from Eq. B.5,

$$(\phi - 1) = \frac{2}{\sum_i m_i} \left[\begin{aligned} & \frac{-A^\phi I^{1.5}}{1+\alpha I^{0.5}} + \sum_c \sum_a m_c m_a (B_{ca}^\phi + ZC_{ca}) + \\ & \sum_c \sum_{c'} m_c m_{c'} \left(\phi_{cc'}^\phi + \sum_a m_a \psi_{cc'a} \right) + \sum_a \sum_{a'} m_a m_{a'} \left(\phi_{aa'}^\phi + \sum_c m_c \psi_{aa'c} \right) + \\ & \frac{1}{2} \sum_n m_n^2 \lambda_{nn} + \sum_n m_n^3 \mu_{nnn} + \sum_n \sum_{n'} m_n m_{n'} \lambda_{nn'} + 3 \cdot \sum_n \sum_{n'} m_n^2 m_{n'} \mu_{nnn'} + \\ & \sum_n \sum_c m_n m_c \lambda_{nc} + 3 \cdot \sum_n \sum_c m_n^2 m_c \mu_{nnc} + \\ & \sum_n \sum_a m_n m_a \lambda_{na} + 3 \cdot \sum_n \sum_a m_n^2 m_a \mu_{nna} + \\ & \sum_n \sum_c \sum_a m_n m_c m_a \zeta_{nca} + \sum_n \sum_c \sum_{c'} m_n m_c m_{c'} \eta_{ncc'} + \sum_n \sum_a \sum_{a'} m_n m_a m_{a'} \eta_{naa'} + \\ & 6 \cdot \sum_c \sum_n \sum_{n'} m_n m_c m_{n'} \mu_{cnn'} + 6 \cdot \sum_a \sum_n \sum_{n'} m_a m_n m_{n'} \mu_{ann'} + 6 \cdot \sum_n \sum_{n'} \sum_{n''} m_n m_{n'} m_{n''} \mu_{nn'n''} \end{aligned} \right] \quad (\text{B.6})$$

$$\begin{aligned} \ln \gamma_M &= z_M^2 F + \sum_a m_a (2B_{Ma} + ZC_{Ma}) + |z_M| \sum_c \sum_a m_c m_a C_{ca} \\ &+ \sum_c m_c \left(2\phi_{Mc} + \sum_a m_a \psi_{Mca} \right) + \sum_a \sum_{a'} m_a m_{a'} \phi_{Maa'} \\ &+ 2 \sum_n m_n \lambda_{Mn} + 3 \sum_n m_n^2 \mu_{Mnn} + 6 \sum_n \sum_{n'} m_n m_{n'} \mu_{Mnn'} \\ &+ 6 \sum_n \sum_a m_n m_a \zeta_{Mna} + 6 \sum_n \sum_c m_n m_c \eta_{Mnc} \end{aligned} \quad (\text{B.7})$$

$$\begin{aligned} \ln \gamma_X &= z_X^2 F + \sum_c m_c (2B_{cX} + ZC_{cX}) + |z_X| \sum_c \sum_a m_c m_a C_{ca} \\ &+ \sum_a m_a \left(2\phi_{Xa} + \sum_c m_c \psi_{cXa} \right) + \sum_c \sum_{c'} m_a m_{a'} \psi_{cc'X} \\ &+ 2 \sum_n m_n \lambda_{Xn} + 3 \sum_n m_n^2 \mu_{Xnn} + 6 \sum_n \sum_{n'} m_n m_{n'} \mu_{Xnn'} \\ &+ 6 \sum_n \sum_c m_n m_c \zeta_{ncX} + 6 \sum_n \sum_a m_n m_c \eta_{Xna} \end{aligned} \quad (\text{B.8})$$

$$\begin{aligned} \ln \gamma_N &= 2 \sum_n m_n \lambda_{Nn} + 3 \sum_n m_n^2 \mu_{Nnn} + 6 \sum_n m_n m_{n'} \mu_{NNn'} \\ &+ 2 \sum_c m_c \lambda_{Nc} + 2 \sum_a m_a \lambda_{Na} + \sum_c \sum_a m_c m_a \zeta_{Nca} \\ &+ 2 \sum_n m_n \lambda_{Xn} + 3 \sum_n m_n^2 \mu_{Xnn} + 6 \sum_n \sum_{n'} m_n m_{n'} \mu_{Xnn'} \\ &+ \sum_c \sum_{c'} m_n m_c \eta_{Ncc'} + \sum_a \sum_{a'} m_a m_{a'} \eta_{Naa'} \\ &+ 6 \sum_n \sum_c m_n m_c \mu_{Nnc} + 6 \sum_n \sum_a m_n m_a \mu_{Nna} \end{aligned} \quad (\text{B.9})$$

The (molal) somatic coefficient, ϕ , of a solution is related to the water activity, a_w , by:

$$\ln a_w = -\frac{M_w}{1000} \phi \sum_i m_i \quad (\text{B.10})$$

The ionic strength of the solution is defined as:

$$I = \frac{1}{2} \sum_i m_i z_i^2 \quad (\text{B.11})$$

The Debye-Hückel term, f_γ , the Debye-Hückel parameter, A_ϕ , and other coefficients can be computed as follows:

$$A_\phi = \frac{1}{3} \left[\frac{2\pi N_o d_w}{1000} \right]^{\frac{1}{2}} \left(\frac{e^2}{\epsilon k T} \right)^{\frac{3}{2}}$$

$$B_{MX}^\phi = \beta_{MX}^{(0)} + \beta_{MX}^{(1)} \exp(-\alpha_1 \sqrt{I}) + \beta_{MX}^{(2)} \exp(-\alpha_2 \sqrt{I})$$

$$C_{MX}^\phi = \frac{C^\phi}{2|Z_M Z_X|^{\frac{1}{2}}}$$

$$F = f^\gamma + \sum_c \sum_a B'_{ca} + \sum_c \sum_{c'} m_c m_{c'} \phi'_{cc'} + \sum_a \sum_{a'} m_a m_{a'} \phi'_{aa'} \quad (\text{B.12})$$

$$\phi'_{cc'} = \phi_{cc'} + I \phi'_{cc'}$$

$$f_\gamma = -A_\phi \left[\frac{\sqrt{I}}{1 + b\sqrt{I}} + \frac{2}{b} \ln(1 + b\sqrt{I}) \right]$$

with $\alpha_1 = 1.4 (1.2) \sqrt{kg/mol}$, $\alpha_2 = 2 (12) \sqrt{kg/mol}$ and $b = 1.2 \sqrt{kg/mol}$

where as Φ' the ionic strength derivative of Φ . The observable binary activity coefficient, γ_{MX} , results from the combination of the corresponding ionic specific activity coefficients.

$$\begin{aligned} \ln \gamma_{MX} = & |z_M z_X| F - \frac{\nu_M}{\nu} \sum_a m_a \left[2B_{Ma} + ZC_{Ma} + 2\frac{\nu_X}{\nu_M} \phi_{Xa} \right] \\ & + \frac{\nu_X}{\nu} \sum_c m_c \left[2B_{cX} + ZC_{cX} + 2\frac{\nu_M}{\nu_X} \phi_{Mc} \right] \\ & + \sum_c \sum_a \frac{1}{\nu} [2\nu_M z_M C_{ca} + \nu_M \Psi_{Mca} + \nu_X \Psi_{caX}] \\ & + \sum_c \sum_{c'} m_c m_{c'} \frac{\nu_X}{\nu} \Psi_{cc'X} + \sum_a \sum_{a'} m_a m_{a'} \frac{\nu_M}{\nu} \Psi_{Maa'} \\ & + 2 \sum_n \frac{m_n}{\nu} (\nu_M \lambda_{nM} + \nu_X \lambda_{nX}) \end{aligned} \quad (\text{B.13})$$

B.3 UNIFAC

The second model implemented in this study is the same as the original UNIFAC (Fredenslund et al., 1975). This model is not used for ion activities, the reference states are the same as in the original UNIFAC. However, in the other models in which ion activities are calculated, ions have different reference states than non-electrolytes. UNIFAC (Fredenslund et al., 1975) is so called group contribution method, where chemical species are constructed from functional groups. Activity coefficient for species i is calculated as a sum of combinatorial and residual contributions

$$\ln \gamma_i = \ln \gamma_i^C + \ln \gamma_i^R, \quad (\text{B.14})$$

The combinatorial contribution is calculated with the equation

$$\ln \gamma_i^C = 1 - V_i + \ln V_i - \frac{z}{2} q_i \left(1 - \frac{V_i}{F_i} + \ln \left(\frac{V_i}{F_i} \right) \right) \quad (\text{B.15})$$

where $V_i = \frac{r_i}{\sum_k r_k x_k}$, $F_i = \frac{q_i}{\sum_k q_k x_k}$ and $z = 10$. x_i is the mole fraction, $q_i = \sum_k \nu_k^{(i)} Q_k$, is the area parameter, $r_i = \sum_k \nu_k^{(i)} R_k$ is volume parameter and $\nu_k^{(i)}$ is the number of functional group k in species i . The only parameters in the combinatorial part are the pure component area (Q_k) and volume (R_k) parameters for sub groups.

Table B.1: UNIFAC group interaction parameters

| $a_{i,j}$ | CH ₂ | OH | CH ₃ OH | H ₂ O | CH ₂ CO | CHO | CCOO | HCOO | CH ₂ O | COOH |
|--------------------|-----------------|--------|--------------------|------------------|--------------------|---------|---------|---------|-------------------|---------|
| CH ₂ | 0.0 | 986.5 | 697.20 | 1318.00 | 476.40 | 677.00 | 232.10 | 507.00 | 251.50 | 663.50 |
| OH | 156.40 | 0.0 | -137.10 | 353.50 | 84.00 | -203.60 | 101.10 | 267.80 | 28.06 | 199.00 |
| CH ₃ OH | 16.51 | 249.1 | 0.0 | -181.00 | 23.39 | 306.40 | -10.72 | 179.70 | -128.60 | -20.002 |
| H ₂ O | 300.00 | -229.1 | 289.60 | 0.0 | -195.4.0 | -116.00 | 72.870 | 233.87 | 540.50 | -14.09 |
| CH ₂ CO | 26.76 | 164.5 | 108.70 | 472.50 | 0.0 | -37.36 | -213.70 | -190.40 | -103.60 | 669.40 |
| CHO | 505.70 | 529.0 | -340.20 | 480.80 | 128.00 | 0.0 | -110.30 | 766.00 | 304.10 | 497.50 |
| CCOO | 114.80 | 245.4 | 249.63 | 200.00 | 372.20 | -185.10 | 0.0 | -241.80 | -235.70 | 660.20 |
| HCOO | 329.30 | 139.4 | 227.80 | 124.63 | 385.40 | -236.50 | 1167.00 | 0.0 | -234.00 | -268.10 |
| CH ₂ O | 83.36 | 237.7 | 238.40 | -314.7 | 191.10 | -7.838 | 461.30 | 457.30 | 0.0 | 664.00 |
| COOH | 315.30 | -151.0 | 339.80 | -66.17 | -297.8 | 165.50 | -256.30 | 193.90 | -338.50 | 0.0 |

The residual contribution is calculated with the equation

$$\ln \gamma_i^R = \sum_k \nu_k^{(i)} \left[\ln \Gamma_k - \ln \Gamma_k^{(ref,i)} \right] \quad (\text{B.16})$$

where $X_k = \frac{\sum_j \nu_k^{(j)} x_j}{\sum_j \sum_m \nu_m^{(j)} x_j}$ is mole fraction of group k in the mixture, $\psi_{mk} = \exp\left(-\frac{a_{km}}{T}\right)$ and a_{km} is the group interaction parameter for main groups k and m . Most of the functional groups (main groups) have sub groups which have the same interaction parameters, but different Q_k and R_k . For example the main group CH_n has sub groups CH₃, CH₂, CH and C. The group volume and surface area parameters can be calculated from the molecular sizes of the functional groups. The UNIFAC parameters are given in the Table. B.1. All non-electrolyte-ion and ion-ion UNIFAC interaction parameters are set to zeros.

B.4 LIFAC

This third model considered in this PhD thesis model is the same as the original LIFAC (Yan et al., 1999) and Modified LIFAC (Kiepe et al., 2006). The total activity coefficients in these approaches are calculated as a sum of three contributions: long range (LR), middle range (MR) and short range (SR) interactions can be write as follows:

$$\ln \gamma_i = \ln \gamma_i^{LR} + \ln \gamma_i^{MR} + \ln \gamma_i^{SR} \quad (\text{B.17})$$

B.4.1 Long-range contribution

The LR term represents the interaction contribution caused by the Coulomb electrostatic forces. Corresponding activity coefficients can be expressed using the extended Debye-Hückel theory (Debye and Hückel, 1923). This concept is also applied to mixtures using the Oster mixing rule (Franks.F, 1973). The physical validity of the LR equation is limited to the very dilute region. The purpose of this term is mainly to provide the true limiting law at infinite dilution. Therefore, this term was not revised in this work. The solvent is a mixture of water and organic compound, and its properties are calculated from pure component properties weighted with salt free volume:

$$\phi'_s = \frac{x'_s \frac{M_s}{\rho_s}}{\sum_{i \neq \text{salt}} x'_i \frac{M_i}{\rho_i}}, \quad (\text{B.18})$$

where M_s (kg/mol) is molecular weight, ρ_s (kg/m^3) is density and x'_s is salt free mole fraction of pure solvent s . Solvent (s) and ion (i) activity coefficients are calculated with the equations

$$\ln \gamma_s^{LR} = \frac{2AM_s\rho}{b^3\rho_s} \left(1 + b\sqrt{I} - \frac{1}{1 + b\sqrt{I}} - 2 \ln(1 + b\sqrt{I}) \right), \quad (\text{B.19})$$

$$\ln \gamma_i^{LR} = \frac{-z^2 A\sqrt{I}}{1 + b\sqrt{I}}, \quad (\text{B.20})$$

where $\rho = \sum_s \phi'_s \rho_s$ is density of the solvent mixture, Z_1 is charge magnitude of ion in the molality (m) scale. The Debye-Hückel parameters A ($\sqrt{kg/mol}$) and b ($\sqrt{kg/mol}$) can be calculated as follows:

$$A = e_0^3 \frac{(2\pi N_A \rho)^{1/2}}{(DkT)^{3/2}}, \quad (\text{B.21})$$

$$b = a \sqrt{\frac{8\pi e_0^2 N_A \rho}{DkT}}. \quad (\text{B.22})$$

Where e_0 (C) is elementary charge, N_A ($1/mol$) is Avogadro's constant, k (J/K) is Boltzmann constant, T (K) is temperature and a (m) is the closest approach parameter, here $a = 10^{-10}m$. Dielectric constant is calculated with equation $D = 4\pi\epsilon_0\epsilon_r$, where ϵ_0 ($C^2/(Jm)$) is permittivity of vacuum and ϵ_r is relative permittivity. In the original model, D is dielectric constant of solvent mixture, but because dielectric constants were not available for all organics, we use that of pure water instead.

B.4.2 Middle-range contribution

The middle range contribution is calculated using functional groups, which are the same as in the UNIFAC part. The equations for solvent group k and ion i are

$$\ln \gamma_k^{MR} = \sum_i B_{k,i} m_i - \frac{M_k \sum_k \sum_i \nu_k^{(i)} x'_i}{M} \sum_k \sum_i [B_{k,i} + I B'_{k,i}] x'_k m_i - M_k \sum_c \sum_a [B_{c,a} + I B'_{c,a}] m_c m_a \quad (\text{B.23})$$

$$\ln \gamma_j^{MR} = \frac{1}{M} \sum_k B_{k,j} x'_k + \frac{z_j^2}{2M} \sum_k \sum_i B_{k,i} x'_k m_i + \sum_i B_{j,i} m_i + \frac{z_j^2}{2} \sum_c \sum_a B'_{c,a} m_c m_a, \quad (\text{B.24})$$

where $B_{k,j}$ (kg/mol) the interaction coefficient for groups j and k is, $B'_{k,i}$ (kg^2/mol^2) is derivative of $B_{k,j}$ with respect to ionic strength, $M = \sum_s x'_s M_s$ is molecular weight of solvent group k , which were calculated from atomic weights. Subscripts k , i , c and a denotes solvent group, any ion, cation and anion respectively. Symmetric interaction coefficients ($B_{j,k} = B_{k,j}$) are functions of ionic strength:

$$B_{c,a}(I) = b_{c,a} + c_{c,a} \exp(-\sqrt{I} + 0.31I) \quad (\text{B.25})$$

$$B_{k,i}(I) = b_{k,i} + c_{k,i} \exp(-1.2\sqrt{I} + 0.31I) \quad (\text{B.26})$$

where $b_{j,k}$ and $c_{j,k}$ are the interaction parameters for the main groups j and k . Ion activity coefficients must be normalized to infinite dilution reference state by subtracting the first term in Eq. B.23 calculated with correct reference state concentrations. The MR activity coefficient of solvent s is calculated as a sum of group activity coefficients:

$$\ln \gamma_s^{MR} = \sum_k \nu_k^{(s)} \ln \gamma_k^{MR} \quad (\text{B.27})$$

The MR interaction parameters are opted directly from the original model. The middle range interaction coefficients between solvent-ion and ion-ion are shown in the Table. C.9.

B.4.3 Short-range contribution

The short range contribution is calculated with UNIFAC, but now the infinite dilution reference state is selected for the ions. Because UNIFAC equations give activity coefficients in mole fraction scale, ion activity coefficients are converted to molality scale with equation:

$$\ln \gamma_i^{(m)} = \ln \gamma_i^{(x)} - \ln \left(M_r / M + M_r \sum_i m_i \right), \quad (\text{B.28})$$

where M_r , molecular weight of the reference state solvent and M is molecular weight of the solvent mixture. Group interaction parameters between solvents can adopt from any model approach, since most of the models used UNIFAC (Fredenslund et al., 1975) for calculating the activity coefficients for the short-range contribution, these parameters are shown in Table. B.1.

B.5 AIOMFAC

B.5.1 Long-range contribution

The Debye-Hückel theory was the first approach to successfully describe the electrolyte effects in highly diluted solutions (Debye and Hückel, 1923). This theory treats the solutes as electrical charges in a solvent medium of a specific density and dielectric constant and was shown to be correct in the limit of infinite dilution. In this model, the extended Debye-Hückel theory modified as by Fowler and Guggenheim (1949) has been used. As a consequence of the choice of the reference solvent water for inorganic ions, the Debye-Hückel expression is different from the one in original LIFAC. Instead of using mixing rules to estimate the density and dielectric constant of the solvent mixture, the water properties have been used for all solvent components. Similar assumptions were made for the LR part of other mixed solvent models (Iliuta et al., 2000). With this constraint, the corresponding LR activity coefficient expressions for the solvents $\ln \gamma_s^{LR,(x)}$ and the ions $\ln \gamma_i^{LR,(x),\infty}$ are:

$$\ln \gamma_s^{LR,(x)} = \frac{2AM_s}{b^3} \left(1 + b\sqrt{I} - \frac{1}{1 + b\sqrt{I}} - 2 \ln(1 + b\sqrt{I}) \right), \quad (\text{B.29})$$

$$\ln \gamma_i^{LR,(x),\infty} = \frac{-z_i^2 A \sqrt{I}}{1 + b\sqrt{I}}, \quad (\text{B.30})$$

Equation Eq. B.30 gives the activity coefficient of ion i in the mole fraction basis (x) with the reference state of infinite dilution in water, indicated by super script ∞ . M_s is the molar mass of solvent s , z_i the number of elementary charges of ion i , and the ionic strength I (mol/kg^{-1}) is:

$$I = \frac{1}{2} \sum_i m_i z_i^2, \quad (\text{B.31})$$

The Debye-Hückel parameters A ($\sqrt{kg/mol}$) and b ($\sqrt{kg/mol}$) depend on temperature $T(K)$, density ρ_w (kg/m^3) and static permittivity ε_w (dimension less) of water, as calculated based on a distance of closest approach of $0.4nm$ between ions

$$A = 1.327757 \cdot 10^5 \frac{\sqrt{\rho_w}}{(\varepsilon_w T)^{3/2}}, \quad (\text{B.32})$$

$$b = 6.359696 \sqrt{\frac{\rho_w}{\varepsilon_w T}}, \quad (\text{B.33})$$

The simplification to a water-properties based expression for LR activity coefficients implicates the advantage of not having to estimate unknown dielectric constants of certain organic compounds (Raatikainen and Laaksonen, 2005) and maintains the thermodynamic consistency regarding the chosen reference states. In a real mixture solvents have densities and dielectric properties different from those of pure water, which was the reason for other authors to avoid applying this simplification. Compensation of these inaccuracies are stemming from this simplification in the semi-empirical MR part (Zuend et al., 2008).

B.5.2 Middle-range contribution

The semi-empirical character of the MR part, containing most of the adjustable parameters, can be regarded as the model part, which describes all the interaction effects involving ions not considered by the LR and SR contributions. This includes corrections to assumptions made in the LR and SR parts with respect to approximations of physical parameters. MR interactions of solvent compounds (organics and water) with ions are calculated using functional main groups.

The three interaction coefficients are parameterized as functions of ionic strength I . In contrast to LIFAC, in AIOMFAC the expressions, which are similar to the ones used for the Pitzer model of Knopf et al. (2003):

$$B_{k,i}(I) = b_{k,i}^{(1)} + b_{k,i}^{(2)} e^{(-b_{k,i}^{(3)}\sqrt{I})}, \quad (\text{B.34})$$

$$B_{c,a}(I) = b_{c,a}^{(1)} + b_{c,a}^{(2)} e^{(-b_{c,a}^{(3)}\sqrt{I})}, \quad (\text{B.35})$$

$$C_{c,a}(I) = c_{c,a}^{(1)} + e^{(-c_{c,a}^{(2)}\sqrt{I})}. \quad (\text{B.36})$$

Where $b_{k,i}^{(1)}$, $b_{k,i}^{(2)}$, $b_{c,a}^{(1)}$, $b_{c,a}^{(2)}$, $c_{c,a}^{(1)}$, $c_{c,a}^{(2)}$ are adjustable parameters, which are determined by fitting AIOMFAC activity coefficients to experimental data sets. The parameter $b_{c,a}^{(3)}$ was found to describe most aqueous salt solutions when assuming a fixed value of $0.8 \text{ (kg}^{1/2}/\text{mol}^{1/2})$. The parameter $b_{k,i}^{(3)}$ was fixed for all mixed organic-inorganic solutions assuming a value of $1.2 \text{ (kg}^{1/2}/\text{mol}^{1/2})$. All interaction coefficients in the MR part are symmetric, i.e. $B_{c,a}(I) = B_{a,c}(I)$.

The MR activity coefficients are obtained for a specific solvent main group k^*

$$\begin{aligned} \ln \gamma_{k^*}^{MR,(x)} &= \sum_i B_{k^*,i}(I) m_i - \frac{M_{k^*}}{M_{av}} \sum_k \sum_i [B_{k,i}(I) + I B'_{k,i}(I)] x'_k m_i \\ &\quad - M_{k^*} \sum_c \sum_a [B_{c,a}(I) + I B'_{c,a}(I)] m_c m_a \\ &\quad - M_{k^*} \sum_c \sum_a [2C_{c,a}(I) + I C'_{c,a}(I)] m_c m_a \sum_i m_i |Z_i| \\ &\quad - M_{k^*} \sum_c \sum_{c'} R_{c,c'} m_c m_{c'} \\ &\quad - M_{k^*} \sum_c \sum_{c' \geq c} \sum_a 2Q_{c,c',a} m_c m_{c'} m_a \end{aligned} \quad (\text{B.37})$$

Where m_i , m_c , m_a are the molalities of ions, cations, and anions respectively, x'_k are the salt-free mole fractions of solvent main groups k , and $M_{av} = \sum_s x'_s M_s$ is the average molar mass of the solvent mixture. M_{k^*} is the molar mass of main group k^* , calculated from the molar masses of the corresponding subgroups and their partial contributions to k^* . $B'_{k,i}(I)$, $B'_{c,a}(I) \text{ (kg}^{1/2}/\text{mol}^{1/2})$. The parameter $b_{k,i}^{(3)}$, and $C'_{c,a}(I) \text{ (kg}^3/\text{mol}^3)$ are the partial derivatives with respect to I , e.g. $B'_{c,a}(I) = \partial B_{c,a}(I) / \partial I$.

The activity coefficient of solvent compound s is then obtained from the main group contributions by:

$$\ln \gamma_s^{MR,(x)} = \sum_k \nu_k^{(s)} \ln \gamma_k^{MR,(x)} \quad (\text{B.38})$$

In analogy to Eq. B.37 the expressions for a specific cation c^* are:

$$\begin{aligned}
\ln \gamma_{c^*}^{MR,(x),\infty} &= \frac{1}{M_{av}} \sum_k B_{k,c^*}(I) x'_k + \frac{z_{c^*}^2}{2M_{av}} \sum_k \sum_i B'_{k,i}(I) x'_k m_i \\
&+ \sum_a B_{c^*,a}(I) m_a + \frac{z_{c^*}^2}{2} \sum_c \sum_a B'_{c,a}(I) m_c m_a \\
&+ \sum_a C_{c^*,a}(I) m_a \sum_i m_i |z_i| \\
&+ \sum_c \sum_a \left[C_{c,a}(I) |z_{c^*}| + C'_{c,a}(I) \frac{z_{c^*}^2}{2} \sum_i m_i |z_i| \right] m_c m_a \\
&+ \sum_c R_{c^*,c} m_c + \sum_c \sum_a Q_{c^*,c,a} m_c m_a,
\end{aligned} \tag{B.39}$$

and for anion a^*

$$\begin{aligned}
\ln \gamma_{a^*}^{MR,(x),\infty} &= \frac{1}{M_{av}} \sum_k B_{k,a^*}(I) x'_k + \frac{z_{a^*}^2}{2M_{av}} \sum_k \sum_i B'_{k,i}(I) x'_k m_i \\
&+ \sum_c B_{c,a^*}(I) m_c + \frac{z_{a^*}^2}{2} \sum_c \sum_a B'_{c,a}(I) m_c m_a \\
&+ \sum_c C_{c,a^*}(I) m_c \sum_i m_i |z_i| \\
&+ \sum_c \sum_a \left[C_{c,a}(I) |z_{a^*}| + C'_{c,a}(I) \frac{z_{a^*}^2}{2} \sum_i m_i |z_i| \right] m_c m_a \\
&+ \sum_c \sum_{c' \geq c} Q_{c,c',a^*} m_c m_{c'}.
\end{aligned} \tag{B.40}$$

Specific interaction coefficients (and the corresponding fit parameters) between the reference solvent, i.e. water, and the inorganic ions are set to zero ($B_{k=w,i}(I) = 0$). Therefore, the unsymmetrical reference state condition for infinite dilution of ions in water $\ln \gamma_i^{MR} \rightarrow 1$ is indeed fulfilled and can write $\ln \gamma_{c^*}^{MR,(x),\infty}$ (normalized) instead of $\ln \gamma_{c^*}^{MR,(x)}$

B.5.3 Short-range contribution

The SR contribution is represented by the group-contribution method UNIFAC (Fredenslund et al., 1975). The UNIFAC expressions in AIOMFAC include some modifications to better meet the specific properties of atmospheric semi-volatile organics, which typically contain molecules carrying several strongly polar functional groups. In this way, the relative distances of a molecule's functional groups are taken into account explicitly.

In UNIFAC the activity coefficient γ_j of mixture component j (j used for solute or solvent) is in general expressed as the contributions of a combinatorial part (C), accounting for the geometrical properties of the molecule, and a residual part (R), which reflects inter-molecular interactions:

$$\ln \gamma_j^{SR} = \ln \gamma_j^C + \ln \gamma_j^R \tag{B.41}$$

The combinatorial contribution is calculated with the equation (Marcolli and Peter, 2005)

$$\ln \gamma_j^C = \ln \frac{\Phi_j}{x_j} + \frac{z}{2} q_j \ln \frac{\Theta_j}{\Phi_j} + l_j - \frac{\Phi_j}{x_j} \sum_{j'} x_{j'} l_{j'}, \tag{B.42}$$

where

$$\Phi_j = \frac{r_j x_j}{\sum_{j'} r_{j'} x_{j'}}; \Theta_j = \frac{q_j x_j}{\sum_{j'} q_{j'} x_{j'}}, \tag{B.43}$$

and where

$$l_j = \frac{z}{2} (r_j - q_j) - (r_j - 1), \tag{B.44}$$

with $z = 10$. x_j is the mole fraction, $q_j = \sum_t \nu_t^{(j)} Q_t$ is the area parameter, $r_j = \sum_t \nu_t^{(j)} R_t$ is volume parameter and $\nu_t^{(j)}$ is the number of functional group k in species i . The only parameters in

the combinatorial part are the pure component area (Q_k) and volume (R_k) parameters for subgroups. The residual contribution is calculated with the equation:

$$\ln \gamma_j^R = \sum_t \nu_t^{(j)} \left[\ln \Gamma_t - \ln \Gamma_t^{(j)} \right], \quad (\text{B.45})$$

where Γ_t and $\Gamma_t^{(j)}$ are the group residual activity coefficients in the mixture and in a reference solution containing only compound j , a (hypothetical) pure liquid of j , respectively.

The expression for the residual activity coefficient of subgroup t is:

$$\ln \Gamma_t = Q_t \left[1 - \ln \left(\sum_m \Theta_m \psi_{m,t} \right) - \sum_m \left(\frac{\Theta_m \psi_{t,m}}{\sum_n \Theta_n \psi_{n,m}} \right) \right], \quad (\text{B.46})$$

with

$$\Theta_m = \frac{\Theta_m X_m}{\sum_n \Theta_n X_n}; \psi_{m,n} = e^{-a_{m,n}/T}, \quad (\text{B.47})$$

where Θ_m is the relative surface area fraction of subgroup m , X_m is the mole fraction of m in the mixture, and $\psi_{m,n}$ is the temperature dependent function of the subgroup interaction parameter $a_{m,n}$. Note that the subgroup interaction parameters are unsymmetrical, i.e. $a_{m,t} \neq a_{t,m}$. The sums are over all different subgroups.

Since ions are treated like solvent components in the SR terms, resulting activity coefficients Eq. B.41 are with respect to the symmetrical convention on mole fraction basis. For ions i , the unsymmetrical normalized activity coefficient is determined from:

$$\ln \gamma_i^{SR,(x),\infty} = \ln \gamma_i^{SR,(x)} - \ln \gamma_i^{SR,(x),ref}. \quad (\text{B.48})$$

The symmetrically normalized value at the reference state is computed from Eq. B.42 and Eq. B.46 by introducing the reference state conditions of the ions (setting $x_w = 1$, $\sum_s x_s = 0$ for $s \neq w$ and $\sum_i x_i = 0$)

$$\begin{aligned} \ln \gamma_i^{SR,(x),ref} = & \ln \frac{r_i}{r_w} + 1 - \frac{r_i}{r_w} + \frac{z}{2} q_i \left[\ln \left(\frac{r_w q_i}{r_i q_w} \right) - 1 + \frac{r_i q_w}{r_w q_i} \right] \\ & + q_i (1 - \ln \psi_{w,i} - \psi_{i,w}), \end{aligned} \quad (\text{B.49})$$

where subscript w stands for the reference solvent (water). The last term on the right-hand side of Eq. B.49, reflecting the residual part reference contribution, becomes zero as we defined the SR ion-solvent interactions to be zero.

B.6 Ming and Russell model

The final model which implemented in this PhD thesis is [Ming and Russel \(2002\)](#) model. The activity coefficients in this model are calculated as a sum of ion-water interactions (IW) and organic-water/organic-ion interactions (OW/OI).

$$\ln \gamma_i = \ln \gamma_i^{IW} + \ln \gamma_i^{OW/OI}. \quad (\text{B.50})$$

Ion-water interactions are calculated with the (Clegg et al., 1992) model and organic-water/organic-ion interactions are calculated with UNIFAC. If the organic concentration is zero, the new model is reduced to (Clegg et al., 1992) model and if the ion concentration is zero the model is reduced to UNIFAC (Fredenslund et al., 1975). Ion-water interaction are calculated with equations from (Clegg et al., 1992) as a sum of LR and SR contributions:

$$\ln \gamma_i^{IW} = \ln \gamma_i^{LR} + \ln \gamma_i^{SR}, \quad (\text{B.51})$$

Ming and Russel (2002) calculated the LR and SR activity coefficients using inorganic-only mole fractions x_i^* (LR^* and SR^*), where organics (subscript o) are ignored. The activity coefficients were then normalized to the solution mole fractions with the equation:

$$\ln \gamma_i^{IW} = \ln \gamma_i^{LR^*} + \ln \gamma_i^{SR^*} - 2 \ln \left(1 - \sum_o x_o \right). \quad (\text{B.52})$$

The long range contribution is a sum of Debye-Hückel (DH) contribution (Debye and Hückel, 1923) and a higher order electrostatic (HOE) contribution to the Debye-Hückel expression.

$$\ln \gamma_i^{LR} = \ln \gamma_i^{DH} + \ln \gamma_i^{HOE} \quad (\text{B.53})$$

The DH contribution of water w and ion i are calculated with equations:

$$\ln \gamma_w^{DH} = \frac{2A_x I_x^{3/2}}{1 + \rho \sqrt{I_x}} - \sum_c \sum_a x_c x_a \left[B_{ca} \exp(-\alpha_{ca} \sqrt{I_x}) + B_{ca}^1 \exp(-\alpha_{ca}^1 \sqrt{I_x}) \right], \quad (\text{B.54})$$

$$\begin{aligned} \ln \gamma_i^{DH} &= \frac{2A_x I_x^{3/2}}{1 + \rho \sqrt{I_x}} - \sum_c \sum_a x_c x_a \left[B_{ca} \exp(-\alpha_{ca} \sqrt{I_x}) + B_{ca}^1 \exp(-\alpha_{ca}^1 \sqrt{I_x}) \right] \\ &+ z_i^2 A_x \left(\frac{2}{\rho} \ln(1 + \rho \sqrt{I_x}) + \frac{\sqrt{I_x}}{1 + \rho \sqrt{I_x}} \right) \\ &+ \sum_{j \neq i} x_j \left(B_{ij} g(\alpha_{ij} \sqrt{I_x}) + B_{ij}^1 g(\alpha_{ij}^1 \sqrt{I_x}) \right) \\ &- \frac{z_i^2}{2I_x} \sum_c \sum_a x_c x_a \left[B_{ca} \left[g(\alpha_{ca} \sqrt{I_x}) - \exp(-\alpha_{ca} \sqrt{I_x}) \right] + \right. \\ &\left. + B_{ca}^1 \left[g(\alpha_{ca}^1 \sqrt{I_x}) - \exp(-\alpha_{ca}^1 \sqrt{I_x}) \right] \right]. \end{aligned} \quad (\text{B.55})$$

Where constant $\rho = 13.0$ and the temperature dependent mole fraction scale Debye-Hückel parameter A_x has a value 2.917 at 298.15 K. I_x is ionic strength in mole fraction scale and function $g(x) = \frac{2(1-(1+x)\exp(-x))}{x^2}$. Most of the symmetric ($B_{ij} = B_{ji}$) parameters are zeros: $B_{cc} = B_{aa} = B_{cc}^1 = B_{aa}^1 = 0$ and $\alpha_{cc} = \alpha_{aa} = \alpha_{cc}^1 = \alpha_{aa}^1 = 0$. Hence, the remaining model parameters for DH part are B_{ca} , $B_{ca}^1 = B_{aa}^1$, α_{ca} and α_{ca}^1 .

The HOE contribution for water w and ion i is needed if the solution have more than two ions (e.g. sulphuric acid). The equations are:

$$\ln \gamma_w^{HOE} = -2 \sum_c \sum_{<c'} x_c x_{c'} (\vartheta_{cc'} + I_x \vartheta'_{cc'}) - 2 \sum_a \sum_{<a'} x_a x_{a'} (\vartheta_{aa'} + I_x \vartheta'_{aa'}), \quad (\text{B.56})$$

$$\begin{aligned} \ln \gamma_i^{HOE} &= 2 \sum_{j \neq i} x_j \left[\vartheta_{ij} - x_i \left(\vartheta_{ij} + \vartheta'_{ij} \left(I_x - \frac{z_i^2}{2} \right) \right) \right] - 2 \sum_{c \neq i} \sum_{c' \neq i} x_c x_{c'} \left(\vartheta_{cc'} + \vartheta'_{cc'} \left(I_x - \frac{z_i^2}{2} \right) \right) \\ &- 2 \sum_{a \neq i} \sum_{a' \neq i} x_a x_{a'} \left(\vartheta_{aa'} + \vartheta'_{aa'} \left(I_x - \frac{z_i^2}{2} \right) \right), \end{aligned} \quad (\text{B.57})$$

where subscript j includes all cations if i is a cation or all anions if i is a anion, and

$$\vartheta_{ij} = \frac{z_i z_j}{4I_x} \left[J(x_{ij}) - \frac{1}{2}J(x_{ii}) - \frac{1}{2}J(x_{ji}) \right], \quad (\text{B.58})$$

$$J(x_{ij}) = \frac{x_{ij}}{4 + C_1 x_{ij}^{C_2} \exp(C_3 x_{ij}^{C_4})}, \quad (\text{B.59})$$

$$x_{ij} = 6z_i z_j A_x \sqrt{I_x} \quad (\text{B.60})$$

The constants are $C_1 = 4.581$, $C_2 = -0.7237$, $C_3 = -0.012$ and $C_4 = 0.528$. Derivatives are $\vartheta'_{ij} = \frac{\partial \vartheta_{ij}}{\partial I_x}$ and $J'(x_{ij}) = \frac{\partial J(x_{ij})}{\partial I_x}$. The short range contributions for water w , cation C and anion A are calculated with following equations.

$$\begin{aligned} \ln \gamma_w^{SR} = & \sum_c \sum_a \left(\frac{1}{F} E_c E_a \frac{z_a + z_c}{z_a z_c} (1 - x_w) W_{ca} + x_c x_a \frac{(z_a + z_c)^2}{z_a z_c} (1 - 2x_w) U_{ca} \right. \\ & \left. + 4x_c x_a x_w (2 - 3x_w) V_{ca} \right), \end{aligned} \quad (\text{B.61})$$

$$\begin{aligned} \ln \gamma_C^{SR} = & \sum_a \sum_{c \neq C} E_a \left[\frac{z_C}{2} E_C \frac{z_a + z_c}{z_a z_c} W_{ca} \right] - \sum_a \sum_c \left[x_w E_c E_a \left(\frac{z_C}{2} + \frac{1}{F} \right) \frac{z_a + z_c}{z_a z_c} W_{ca} \right. \\ & \left. + 2x_w x_c x_a \frac{(z_a + z_c)^2}{z_a z_c} U_{ca} + 12x_w^2 x_c x_a V_{ca} \right] + \sum_a \left[x_w E_a \frac{z_a + z_C}{z_a} W_{Ca} \right. \\ & \left. + x_w x_a \frac{(z_a + z_C)^2}{z_a z_C} U_{Ca} + 4x_w^2 x_a V_{Ca} - E_a \left(1 - \frac{E_C}{2} \right) \frac{z_a + z_C}{z_a} W_{Ca} \right], \end{aligned} \quad (\text{B.62})$$

$$\begin{aligned} \ln \gamma_A^{SR} = & \sum_c \sum_{a \neq A} E_c \left[\frac{z_A}{2} E_a \frac{z_a + z_c}{z_a z_c} W_{ca} \right] - \sum_c \sum_a \left[x_w E_c E_a \left(\frac{z_A}{2} + \frac{1}{F} \right) \frac{z_a + z_c}{z_a z_c} W_{ca} \right. \\ & \left. + 2x_w x_c x_a \frac{(z_a + z_c)^2}{z_a z_c} U_{ca} + 12x_w^2 x_c x_a V_{ca} \right] + \sum_c \left[x_w E_c \frac{z_c + z_A}{z_c} W_{Ca} \right. \\ & \left. + x_w x_a \frac{(z_a + z_C)^2}{z_a z_C} U_{Ca} + 4x_w^2 x_a V_{Ca} - E_a \left(1 - \frac{E_C}{2} \right) \frac{z_a + z_C}{z_a} W_{Ca} \right], \end{aligned} \quad (\text{B.63})$$

where lower case letters refer to any other cation and anion, $E_c = \frac{x_c z_c}{\sum_c x_c z_c}$, $E_a = \frac{x_a z_a}{\sum_a x_a z_a}$. The parameters for the SR part are symmetric i.e. W_{ca} , U_{ca} and V_{ca} . These equations give ion activity coefficients in mole fraction scale, so these must be converted to molality scale with Eq. B.28. Parameters for IW part were collected from Clegg et al. (1992); Clegg and Brimblecombe (1995); Clegg et al. (1998a).

OW/OI interactions are calculated with UNIFAC (Fredenslund et al., 1975). Also here, the ion activity coefficients are normalized to infinite dilution reference state and from mole fraction scale to molality scale with Eq. B.28. In this model, surface area and volume parameters for ions were the same as for water, and all ion-water and ion-ion interaction parameters were zeros (see Ming and Russel (2002)). Hence, the OW/OI contribution for water and electrolytes is zero if the organic fraction is zero. The same values were used in the current implementation.

Appendix C

Multiphase processing in aqueous particles and clouds (Supplementary material to Chapter. 6.2)

C.1 Modeled activity coefficients

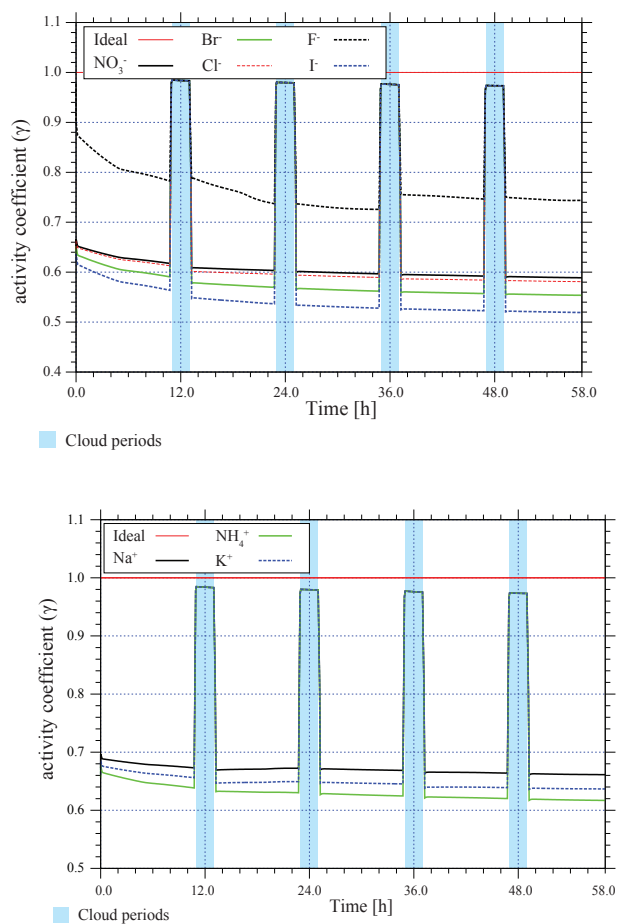


Figure C.1: Modeled activity coefficients of inorganic ions vs. modeling time for urban scenario for the simulations 90%-IDU vs. 90%-NIDU.

C.2 Multiphase processing of inorganic compounds

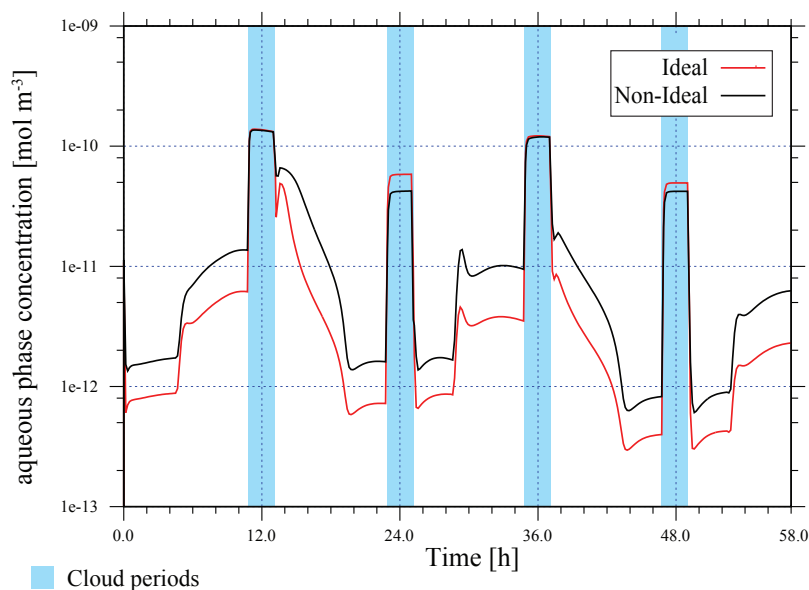


Figure C.2: Modeled Fe(II) aqueous phase concentration in mol l^{-1} vs. modeling time for the remote scenario for the simulations 90%-IDR vs. 90%-NIDR.

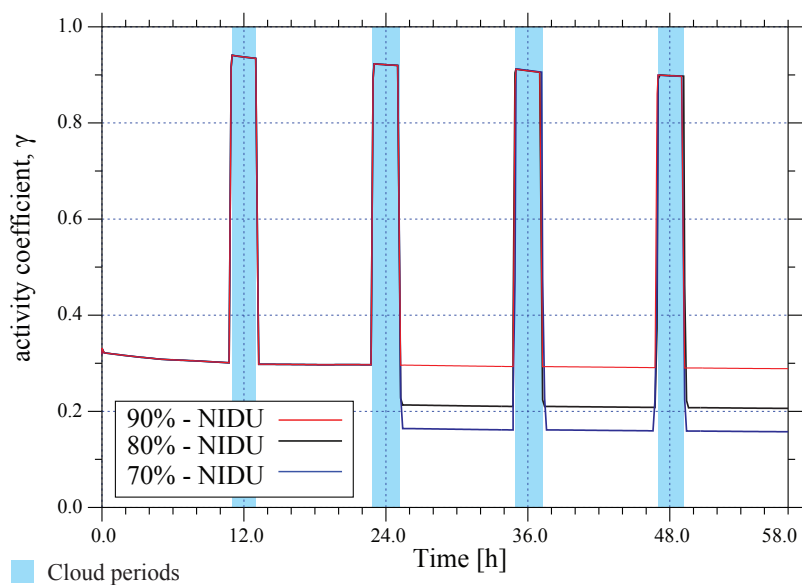


Figure C.3: Modeled activity coefficients of Fe(II) vs. modeling time for urban scenario at three different relative humidity levels. (—) Basecase (90% RH), (—) 80% RH, (—) 70% RH.

Table C.1: Integrated percentage contributions of the most important Fe(II) sources and sink reactions for the remote case classified regarding to the various microphysical conditions during the simulation time (Total = Total contributions throughout the simulation time, Total clouds = Contribution throughout all cloud events, Aqueous aerosol particles = Contribution through out the deliquescent particle conditions, Δ Difference = Difference between the aqueous phase particle fluxes (90%-NIDR - 90%-IDR), only sinks and sources with a contribution larger than \pm % presented.)

| Reaction | Ideal | | Non-ideal | | Δ Difference |
|--|---------|----------------|-----------|-------------------|---------------------|
| | Total | Aqueous clouds | Total | Aqueous particles | |
| $\text{FeOH}^{2+} + h\nu \rightarrow \text{Fe}^{2+} + \text{HO}$ | 8.7% | 11.2% | 9.2% | 11.3% | 0.7% |
| $\text{Fe}(\text{C}_2\text{O}_4)_2^- \rightarrow$ | 4.4% | 0.2% | 4.6% | 0.3% | 0.4% |
| $\text{H}_2\text{O}_2 + \text{Fe}^{2+} \rightarrow$ | -53.1% | -43.0% | -51.7% | -41.9% | 1.1% |
| $\text{O}_2^- + \text{Fe}^{3+} \rightarrow$ | 1.0% | 1.5% | 1.0% | 1.5% | 0.0% |
| $\text{O}_2^- + \text{FeOH}^{2+} \rightarrow$ | 45.9% | 72.9% | 47.2% | 72.9% | 1.4% |
| $\text{O}_2^- + \text{FeOH}^+ \rightarrow$ | 3.6% | 6.4% | 3.8% | 6.5% | 0.0% |
| $\text{O}_2^- + \text{Fe}^{2+} \rightarrow$ | -18.9% | -31.6% | -20.0% | -32.5% | -0.6% |
| $\text{Fe}^{3+} + \text{Cu}^+ \rightarrow \text{Fe}^{2+} + \text{Cu}^{2+}$ | 25.5% | 0.1% | 24.7% | 0.1% | -0.3% |
| $\text{FeOH}^{2+} + \text{Cu}^+ \rightarrow$ | 9.8% | 6.3% | 8.5% | 6.0% | -2.5% |
| $\text{HSO}_5^- + \text{Fe}^{2+} \rightarrow \text{SO}_4^- + \text{FeOH}^{2+}$ | -1.6% | -3.3% | -1.7% | -3.4% | 0.0% |
| $\text{Fe}^{2+} + \text{CH}_3\text{O}_2 \rightarrow \text{Fe}(\text{CH}_3\text{O}_2)^{2+}$ | -8.3% | -11.0% | -8.6% | -11.1% | -0.3% |
| $\text{HO}_2 + \text{Fe}^{2+} \rightarrow$ | -4.9% | -7.3% | -5.3% | -7.4% | -0.5% |
| $\text{OH} + \text{Fe}^{2+} \rightarrow \text{FeOH}^{2+}$ | -0.4% | -0.3% | -0.3% | -0.3% | 0.0% |
| $\text{Fe}^{2+} + \text{O}_3 \rightarrow \text{FeO}^{2+} + \text{O}_2$ | -1.1% | -1.6% | -1.1% | -1.5% | 0.1% |
| $\text{Fe}^{2+} + \text{SO}_4^- \rightarrow$ | -7.9% | -1.1% | -7.2% | -1.1% | 0.9% |
| $\text{Cl}_2^- + \text{Fe}^{2+} \rightarrow \text{Cl}^- + \text{Fe}^{3+}$ | -1.7% | 0.0% | -2.1% | 0.0% | -1.0% |
| $\text{Cl}_2^- + \text{Fe}^{2+} \rightarrow \text{FeCl}^{2+} + \text{Cl}^-$ | -0.6% | 0.0% | -0.77% | 0.0% | -0.4% |
| $\text{Br}_2^- + \text{Fe}^{2+} \rightarrow \text{Br}^- + \text{Fe}^{3+}$ | -1.1% | 0.0% | -0.8% | 0.0% | 0.7% |
| Total Sources | 100.0% | 100.0% | 100.0% | 100.0% | 100.0% |
| Total Sinks | -100.0% | -100.0% | -100.0% | -100.0% | -100.0% |

C.3 Multiphase processing of radical oxidants

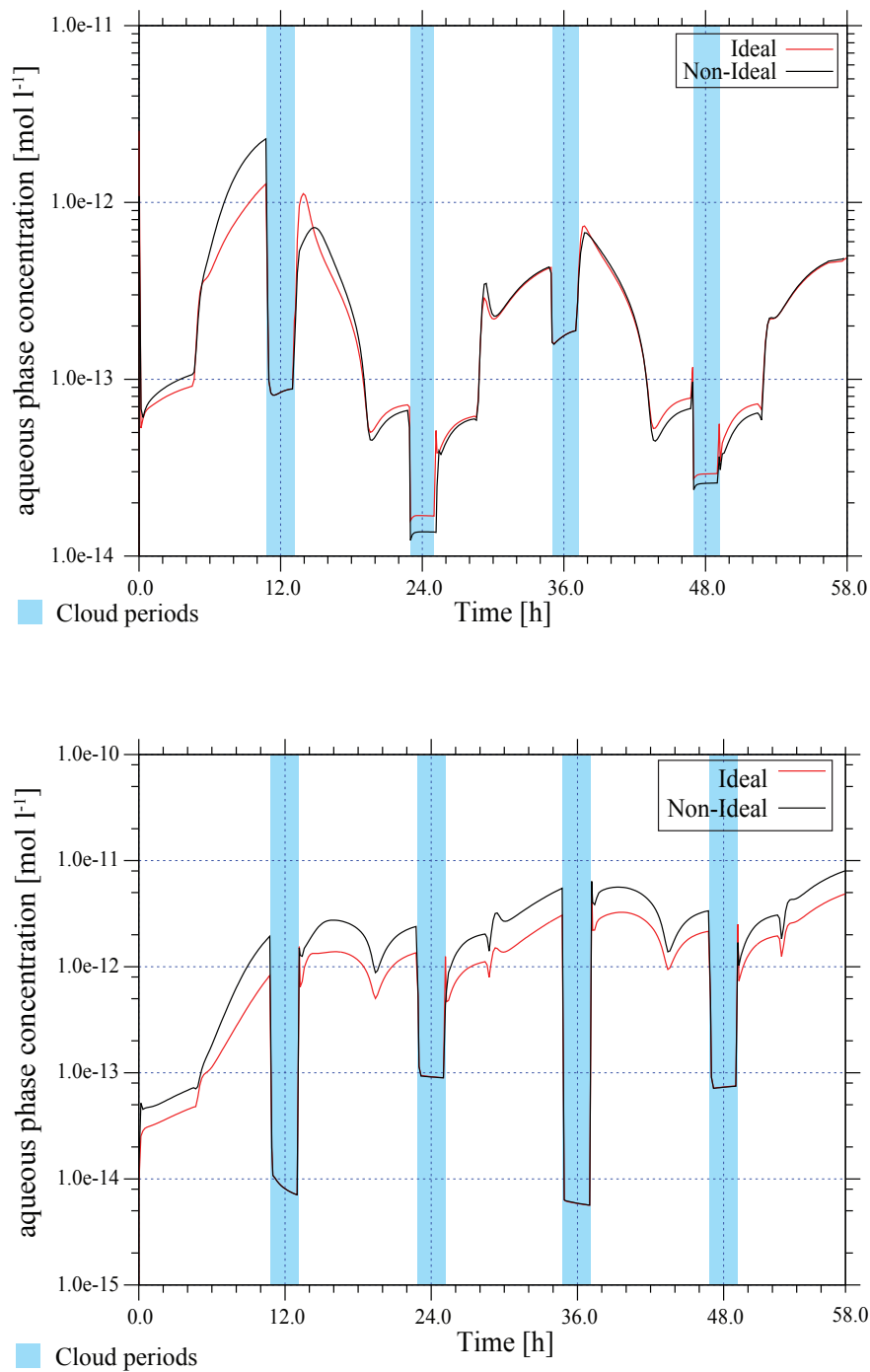


Figure C.4: Modeled OH (top) and NO₃ (bottom) aqueous phase concentration in mol l⁻¹ vs. modeling time for the remote scenario for the simulations 90%-IDR vs. 90%-NIDR.

Table C.2: Integrated percentage contributions of the most important OH radical sources and sink reactions for the remote case classified regarding to the various microphysical conditions during the simulation time (Total = Total contributions throughout the simulation time, Total clouds = Contribution throughout all cloud events, Aqueous aerosol particles = Contribution through out the deliquescent particle conditions, Δ Difference = Difference between the aqueous phase particle fluxes (90%-NIDR - 90%-IDR), only sinks and sources with a contribution larger than \pm % presented)

| Reaction | Ideal | | Non-ideal | | Δ Difference in Aqueous particle fluxes |
|--|--------|----------------|-----------|----------------|--|
| | Total | Aqueous clouds | Total | Aqueous clouds | |
| phase transfer: $\text{OH} \rightleftharpoons \text{OH}_{(aq)}$ | 25.8% | 36.0% | 27.2% | 34.8% | 1.4% |
| $\text{Cl}^- + \text{OH} \rightleftharpoons \text{ClOH}^-$ | -12.8% | 1.62% | -12.1% | 2.2% | 0.4% |
| $\text{Br}^- + \text{OH} \rightleftharpoons \text{BrOH}^-$ | -1.7% | 0.0% | -0.8% | 0.0% | 1.8% |
| $\text{FeOH}^{2+} + h\nu \rightarrow \text{Fe}^{2+} + \text{OH}$ | 7.4% | 8.6% | 7.5% | 7.9% | 0.5% |
| $\text{H}_2\text{O}_2 \rightarrow \text{OH} + \text{OH}$ | 8.6% | 10.3% | 9.4% | 10.3% | 0.5% |
| $\text{H}_2\text{O}_2 + \text{Fe}^{2+} \rightarrow \text{Fe}^{3+} + \text{OH} + \text{OH}^-$ | 45.0% | 28.3% | 41.7% | 29.0% | -3.8% |
| $\text{H}_2\text{O}_2 + \text{Cu}^+ \rightarrow$ | 6.0% | 7.0% | 6.7% | 7.5% | 0.9% |
| $\text{OH} + \text{HSO}_4^- \rightarrow$ | -0.5% | 0.0% | -0.3% | 0.0% | 0.4% |
| $\text{OH} + \text{CH}_2(\text{OH})\text{COOH} \rightarrow$ | -1.9% | -0.4% | -1.9% | -0.4% | -0.2% |
| $\text{OH} + \text{CH}_2(\text{OH})\text{COO}^- \rightarrow$ | -0.6% | -1.0% | -0.6% | -1.0% | 0.0% |
| $\text{OH} + \text{OHCCH}_2(\text{OH}) \rightarrow$ | -0.7% | -1.2% | -0.8% | -1.2% | 0.0% |
| $\text{OH} + \text{CH}(\text{OH})_2\text{CH}_2(\text{OH}) \rightarrow$ | -2.1% | -3.4% | -2.2% | -3.5% | 0.0% |
| $\text{OH}_3 \rightarrow \text{OH} + \text{O}_2$ | 5.1% | 7.2% | 5.5% | 7.6% | 0.3% |
| $\text{OH} + \text{H}_2\text{O}_2 \rightarrow$ | -6.4% | -6.6% | -6.7% | -6.6% | 0.0% |
| $\text{OH} + \text{CH}_3\text{OH} \rightarrow$ | -3.1% | -3.8% | -3.2% | -3.8% | -0.1% |
| $\text{OH} + \text{CH}_2(\text{OH})_2 \rightarrow$ | -35.7% | -47.1% | -36.5% | -47.4% | -0.8% |
| $\text{OH} + \text{HCOO}^- \rightarrow$ | -23.8% | -28.4% | -24.2% | -28.1% | -1.1% |
| $\text{OH} + \text{CH}(\text{OH})_2\text{CH}(\text{OH})_2 \rightarrow$ | -1.5% | -2.3% | -1.5% | -2.3% | 0.0% |
| $\text{OH} + \text{CH}(\text{OH})_2\text{COOH} \rightarrow$ | -3.0% | -0.1% | -2.8% | -0.1% | 0.0% |
| $\text{OH} + \text{CH}_3\text{C}(\text{O})\text{CH}(\text{OH})_2 \rightarrow$ | -0.8% | -1.1% | -0.9% | -1.1% | 0.0% |
| Total Sources | 100.0% | 100.0% | 100.0% | 100.0% | 100.0% |

Table C.2: Integrated percentage contributions of the most important OH radical sources and sink reactions for the remote case (Continued)

| Reaction | Ideal | | Non-ideal | | Δ Difference in Aqueous particle fluxes |
|-------------|-----------------|----------------------|-----------------|----------------------|--|
| | Total clouds | Aqueous particles | Total clouds | Aqueous particles | |
| Total Sinks | -100.0% | -100.0% | -100.0% | -100.0% | -100.0% |

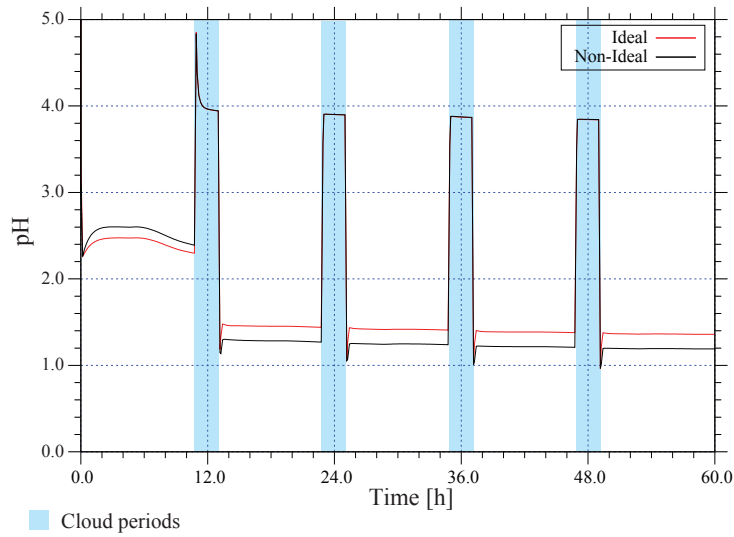


Figure C.5: Modeled pH value as a function of time for the remote environmental conditions for the simulations 90%-IDR vs. 90%-NIDR.

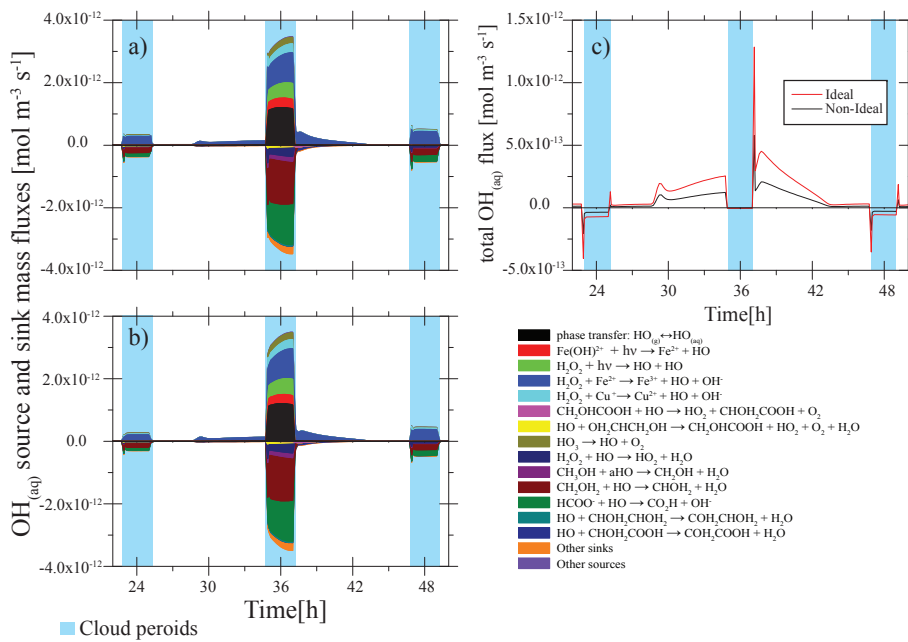


Figure C.6: Modeled chemical sinks and sources mass fluxes of OH in aqueous phase in $\text{mol m}^{-3} \text{ s}^{-1}$ for the second day of modeling time for the remote scenario for the simulations 90%-IDR vs. 90%-NIDR. a) ideal solutions (90%-IDR), b) non-ideal solutions (90%-NIDR), c) corresponding total fluxes. Only sinks and sources with a contribution larger than $\pm 1\%$ presented.

Table C.3: Integrated percentage contributions of the most important NO_3 radical sources and sink reactions for the remote case classified regarding to the various microphysical conditions during the simulation time ($\text{Total} = \text{Total contributions throughout the simulation time}$, $\text{Total clouds} = \text{Contribution throughout all cloud events}$, $\text{Aqueous aerosol particles} = \text{Contribution through out the deliquescent particle conditions}$, Δ Difference = Difference between the aqueous phase particle fluxes (90%-NIDR - 90%-IDR), only sinks and sources with a contribution larger than \pm % presented)

| Reaction | Ideal | | Non-ideal | | Δ Difference |
|---|---------|--------------------------|-----------|--------------------------|---------------------|
| | Total | Aqueous clouds particles | Total | Aqueous clouds particles | |
| phase transfer: $\text{NO}_3 \rightleftharpoons \text{NO}_{3(aq)}$ | 11.4% | 98.9% | -0.7% | 99.0% | -14.9% |
| $\text{NO}_3 + \text{Cl}^- \rightleftharpoons \text{NO}_3^- + \text{Cl}$ | 58.2% | -51.3% | 62.3% | -50.7% | 4.8% |
| $\text{NO}_3 + \text{HSO}_4^- \rightarrow \text{NO}_3^- + \text{H}^+ + \text{SO}_4^-$ | -36.5% | -0.0% | -33.4% | -0.0% | 4.1% |
| $\text{NO}_3 + \text{SO}_4^{2-} \rightarrow \text{NO}_3^- + \text{SO}_4^-$ | -6.5% | -0.7% | -4.1% | -0.7% | 3.0% |
| $\text{SO}_4^- + \text{NO}_3^- \rightarrow \text{SO}_4^{2-} + \text{NO}_3$ | 4.0% | 0.1% | 2.5% | 0.1% | -1.9% |
| $\text{Br}^- + \text{NO}_3 \rightarrow \text{NO}_3^- + \text{Br}$ | -9.4% | -0.5% | -4.6% | -0.3% | 6.0% |
| $\text{NO}_3 + \text{CH}_3\text{C}(\text{O})\text{CH}(\text{OH})_2 \rightarrow$ | -0.6% | -2.5% | -0.5% | -2.5% | 0.0% |
| $\text{NO}_3 + \text{CH}_3\text{C}(\text{O})\text{COO}^- \rightarrow$ | -3.2% | -1.2% | -3.6% | -1.2% | -0.4% |
| $\text{NO}_3 + \text{CH}_2\text{OHCOO}^- \rightarrow$ | -1.6% | -4.9% | -1.7% | -4.6% | -0.1 % |
| $\text{NO}_3 + \text{HOCH}_2\text{C}(\text{O})\text{COO}^- \rightarrow$ | -0.9% | -0.3% | -0.9% | -0.4% | 0.0% |
| $\text{NO}_3 + \text{CHOC}(\text{O})\text{COO}^- \rightarrow$ | -6.0% | -1.7% | -5.7% | -1.8% | 0.4% |
| $\text{NO}_3 + \text{H}_2\text{O}_2 \rightarrow$ | -5.8% | -25.5% | -6.1% | -26.2% | -0.3% |
| $\text{HCOO}^- + \text{NO}_3 \rightarrow$ | -1.7% | -7.7% | -1.6% | -7.5% | 0.0% |
| Total Sources | 100.0% | 100.0% | 100.0% | 100.0% | 100.0% |
| Total Sinks | -100.0% | -100.0% | -100.0% | -100.0% | -100.0% |

C.4 Aqueous multiphase processing of organic compounds

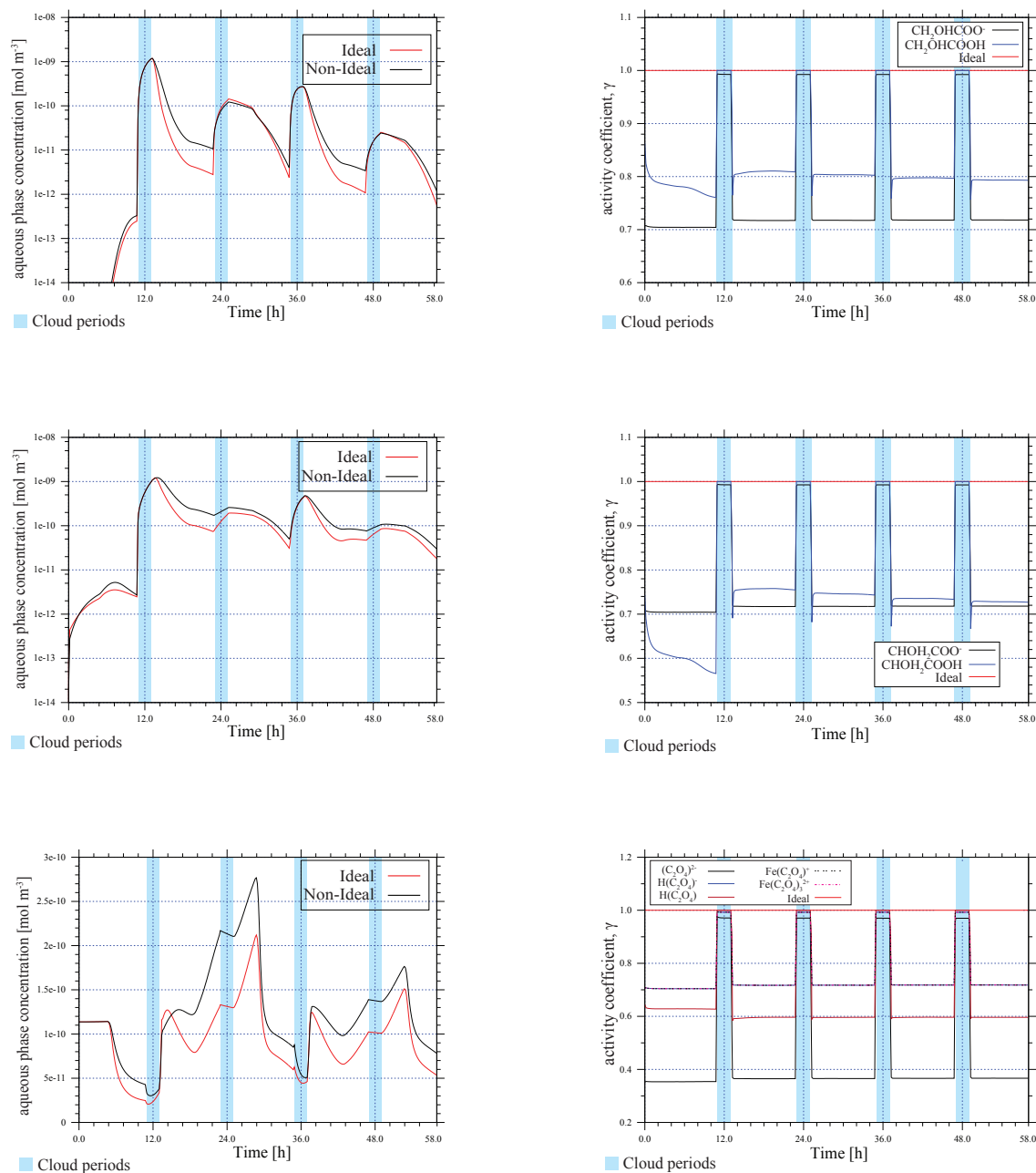


Figure C.7: Modeled aqueous phase mol m⁻³_(air) and corresponding activity coefficients for the most important C₂ oxidation products for the remote scenario for the simulations 90%-IDU vs. 90%-NIDU, Glycolic acid (top), Glyoxylic acid (center), Oxalic acid (bottom).

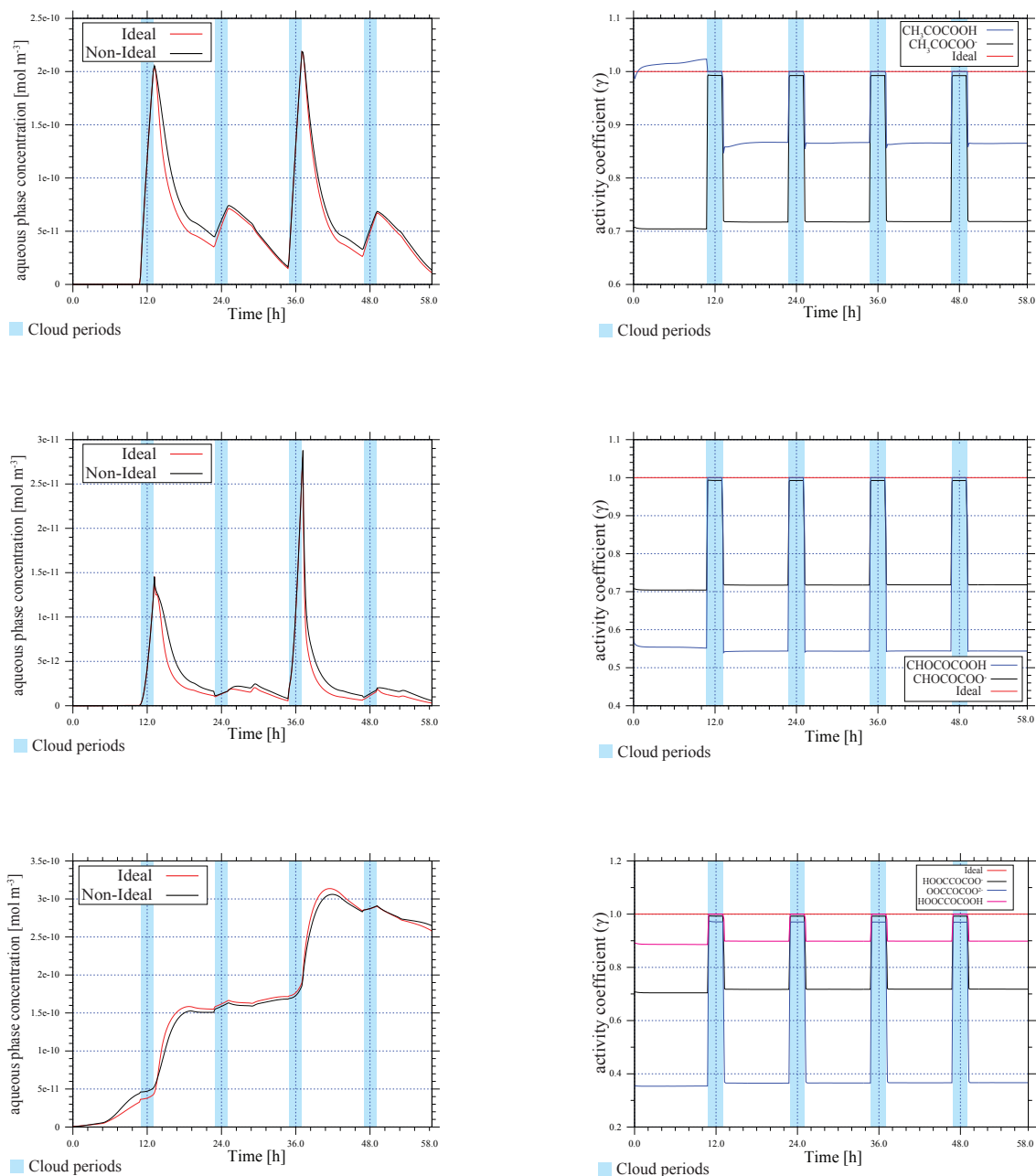


Figure C.8: Modeled aqueous phase $\text{mol m}^{-3}_{(air)}$ and corresponding activity coefficients for the most important C_3 oxidation products for the remote scenario for the simulations 90%-IDU vs. 90%-NIDU, Pyruvic acid (top), Oxopyruvic acid (center), Ketomalonic acid (bottom)

C.5 Activity coefficient parameters

Table C.6: Binary cation-anion MR interaction parameters (Zuend et al., 2008).

| Cation | Anion | $b_{c,a}^{(1)}$ (kg mol ⁻¹) | $b_{c,a}^{(2)}$ (kg mol ⁻¹) | $b_{c,a}^{(3)}$ (kg ^{1/2} mol ^{-1/2}) | $c_{c,a}^{(1)}$ (kg ² mol ⁻²) | $c_{c,a}^{(2)}$ (kg ^{1/2} mol ^{-1/2}) |
|-----------|-------------|--|--|---|---|---|
| H^+ | Cl^- | 0.182003 | 0.243340 | 0.8 | 0.033319 | 0.504672 |
| H^+ | Br^- | 0.120325 | 0.444859 | 0.8 | 0.080767 | 0.596776 |
| H^+ | NO_3^- | 0.210638 | 0.122694 | 0.8 | -0.101736 | 1.676420 |
| H^+ | SO_4^{2-} | 0.097108 | -0.004307 | 1.0 | 0.140598 | 0.632246 |
| H^+ | HSO_4^- | 0.313812 | -4.895466 | 1.0 | -0.358419 | 0.807667 |
| Li^+ | Cl^- | 0.106555 | 0.206370 | 0.8 | 0.053239 | 0.535548 |
| Li^+ | Br^- | 0.106384 | 0.316480 | 0.8 | 0.057602 | 0.464658 |
| Li^+ | NO_3^- | 0.076313 | 0.300550 | 0.8 | 0.046701 | 0.664928 |
| Li^+ | SO_4^{2-} | 0.114470 | 0.035401 | 0.8 | -0.263258 | 1.316967 |
| Na^+ | Cl^- | 0.053741 | 0.079771 | 0.8 | 0.024553 | 0.562981 |
| Na^+ | Br^- | 0.180807 | 0.273114 | 0.8 | -0.506578 | 2.209050 |
| Na^+ | NO_3^- | 0.001164 | -0.102546 | 0.410453 | 0.002535 | 0.512657 |
| Na^+ | SO_4^{2-} | 0.001891 | -0.424184 | 0.8 | -0.223851 | 1.053620 |
| Na^+ | HSO_4^- | 0.021990 | 0.001863 | 0.8 | 0.019921 | 0.619816 |
| K^+ | Cl^- | 0.016561 | -0.002752 | 0.8 | 0.020833 | 0.670530 |
| K^+ | Br^- | 0.033688 | 0.060882 | 0.8 | 0.015293 | 0.565063 |
| K^+ | NO_3^- | 0.000025 | -0.413172 | 0.357227 | -0.000455 | 0.342244 |
| K^+ | SO_4^{2-} | 0.004079 | -0.869936 | 0.8 | -0.092240 | 0.918743 |
| NH_4^+ | Cl^- | 0.001520 | 0.049074 | 0.116801 | 0.011112 | 0.653256 |
| NH_4^+ | Br^- | 0.002498 | 0.081512 | 0.143621 | 0.013795 | 0.728984 |
| NH_4^+ | NO_3^- | -0.000057 | -0.171746 | 0.260000 | 0.005510 | 0.529762 |
| NH_4^+ | SO_4^{2-} | 0.000373 | -0.906075 | 0.545109 | -0.000379 | 0.354206 |
| NH_4^+ | HSO_4^- | 0.009054 | 0.214405 | 0.228956 | 0.017298 | 0.820465 |
| Mg^{2+} | Cl^- | 0.195909 | 0.332387 | 0.8 | 0.072063 | 0.397920 |
| Mg^{2+} | NO_3^- | 0.430671 | 0.767242 | 0.8 | -0.511836 | 1.440940 |
| Mg^{2+} | SO_4^{2-} | 0.122364 | -3.425876 | 0.8 | -0.738561 | 0.864380 |
| Ca^{2+} | Cl^- | 0.104920 | 0.866923 | 0.8 | 0.072063 | 0.365747 |
| Ca^{2+} | NO_3^- | 0.163282 | 0.203681 | 0.8 | -0.075452 | 1.210906 |

Table C.7: Additional aqueous electrolyte interaction parameters $R_{c,c'}$ and $Q_{c,c',a}$ (Zuend et al., 2008)

| Cation | Anion | a | R (kg mol ⁻¹) | Q (kg ² mol ⁻²) |
|----------|-------|-----------|------------------------------|---|
| NH_4^+ | H^+ | 0.0 | -0.220938 | 0.0 |
| NH_4^+ | H^+ | HSO_4^- | 0.0 | 0.002414 |

Table C.8: AIOMFAC binary MR parameters of organic-inorganic interactions between the functional main groups and the ions. (Zuend et al., 2008).

| k | ion (i) | $\mathbf{b}_{k,i}^{(1)}$ | $\mathbf{b}_{k,i}^{(2)}$ |
|-----------------|-------------------------------|--------------------------|--------------------------|
| CH _n | Li ⁺ | 0.242840 | 0.004770 |
| OH | Li ⁺ | -0.029646 | -1.033024 |
| CH _n | Na ⁺ | 0.124972 | -0.031880 |
| OH | Na ⁺ | 0.080254 | 0.002201 |
| CH _n | K ⁺ | 0.121449 | 0.015499 |
| OH | K ⁺ | 0.065219 | -0.170779 |
| CH _n | NH ₄ ⁺ | 0.103096 | -0.006344 |
| OH | NH ₄ ⁺ | 0.039373 | 0.001083 |
| CH _n | Ca ²⁺ | 0.000019 | -0.060807 |
| OH | Ca ²⁺ | 0.839628 | -0.765776 |
| CH _n | Cl ⁻ | 0.014974 | 0.142574 |
| OH | Cl ⁻ | -0.042460 | -0.128063 |
| CH _n | Br ⁻ | 0.000042 | -0.025473 |
| OH | Br ⁻ | -0.007153 | 0.483038 |
| CH _n | NO ₃ ⁻ | 0.018368 | 0.669086 |
| OH | NO ₃ ⁻ | -0.128216 | -0.962408 |
| CH _n | SO ₄ ²⁻ | 0.101044 | -0.070253 |
| OH | SO ₄ ²⁻ | 4 -0.164709 | 0.574638 |

Table C.9: Modified LIFAC binary MR interaction parameters of organic ↔ inorganic interactions between the functional main groups and the ions. (Kiepe et al., 2006).

| k | ion (i) | $\mathbf{b}_{k,ion}^a$ | $\mathbf{c}_{k,ion}^b$ |
|--------------------|----------------------------------|------------------------|------------------------|
| OH | Ca ²⁺ | 0.56414 | -0.00972 |
| CH _n | Na ⁺ | 0.12850 | -0.17353 |
| CH _n | Mg ²⁺ | -0.34610 | -0.44995 |
| CH _n | Zn ²⁺ | -0.10163 | -0.06578 |
| CH _n | F ⁻ | 0.07614 | -0.28255 |
| CH _n | CH ₃ COO ⁻ | 0.09461 | -0.02404 |
| OH | Zn ²⁺ | 0.03648 | 0.02249 |
| OH | F ⁻ | 0.15233 | -0.04145 |
| OH | I ⁻ | -0.04479 | 0.04151 |
| OH | CH ₃ COO ⁻ | 0.02672 | -0.02117 |
| CH ₂ CO | Li ⁺ | -0.44806 | 1.17835 |
| CH ₂ CO | Na ⁺ | -0.21019 | 0.94813 |
| CH ₂ CO | K ⁺ | -0.44195 | 1.10287 |
| CH ₂ CO | Cl ⁻ | 0.54064 | -0.62981 |

Table C.9: Modified LIFAC binary MR interaction parameters (Continued)

| k | ion (i) | $b_{k,ion}^a$ | $c_{k,ion}^b$ |
|--------------------|----------------------------------|---------------|---------------|
| CH ₂ CO | Br ⁻ | 0.48898 | -0.96778 |
| CH ₂ CO | I ⁻ | 0.08245 | 0.03292 |
| CH ₂ CO | CH ₃ COO ⁻ | 0.26560 | -0.93032 |
| CH ₃ OH | Li ⁺ | 0.21353 | -0.03937 |
| CH ₃ OH | Na ⁺ | 0.16617 | 0.03928 |
| CH ₃ OH | K ⁺ | 0.10797 | 0.19164 |
| CH ₃ OH | Ca ²⁺ | 0.37818 | 0.00247 |
| CH ₃ OH | NH ₄ ⁺ | 0.20529 | -0.10550 |
| CH ₃ OH | Cu ²⁺ | 0.00789 | -0.06944 |
| CH ₃ OH | Zn ²⁺ | 0.16775 | -0.44229 |
| CH ₃ OH | F ⁻ | 0.07436 | -0.04388 |
| CH ₃ OH | Cl ⁻ | -0.03352 | 0.00242 |
| CH ₃ OH | Br ⁻ | -0.00944 | -0.06080 |
| CH ₃ OH | I ⁻ | -0.02090 | -0.14894 |
| CH ₃ OH | OH ⁻ | -0.01664 | 0.48879 |
| CH ₃ OH | NO ⁻ | -0.07716 | -0.00669 |

^{a,b} Values are assigned to 0 for the remaining organic ↔ ion interaction parameters.

Table C.10: Relative van der Waals subgroup volume (R_t) and surface area (Q_t) parameters for solvent subgroups used in this study (source *E-AIM*)

| | Family name | Main group (k) | Subgroup (t) | R_t | Q_t |
|------------|--------------------|----------------------------------|---------------------|--------|-------|
| G1 | Alkane | CH _n (n = 0, 1, 2, 3) | CH ₃ | 0.9011 | 0.848 |
| | | | CH ₂ | 0.6744 | 0.540 |
| | | | CH | 0.4469 | 0.228 |
| | | | C | 0.2195 | 0.000 |
| G2 | Alcohol | OH | OH | 1.0000 | 1.200 |
| G3 | Water | H ₂ O | H ₂ O | 0.9200 | 1.400 |
| G4 | Methanol | CH ₃ OH | CH ₃ OH | 1.4311 | 1.432 |
| G5 | Carbonyl | CH ₂ CO | CH ₃ CO | 1.6724 | 1.488 |
| | | | CH ₂ CO | 1.4457 | 1.180 |
| G6 | Aldehyde | CHO | CHO | 0.9980 | 0.948 |
| G7 | Acetate | CCOO | CH ₃ COO | 1.9031 | 1.728 |
| | | | CH ₂ COO | 1.6764 | 1.420 |
| G8 | Formate | HCOO | HCOO | 1.2420 | 1.188 |
| G9 | Ether | CH ₂ O | CH ₃ O | 1.1450 | 1.088 |
| | | | CH ₂ O | 0.9183 | 0.780 |
| | | | CH-O | 0.6908 | 0.468 |
| G10 | Carboxylic acid | COOH | COOH | 1.3013 | 1.224 |
| | | | HCOOH | 1.5280 | 1.532 |

Table C.11: Relative van der Waals subgroup volume (R_t^H) and surface area (Q_t^H) parameters for cations and anions considering dynamic hydration.

| Ion | ADHN ^a | R_t | Q_t | $R_t^{H^c}$ | $Q_t^{H^c}$ | Reference |
|---|-------------------|-------|-------|-------------|-------------|---------------------|
| H ⁺ | 1.93 | 0.0 | 0.0 | 1.78 | 2.70 | Zuend et al. (2008) |
| Na ⁺ | 0.22 | 0.18 | 0.18 | 0.38 | 0.62 | Zuend et al. (2008) |
| K ⁺ | 0.00 | 0.44 | 0.58 | 0.440 | 0.58 | Zuend et al. (2008) |
| NH ₄ ⁺ | 0.00 | 0.69 | 0.78 | 0.69 | 0.78 | Zuend et al. (2008) |
| Mg ²⁺ | 5.85 | 0.06 | 0.16 | 5.44 | 8.35 | Zuend et al. (2008) |
| Ca ²⁺ | 2.10 | 0.31 | 0.46 | 2.24 | 3.40 | Zuend et al. (2008) |
| Fe ²⁺ | 0.00 | 0.90 | 0.84 | 0.901 | 0.84 | – ^d |
| Cu ²⁺ | 0.00 | 0.13 | 0.26 | 0.13 | 0.26 | Kiepe et al. (2006) |
| Mn ²⁺ | 0.00 | 0.90 | 0.84 | 0.901 | 0.84 | – ^d |
| Zn ²⁺ | 2.18 | 0.12 | 0.24 | 2.12 | 3.29 | Kiepe et al. (2006) |
| Cl [–] | 0.00 | 0.99 | 0.99 | 0.99 | 0.99 | Zuend et al. (2008) |
| Br [–] | 0.00 | 1.25 | 1.16 | 1.25 | 1.16 | Zuend et al. (2008) |
| NO ₃ [–] | 0.00 | 0.95 | 0.97 | 0.95 | 0.97 | Zuend et al. (2008) |
| HSO ₄ [–] | 0.00 | 1.65 | 1.40 | 1.65 | 1.40 | Zuend et al. (2008) |
| SO ₄ ^{2–} | 1.83 | 1.66 | 1.40 | 3.34 | 3.96 | Zuend et al. (2008) |
| OH [–] | 2.80 | 1.16 | 1.27 | 3.74 | 5.196 | Kiepe et al. (2006) |
| CO ₃ ^{2–} | 0.00 | 2.06 | 2.25 | 2.06 | 2.26 | Kiepe et al. (2006) |
| NO ₂ [–] | 0.00 | 1.52 | 1.68 | 1.52 | 1.6 | Kiepe et al. (2006) |
| I [–] | 0.00 | 1.55 | 1.34 | 1.55 | 1.34 | Kiepe et al. (2006) |
| F [–] | 5.02 | 0.29 | 0.44 | 4.92 | 7.45 | Kiepe et al. (2006) |
| HCOO [–] | 0.00 | 0.901 | 0.84 | 0.901 | 0.84 | – ^d |
| CH ₃ COO [–] | 0.00 | 1.74 | 1.04 | 1.74 | 1.0437 | Kiepe et al. (2006) |
| HOOCCH ₄ COO [–] | 0.00 | 0.901 | 0.84 | 0.901 | 0.84 | – ^d |
| HOCC ₂ H ₄ COO [–] | 0.00 | 0.901 | 0.84 | 0.901 | 0.84 | – ^d |
| HCO ₃ [–] | 0.00 | 0.901 | 0.84 | 0.901 | 0.84 | – ^d |
| CHOCOO [–] | 0.00 | 0.901 | 0.84 | 0.901 | 0.84 | – ^d |

^a The apparent dynamic hydration numbers (ADHN) at 303.15 K and 0.1 M taken from Kiriukhin and Collins (2002).

^b Values of NADH = 0 are assigned to the ions for those the data is unavailable

^c Calculated using Eq. 3.47 and Eq. 3.48, respectively

^d NADH data is not available